2010

MONITORING OF FLUIDIZATION QUALITY, DRYING AND SPRAY STABILITY IN A FLUIDIZED BED

Garret Book
Western University

MONITORING OF FLUIDIZATION QUALITY, DRYING AND SPRAY STABILITY IN A FLUIDIZED BED

(Spine title: Monitoring of Fluidized Beds)

(Thesis format: Integrated-Article)

by

Garret Book

Graduate Program in Engineering Science
Department of Chemical and Biochemical Engineering

A thesis submitted in partial fulfillment
of the requirements for the degree of
Master of Engineering Science

School of Graduate and Post-Doctoral Studies
The University of Western Ontario
London, Ontario, Canada

CERTIFICATE OF EXAMINATION

Supervisor

Dr. Lauren Briens

Supervisory Committee

Dr. Cedric Briens

Dr. Franco Berruti

Examiners

Dr. Paul Charpentier

Dr. Vijay Parsa

Dr. Don Hewson

The thesis by

Garret Book

entitled:

Monitoring of Fluidization Quality, Drying and Spray Stability in a Fluidized Bed

is accepted in partial fulfilment of the
requirements for the degree of
Master of Engineering Science

Date_____

Chair of the Thesis Examination Board

Abstract

Experimental studies were conducted for monitoring fluidization quality, drying and nozzle spray stability in gas – solid fluidized beds of powders. The research focused on the development of triboelectric, acoustic emission and vibration monitoring methods as these can be reliably applied to a wide range of operating conditions at low cost and also often non – intrusively.

In a small scale vibrated fluidized bed of powder, it was found that the minimum bubbling velocity and minimum fluidization velocity decreased with increasing vibration. This was because vibration aided in the breakup of inter-particle cohesive forces. Vibration also accelerated the drying of wet, fine and cohesive particles by breaking up wet agglomerates. Triboelectric probes were successfully used to monitor this drying and to determine the effect of vibration on the drying.

Liquid injection into gas-solid fluidized beds has an adverse effect on bed fluidity. Acoustic and vibration measurements were extensively analyzed and correlated to bed fluidity through avalanche testing to successfully detect the bed fluidity of a large scale gas-solid fluidized bed. In addition, the acoustic and vibration measurements provided an indication of the time required to mix the solids after liquid injection into the bed.

Spray stability is a critical factor when injecting liquid into gas-solid fluidized beds. The signals from an accelerometer placed on the conduit leading up to industrial nozzles were correlated to the spray stability in open air. However, when the nozzles were inserted

into a large scale gas-solid fluidized bed the accelerometer signals were different. The mounting in the bed kept the nozzle assembly more stable, affecting the amplitude of the measured signal fluctuations but the effects of fluidization prevented direct calibration of spray stability in the bed to open air results. The accelerometer could still be used to evaluate the relative stability in the bed. In addition the accelerometer allowed the effects of gas properties and gas to liquid ratio on spray stability to be investigated.

Keywords: Fluidization quality, acoustics, vibrometrics, signal analysis, wavelets, spray stability, triboelectric probes

Statement of Co-Authorship

Chapters 2 through 4 are research studies that have been published, submitted or are ready for submission to refereed journals. Appendix 1 is a research study demonstrating one of the applications of the work in Chapter 3 in paper format. Appendix 2 is a research study presented at Acoustics Week in Canada 2005 and published in the non-refereed proceedings, Canadian Acoustics - Acoustique Canadienne. Appendix 3 is a research study presented at Acoustics Week in Canada 2005 and published in the non-refereed proceedings, Canadian Acoustics - Acoustique Canadienne. Appendix 4 is a research study published in the refereed journal, Chemical Engineering and Processing. Due the integrated article format of this thesis, not all signal analysis techniques are described in detail in the main chapters. Appendix 5 provides additional details and references on the various statistics and analysis techniques discussed.

Chapter 2:

Development of a Tribolelectric Procedure for the Measurement of Mixing and Drying in a Vibrated Fluidized Bed

Authors: William Brennan, Mike Jacobson, Garret Book, Lauren Briens, Cedric Briens

Status: Presented at Particulate Processes in the Pharmaceutical Industry I (2005) and published in the refereed journal Powder Technology

The experimental work for this study was conducted by William Brennan, Mike Jacobson and Garret Book. Consultation regarding experimental work and interpretation of experimental data was provided by Lauren Briens and Cedric Briens. The manuscript was written by William Brennan, Mike Jacobson and Garret Book and was revised by

Garret Book. The manuscript was reviewed by Lauren Briens and Cedric Briens. The study was presented by Garret Book at the conference.

Chapter 3:

On-line detection of bed fluidity in gas-solid fluidized beds with liquid injection by passive acoustic and vibrometric methods

Authors: Garret Book, Katherine Albion, Lauren Briens, Cedric Briens, Franco Berruti

Status: Submitted to Powder Technology

All experimental work for this study was conducted by Garret Book. Katherine Albion provided consultation and demonstration of appropriate signal analysis techniques so that Garret Book could fully develop the methods for this chapter. Consultation regarding experimental work and interpretation of experimental data was provided by Lauren Briens, Cedric Briens and Franco Berruti. The manuscript was written and revised by Garret Book, and reviewed by Lauren Briens, Cedric Briens and Franco Berruti.

Chapter 4:

Evaluation of the nozzle stability on liquid injection in gas-solid fluidized beds by passive vibrometric methods

Authors: Garret Book, Katherine Albion, Lauren Briens, Cedric Briens, Franco Berruti

Status: Will be submitted to Canadian Journal of Chemical Engineering

All experimental work for this study was conducted by Garret Book. Katherine Albion provided consultation and demonstration of appropriate signal analysis techniques so that Garret Book could fully develop the methods for this chapter. Consultation regarding

experimental work and interpretation of experimental data was provided by Lauren Briens, Cedric Briens and Franco Berruti. The manuscript was written and revised by Garret Book, and reviewed by Lauren Briens, Cedric Briens and Franco Berruti.

Appendix 1:

On-line detection of drying end point in gas-solid fluidized beds with liquid injection by passive acoustic and vibration methods

Authors: Garret Book, Katherine Albion, Lauren Briens, Cedric Briens, Franco Berruti

All experimental work for this study was conducted by Garret Book. Katherine Albion provided consultation and demonstration of appropriate signal analysis techniques so that Garret Book could fully develop the methods for this chapter. Consultation regarding experimental work and interpretation of experimental data was provided by Lauren Briens, Cedric Briens and Franco Berruti. The manuscript was written and revised by Garret Book, and reviewed by Lauren Briens, Cedric Briens and Franco Berruti.

Appendix 2:

Development of an Acoustic Method for the Measurement of Mixing and Drying in a Vibrated Fluidized Bed

Authors: Garret Book, Lauren Briens, Cedric Briens

Status: Presented at Acoustics Week in Canada 2005 October 11-14, 2005, London, Ontario, Canada and published in the non-refereed conference proceeding Canadian Acoustics - Acoustique Canadienne.

All experimental work for this study was conducted by Garret Book. Consultation regarding experimental work and interpretation of experimental data was provided by Lauren Briens and Cedric Briens. The manuscript was written and revised by Garret Book, and reviewed by Lauren Briens and Cedric Briens. The study was presented by Lauren Briens at the conference.

Appendix 3:

Flow Regime Detection in Pneumatic Transport of Particulates Using Non-Intrusive Acoustic Probes

Authors: Katherine Albion, Lauren Briens, Cedric Briens, Franco Berruti, Garret Book

Status: Presented at Acoustics Week in Canada 2005 October 11-14, 2005, London, Ontario, Canada and published in the non-refereed conference proceeding Canadian Acoustics - Acoustique Canadienne.

The experimental work of acquiring acoustic measurements was performed by Katherine Albion and Garret Book. All signal analysis and technique development was completed by Katherine Albion. Consultation regarding experimental work and technique development was provided by Lauren Briens, Cedric Briens and Franco Berruti. The manuscript was written and revised by Katherine Albion, and reviewed by Lauren Briens, Cedric Briens and Franco Berruti. The study was presented by Katherine Albion at the conference.

Appendix 4:

Flow Regime Determination in Upward Inclined Pneumatic Transport of Particulates Using Non-Intrusive Acoustic Probes

Authors: Katherine Albion, Lauren Briens, Cedric Briens, Franco Berruti and Garret Book

Status: Published in Chemical Engineering and Processing, 46(6), 520-531, 2007.

The majority of the experimental work, acquiring acoustic and pressure measurements, was performed by Katherine Albion with the remaining experimental work performed by Garret Book. All signal analysis and technique development was completed by Katherine Albion. Consultation regarding experimental work and technique development was provided by Lauren Briens, Cedric Briens and Franco Berruti The manuscript was written and revised by Katherine Albion, and reviewed by Lauren Briens, Cedric Briens and Franco Berruti.

Epigraph

"However beautiful the strategy, you should
occasionally look at the results."

Sir Winston Leonard Spencer-Churchill[1]
KG, OM, CH, TD, FRS, PC
(30 November 1874 – 24 January 1965)

[1] While this quote is widely attributed to Churchill, according to Richard M. Langworth, of The Churchill Centre, after scanning 15 million of Churchill's words, there is no proof, that they are, in fact, Churchill's words. Despite this, the spirit of the words carries weight, no matter who said them first.

Dedication

Dedicated to my Bubby Irma, who saw me start the research for this thesis but who was not here to see me defend.

Acknowledgements

I would like to express my extreme gratitude to my supervisor Dr. Lauren Briens for her patience, encouragement and advice. Without her I would not have been able to complete this work. Her guidance has allowed me to navigate through this project and academia in general. I would also like to thank my advisory committee Dr. Cedric Briens and Dr. Franco Berruti, for their continuing support and aid in completing this thesis.

I would like to thank Syncrude Canada Ltd. for their financial and material support. Specifically I want to thank Dr. Jennifer McMillan, Edward Chan and Eb Mueller for their all their advice and support of this project.

I would like to thank Ontario Graduate Scholarships (OGS) and Ontario Graduate Scholarships in Science and Technology (OGSST) for their financial support.

I would like to express my utmost thanks to University Machine Shop and Engineering Stores for all the help they have provided over the course of this research. Without their patience and hard work I would not have been successful.

Finally I would like to thank my family and my friends for all of their support. Without them I could not have made it through.

Table of Contents

List of Tables

List of Figures

List of Appendices

List of Symbols

A	Vibrational amplitude (mm)
A_c	Critical vibrational amplitude (mm)
C	Energy of the signal, Coefficient in the definition of Hölder exponent (units)
d_{p50}	Median particle size (μm)
f	Frequency, (Hz)
F	Maximum frequency, (Hz)
g	Acceleration due to gravity = 9.81 m/s^2
G_{bed}	Bed conductance, (Siemens/mhos)
h	Hölder exponent, (−)
i	Numerical indices of an element in a series
I	current, (ampres)
I	Local Intermittency index, (units)
j	Positive integer, number of power spectral density bin, (-)
J	Positive integer, number of power spectral density bins, (-)
K	Vibration intensity, (−)
m	Positive integer, number of level in a wavelet decomposition of a signal, (-)
n	Positive integer, number of points in a series or signal, Degree of polynomial P (-)
p	Power at a given frequency, (units)
r	Radial placement of triboelectric probes, (m)
R	Radius of column, (m)
R_1	Resistor used in the active conductivity circuit, (kΩ)
R_{bed}	Bed resistance, (kΩ)

s	Independent variable of P, (units), s
t	time, (s, min)
U_g	Superficial gas velocity, (m/s)
U_{mb}	Minimum bubbling velocity, (m/s)
U_{mf}	Minimum fluidization velocity, (m/s)
X	Function, (units)
x	Axial distance from distributor plate, (m)
z	Height, (m)
z_{max}	Maximum bed height, (m)
V_{app}	Applied voltage, (Volts)
V_m	Measured voltage, (Volts)

Greek symbols

α	Noise index of the signal, (units)
β	Linear constant, (units)
μ	Mean of a series or signal, (units)
σ	Standard deviation, (units)
ω	Angular frequency = $2\pi f$ rad/s

Chapter 1. Introduction

This thesis deals with experimental studies of passive methods for the monitoring of fluidization quality, drying and spray stability in gas-solid fluidized beds of powders. The research focused on the development of passive tribroelectric, acoustic emission and vibration monitoring methods as these can be applied to a wide range of operating conditions at low cost and still be reliable and be non-intrusive in most cases.

This chapter introduces each experimental study, discusses the research motivation for each study, previous studies and how each study fits into the thesis as a whole.

1.1. Triboelectric monitoring of mixing and drying in a vibrated gas-solid fluidized bed

1.1.1. Research motivation – Vibrated Fluidized Bed Drying

Fluidized beds are one of the most widespread technologies used in industrial drying operations. Fluidized bed dryers are prevalent in many chemical industries where drying or wet granulation of solid materials is required such as the pharmaceutical, food, fertilizer and energy industries [1]. Coal, biosynthesis products, pharmaceutical granules and food stuffs are all being dried in industry by fluidized beds [2].

The effective drying of these products is of great importance. Drying food products can affect the way a product tastes, as well as the amount of time it takes to spoil. Pharmaceutical granules are turned to tablets for consumption. The way pharmaceutical granules are dried affects granule size distribution and moisture content which in turn affects crucial properties of the produced tablets (e.g. hardness, friability, disintegration

time, etc) [2]. Coal particles tend to contain a considerable amount of moisture in thermal power stations and may require drying. If the coal is not dry and flowable, transport becomes very difficult [3].

As the solids in fluidized beds are moving rapidly, there is good solid's mixing and there is a large surface area between the solids and drying gas for heat and mass transfer to occur. This shortens the required time to dry the product without damaging heat sensitive materials by raising the temperature. Additionally, the fluidized solids can be moved easily in and out of the dryer via gravity, as well by pneumatic transport. The high rates of heat and mass transfer as well as high rates of solids transport to and from fluidized beds make them an important addition in industrial drying operations [2].

Although there are many advantages to using fluidized beds for drying, there are still several difficulties. One issue is that the fluidization quality in the beds is degraded when the particles are cohesive or just difficult to fluidize. Moisture content itself tends to make the particles more cohesive [2]. Raising the fluidization gas velocity can help improve fluidization, however, higher fluidization velocities can cause several undesirable phenomena such as particle entrainment and attrition [2, 4].

In fluidized bed drying it is critical to maintain good mixing through fluidization quality. Daud [2] reviewed recent advances in methods aimed to reduce the difficulties associated with fluidized bed drying. There are several external means of improving fluidization via vibration, agitation, rotation and centrifugation. The mathematical models for these

innovative types of fluidized beds are not well developed however both vibrated and agitated beds have been used successfully in industry [2].

In fluidized bed drying of cohesive particles, it is critical to maintain good fluidization. This can be achieved through mechanical vibration. It is also critical to monitor drying in order to determine the drying end point. Triboelectric probes provide inexpensive sensors that are capable of reliably monitoring drying and mixing in vibrated fluidized beds.

1.1.2. Literature Review

A number of ways of monitoring drying end points have been developed. In almost all cases they focused on the determination of the moisture content and ignored the flowability of the solids.

Alden et al. [5] developed a working model for the determination of moisture content via temperature difference. They assumed that the temperature of the moist solids in the bed was equivalent to the temperature read by a wet-bulb thermometer operating in similar conditions. Measuring the instantaneous temperature difference between the temperature of the solids and the wet bulb temperature that would be measured for a saturated sample when heated by the drying air, provided the moisture content of the sample. A specific temperature difference was identified for the system by taking frequent samples and calibrating with the measured moisture content. There are two problems with this approach:

1) With wet beds, it would be impossible to achieve fluidization if moisture was uniformly distributed on the surface of the bed particles, since the particles would be too cohesive for proper fluidization. In reality, most of the moisture is trapped within agglomerates or granules whose surface is relatively dry. The surface temperature of an agglomerate is affected not only by its average moisture but also by heat and mass transfer within the agglomerate.
2) The temperature measured by a thermocouple immersed in a fluidized bed is an unknown combination of the fluidization gas temperature, the dry particles temperature and the surface temperature of the wet agglomerates.

Wet granulation is the process of using a binder liquid, added to constituent powders to agglomerate the powders into granules. In the pharmaceutical industry these wet granules need to be dried to a specific moisture content depending on the desired tablet properties. Therefore a great deal of research has gone into determining the drying end point of pharmaceutical granules.

Watano et al. [6] used the fact that wet granules have different infrared (IR) absorption characteristics than dry granules, demonstrating that with increasing moisture content there was increasing IR absorption, to develop infrared moisture sensors. These sensors were used to monitor the drying of lactose and cornstarch granules, although the IR absorption characteristics were not specifically calibrated to moisture content. Other works built on these results by calibrating near IR absorbtion to the moisture content measured by Karl-Fischer titration, a titration where water is reacted with a base. The

technique was capable of monitoring in real time so that process conditions could be altered to improve product characteristics and reliability [7-9].

Räsänen et al. [10] used near infrared (NIR) to study the influence of process parameters in the dehydration behaviour of two pharmaceutical solids, wet theophylline granules and disodium phosphate. It was found that three carefully selected wavelengths from NIR absorption spectra were sufficient to indicate the moisture content of the solids. .

Wildfong et al. [11] and Morris et al. [12] used the NIR technique to successfully accelerate drying by appropriate monitoring and control. This was accomplished by initially setting the inlet air temperature above the melting point of the pharmaceutical product. In the first part of drying the evaporative cooling protects the product and, then, as the NIR identifies a critical moisture content where evaporation can no longer cool the product sufficiently, the inlet gas temperature is reduced to a level which is unlikely to harm the product. This managed to reduce the drying time required for most pharmaceutical products tested, demonstrating the usefulness of NIR techniques.

One potential problem with IR adsorption based process control is that dust will adhere to the surface of the sensors, causing changes in the IR adsorption that are unrelated to the changes in bed moisture.

Chaplin et al. [13] calibrated capacitance tomography with X-ray tomography to study the hydrodynamics of fluidized bed drying of pharmaceutical granules. They found that

capacitance tomography gave similar radial profiles to X-ray tomography on a time averaged basis. Capacitance tomography is a method that allows the dielectric permittivity distribution in the interior of the bed to be measured from external capacitance measurements. As expected, the hydrodynamics of the bed changed as the product was dried. Later, Chaplin and Pugsley [14] used the S-statistic chaotic attractor comparison method on the tomographs to indicate the solid moisture content. A reference state of 9-wt% moisture was selected. The S-statistic then compared the tomographs from a drying trial to the reference state to evaluate the statistical differences. Chaplin et al. [15] later performed S-statistic analysis on dynamic pressure signals to the same effect. Unfortunately this method could only indicate if the bed was at the reference moisture content level and could not monitor the progress of drying.

Acoustic and vibration sensors have been investigated for monitoring fluidization quality and fluidized bed drying. Tsujimoto et al. [16] used a single high frequency (140 kHz) passive acoustic sensor on both agitated and traditional fluidized bed granulators and found that unstable fluidization due to increases in moisture content could be monitored. Bojarra and Briens [17] investigated acoustic and vibration monitoring of fluidized bed drying of pharmaceutical placebo granules. Although passive acoustic emissions could not reliably monitor the granule moisture content, vibrations of the bed could indicate a specific criterion while drying in order to indentify an appropriate end point. Book et al. [18] found that by placing a microphone in the bag house exhaust above a vibrated fluidized bed of cohesive particles, it was possible to monitor the drying, including the breakup of agglomerates in the audible frequency band.

Vervloet et al. [19] recorded acoustic and vibration signals at 400 Hz in order to compare analysis techniques with pressure fluctuations, also recorded at 400 Hz. Time-domain, frequency and state-space methods were used to analyze the signals. Vervloet et al. [19] found that time-domain analysis and frequency analysis of the signals were insufficient to detect gradual changes in the process. However, it was noted that the power spectral density did change between dry and wet beds for the pressure, acoustic and vibration signals. The state-space attractor comparison method successfully detected changes in the process hydrodynamics in all 3 sensor types, however, this method could only compare the signals to a reference level.

Inexpensive, passive triboelectric probes were successfully used to reliably measure moisture contents down to 100 ppm and detect drying end points in fluidized beds of glass beads, ceramic microspheres and silica sand [1, 13, 20]. These probes are constructed easily by inserting a metal rod into the fluidized bed. The rod is insulated from the bed wall to prevent grounding. The friction resulting from the impact of particles on the probe causes surface or tribo charging of the solids which results in a current through the probe. The current generated is highly dependent on the surface properties of the solids which are in turn highly dependent on the moisture content of the bed.

Portoghese et al. [1] correlated the W-statistic of the triboelectric signal to the moisture content of fluidized beds of glass beads and silica sand measured via Karl-Fischer

titration. Interestingly, Portoghese et al. [1] found that, during the drying procedure, the surface moisture of the bed particles would initially increase as the breakup of wet agglomerates overwhelmed moisture removal by evaporation.

Fine, cohesive powders typically exhibit channeling rather than good fluidization as the forces holding them together resist free flowing fluidization and bubble formation. Vibration can improve the fluidization quality by disrupting channels and making bubbles appear. Valverde et al. [21] found that vibrated fluidized beds of cohesive powders exhibit two different regimes. In the solid-like regime, the bed will compact much like a bed of non-cohesive particles being vibrated into a settled state. It was found that if vibration is then stopped, the bed does not expand back to its original height. In the fluid-like regime, the bed will expand until a critical vibration amplitude is reached. At this point, bed bubble instabilities cause sloshing at the top of the bed as shown in Figure 1.1. If the vibration is then stopped the bed expands back to its original height.

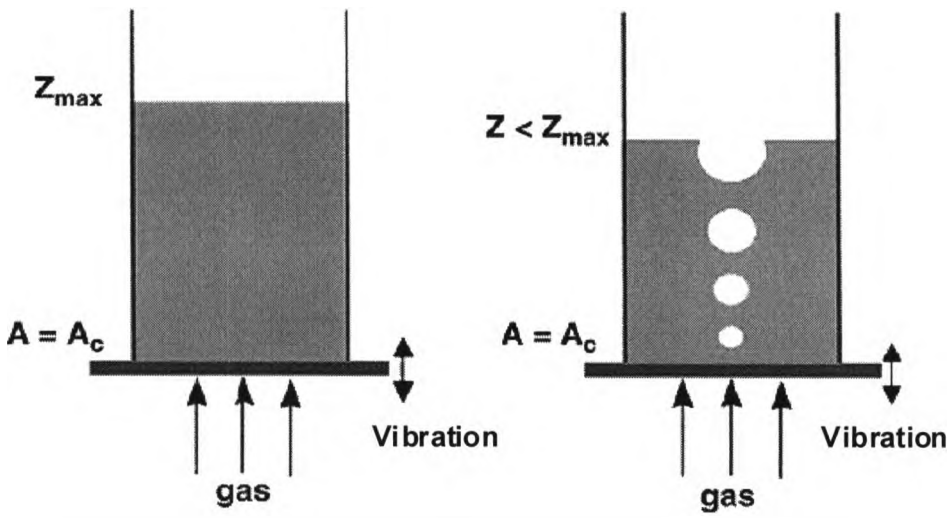

Figure 1.1 Bubble Instabilities at Greater than Critical Amplitude (Adapted from [21])

1.2. On-line detection of bed fluidity in gas-solid fluidized beds

1.2.1. Research motivation - The Syncrude Fluid Coking Process

Industrial processes make use of gas-solid fluidized beds extensively for both chemical and physical operations. Liquid can be sprayed directly into a fluidized bed where it can dry as in fluidized bed dryers, evaporate as in gas-phase polymerization or react as in fluid cokers [22, 23].

According to the Syncrude Canada Ltd. website the synthetic crude they produced in 2008 accounted for 15% of all Canada's oil production. Syncrude Canada extracts bitumen (heavy oil) from the Alberta tar sands and proceeds to upgrade the bitumen to more usable synthetic crude oil. This is accomplished by the fluid coking process. Figure 1.2 shows a flow diagram of fluid coking.

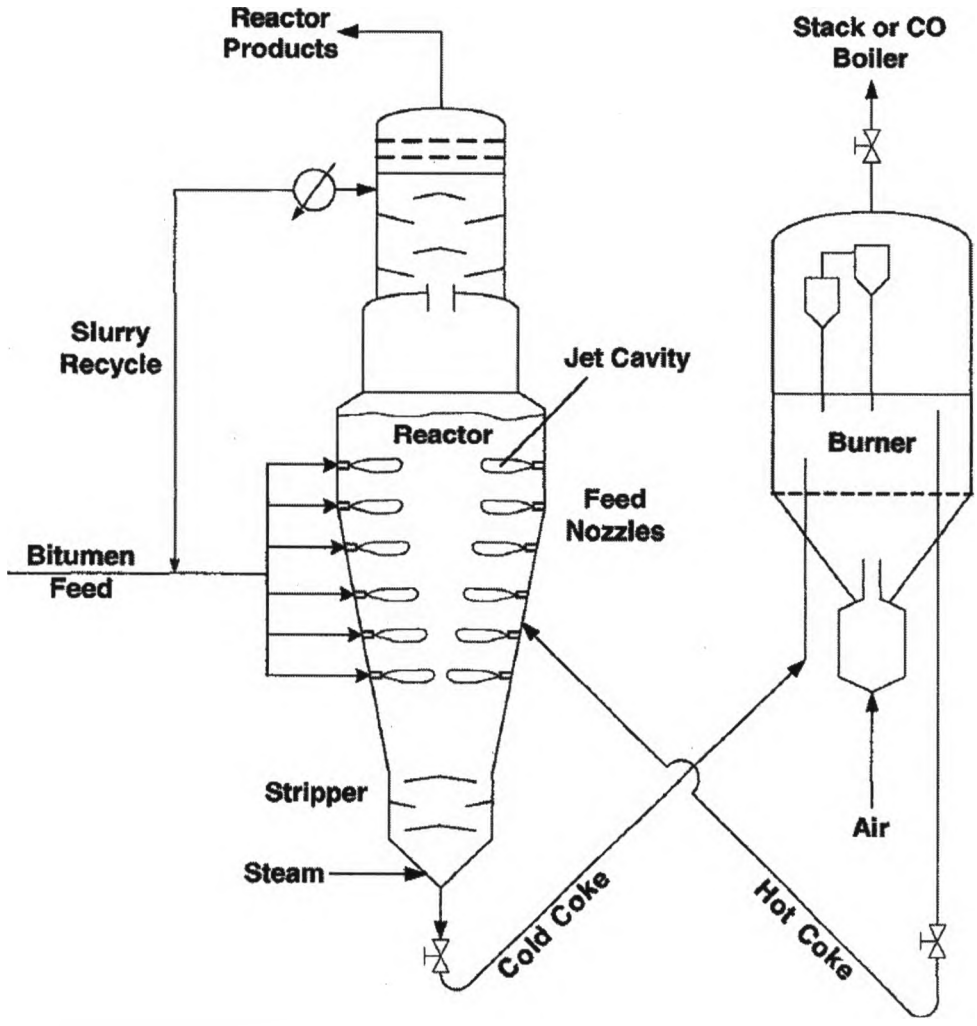

Figure 1.2 Flow diagram of fluid coking (adapted from [3])

In the fluid coking process the bitumen feed stock at 300 - 350 °C is injected into a bubbling or turbulent fluidized bed of coke particles at 500 – 550 °C. Within the fluidized bed reactor the heavy bitumen undergoes several cracking reactions resulting in lighter, more volatile fractions which leave as products and heavier fractions which deposit on the catalyst particles as coke [24]. The coke is circulated continuously through the burner in order to heat the rest of the particles. Any excess coke is removed from the system [25].

As with most gas-solid fluidized beds, the presence of liquid in fluid cokers has an adverse effect on bed fluidity. Operating fluid cokers at high liquid loadings, at lower temperatures increase yields and reduce sulphur oxide emissions providing a strong incentive, but such operation increases bed wetness [23]. The increase of liquid loading can result in local poor mixing zones, local defluidization, an increase of fouling of stripper sheds and a general reduction in fluidization quality, all of which reduce reactor performance and stability [23, 25]. With the loss of bed fluidity, heat transfer and mass transfer become extremely poor to the point the bed is ineffective and the bed behaviour is referred to as "bogging" [25].

Monitoring the bed fluidity in operations where liquid is injected into fluidized beds is, in general, difficult. With strong incentives to operate at higher liquid loadings, it becomes a necessity [23]. Sensor development is required to improve process control and safety [26].

1.2.2. Literature Review

The basis of many studies is the analogy between a bubbling liquid and a fluidized bed. The hydrodynamics of a bubbling liquid are strongly influenced by its viscous properties. Therefore it is proposed that a fluidized bed, behaving like a liquid, has an 'apparent viscosity' affecting fluidity. In general, there have been two types of studies performed in order to characterize bed fluidity through indirect signal analysis methods [25, 27] correlated to apparent viscosity or fluidity: the focus of the study can be on either the local fluidities in the bed or the general overall fluidity of the bed. Recently, Rees et al. [28] performed an updated literature review only to find that the principal measurement

techniques for measuring bed viscosity have not been advanced greatly since they were initially reviewed in 1971 by Schügerl [29]. Although the measurement techniques have not changed they can be useful since the apparent viscosity and fluidization quality of a fluidized bed are related [30].

1.2.2.1. Apparent Viscosity Measurements

A number of studies have attempted to measure the apparent viscosity of fluidized beds using the tools normally applied to liquids such as paddles, rotating spheres, falling ball and Couette-type viscometers [30]. Typically viscosity of a liquid is measured by the time it takes for it to flow through an orifice. Since the emulsion phase of a fluidized bed cannot be removed for this type of test, the time for a weight to pass through the bed is measured. Unfortunately the results have wide variations at least partially due to the difficulty estimating the viscosities of fluidized systems where the peripheral velocities of submerged objects are equal in magnitude to particle velocities in the undisturbed bed [31].

A)

B)

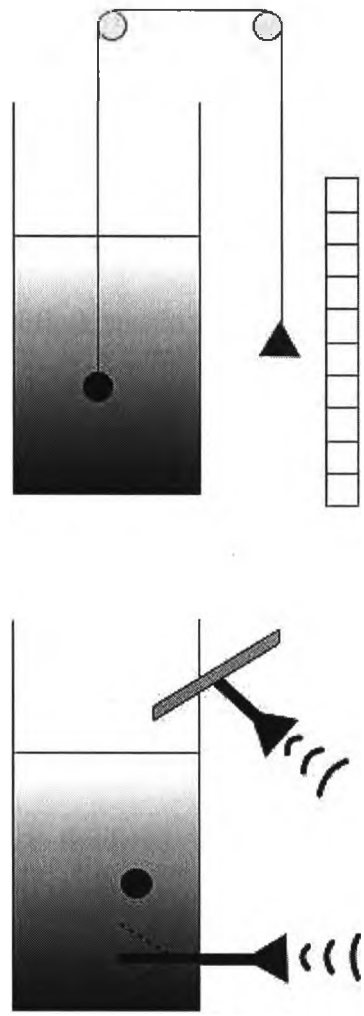

Figure 1.3 A) Falling Tethered Ball Viscometer B) Free Falling Ball Viscometer

Figure 1.3 shows two types of falling ball viscometers: tethered and free falling. With a tethered ball viscometer, the ball is attached to counter weight which is easily read against a ruler. It is then relatively easy to calculate the velocity of the falling sphere. In a free falling ball viscometer, the ball enters the bed then falls through the bed striking a

rod. Both of these actions generate acoustic signals and the time between them can easily be determined giving similar results to the tethered ball.

Falling ball methods are affected not only by the apparent viscosity but also by solids' circulation patterns and fluctuations due to the passage of bubbles resulting in error [31, 32]. Inertial effects of each fluctuation in the emulsion phase tend to cause the density inhomogenities throughout the bed. This, along with uneven gas distribution, makes it probable that there are some modifications in the theoretical laws governing particle interaction forces [33]. The sphere must be small enough to avoid significant wall effects but local defluidization zones may still form over the top surface of the falling [31, 32].

In order to avoid some of these problems, Rees et al. [28] stated that apparent viscosity measurements must be made when there are no bubbles. Unfortunately, the low gas velocity to achieve these conditions can result in a non-homogenous fluidization where some parts of the bed are better fluidized than others. Grace [31] used X-ray photography to infer the apparent viscosity based on bubble shapes. He observed the bubble shapes in the fluidized bed and then compared them to bubble shapes in viscous liquids. By this method, the apparent viscosity could be measured at any superficial gas velocity where bubbles were present.

The deaeration method has been used extensively to determine emulsion phase properties in fluidized beds [34]. The procedure involves defluidizing the bed while measuring the pressure drop as the gas exits. Lorences et al. [35] indicated that, in bubbling beds, the

de-aeration rates were independent of the initial fluidization velocities. This means that the bubbles tend to escape very quickly and that the emulsion phase properties are independent of the fluidization velocity [37]. This means once emulsion phase properties are determined at a single gas velocity it can be used at any gas velocity in the bubbling bed.

All methods for the direct measurement of apparent bed viscosity are interesting within the laboratory setting but none would be practical in industrial coking operations. The operating conditions of industrial coking units are too rigorous for fragile sensors or sensors that easily become fouled. Additionally the alterations to existing units would be expensive and could potentially damage the process efficiency.

1.2.2.2. Local fluidity measurements

Local defluidization will generally occur first near the gas distributor in gas-solid fluidized beds. There are many reasons that local defluidization zones can form near the gas distributor: the gas distribution is uneven because of faulty distributor design or plugging, larger particles in the distributor zone segregate, if sintering and caking make the particles more difficult to fluidize, or if agglomerates that have formed elsewhere in the bed settle near the distributor [25].

Yutani et al. [36] used the autocorrelation of local capacitance measurement to detect defluidized zones between adjacent gas jets in the grid zone of a fluidized bed of sand. Capacitance probes are hard to use in industrial applications because they require large electrical potentials and are sensitive to electrical noise. Additionally they tend to be too

fragile for many processes [25]. The hostile environment of fluid cokers would result in capacitance probes becoming quickly fouled or broken.

Defluidized zones lack the heat transfer typical of fluidized conditions. Ropchan [37] used a self heating thermistor and measured the flucuations in heat transfer coefficients in order to detect defluidized zones. Using the Hurst exponent of temperature fluctuations, Karamavruç et al. [38] detected defluidized zones around a horizontal heat transfer tube. Heat transfer measurements however are not a suitable method for detection of defluidized zones in fluidized beds of polymer particles as thermistors and other heat transfer probes form hot spots that may result in sintering and themselves promote the formation of defluidized zones [25]. In fluid cokers, heat transfer surfaces would quickly be fouled by coke deposits.

Triboelectric currents are generated by the potential difference developed by the charging of particles by friction between two materials [39]. Triboelectric current generated at electrodes in the distributor zone of gas-solid fluidized beds have been shown to reliably and rapidly detect defluidized zones [25]. This method required the V-statistic signal analysis technique and found that when the V-statistic of the signal fell below a certain level, it indicated a defluidized zone [40]. The V-statistic is a tool that was developed to identify cycles in the stock market [41]. Like other local probes, triboelectric probes would likely become fouled in fluid coker applications.

1.2.2.3. Overall Fluidity Measurements

Any property which is measured for the purposes of determining global bed fluidity, must be affected by small changes in fluidization quality anywhere in the bed, not just in the vicinity of the sensor. As pressure transducers can measure global fluctuations, many investigators have studied pressure signal fluctuations to characterize the global quality of fluidization. These investigations use a variety of analytical methods. Industrial installations often have fluctuations in gas velocity which are relatively small. This makes it desirable to use a method insensitive to velocity but sensitive to small changes in particle properties [27].

Tardos et al. [42] and McLaughlin et al. [43] used time averaged pressure drop in order to detect defluidization, but were unable to use the technique to provide early warning. The application of chaos analysis on the bed pressure drop fluctuations provides a tool to determine small changes in particle size distribution [44, 45]. Van Ommen et al. [46] used an enhanced attractor comparison method on pressure fluctuation measurements for an early warning of agglomerate formation in fluidized beds. Briens et al. [25] used an analytical tool called W-statistic on signals recorded from a dynamic pressure transducer to determine bed fluidity in a 1 m diameter pilot coker. They found very good agreement with traditional coke sampling methods. Chaplin et al [15] used the S-statistic to determine the moisture content in fluidized beds of drying pharmaceutical granules from dynamic pressure signals. It was concluded that the changes in hydrodynamic state, related to the changes in moisture, accounted for the changes in pressure fluctuations.

Benoni et al. [47] determined particle agglomeration in a fluidized bed by a simple process of monitoring the entrainment of fine particles.

Recent studies in the innovative field of non-intrusive passive acoustic monitoring as an alternative to direct pressure measurements indicate a large potential for these sensors as an analytical tool. An ultra high frequency acoustic emission sensor was used by Tsujimoto et al. [16] to detect the start of unstable fluidization leading to defluidization due to increases of moisture content. The major difficulties with this technique occurred when the bed humidity was too high, the inducing channeling in the bed and attenuating the acoustic signal. Additionally the massive digital processing power required to manage signals at 140 kHz is excessive. Briongos et al. [48] focused on extremely low frequency noise between 0 – 20 Hz which greatly improved the ease of data processing. This frequency band corresponded to the bubbling properties of the fluidized bed leading to conclusions on the fluidization regime. These studies considered background noise and selected the frequency bands of interest partly to avoid the background noise affecting the results; however by proper sensor selection and advanced signal filtering, detailed information about the process may be obtained from the acoustic emissions in the audible range (20 Hz – 20 kHz). Book et al. [18] acquired acoustic data in the audible frequency range with a microphone in exhaust of a small vibrated fluidized bed of cohesive powder to determine the minimum bubbling velocity of the bed and the evaluate the drying of the bed. This clearly demonstrated the usefulness of this frequency range and passive acoustics for the determination of bed hydrodynamics.

1.3. Evaluation of the Spray Stability on Liquid Injection

1.3.1. Research motivation - Spray Stability

Many gas-solid fluidized bed operations involve the injection of gas atomized liquid feed via spray nozzles of varying types. Gas-liquid spray nozzles can be used to introduce feedstocks or coolants to different chemical reactors such as gas-phase polymerization reactors, fluid cokers and fluidized catalytic cracking (FCC) units [25, 49-53].

In Syncrude Canada Ltd. fluid coking units, bitumen is mixed with steam in order to atomize it and disperse it throughout the bed by injection nozzles [49]. Efficiency and rate of cracking depends on the liquid-solid contact within the unit which is determined by the initial effectiveness of liquid dispersion from the injection [50].

In almost all cases, a stable or non-pulsating spray with a controlled droplet size is considered optimal for reactor operation as this avoids large liquid-solid agglomerates which settle to the bottom of the reactor, potentially causing an extreme loss of fluidization or "bogging" [50, 51].

1.3.2. Literature Review

There are two main strategies used to investigate nozzles: a direct investigation of their performance by measuring the contact between solids and liquids in the bed or measuring the spray stability, assuming that it is the critical factor in ensuring good liquid solid contact in the fluidized bed.

1.3.2.1. Spray Performance

To fully investigate nozzle behavior, spraying into open air and spraying into fluidized beds of solids are required. Many studies [49, 50, 51, 53] involved experiments both in open air and in fluidized beds. There are two approaches to evaluating nozzle behavior. The first is to evaluate the nozzle based on the characteristics of the spray pattern downstream from the tip of the nozzle, and, the second approach is to evaluate the gas-liquid flow upstream of the nozzle tip.

A basic optical way of evaluating nozzle stability uses high speed video or images in open air tests [49-54]. The imaging techniques are relatively easy and the spray expansion angle is measured using programmed optical algorithms [53] by assigning pixels as either black or white based on the spray and counting the different coloured pixels. Translating the results to fluidized bed experiments can be difficult because the spray interacts with the solids in the bed. In order to validate a model of the entrainment of solids in the gas-liquid jet within a fluidized bed, Ariyapadi et al. [51] used an X-ray observation technique.

House et al. [52] used a tracer in the liquid to determine the dispersion after spraying; a small injection of volatile *n*-propanol was sprayed into the bed in order to allow the spray to stabilize followed by a sugar solution in water. The gas velocity was then brought just below fluidization velocity and the fluidized bed was allowed to dry. Finally the bed was emptied and then sieved. House et al. [52] found that the sugar had formed bridges so the solids were trapped in granules of different sizes. By measuring the mass of sugar in

these granules, the liquid to solid ratios were calculated, providing a rating of the dispersion of nozzles as well as indicating four mechanisms for the distribution of liquid.

Knapper et al. [55] used a more advanced tracer technique where copper naphthenate dissolved in bitumen was injected into the pilot scale hot coker. The coke particles were sampled during the injection and were analyzed offline by Inductively Coupled Plasma (ICP) to evaluate the gross concentration of copper left on the coke particles and Energy dispersive X-ray (EDX) determined the surface coating of copper on individual particles. This method was successful at differentiating between low and high performance spray nozzles.

Temperature tracer techniques have also been used to evaluate liquid dispersion of nozzles. The local solid-liquid mixing of a free spraying nozzle and the same nozzle with a draft tube in a fluidized bed were compared by McMillan et al. [56] using a temperature tracer. Cold ethanol was sprayed into a fluidized bed and then a series of fast response thermocouples at various lengths along the jet and radial positions from the center of the jet to measured the temperature. If mixing was perfect the temperature should have been the same all through the jet. However, McMillan et al. [56] found that this was not the case, even though the presence of a draft tube increased the local liquid – solids mixing.

Portoghese et al. [53] used multiple and novel techniques to investigate the effect of varying gas to liquid ratio, liquid mass flow rate and nozzle size on the contact efficiency of the spray. In open air, a laser was passed through the gas-liquid jet onto a photocell

target and the signal attenuation was recorded where the signal attenuation was defined as the difference between the value of the undisturbed signal (when there was no spray) and the average of the signal calculated over a steady state spray. Automatic computer algorithms calculated the spray expansion angle. The nozzles were then tested at the same conditions in a gas fluidized bed of silica sand. A triboelectric probe was made by inserted into the bed opposite from the nozzle. When particles in the fluidized bed contacted the probe they became triboelectrically charged creating a current in the probe. The current was amplified, converted to a voltage and recorded. The signal was compared to a reference signal in order to develop a nozzle performance index (NPI) validated previously with temperature measurements [53].

Leach et al. [57] improved on this technique by adding a defluidization step after spraying which allowed for wet agglomerates to segregate as well as letting the charged solids in the bed return to a electrically neutral state more slowly providing a more distinctive signal to be analyzed. Leach et al. [49] provided even further improvements by adding an active voltage to the probe. Rather than measuring passive tribo charging of the particles the effective resistance and conductance of the fluidized bed was calculated. The initial distribution of the water in the bed was highly correlated with that of the conductance of the bed and a new nozzle performance index was calculated. Leach et al. [49] tested the nozzles in open air and a Malvern Mastersizer evaluated the size distribution of the droplets. The findings showed that droplet size had a strong impact on solid liquid contact when the droplet size was significantly larger than that of the solids.

Using a patented Phase Doppler Particle Analyzer (PDPA), Rahman et al. [58] managed to fully characterize the atomization of nozzles in open air. The Stokes, Reynolds and Weber numbers characterized the spray at many distances from the tip of the nozzle, both axially and radially. This method defined the size and velocity of droplets at a wide variety of locations within the gas liquid jet.

1.3.2.2. Spray Stability

Stable spray is defined as a spray that is non-pulsating with a controlled droplet size. Spray stability coefficients have been calculated from a static pressure transducer upstream of a nozzle and correlated to a stability coefficient calculated from the signal of a triboelectric probe downstream of the nozzle located inside a fluidized bed of solids [50]. In open air tests, the stability of the nozzle spray was measured with a static pressure transducer and then correlated with acoustic results, measured by a microphone encased in copper and placed directly in the spray. Ariyapadi et al. [50] showed that upstream measurements were sufficient to evaluate downstream characteristics and additionally began applying the wavelet transform on signals in order to refine the results.

Cody et al. [59] filed an American patent before the previous study on the upstream monitoring of nozzles on industrial cokers at Exxon in the hopes of controlling operating parameters. Accelerometers and dynamic pressure transducers were used on the conduit outside industrial cokers on 2 phase feed nozzles and the signals were analyzed using fast Fourier transforms in order to be compared to a reference power spectral density at known and correct operating conditions.

Building on the previous two studies Maldonado et al. [54] used an advance dynamic pressure transducer at a frequency of 2 kHz in order to evaluate nozzle stability in open air. Once again the fast Fourier transform was used to analyze the pressure signal. In this case a parameter was calculated based upon the power of the frequencies from 0 to 40 Hz where the dominant frequencies were.

1.4. Thesis Objectives

The overall objective of the research described in this thesis was to investigate and then develop monitoring methods and analysis methods to monitor fluidization quality, drying and spray stability in gas-solid fluidized beds. This included triboelectric methods, passive acoustic emission and vibration measurements.

From this, specific objectives included the monitoring of the effects of vibration on fluidization and drying, identification of conditions that lead to bogging and a performance ranking of nozzle and pre-mixer combinations.

1.5. References

[1] Portoghese, F., Berruti, F., Briens, C., Continuous on-line measurement of solid moisture content during fludized bed drying using triboelectric probes. *Powder Technology.* 181 (2008) 169 – 177.

[2] Daud, W. R. W., Fluidized Bed Dryers - Recent Advances. *Advanced Powder Technology.* 19 (2008) 403 - 418.

[3] Medhe, M., Pitchumani, B., Effect of moisture induced capilliary forces on coal flow properties. *AIChE Annual Meeting. Conference Proceedings 2006.* (2006)

[4] Wormsbecker, M., Pugsley, T., The influence of moisture on the fluidization behaviour of porous pharmaceutical granule. *Chemical Engineering Science.* 63 (2008) 4063 – 4069.

[5] Alden. M., Torkington, P., Strutt, A. C. R., Control and Instrumentation of a Fluidized-Bed Drier Using the Temperature Difference technique I. Development of a Working Model. *Powder Technology.* 54(1988) 15-25.

[6] Watano, S., Takashima, H., Sato, Y., Miyanami, K., Yasutomo, T., IR Absorbstion characteristics of an IR moisture sensor and mechanism of water transfer in a fluidized bed granulation. *Advanced Powder Technology.* 7 (1996) 279-289.

[7] Rantanen, J., Lehtola, S., Rämet, P., Mannermaa, J-K., Yliruusi, J., On-line monitoring of moisture content in an instrumented fluidized bed granulator with a multi-channel NIR moisture Sensor. *Powder Technology.* 99 (1998) 163-170.

[8] Frake, P., Greenhalgh, D., Grierson, S. M., Hempenstall, J. M., Rudd, D. R., Process control and end-point determination of a fluid bed granulation by application of near infra-red spectroscopy. *Internation Journal of Pharmaceutics.* 151 (1991) 75-80.

[9] Green, R. L., Thurau, G., Pixley, N. C., Mateos, A., Reed, R. A., Higgins, J. P., In-Line Monitoring of Moisture Content in Fluid Bed Dryers Using Near-IR Spectroscopy with Consideration of Sampling Effects on Method Accuracy. *Analytical Chemistry.* 77 (2005) 4515-4522.

[10] Räsänen, E., Rantanen, J., Mannermaa, J-K., Yliruusi, J., Vuorela, H., Dehydration Studies Using a Novel Multichamber Microscale Fluid Bed Dryer with In-Line Near-Infrared Measurement. *Journal of Pharmaceutical Sciences.* 92 (2003) 2074-2081.

[11] Wildfong, P. L. D., Samy, A-S., Corfa, J., Peck, G. E., Morris, K. R., Accelerated Fluid Bed Drying Using NIR Monitoring and Phenomenological Modeling: Method Assessment and Formulation Suitability. *Journal of Pharmaceutical Sciences.* 91 (2002) 631-639.

[12] Morris, K. R., Stowell, J. G., Byrn, S. R., Placette, A. W., Davis, T. D., Peck, G. E., Accelerated Fluid Bed Drying Using NIR Monitoring and Phenomenological Modeling. *Drug Development and Industrial Pharmacy.* 26 (2000) 985-988.

[13] Chaplin, G., Pugsley, T., van der Lee, L., Kantzas, A., Winters, C., The dynamic calibration of an electrical capacitance tomography sensor applied to the fluidized bed drying of pharmaceutical granule. *Measurement Science and Technology.* 16 (2005) 1281-1290.

[14] Chaplin, G., Pugsley, T., Application of electrical capacitance tomography to the fluidized bed drying of pharmaceutical granule. *Chemical Engineering Science.* 60 (2005) 7022-7033.

[15] Chaplin, G., Pugsley, T., Winters, C., Application of chaos analysis to pressure fluctuation data from a fluidized bed dryer containing pharmaceutical ganule. *Powder Technology.* 142 (2004) 110-120

[16] Tsjujimoto, H., Yokoyama, T., Huang, C.C., Sekiguchi, I., Monitoring particle fluidization in a fluidized bed granulator with an acoustic emission sensor. *Powder Technology.* 113 (2000) 88-96

[17] Bojarra, M., MONITORING FLUIDIZED BED DRYING OF PHARMACEUTICAL GRANULES. MESc Thesis, The University of Western Ontario, 2008.

[18] Book. G., Briens, L., Briens, C., Development of an acoustic method for the measurement of mixing and drying in a vibrated fluidized bed. *Canadian Acoustics - Acoustique Canadienne.* 33 (2005) 20-21

[19] Vervloet, D., Nijenhuis, J., van Ommen, J.R., Monitoring a lab-scale fludized bed dryer: A comparison between pressure transducers, passive acoustic emissions and vibration measurements. *Powder Technology.* 197 (2010) 36 - 48.

[20] Brennan, W., Jacobson, M., Book, G., Briens, C., Briens, L., Development of a triboelectric procedure for the measurement of mixing and drying in a vibrated fluidized bed. *Powder Technology.* 181 (2008) 178-185.

[21] Valverde, J., Castellanos, A., Quintanilla, M. Effect of vibration on the stability of a gas-fluidized bed of fine powder. In: *Physical Review E: Statistical Physics, Plasmas, Fluids, and Related Interdisciplinary Topics.* 64 (2001) 21302.

[22] McDougall, S., Saberian, M., Briens, C., Berruti, F., Chan, E., Effect of liquid properties on the agglomerating tendency of a wet gas-solid fluidized bed. *Powder Technology.* 149 (2005) 61-67

[23] McDougall, S., Saberian, M., Briens, C., Berruti, F., Chan, E., Using dynamic pressure signals to assess the effects of injected liquid on fluidized bed properties. *Chemical Engineering and Processing.* 44 (2005) 701-708

[24] House, P. K., Interaction of Gas-Liquid Jets with Gas-Solid Fluidized Beds: Effect of Liquid Solid Contact and Impact on Fluid Coker Operation, *PhD Thesis,* University of Western Ontario, (2007).

[25] Briens, C., McDougall, S., Chan, E., Online Detection of Bed Fluidity in a fluidized bed coker. *Powder Technology.* 138 (2003) 160-168

[26] Boyd, J.W.R., Varley, J., The uses of passive measurement of acoustic emissions from chemical engineering processes. *Chemical Engineering Science.* 56 (2001) 1749 - 1767.

[27] McDougall, S., Saberian, M., Briens, C., Berruti, F., Chan, E., Characterization of Fluidization Quality in Fluidized Beds of Wet Particles. *International Journal of Chemical Reactor.* 2 (2004) A26

[28] Rees, A. C., Davidson, J. F., Dennis, J. S., Hayhurst, A. N., THE APPARENT VISCOSITY OF THE PARTICULATE PHASE OF BUBBLING GAS-FLUIDIZED BEDS: A comparison of the falling or rising sphere technique with other methods, *IChemE J.* 85 (2007) A10, 1341-1347

[29] Schügerl, K., Rheological behaviour of fluidized systems, Davidson, J.F. and Harrison, D. (eds). *Fluidization,* (Academic Press, London and New York) 261-292

[30] Kai, T., Murakami, M., Yamaskai, K., Takahashi, T, RELATIONSHIP BETWEEN APPARENT BED VISCOSITY AND FLUIDIZATION QUALITY IN A FLUIDIZED BED WITH FINE PARTICLES, *Journal of Chemical Engineering of Japan.* 24 (1991) 4, 494-500

[31] Grace, J. R., The Viscosity of Fluidized Beds, *Canadian Journal of Chemical Engineering.* 48 (1970) 30-33

[32] King, D. F., Mitchell, F. R. G., Harrison, D., Dense Phase Viscosities of Fluidised Beds at Elevated Pressures, *Powder Technology.* 28 (1981) 55-58

[33] Daniels, T.C., Measurement of the Drag on Spheres Moving Through Gaseous Fluidized Beds, *Journal of Mechanical Engineering.* 4 (1962) 2, 103-110

[34] Geldart, D., Wong, A.C., FLUIDIZATION OF POWDERS SHOWING DEGREES OF COHESIVENESS—II.EXPERIMENTS ON RATES OF DE-AERATION, *Chemical Engineering Science.* 40 (1985) 4, 653-661

[35] Lorences, M. J., Patience, G.S., Diez, F.V., Coca, J., Fines effects on collapsing fluidized beds, *Powder Technology.* 131 (2003) 234-240

[36] Yutani, N., Ho, T.C., Fan, L.T., Walawender, W.P., Song, J.C., STATISTICAL STUDY OF THE GRID ZONE BEHAVIOR IN A SHALLOW GAS-SOLID FLUIDIZED BED USING A MINI-CAPACITANCE PROBE, *Chemical Engineering Science.* 38 (1983) 4, 575-582

[37] Ropchan, W.T., Heat transfer and grid jets, *PhD Thesis,* Stanford University, (1981).

[38] Karamavruç, A.I., Clark, N.N., A fractal approach for interpretation of local instantaneous temperature signals around a horizontal heat transfer tube in a bubbling fluidized bed, *Powder Technology.* 90 (1997) 235-244

[39] Moore, A.D. (Ed.), Electrostatics and its Applications, *Wiley*, USA, (1974)

[40] Briens, C. L., Briens, L. A., Barthel, E., Le Blévec, J. M., Tedoldi, A., Margaritis, A., Detection of local fluidization characteristics using the V statistic, *Powder Technology.* 102 (1999) 95-103

[41] Briens, L.A., Briens, C.L., Cycle Detection and Characterization in Chemical Engineering, *AIChE Jounal.* 48 (2002) 5, 970-980

[42] Tardos, G., Mazzone, D., Pfeffer, R., Destabilization of Fluidized Beds Due to Agglomeration – Part II: Experimental Verification, *Canadian Journal of Chemical Engineering.* 63 (1985) 384-389

[43] McLaughlin, L.J., Rhodes, M.J., Prediction of fluidized bed behaviour in the presence of liquid bridges, *Powder Technology.* 114 (2001) 213-233

[44] van Ommen, J.R., Schouten, J., Coppens, M.O., van den Bleek, C.M., Monitoring Fluidization by Dynamic Pressure Analyis, *Chemical Engineering Technology.* 22 (1999) 9, 773-775

[45] Schouten, J.C., van den Bleek, C.M., Monitoring the Quality of Fluidization Using the Short-Term Predictability of Pressure Fluctuations, *AIChE Journal.* 44 (1998) 1, 48-60

[46] van Ommen, J.R., Coppens, M.O., van den Bleek, C.M., Schouten, J.C., Early Warning of Agglomeration in Fluidized Beds by Attractor Comparison, *AIChE Journal.* 46 (2000) 11, 2183-2197

[47] Bénoni, D., Briens, C.L., Baron, T., Duchesne, E., Knowlton, T.M., A procedure to determine particle agglomeration in a fluidized bed and its effect on entrainment, *Powder Technology.* 78 (1994) 33-42

[48] Villa Briongos, J., Aragón, J. M., Palancar, M. C., Fluidised bed dynamics diagnosis from measurements of low frequency out-bed passive acoustic emission, *Powder Technology.* 162 (2006) 145-156

[49] Leach, A., Chaplin, G., Briens, C., Berruti, F., Comparison of the permformance of liquid-gas injection nozzles in a gas-solid fluidized bed. *Chemical Engineering and Processing: Process Intensification.* 48 (2009) 780-788

[50] Ariyapadi, S., Berruti, F., Briens, C., Knapper, B., Skwarok, R., Chan, E., Stability of Horizontal Gas-Liquid Sprays in Open-Air and in Gas-Solid Fluidized Bed. *Powder Technology.* 155 (2005) 161-174

[51] Ariyapadi, S., Berruti, F., Briens, C., Griffith, P., Hulet, C., Modeling the Injection of Gas-Liquid Jets into Fluidized Beds of Fine Particles. *The Canadian Journal of Chemical Engineering.* 81 (2003) 891-899

[52] House, P., Briens, C., Berruti, F., Chan, E., Effect of spray nozzle design on liquid-solid contact in fluidized beds. *Powder Technology.* 186 (2008) 89-98

[53] Portoghese, F., Ferrente, L., Berruti, F., Briens, C., Chan, E., Effect of injection-nozzle operating parameters on the interaction between a gas-liquid jet and a gas-solid fluidized bed. *Powder Technology.* 184 (2008) 1-10

[54] Maldonado, S., Fleck, B., Heidrick, T., Amirfazli, A., Chan, E., Knapper, B., Development of an Experimental method to evaluate stability of gas-liquid sprays. *Atomization and Sprays.* 18 (2008) 699-722

[55] Knapper, B., Chan, E., Gray, M., Mikula, R., Meauserment of Efficiency of Distribution of Liquid Feed in a Gas-Solid Fluidized Bed Reactor. *International Journal of Chemical Reactor Engineering.* 1 (2003) A35

[56] McMillan, J., Zhou, D., Ariyapadi, S., Briens, C., Berruti, F., Characterization of the contact between Liquid Spray Droplets and Particles in a Fluidized Bed. *Industrial Chemical Engineering Res.* 44 (2005) 4931-4939

[57] Leach, A., Portoghese, F., Berruti, F., Briens, C., A new and rapid method for the evaluation of the liquid-solid contact resulting from liquid injection into a fluidized bed. *Powder Technology.* 184 (2008) 44-51

[58] Rahman, M., McMillan, J., Hiedrick, T., Fleck, B,. Charactering the Two-phase, Air/Liquid Spray Profile Using a Phase Doppler Particle Analyzer. *14th Int Symp on Applications of Laser Techniques to Fluid Mechanics*, Lisbon, Portugal, 07-10 July, 2008

[59] Baker, C., Cody, G., Joseph, C., Sela, U,. Acoustic Monitoring of Two-Phase Feed Nozzles. US Patent 5 004 152, 1991

Chapter 2. Development of a Tribolelectric Procedure for the Measurement of Mixing and Drying in a Vibrated Fluidized Bed

William Brennan, Mike Jacobson, Garret Book, Cedric Briens, Lauren Briens

Note: This chapter was presented at Particulate Operations in the Pharmaceutical Industry I (2005) and published in the refereed journal Powder Technology 181 (2008) 178–185

2.1. Introduction

Currently some of the most important applications of gas-solid fluidized beds are physical processes in the pharmaceutical industry [1]. However, many fine powders are very difficult to fluidize. Vibration can be used to facilitate fluidization as well as decrease the required gas velocity. This is particularly useful in fluidizing cohesive powders [1-6].

Along with the difficulties of fluidization of cohesive powders, there are difficulties associated with the detection of their fluidization regime. Traditionally, the minimum gas velocity for fluidization [U_{mf}] and bubbling [U_{mb}] in fluidized beds are determined through pressure profiles and bed height measurements. In industrial applications, accurate bed height measurements are nearly always impossible while pressure measurements not only require invasive pressure taps but often do not provide clear information with very fine powders, lacking distinctive maximums. In addition, to ensure that the pressure transducers do not become plugged with fine powder, continual

backflushing with instrument gas or membranes, which are expensive and reduce sensitivity, are required. In a vibrated fluidized bed, selection of the appropriate gas velocity and vibration amplitude is essential for good mixing and drying.

2.1.1. Vibration

Fine, cohesive powders typically exhibit channeling rather than good fluidization as the forces holding them together resist free flowing fluidization and bubble formation. Vibration can improve the fluidization quality by disrupting channels and making bubbles appear. Valverde et al. [7] found that vibrated fluidized beds of cohesive powders exhibit two different regimes. In the solid-like regime, the bed will compact much like a bed of non-cohesive particles being vibrated into a settled state. It was found that if vibration is then stopped, the bed does not expand back to its original height. In the fluid-like regime, the bed will expand until a critical vibration amplitude is reached. At this point, bed bubble instabilities cause sloshing at the top of the bed as shown in Figure 2.1. If the vibration is then stopped the bed expands back to its original height.

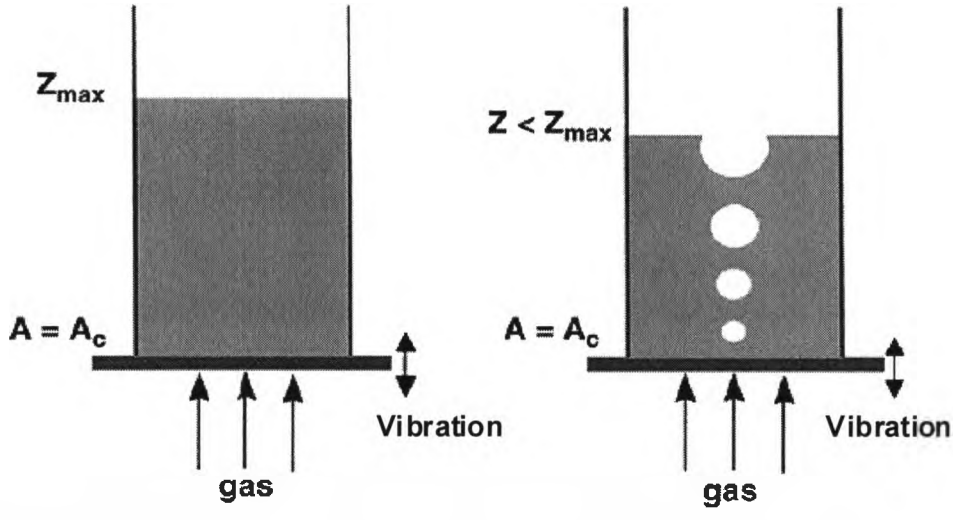

Figure 2.1 Bubble Instabilities at Greater than Critical Amplitude (Adapted from [7])

2.1.2. Triboelectric probes

The triboelectric effect refers to the charging of particles by friction between two different materials. The ancient Greeks knew about triboelectrification. However, even after many years of study, the process is still considered quite complex and is not very well understood [8]. A triboelectric probe is made by coating a metal rod with an electrically insulating material except for its tip. When the probe is inserted into a fluidized bed, triboelectric current is generated by the friction of bed solids against the metal tip of the probe. The triboelectric current depends upon the surface properties, the collision rate and the kinetic energy of the solids. Fluidization quality affects the triboelectric current by influencing the energy and the collision rate. Briens et al. [9] found that by using triboelectric probes in a fluidized bed, localized defluidization could be detected within 100 ms. This detection was made by taking the V-statistic of the triboelectric current from the probes. These findings suggest that triboelectric probes can be used to detect changes in global fluidization quality and therefore the transition between fluidization regimes.

2.1.3. Minimum Bubbling Velocity

Determining the minimum bubbling velocity is particularly useful as it is indicative of a well mixed bed [6]. Bubbles are formed at gas velocities higher than the minimum bubbling velocity. Bubbles promote mixing in the fluidized bed by carrying solids in their wakes. This provides good top to bottom mixing of the solids, as shown in Figure

2.2. The minimum bubbling velocity can be difficult to determine with traditional pressure measurements in beds of fine powders.

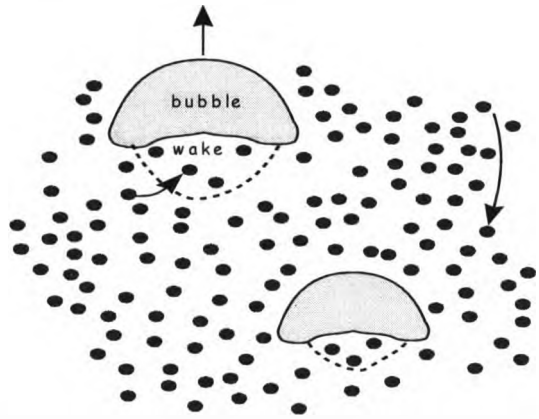

Figure 2.2 Bubbles in a Gas-Solid Fluidized Bed Carrying Solids in their Wakes

2.1.4. Solids Drying

Fluidized beds are commonly used to dry powders. The fluidizing gas dries wet particles as it flows through the bed and heat exchangers may be used to speed up drying. A bubbling fluidized bed provides the agitation, mixing and good heat transfer required for effective drying.

Wet solids have different surface properties than dry particles. Therefore, as the solids dry, their surface properties change thereby changing the local triboelectric current. This allows for the detection of drying in a fluidized bed by triboelectric probes [10].

2.1.5. Signal Analysis

As triboelectric signals are very sensitive to electrical noise, their reliable use requires sophisticated analysis. Examination of the way the signal fluctuates over time can

provide important information [6, 9, 11-13]. A few analysis techniques are reviewed below.

2.1.6. Time-averages

The time-average of a signal is the arithmetic mean of the signal over a specified length of time.

2.1.7. Power Spectra

The power spectra decomposes the frequency components of the signal into frequency ranges allowing for the detection of periodic cycles.

2.1.8. Hölder Exponent

For stochastic processes or functions X(t), the local regularity of sample paths is usually measured in terms of the Hölder exponent. This is performed by a comparison of X(t) at time t to a power law. A process X is said to have Hölder regularity $h \geq 0$ at time t if there exists a local polynomial P(s) of degree n = h and a constant C, as shown in Equation 2.1.

$$\left|X(t+s)-P(s)\right| \leq C\left|s\right|^{h} \qquad \textbf{(2.1)}$$

Where 's' is an independent variable of the poloynomial 'P'. The Hölder exponent [h] quantifies the roughness of X [14, 15]. If h is close to 0 then the signal is considered to be rough and variable whereas an "h" close to 1 indicates a smooth and regular signal.

For the derivative of the function, the Hölder exponent is in the range 1<h<2; where an "h" closer to 1, the rougher the signal. The Hölder exponent therefore is a measure of signal singularity. The present study used a Hölder exponent estimated by using a transform of order 3. Therefore, the exponent calculated is referred to as the Hölder exponent of the 3rd order [14, 15].

2.2. Objectives

There were three main objectives of this research. First, to use triboelectric probes to identify the minimum bubbling velocity and thus ensure good solids mixing within the bed. Second, to use triboelectric probes to monitor the drying of wet solids in a fluidized bed. The third objective was to study the effect of vibration on solids mixing and drying in a fluidized bed at low gas velocities and low vibration amplitudes.

2.3. Equipment

There were two main parts to the experimental set-up of this lab: the vibrating fluidized bed and the data acquisition system.

2.3.1. Vibrating Fluidized Bed

The laboratory fluidized bed used in this study, as seen in Figure 2.3, was made of Plexiglas.

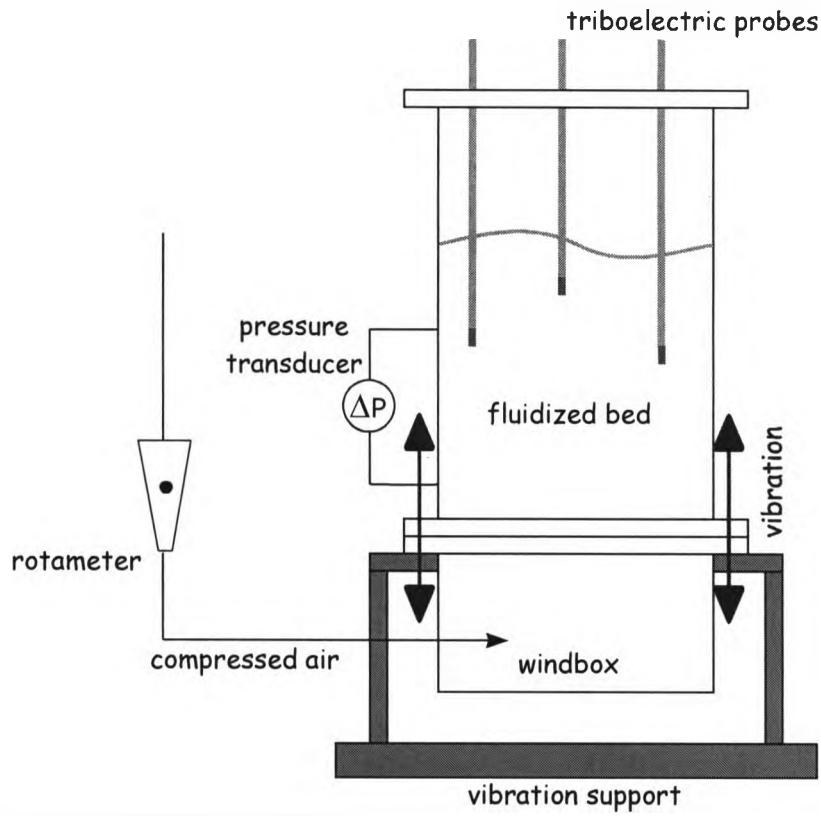

Figure 2.3 Vibrated Gas-Solid Fluidized Bed

The column itself was 11.3 cm in inner diameter and 27.4 cm in height. This column was separated from a 20.9 cm high windbox by a porous plate distributor. A lid was constructed for the column so that the triboelectric probes could be inserted into the bed from the top. The lid had 24, 0.95 cm diameter ports and one, 1.6 cm diameter port, at the locations shown in Figure 2.4.

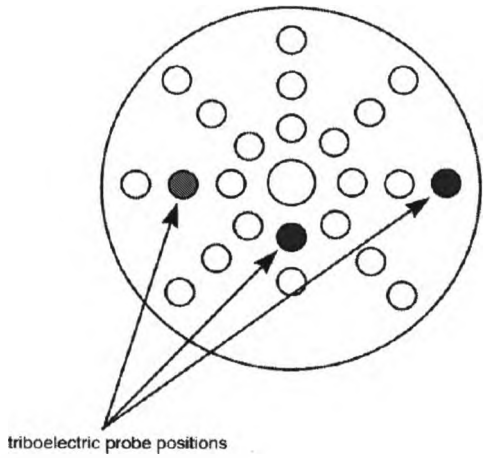

Figure 2.4 Positioning of the Triboelectric Probes

A measuring tape was attached to the outside of the column for use in the recording of visual height measurements. The tips of the three triboelectric probes were placed at 0.074, 0.096, and 0.134 m from the distributor, and at r/R = 0.35, 0.71 and 0.88, respectively. The remaining holes were covered with filter paper to minimize solids loss due to entrainment.

The vibrating base was connected to the apparatus at the flange connecting the column to the windbox. This the shaker produced a vibration that had a constant frequency of 60 Hz and a range of possible amplitudes. A calibration curve was produced by measuring the vibration amplitude with accelerometers.

Differential pressure drop measurements within the bed were taken using a PX-163 pressure transducer from Omega. The ports for this pressure transducer were located at 0.07 m and 0.12 m above the grid. A 60 mesh size screen was attached to the entering ports in order to prevent the flow of solids into the pressure transducer.

2.3.2. Triboelectric Probes

Triboelectric probes produce a very small current that must be amplified. As the flux of electrons is going from particles to the probes or from the probes to particles, the current ranges from negative to positive. The triboelectric probes consisted of stainless steel rods coated with an insulating polymer. The probes were approximately 0.28 m long and 0.003 m in diameter with 0.01 m at each end uncoated for electrical contact. The current from the probes was transferred to a grounded amplification box before output to a NI 6034E series multifunction data acquisition card from National Instruments and sampled at 900 Hz. Once the data was acquired on a computer, time series signal analysis was performed. By examining the way the signal fluctuates over time important information may be obtained [6].

2.3.3. Powders

The powders tested in this experiment were ceramic microspheres [G-850] and FCC Catalyst. The FCC Catalyst was an A-type powder as classified by Geldart [2] while the G-850 was at the A-C boundary between A and C types [2]. The G-850 was mildly cohesive and became very cohesive with low concentrations of water [2]. The physical properties of these particles are summarized in Table 2.2.

Figure 2.5 shows scanning electron micrograph of the two powders. The G-850 powder consisted of non-porus particles and were analogous to glass beads. It had a relatively wide size distribution with fines as small as 5 μm and particles as large as 260 μm. Water distributed on the surface of the particles making them cohesive enough to form

large agglomerates. The FCC were porous particles with a size distribution between 30 μm and 250 μm.

Table 2.1 Physical Properties of Tested Powders

Powder	**Sauter-mean diameter (μm)**	**Particle Density (kg/m^3)**	**Source of Powder**
Ceramic Microspheres [G-850]	33	2200	3M Canada
FCC Catalyst	83	1400	GRACE Davidson

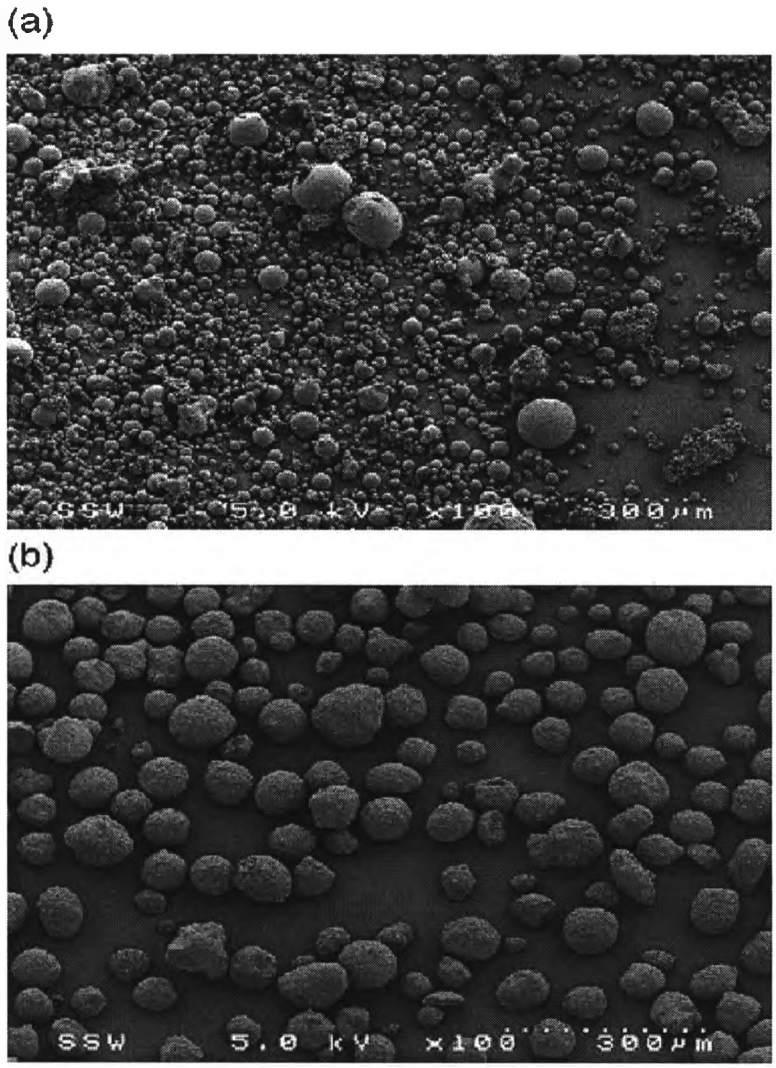

Figure 2.5 (a) Scanning Electron Micrograph of G-850 Ceramic Microspheres (b) Scanning Electron Micrograph of FCC Catalyst

2.4. Experimental Procedures

2.4.1. Minimum Bubbling Experiments

Four vibration amplitudes were tested: 0 mm, 0.01 mm, 0.05 mm and 0.14 mm. At a frequency of 60 Hz these amplitudes correspond to vibration intensities of K=0, 0.145, 0.724 and 2.03 by the relation given in Equation 2.2.

$$K = \frac{A\omega^2}{g} \qquad (2.2)$$

For each vibration amplitude, starting at a very well fluidized state, measurements were made at a various decreasing gas velocities. Each condition was given 5 minutes to reach equilibrium before the 30 second measurements were recorded. The bed height was also visually recorded. These measurements confirmed results reported by Ruzich [6].

2.4.2. Solids Drying Experiments

Drying was studied only with the G-850 microspheres. A portion of the powder was removed from the bed, wetted with distilled water in a low shear mixer, re-introduced into the column, and the bed was fluidized. The overall moisture content of the bed at the beginning of drying was 100 ppm by mass. The triboelectric signals were continuously recorded over at a sampling frequency of 900 Hz over a 2 hour period. These experiments were performed at two gas velocities of 0.008 m/s and 0.01 m/s, at vibration amplitudes of 0 mm and 0.14 mm.

2.5. *Results*

2.5.1. Bed Height

The bed height was visually determined for all of the experiments. Bed height was then plotted against superficial gas velocity to determine the minimum bubbling velocity. In the absence of vibration, the minimum bubbling velocity or U_{mb}, corresponded to the maximum bed height. Above U_{mb}, the bed height decreased as a large fraction of the gas previously flowing between particles went to form bubbles. However, as seen in Figure 2.6, with vibration the bed height reached a maximum but did not decrease at higher superficial gas velocities. Similar results were found with FCC and the ceramic microspheres.

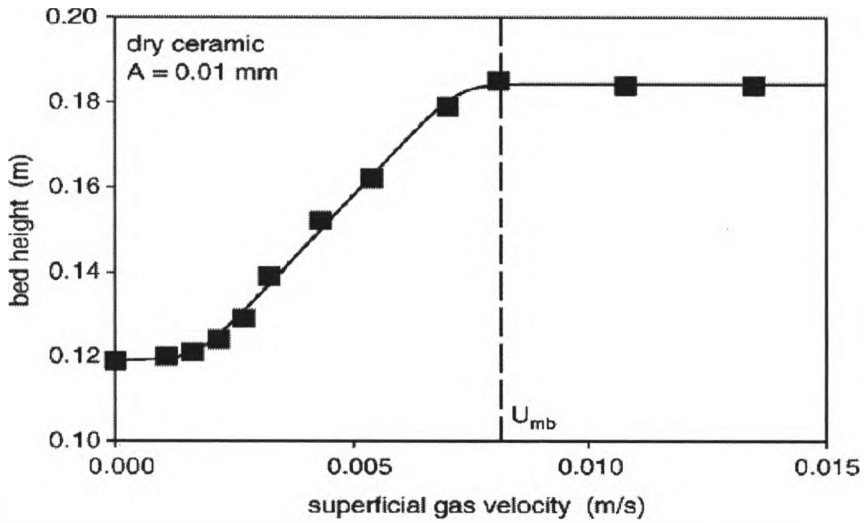

Figure 2.6 Bed Height vs Gas Velocity for G-850 with Vibration Amplitude = 0.01 mm

2.5.2. Pressure Gradients

A notch frequency filter was used to remove 60 Hz noise from the pressure signals before any signal analysis was performed. Time-averaged pressure gradient profiles at constant vibration level allowed the minimum fluidization and bubbling velocities to be estimated.

For a typical fluidization, the minimum bubbling velocity corresponds to a minimum pressure gradient after the maximum gradient characterizing minimum fluidization. As seen in Figure 2.7, a maximum occurred at minimum fluidization, but the minimum bubbling velocity corresponded to the start of a constant pressure gradient rather than a local minimum. This profile was observed both with and without vibration and was thus a characteristic of the powders used and not a result of the vibration. Clear detection of the minimum bubbling velocity therefore required very accurate pressure gradient measurements, which would be difficult to achieve under industrial conditions. There was also a large correlation between the magnitude of the pressure gradient and the vibration amplitude. As the vibration amplitude increased, the pressure gradient at U_{mf} increased, changing from just above 7500 Pa/m with no vibration to just above 10000 Pa/m at a vibration amplitude of 0.14 mm. This was due to the fact that as the bed reached U_{mf}, the vibration compacted the defluidizing bed, making the fixed bed have a larger pressure drop. The pressure gradient at U_{mb}, however, remained relatively constant at around 6750 Pa/m, with the exception of the ceramic microspheres [G-850] at a vibration amplitude of 0.14 mm where U_{mb} occurred at a pressure gradient of 7500 Pa/m.

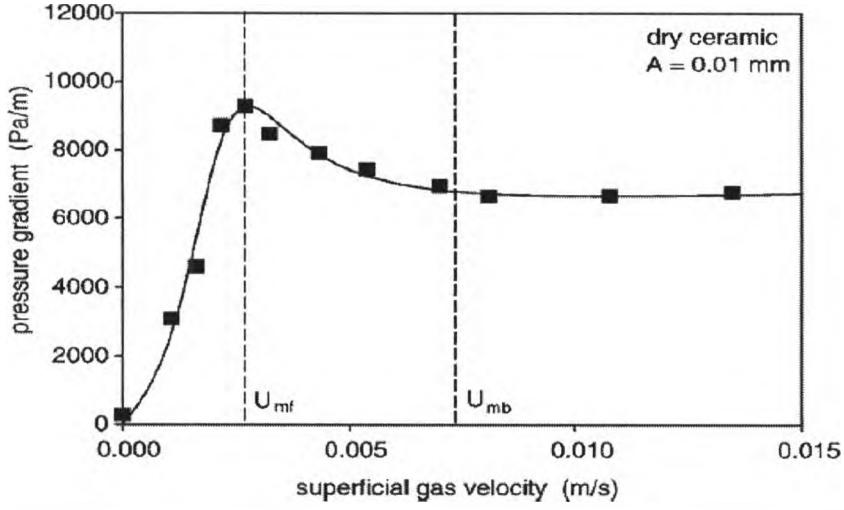

Figure 2.7 Pressure Gradient vs Gas Vvelocity for G-850 and Vibration Amplitude = 0.01 mm

2.5.3. Minimum Fluidization Velocity

The minimum fluidization velocities for different vibration levels were determined from the bed height and bed pressure gradients. The two curves are offset as the particles tested had different properties (size, shape, density, etc). The effects of vibration are shown in Figure 2.8. As the vibrational amplitude was increased the required gas velocity for fluidization initially decreased. Beyond a critical amplitude of approximately 0.08mm, there appeared to be little effect of vibration amplitude on the minimum fluidization velocity. This pattern appears to continue beyond an amplitude of 0.15 mm, but would need to be confirmed by additional measurements at much larger vibration amplitudes.

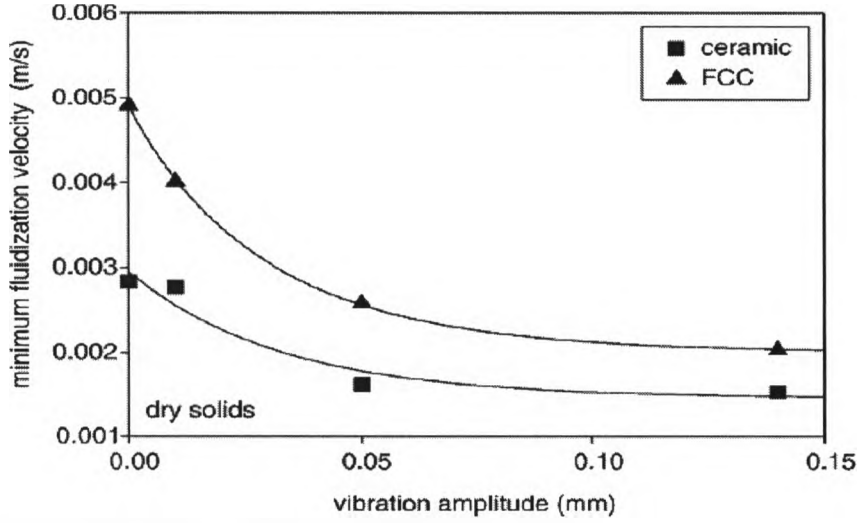

Figure 2.8 Effect of Vibration on Minimum Fluidization Velocity

2.5.4. Minimum Bubbling Velocity

The minimum bubbling velocity showed a similar trend to that of the minimum fluidization velocity. As the vibrational amplitude increased the minimum bubbling

velocity decreased, as shown by Figure 2.9. However, over the amplitudes tested, there did not appear to be an amplitude above which there was no further effect on the minimum bubbling velocity. Once again the two curves were offset due to the differences in particle properties.

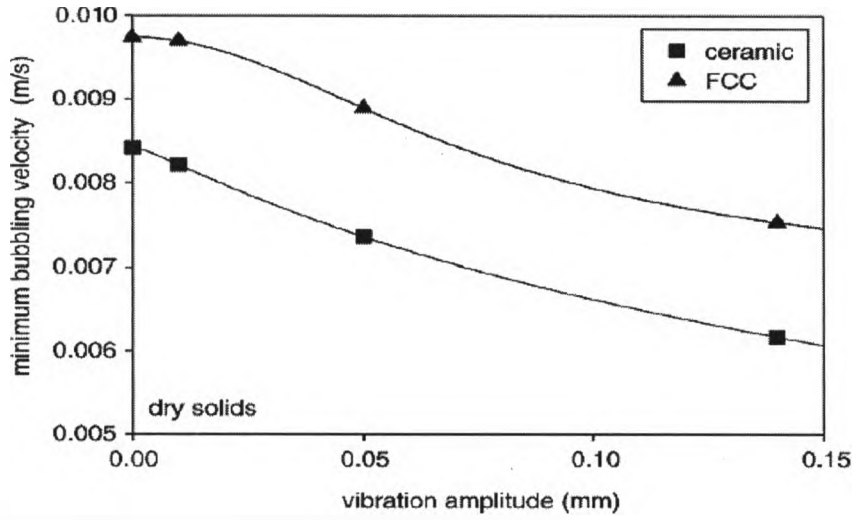

Figure 2.9 Effect of Vibration on Minimum Bubbling Velocity

2.5.5. Triboelectric Current

Figure 2.10 shows raw triboelectric signals normalized to have a mean of zero. Bubbles could not be detected unprocessed from looking at the raw signals of the triboelectric probes. Signal analysis was therefore required to extract information from the measurements.

Figure 2.11 shows the variation the Hölder exponent of the signals with the gas velocity. The Hölder exponent decreased sharply with the appearance of bubbles beyond U_{mb}. As the fluidization quality improved, the appearance of bubbles cause more chaotic

movement of the particles striking the triboelectric probes. This resulted in a rougher signal and a lower Hölder exponent.

Power spectra analysis was also performed to further characterize bubbling behavior. Figure 2.12 shows a section of the power spectra of the triboelectric probe signals at x = 0.096 m in the bed of ceramic powder. Although there were several portions of the power spectral density that changed with the fluidization quality, there was a consistent difference in the spectra power below and above U_{mb} at a frequency of 175 Hz.

A bubbling index was developed to characterize bubbling behaviour. Its value is 1 below U_{mb} and 2 above U_{mb}. This index could also be predicted from a linear combination of the time average, the power of the frequency at 175 Hz and the 3rd order Hölder exponent of the triboelectric probe signals. Figure 2.13 shows the predicted bubbling index for G-850 ceramic microspheres at various vibration levels. This index corresponds perfectly to the index determined from the bed height and visual observations of bubbling.

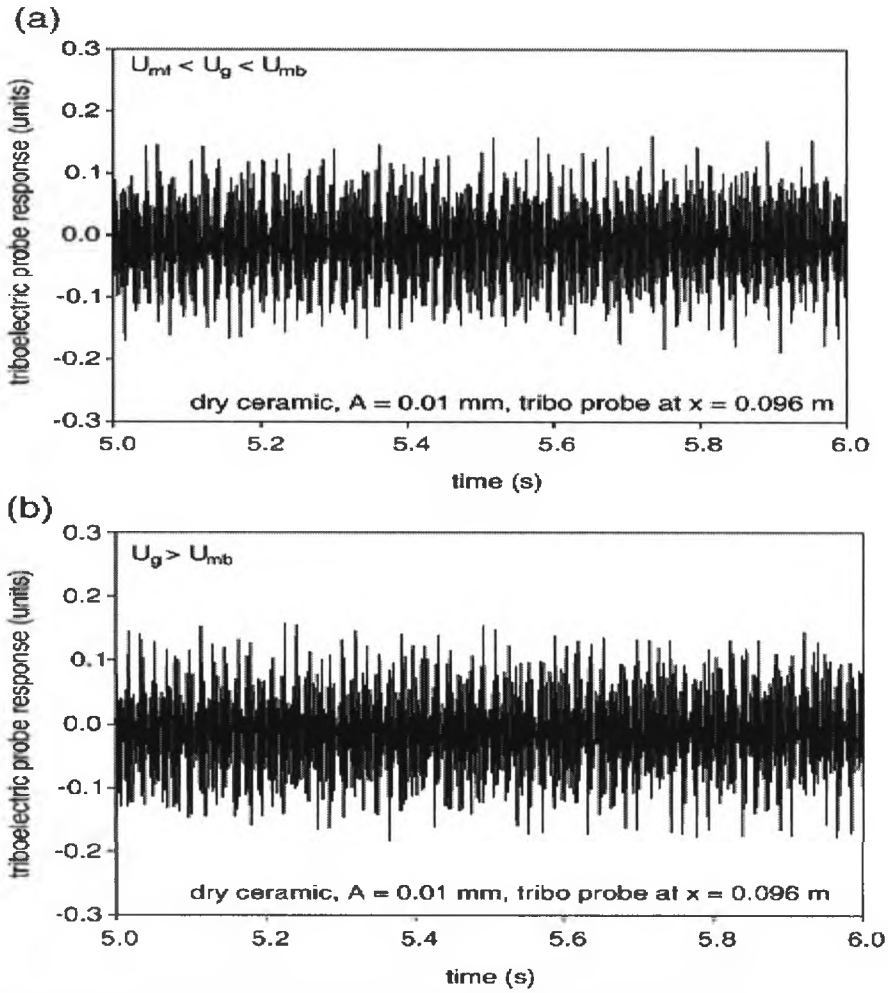

Figure 2.10 Raw Triboelectric Probe Signals at (a) $U_{mf}<U_g<U_{mb}$ and (b) $U_g>U_{mb}$

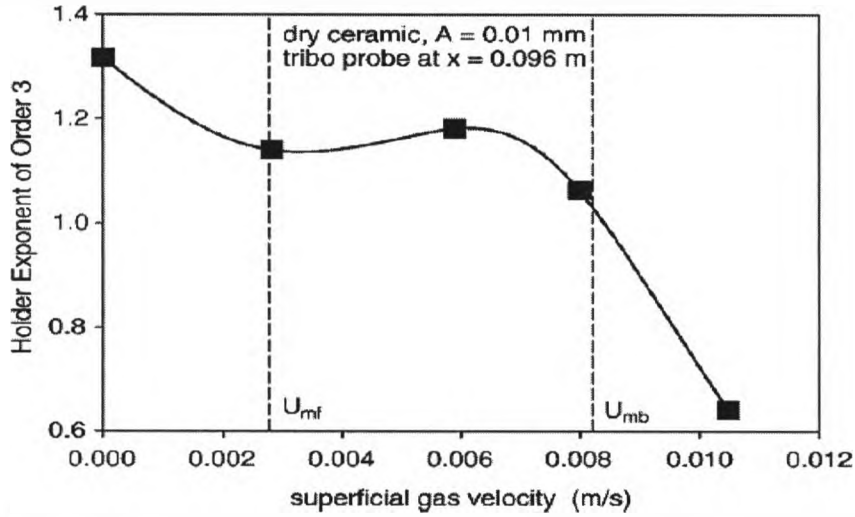

Figure 2.11 Hölder Exponent of the Triboelectric Signal as a Function of the Gas Velocity

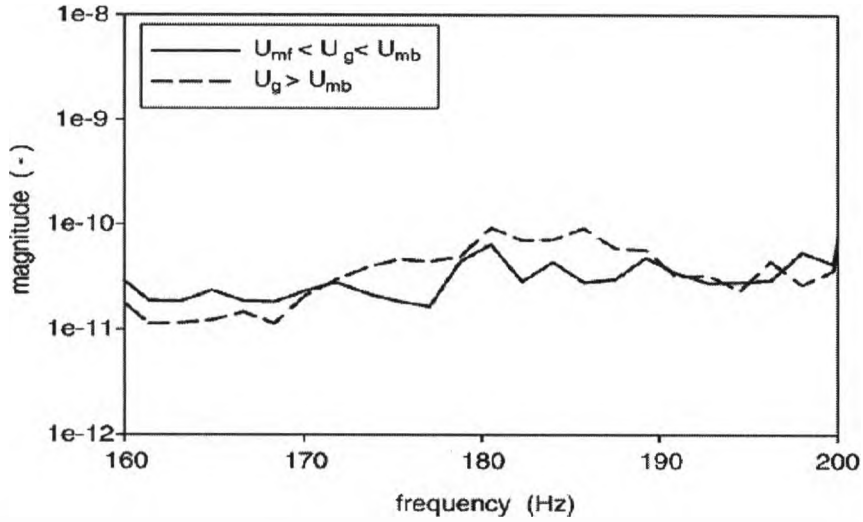

Figure 2.12 Power Spectrum Density of the Triboelectric Signal Above and Below U_{mb}

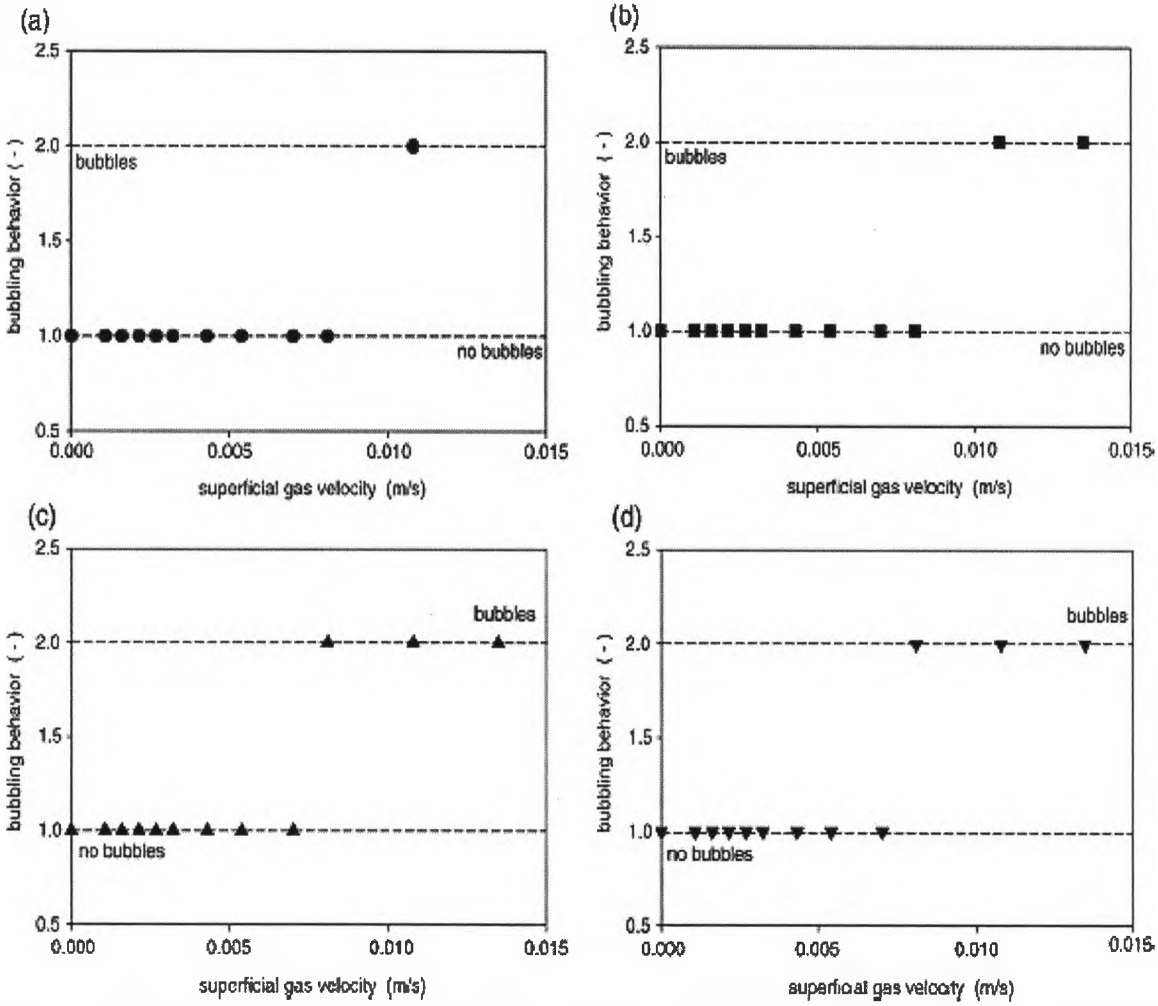

Figure 2.13 Minimum Bubbling Velocities using Bubbling Index for G-850 at Vibrational Amplitudes of (a) A=0.00mm (b) A=0.01mm (c) A=0.05mm (d) A=0.14mm, and using the Triboelectric Probe at x=0.096m

Figure 2.14 shows the moving average of the triboelectric currents calculated over 1 second intervals re-scaled between 0 and 1. This was done to compare for ease of comparing the signals on the same y-axis. The superficial gas velocity was 0.008 m/s. At this gas velocity the bed was below U_{mb} unless it was vibrated with an amplitude of at least 0.05 mm. When the bed was thus vibrated at this gas velocity, the moisture was distributed very quickly and the drying progressed fairly smoothly until an end point. Without vibration, the bed was not bubbling and required a much longer time for the moisture to be distributed and detected by the probes. Once distributed, moreover, most of the moisture was then contained within agglomerates that did not easily break up and thus the bed remained wet for a very long period of time, far beyond what was measured with vibration.

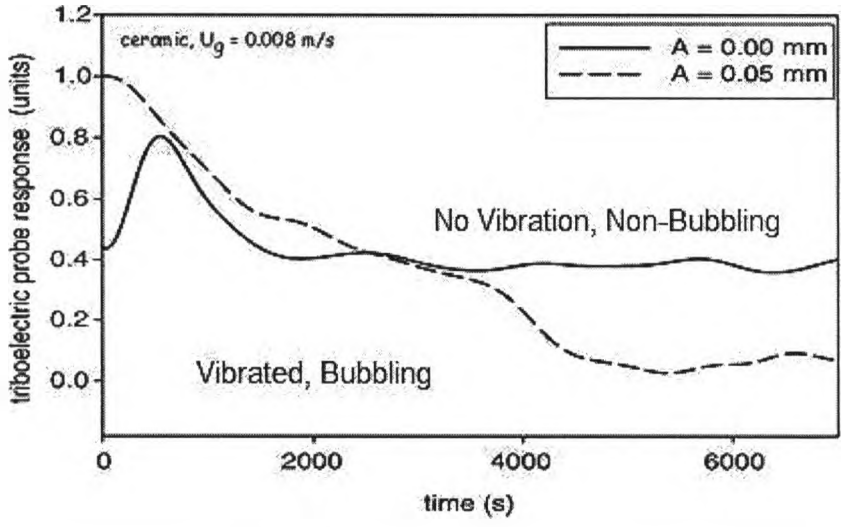

Figure 2.14 Drying Curves for Ceramic Powder [G-850] at Superficial Gas Velocity of 0.008m/s

Figure 2.15 shows the time-average of the triboelectric currents measured over 1 second intervals with a superficial gas velocity of 0.010 m/s. It shows the effect of vibration on drying in a gas-solid fluidized bed operating at a gas velocity above the minimum bubbling velocity, even without vibration. Both with and without vibration, the bed is

well mixed with the moisture distributed quickly over the entire bed of particles. Once again, with vibration, it is seen that drying occurred fairly smoothly and reached an end point. Without vibration, agglomerates were slowly broken up, as shown by the spikes in the signal, and drying was much slower.

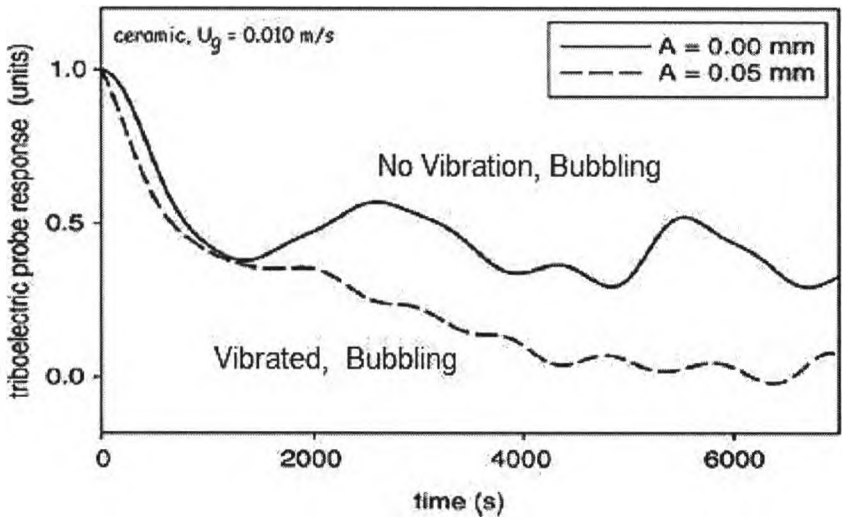

Figure 2.15 Drying Curves for Ceramic Powder [G-850] at Superficial Gas Velocity of 0.01m/s

2.6. Conclusions

It was found that minimum bubbling velocity and minimum fluidization velocity decreased with increasing vibration amplitude. A critical vibrational amplitude was observed such that with higher amplitudes minimum fluidization velocity is not affected. A bubbling index was developed to detect bubbles using triboelectric probes. Triboelectric probes were also used to monitor drying and determine the effect of vibration on drying. Vibration greatly accelerates the drying of fine powders by breaking up wet agglomerates.

2.7. Acknowledgements

The authors would like to acknowledge NSERC for the initial funding that purchased this equipment. Additional thanks to Derek Daniher for his help setting up the equipment.

2.8. Symbols

A	Vibrational amplitude (mm)
A_c	Critical vibrational amplitude (mm)
C	Coefficient in the definition of Hölder exponent (−)
f	Frequency (Hz)
g	Acceleration due to gravity = 9.81 m/s^2
h	Hölder exponent, (−)
K	Vibration intensity, (−)
n	Degree of polynomial P, (−)
P	Polynomial of the nth degree, (−)
r	Radial placement of triboelectric probes, (m)
R	Radius of column, (m)
s	Independent variable of P, (−), s
U_g	Superficial gas velocity ,(m/s)
U_{mb}	Minimum bubbling velocity, (m/s)
U_{mf}	Minimum fluidization velocity, (m/s)
X	Function, (units)
x	Axial distance from distributor plate, (m)
z	Height, (m)
z_{max}	Maximum bed height, (m)

Greek Symbols

ω	Angular frequency = 2πf rad/s

2.9. References

[1] Avidan, A., King, D., Knowlton, T., Pell, M. Fluidization. *In: Kirk-Othmer Encyclopedia of Chemical Technology.* 11(2000) 791-825.

[2] Geldart, D. Types of gas fluidization. *Powder Technology.* 7 (1973) 285-92.

[3] Marring, E., Hoffmann, A., Janssen, L. The effect of vibration on the fluidization behaviour of some cohesive powders. *Powder Technology.* 79 (1994)1-10.

[4] Mawatari, Y., Tatemoto, Y., Noda, K. Prediction of minimum fluidization velocity for vibrated fluidized bed. *Powder Technology.* 131 (2003) 66-70.

[5] Noda, K., Mawatari, Y., Uchida, S. Flow patterns of fine particles in a vibrated fluidized bed under atmospheric or reduced pressure. *Powder Technology.* 99 (1998) 11-4.

[6] Ruzich N. (2004) The effect of vibration on gas-solid fluidization. MESc Thesis, University of Western Ontario.

[7] Valverde, J., Castellanos, A., Quintanilla, M. Effect of vibration on the stability of a gas-fluidized bed of fine powder. In: *Physical Review E: Statistical Physics, Plasmas, Fluids, and Related Interdisciplinary Topics.* 64 (2001) 21302.

[8] Guardiola, J., Rojo, V., Ramos, G. Influence of particle size, fluidization velocity and relative humidity on fluidized bed electrostatics. *Journal of Electrostatics.* 37 (1996) 1-20.

[9] Briens, C., Briens, L., Barthel, E., LeBlévec, J., Tedoldi, A., Margaritis, A. Detection of local fluidization characteristics using the V statistic. *Powder Technology.* 102 (1999) 95-103.

[10] Portoghese, F., Berruti, F., Briens, C., Continuous on-line measurement of solid moisture content during fluidized bed drying using triboelectric probes. *Powder Technology.* 181 (2008)169-177.

[11] Briens, L., Briens, C. Cycle detection and characterization in chemical engineering. *American Institute of Chemical Engineers Journal.* 48 (2002) 970-80.

[12] Briens, C., McDougall, S., Chan, E. On-line detection of bed fluidity in a fluidized bed coker. *Powder Technology.* 138 (2003) 160-8.

[13] Hulet, C., Briens, C., Berruti, F., Chan, E., Ariyapadi, S. Entrainment and stability of a horizontal gas-liquid jet in a fluidized bed. *International Journal of Chemical Reactor Engineering.* 1 (2003) A60.

[14] Park, K., Willinger, W. [Ed] Self-Similar Network Traffic and Performance Evaluation. *New York. Wiley-Interscience.* (2000)

[15] Riedi, R. Multifractal processes. In: Doukhan P, Oppenheim G, and Taqqu M [Ed.] *Theory and Applications of long range dependence*. Springer, (2003) 625-716.

Chapter 3. On-line detection of bed fluidity in gas-solid fluidized beds with liquid injection by passive acoustic and vibrometric methods

Garret Book, Katherine Albion, Lauren Briens, Cedric Briens, Franco Berruti

3.1. Introduction

Gas-solid fluidized beds are used extensively in many industrial processes for both chemical and physical operations. In some processes, liquid is sprayed directly into the fluidized bed where it can dry as in fluidized bed dryers, evaporate as in gas-phase polymerization or react as in fluid cokers [1, 2].

In 2008, synthetic crude produced by Syncrude Canada from the Alberta oil sands represented about 15% of Canada's oil production. Syncrude Canada upgrades bitumen extracted from the oil sands with fluid cokers, where the heavy feed stock is sprayed onto hot coke particles to undergo thermal cracking, yielding lighter hydrocarbons and solid coke. Coke particles are continuously recirculated to a burner where some of the coke is burned to reheat the rest of the particles. Any excess coke is removed from the system [3].

The presence of liquid has generally an adverse effect on the quality of fluidization as it coats the surface of particles making them cohesive; however, there are strong incentives to operate at high liquid loading, especially in fluid coking processes [2]. Operation of fluid cokers at lower temperatures increases yield of desirable condensable products and

reduces sulphur oxide emissions but increases bed wetness [2, 3]. This increase in bed wetness or liquid loading may lead to local poor mixing zones, local defluidization, an increase of fouling of walls and stripper sheds and a general reduction in fluidization quality, all of which reduces the reactor performance, stability and run length [2, 3]. When the bed becomes less fluid, heat and mass transfer are hindered and, if the problem is not corrected, a catastrophic loss of fluidization can even occur, referred to as "bogging" [3].

Monitoring of fluidization quality is a difficult operating challenge for many processes where liquid is injected into the bed, including fluid coking [2]. Ideally, a monitoring system should be able to be applied to a wide range of operating conditions, have low cost, be reliable and be non-intrusive. Passive acoustic and vibrometric methods have the potential to meet all these requirements [4].

The general objective of this study was, therefore, to apply passive acoustic and vibrometric methods to monitor the bed fluidity of a large gas-solid fluidized bed after liquid injection has occurred. Advanced signal analysis was performed on acoustic and vibration signals and compared with physical tests performed on samples from the bed.

3.2. Literature Review

There have been several direct measurement methods developed where the 'apparent viscosity' of a fluidized bed is physically measured. Since viscosity is typically measured by recording the time it takes a liquid to flow through an orifice. As this is impossible

with the emulsion phase of a fluidized bed, the time it takes for a weight to move through the bed is measured giving the 'apparent viscosity'. As well, however, there are essentially two types of studies that have been attempted to characterize the fluidity of a fluidized bed through indirect signal analysis methods [3, 5]: studies focused on local fluidity, and studies concentrated on global fluidization. In a recent review update, Rees et al. [6] found that the principal measurement techniques for measuring bed viscosity have not advanced greatly since they were reviewed in 1971 by Schügerl [7]. These measurements, however, can be useful as the apparent viscosity and fluidization quality of a fluidized bed are related [8].

3.2.1. Apparent Viscosity Measurements

The apparent viscosity of a fluidized bed has been measured with paddles, rotating spheres, a falling ball or Couette-type viscometers [8]. Typically viscosity of a liquid is measured by the time it takes for it to flow through an orifice. Since the emulsion phase of a fluidized bed cannot be removed for this type of test, the time for a weight to pass through the bed is measured. These results have wide variations that are partly due to the difficulties in estimating the viscosity of a fluidized system where the peripheral velocities of submerged objects are equal in magnitude to particle velocities in the undisturbed bed [9].

When using the falling ball method, the viscosity measurements are affected not only by the apparent viscosity, but also by solids circulation patterns and fluctuations due to the passage of bubbles [9, 10]. Moreover, the inertial effects of each fluctuation tend to cause non-homogeneous density throughout the bed. As well, with uneven gas

distribution, it is probable that there is some modification in the theoretical laws governing particle interaction forces [11]. An additional reason this technique is disputed is that local defluidization zones may form over the top surface of the falling sphere. An important property of the sphere is that it must be small enough to avoid significant wall effects [9, 10].

Rees et al. [6] stated that apparent viscosity measurements must be made when there are no bubbles in the fluidized bed to avoid some of these problems, but the low gas velocity required for these conditions can result in a non-homogenous fluidization. Grace [9] used X-ray photography to observe the bubble shapes in the fluidized bed and then compared them to bubble shapes in viscous liquid to infer the apparent bed viscosity. This allowed for the apparent viscosity to be measured at any superficial gas velocity above the minimum fluidization velocity.

Another method that has been used extensively is the de-aeration method for the characterization of emulsion phase properties in gas-solids fluidization [12]. The de-aeration procedure involves defluidizing the bed while measuring the pressure drop as the gas exits. The findings of Lorences et al. [13] indicated that, in bubbling beds, the de-aeration rates are independent of the initial fluidization velocities. This means that the bubbles tend to escape very quickly and that the emulsion phase properties are independent of the bubble flow [5].

Direct measurements of a fluidized bed apparent viscosity are useful for laboratory experiments, but it would certainly be impossible to implement these methods in industrial cokers.

3.2.2. Local fluidity measurements

In gas-solid fluidized beds, local zones of defluidization will generally occur first near the gas distributor. Defluidized zones can form when the gas distribution is uneven because of faulty distributor design or plugging. Local defluidization may also occur due to segregation of larger particles in the distributor zone, if local conditions, such as sintering and caking, make the particles more difficult to fluidize, or if agglomerates that have formed elsewhere in the bed settle near the distributor [3].

Autocorrelation of local capacitance measurements was used by Yutani et al. [14] to detect defluidized zones between adjacent gas jets in the grid zone of a fluidized bed of sand. The difficulty in using capacitance probes in industry is that these probes require large electrical potentials, are sensitive to electrical noise, and may be too fragile for many processes [3]. In fluid cokers, the probes would quickly be fouled by coke deposits.

Measurements of heat transfer can also be used for the detection of defluidized zones. Ropchan [15] used a self heating thermistor and found that defluidized zones could be detected by analyzing the fluctuations in the measured heat transfer coefficient. Karamavruç et al. [16] used the Hurst exponent of temperature fluctuations to detect defluidized zones around a horizontal heat transfer tube. In many applications, heat

transfer measurements are not a suitable method for detection of defluidized zones. In fluidized beds of polymer particles, thermistors and other heat transfer probes form hot spots that may result in sintering and themselves promote the formation of defluidized zones [3]. In fluid cokers, heat transfer surfaces would quickly be fouled by coke deposits.

Triboelectric current generated at electrodes in the distributor zone of gas-solid fluidized beds have been shown to reliably and rapidly detect defluidized zones [3]. Currents that are generated by the potential difference developed by the charging of particles due to friction between two materials are termed "triboelectric" [17]. The accurate detection of defluidized zones using triboelectric current measurement required the V-statistic signal analysis technique [18, 19]. However, in fluid cokers, the electrodes would quickly be fouled by coke deposits.

3.2.3. Global Fluidity Measurements

In order to monitor the global fluidity of a fluidized bed, the measured property must be affected by small changes that can happen anywhere in the bed, not just at the sensor location. For this reason, several investigators have studied pressure signal fluctuations to characterize the quality of the fluidization with a variety of analytical methods. Industrial installations often have small fluctuations in gas velocity, making it desirable to have a method insensitive to velocity but sensitive to even small changes in particle properties [5].

Tardos et al. [20] and McLaughlin et al. [21] investigated destabilization or defluidization of fluidized beds due to agglomeration with the time averaged pressure drop. This method, however, was unable to provide early warning of poor bed fluidity. By applying chaos analysis to bed pressure drop fluctuations, several investigators were able to detect small changes in the particle size distribution [22, 23]. Van Ommen et al. [24] used an enhanced attractor comparison method on pressure fluctuation measurements for an early warning of agglomerate formation in fluidized beds. Briens et al. [3] used a new analytical tool called W-statistic on dynamic pressure signals to determine bed fluidity in a 1 m diameter pilot coker and found very good agreement with traditional coke sampling methods. Chaplin et al. [25] found that the moisture content could be monitored in a fluidized bed dryer of pharmaceutical granules by applying the S-statistic to dynamic pressure signals since the moisture content was related to different hydrodynamic states in the fluidized bed. Benoni et al. [26] used a method that determined particle agglomeration in a fluidized bed by monitoring the entrainment of fine particles which is significantly easier than the dynamic pressure measurements and chaos analysis.

Recently, there have been studies in the innovative field of non-intrusive passive acoustic monitoring as an alternative to direct pressure measurements. Tsujimoto et al. [27] used an ultra high frequency acoustic emission sensor to detect the start of unstable fluidization leading to defluidization due to increases of moisture content. Two major difficulties with this technique were its limitations when the bed humidity was too high, inducing channeling and attenuating the acoustic signal, and the large digital processing power required to manage signals at 140 kHz. On the other end, Briongos et al. [28]

focused on extremely low frequency noise between 0 – 20 Hz, which greatly improved the ease of data processing. This frequency corresponded to the bubbling properties of the bed and thus conclusions were made about the fluidization regime. Both these studies considered background noise in selecting the sampling frequency; however, through proper sensor selection and advanced signal filtering, detailed information about the process can be obtained from acoustic emissions in the audible range (20 Hz – 20 kHz). Experienced operators can often just listen to a fluidized bed and use this information in taking corrective action, for example, loud thudding can indicate sloshing due to gas misdistribution due to large agglomerates on the gas-distributor. The current study focuses on the audible range of frequencies to quantify this ability and link it to physically measured attributes of the bed.

3.3. Experimental Equipment

All experiments were performed using a large fluidized bed that is shown schematically in Figures 3.1 and 3.2. The bed was 5.6 m high and trapezoidally shaped with a 0.2 m wide short end and a 1.2 m wide long end. The bed was fluidized with air, where properties were kept constant at approximately 22 °C and 15 % relative humidity. The air entered through a windbox at the bottom of the column and then into the bed through a perforated plate distributor. Any entrained solids were returned to the bed through a system of internal cyclones.

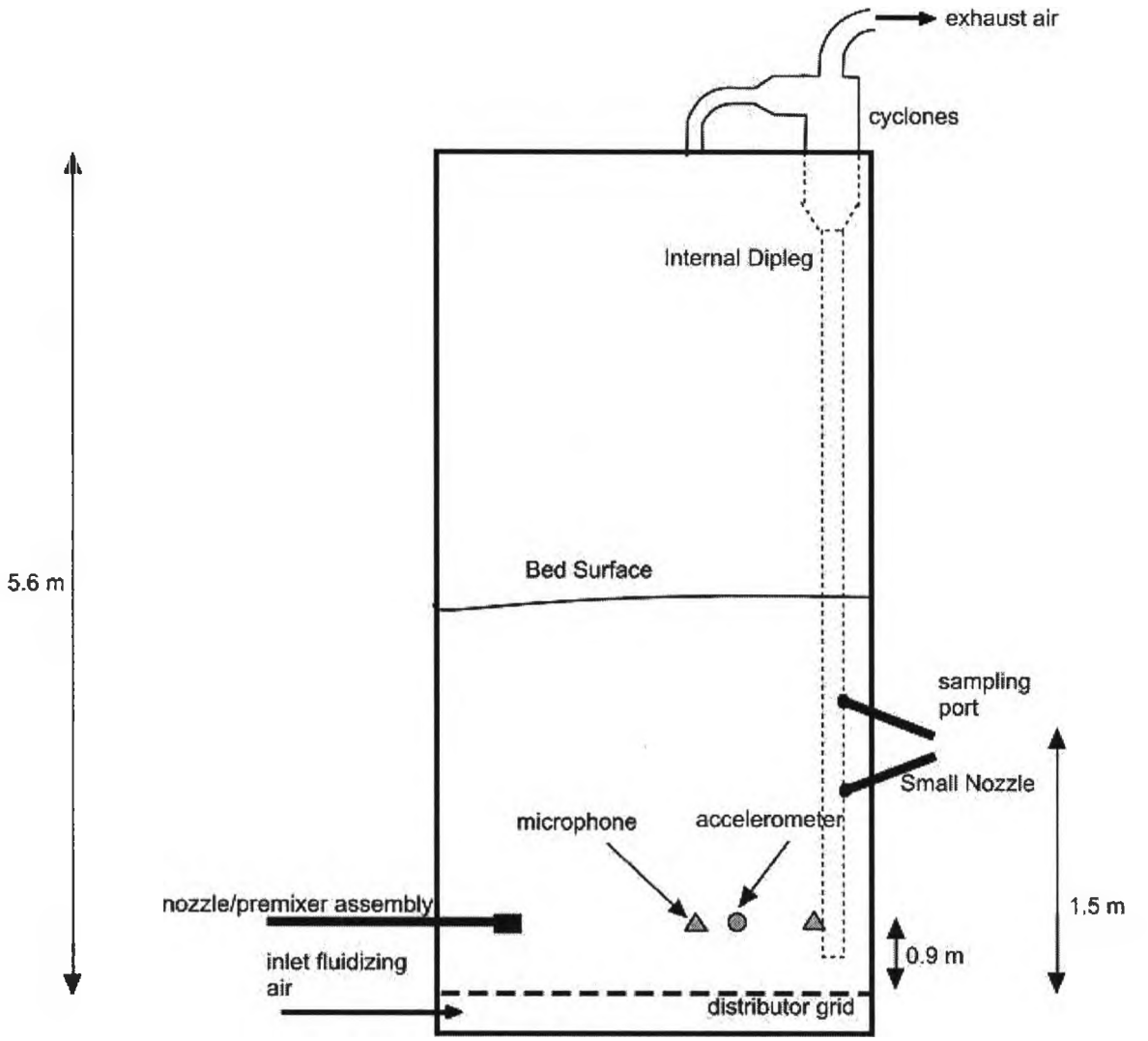

Figure 3.1 Schematic diagram of the fluidized bed, side view

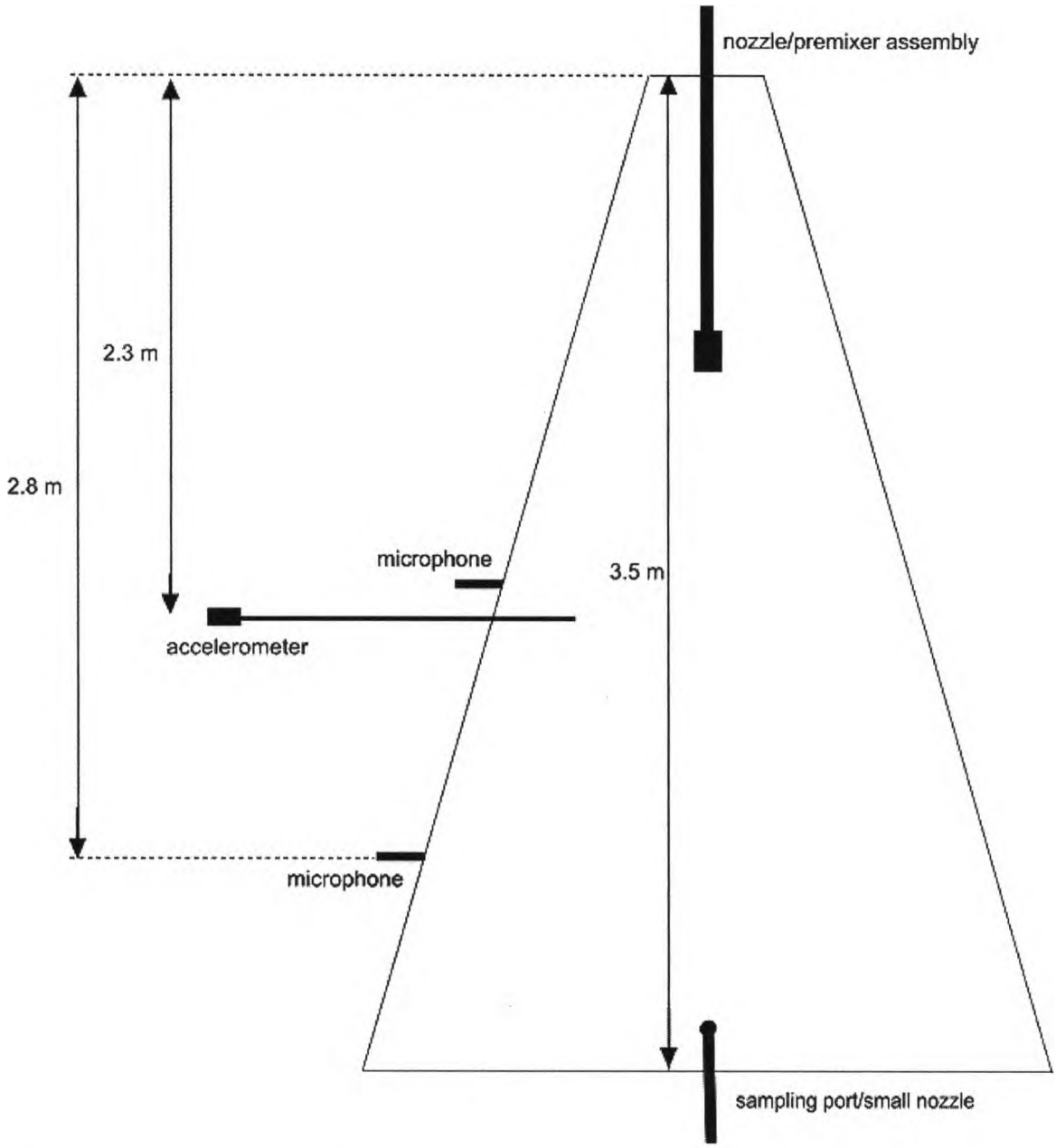

Figure 3.2 Schematic diagram of the cross section of the fluidized bed, top view

A series of large nozzle and premixer assemblies with differing spray characteristics were inserted 1 m into the bed and 0.9 m above the distributor grid, at the short end of the bed. There were two basic types of gas-liquid pre-mixers where the atomization gas was mixed the pressurized water before flowing down a conduit to the nozzle. The bilateral flow conditioner (BFC) was the simplest pre-mixer. Pipes for the atomization air and

pressurized liquid entered a mixing chamber at an angle in the direction of flow. The two injection ports were located 90 ^{o} from each other along the circumference of the mixing chamber. At the end of the mixing chamber there was a contraction to reduce the diameter to the nozzle conduit diameter of 1 inch (0.0254 m).

The simple constriction nozzle constricted the flow of the liquid and atomization gas causing a two-phase jet to form into the open air or fluidized bed. The angles of decrease in this constriction as well as the final outlet diameter are design parameters of this nozzle. For the TEB nozzle, as the two phase flow enters the nozzle, it passes through a fast constriction followed by a slow expansion and finally through another constriction to form the two phase jet. The angles of these constrictions and expansions as well as their final diameters can be changed.

A small, shaped shroud could be screwed onto the end of the simple constriction nozzle in order to reshape the spray. The nozzle injected de-ionized water from a pressurized tank. Nitrogen was used as atomization gas. For selected experiments, a small nozzle set up was located 1.5 m above the grid on the wide side of the bed. The small nozzle set up was a TEB nozzle and BFC premixer roughly 1/25th the size of the industrial setup.

Two prepolarized microphones were mounted flush onto the side of the bed, 0.9 m above the distributor grid and 2.3 and 2.8 m from the short end of the bed.

A uni-directional accelerometer was mounted on the end of a 6.4 mm diameter, 0.35 m long steel rod. This rod was inserted 0.10 m into the bed at a location 0.9 m above the distributor grid and 2.3 m from the short end of the bed. This rod was of similar demensions as thermocouples currently used in coking units. In this way the rod simulated a thermocouple that would be inserted into a fluid bed coker and therefore a potential, easy to implement location for measurements on a commercial unit.

Silica sand was fluidized in the bed. The sand was Barco 71 supplied by Opta Minerals Inc. The sand had a Mohs hardness of 7, was resistant to grinding, was inert and maintained its initial properties throughout the experiments. The sand had a Sauter mean diameter of 150 μm and d_{p50} of 212 μm, a specific gravity of 2650 kg/m^3, and a bulk density of 1590 kg/m^3.

Figure 3.3 shows the particle size distribution of the sand, and Figure 3.4 shows a photograph of the sand obtained using a scanning electron micrograph. Nine tonnes of sand were added to the bed and the defluidized bed height was about 2 m above the distributor.

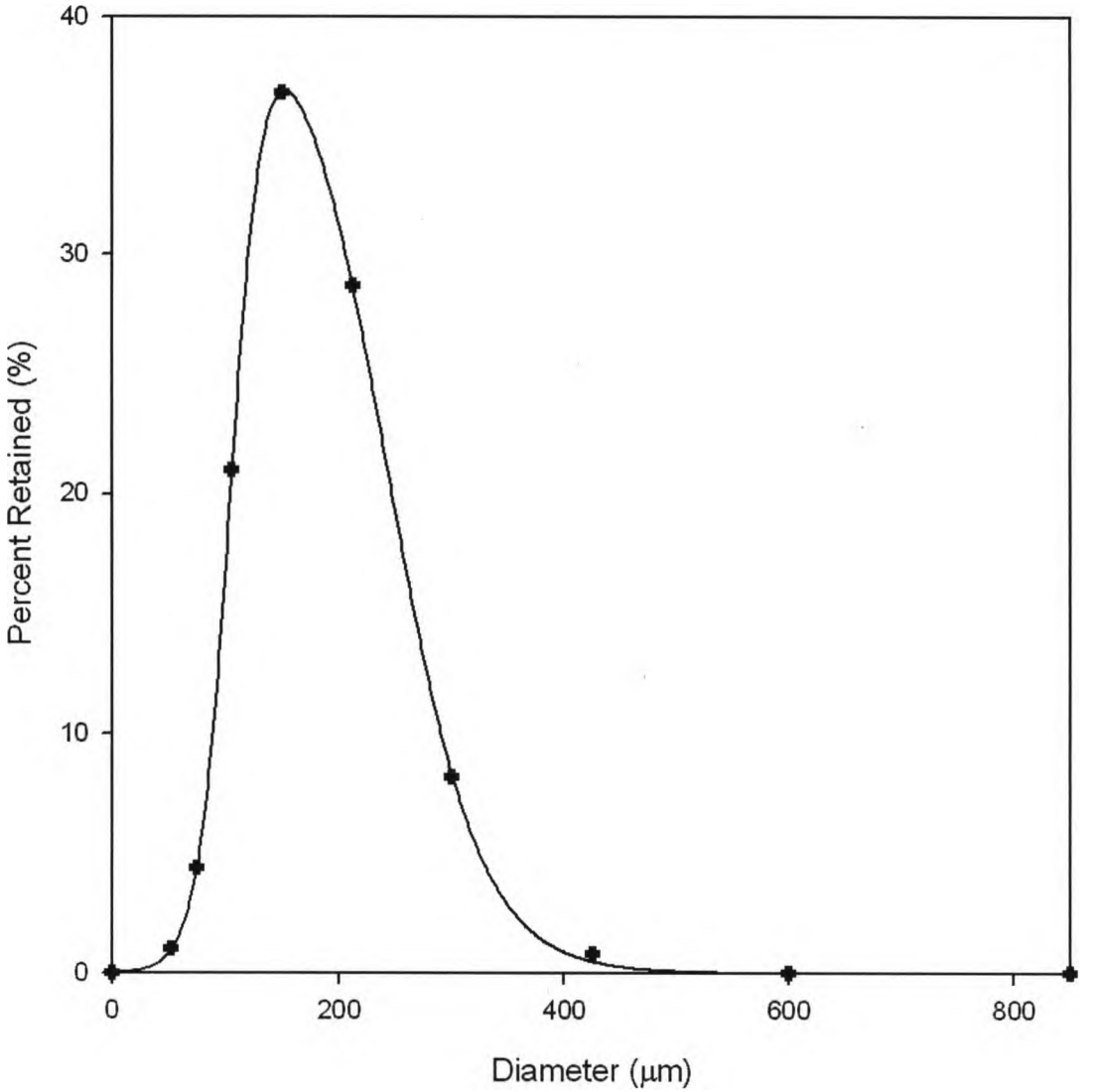

Figure 3.3 Particle size distribution of the silica sand

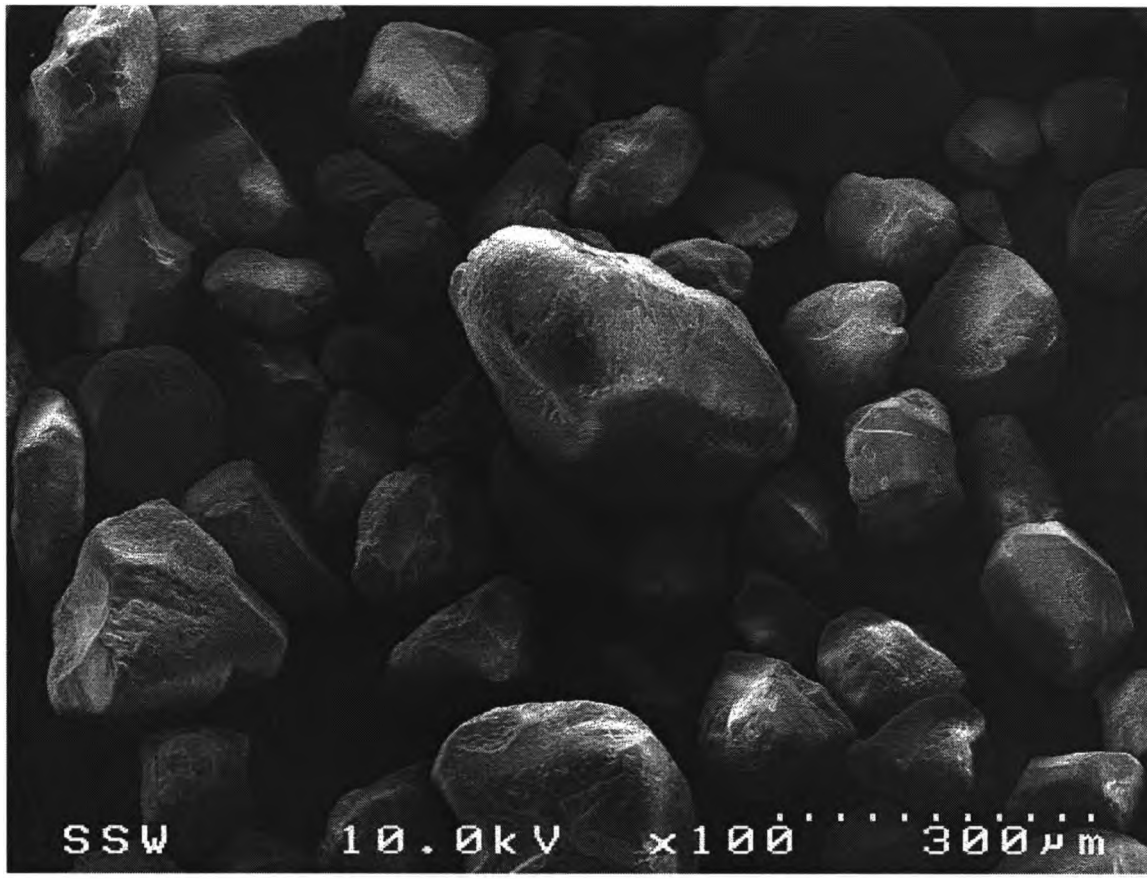

Figure 3.4 Scanning electron micrograph of the silica sand

The flowability of samples of sand withdrawn from the bed was measured using a Mercury Revolution Analyzer ®. The Revolution Analyzer rotated samples in a transparent drum at 0.3 RPM and used optical algorithms to characterize the sample surface as it was rotated. An avalanche was defined as a surface movement of 0.65% of the volume of the drum. The size and duration of each avalanche was measured as well as the angle of the sample surface relative to the horizontal. The measurements were summarized using a variety of statistics including the median avalanche time of 128 avalanches.

The moisture content of the sand was determined using a Mettler-Toledo Moisture Analyzer. The moisture content was determined through loss-on-drying measurements at 110 °C to make sure all the water was removed.

3.4. Experimental Procedure

The bed was initially fluidized at a superficial gas velocity of 0.15 m/s. Water was then injected into the bed using either a large nozzle and pre-mixer assembly or a small nozzle assembly. Immediately following an injection, the superficial gas velocity of the fluidizing air was reduced to 0.06 m/s for 40 s to allow the injected water to be mixed into the bed and for any very large wet agglomerates to settle on the gas distributor plate. The bed was then defluidized for 10 minutes. The bed was refluidized at superficial gas velocity of 0.12 m/s for 90 minutes to allow all the solids in the bed to thoroughly dry.

With the large nozzle and pre-mixer assembly, 21 liters of water were injected into the bed over 9.5 seconds. This injection flowrate was similar to flowrates used in commercial coking units. Trials using a wide range of nozzle and pre-mixer combinations allowed any effects of nozzles and pre-mixers to be studied.

With the small nozzle assembly, either 7 liters or 10.5 liters of water were injected over 100 s and 150 s respectively. This slower injection flowrate provided better distribution of the liquid injected into the bed with the formation of fewer very large agglomerates.

During the drying phase, acoustic and vibration data from the microphones and accelerometer were recorded at 40 kHz for 90 minutes. Also, samples of the sand in the bed of about 5 x 10^{-4} m^3 were removed from the bed using the sampling port (Figures 3.1 and 3.2). First, any solids in the port were purged from the port using compressed air, then the fresh fluidized solids were allowed to flow out into air tight sample containers. These samples were immediately analyzed for fluidity and moisture content using the Revolution Analyzer and Moisture Analyzer respectively.

3.4.1. Experiments

Table 3.1 shows the trials performed for this study. Trials were performed over a wide range of gas to liquid ratios (GLR %), different nozzle configurations, pre-mixer configurations and with an inert atomization gas mixture as opposed to air.

Table 3.1 Summary of trials

Trial	Nozzle	Gas – Liquid Pre-mixer	Atomization gas	Volume injected (litres)	Gas to Liquid Ratio (mass %)
1	Simple Constriction	Venturi	Air	21	2.8
2 a, b	TEB	Venturi	Air	21	2.8
3	Shaped Shroud	Venturi	Air	21	0.5
4	TEB	BFC	Air	21	1.5
5	TEB	BFC	Air	21	2.8
6	TEB	Venturi	Helium/Nitrogen	21	0.8
7 a, b, c	Small Nozzle	Small BFC	Air	7.0	2.0
8 a, b, c	Small Nozzle	Small BFC	Air	10.5	2.0

The atomization gas and water were combined into one of two gas liquid pre-mixer assemblies: a venturi type and a bilateral flow conditioner type (BFC). The two phase flow then transferred through a smooth conduit to the nozzle inserted into the bed. Three

nozzles were used and were of the expansion-constriction, simple constriction and the simple constriction nozzle with a shroud on the end types. For the small nozzle tests, the BFC pre-mixer and nozzle were similar but at roughly 1:25 the scale. A helium/nitrogen gas mixture trial was also completed to ensure the atomization gas properties were accounted for in any relationship developed. This wide variety of nozzle and pre-mixer assemblies ensured that any relationship developed between bed fluidity and acoustic or vibration measurements would be independent of the spray nozzle type due to the fact that it was developed from many scenerios.

3.5. Signal analysis methods

Acoustic and vibration data from the microphones and the accelerometer were recorded at 40 000 Hz in order to make use of the audible sound range (20 – 20 000 Hz) without the risk of alias according to Nyquist-Shannon theorem. One of the corollaries of this theorm is the Nyquist rate which is the rate of sampling such that aliasing is avoided is twice that of the frequency band of interest. Frequencies that are not audible in the range of 0 – 20 Hz were also used. The signals were analyzed offline in 60 second consecutive intervals for the frequency of fluctuations using fast Fourier and wavelet techniques. This time period was deemed to have a sufficient number of data points such that physical changes in the signal were dominant in the analysis over any random noise. A large number of parameters were calculated based on the power and wavelet spectra and were combined using multi-linear and power law regressions.

3.5.1. Frequency analysis using fast Fourier techniques

The spectral density is calculated from the product of the Fourier transform of a signal and its complex conjugate. A plot of the spectral density versus frequency allows identification of the frequencies of any dominant fluctuations in a signal. Beyond simply calculating the power of the signal in different frequency bands, other parameters were calculated from the power spectral density such as average power, average frequency and noise index. After performing multi-linear regression on these power spectral density parameters, two additional parameters were found to be significant: average frequency and noise index. The average frequency of a signal was calculated by:

$$\mu = \frac{\sum_{j=0}^{J-1} f(j)p(j)}{\sum_{j=0}^{J-1} p(j)} \qquad \textbf{(3.1)}$$

Where *f(j)* is the midpoint frequency of at bin '*j*' and *p(j)* is the power of the frequency at bin '*j*'

The noise index (α) of a signal is defined as the slope of line of the natural logarithms of power and frequency, shown by:

$$\ln(p) = \beta + \alpha \ln(f) \qquad \textbf{(3.2)}$$

3.5.2. Frequency analysis using wavelet techniques

During the wavelet analysis of a signal, the signal is divided into *m* multiple levels or scales. Each of these levels corresponds to a frequency band, and due to the halving effect of the frequency, can further be defined as octaves. At each octave, using a Debauchies 4 wavelet, the signal was separated into two parts: the averages and the coefficients. The coefficients indicated the fluctuations in the signal at a specified scale. It is then possible to calculate statistics on this set of coefficients. The regressions were performed on the wavelet spectrum and the corresponding coefficients, and it was found that the average, the standard deviation, and the intermittency of the coefficients were relevant. The standard deviation of the coefficients was calculated at each scale by:

$$\sigma_m = \sqrt{\frac{\sum_{i=1}^{n} (x_i - \mu_{coeff})^2}{n}} \qquad \textbf{(3.3)}$$

In most cases, it was useful to normalize the standard deviation of coefficients with the standard deviation of the signal in that it was more effective in the regression. Similarly, by computing the energy of the coefficients at specified scale and dividing by the global (average) energy of the entire signal the intermittency of the coefficients was determined by:

$$I_{m,n} = \frac{(C_{m,n})^2}{< C^2_{m,n} >} \qquad \textbf{(3.4)}$$

Where < > indicates the mean energy of the signal and ( ) indicates the average value of the coefficients at the specific octave.

3.6. Results & Discussion

3.6.1. Effect of moisture on solids flowability

Figure 3.5 shows images of sample surfaces in the Revolution Analyzer. When the sand was wet, with a moisture content of 0.1 wt % (Figure 3.5a), it was visually cohesive: the sample surface was irregular and showed large avalanches of material as the sample was rotated in the drum. On the other hand, the sample surface was much smoother when the sand was dry (Figure 3.5b), as the dry particles flowed easily; only very small and frequent avalanches were recorded.

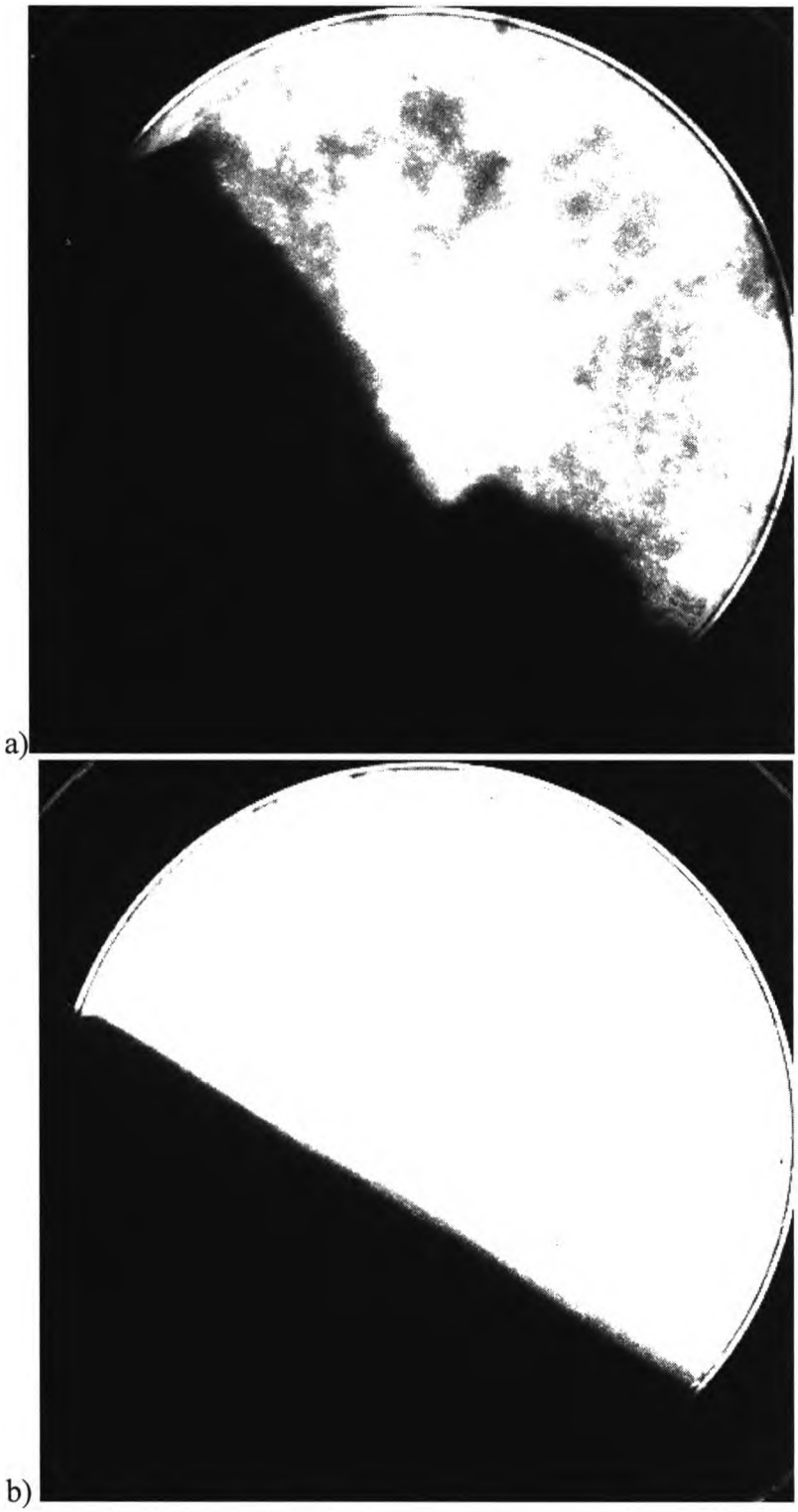

Figure 3.5 Images of silica sand samples in the Revolution Analyzer when (a) the sand was cohesive and wet (0.1 wt%) and when (b) the sand was dry and free flowing

Samples were taken at intervals during the 90 minute drying time and analyzed for flowability and moisture content. Figure 3.6 shows a typical trial. Initially (at time t=0 minutes in the drying run), the median avalanche time was low at 4 s and the moisture content was about 0.05 wt %. At 10 minutes into the drying phase, both the median avalanche time and the moisture content of the sand reached a maximum and then subsequently decreased as drying proceeded. The initial (time t = 0 min) low median avalanche time and low moisture content of the sand was attributed to the non-uniform dispersion of water in the bed as the injected water did not have sufficient time to be completely mixed into the bed and uniformly distributed.

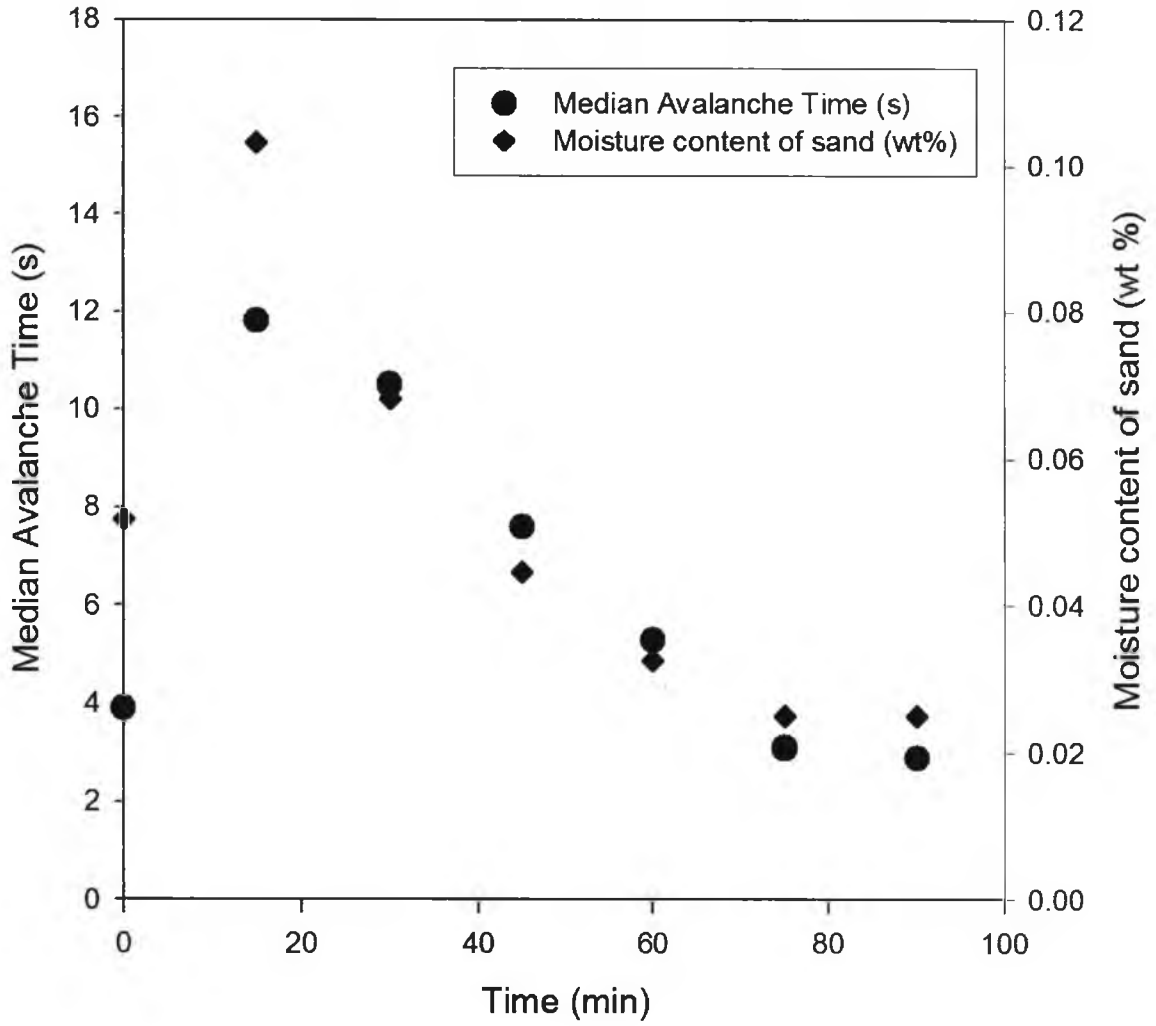

Figure 3.6 Flowability and moisture content of the sand during the drying phase of Trial #4

Figure 3.7 relates the flowability of the sand, using the median avalanche time to the moisture content of the sand. It was compiled from a range of nozzle and pre-mixer combinations with varying gas to liquid ratios, small nozzle injections, and by mechanically mixing water and solids. Samples of sand were mechanically mixed with water to eliminate all agglomerates and determine the avalanche time for agglomerate-free solid-liquid mixtures. The moisture measurements used samples of a very small size

(≈ 8 g) compared to the industrial size of the bed. Even in a very well mixed fluidized bed of 9 tonnes, this can only be considered a local measurement of moisture.

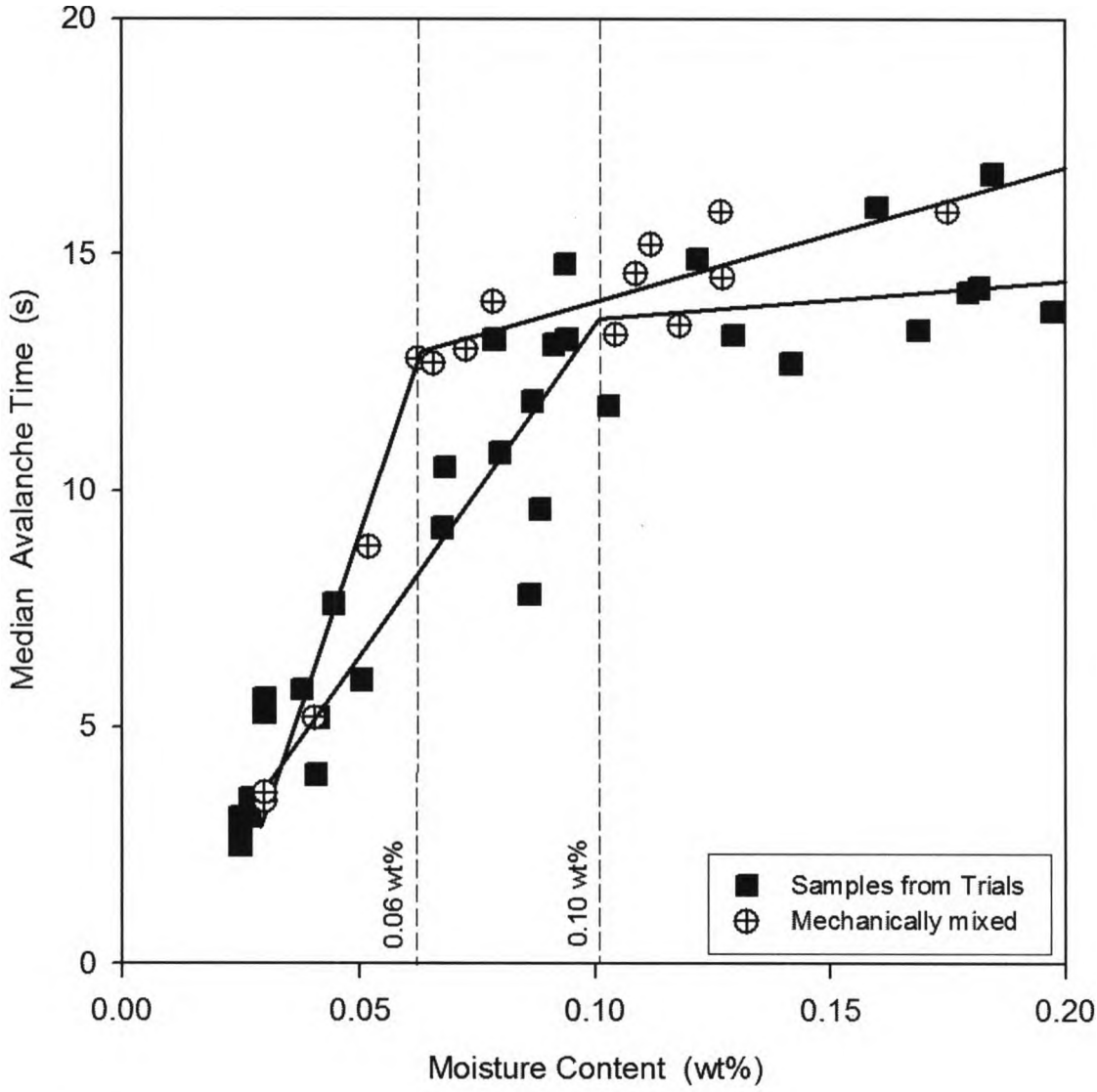

Figure 3.7 Relationship between the median avalanche time and moisture content

Below a moisture content of 0.06 wt %, there was a positive linear relationship between the flowability and moisture content of the sand for the mechanically mixed samples. A change in slope occurred at about 0.1 wt % for the samples withdrawn from the fluidized

bed. At higher moisture content levels, there was almost no change in the median avalanche times for both mechanically mixed and fluidized bed samples.

It was found that the mechanically mixed samples had higher avalanche times than the bed samples for a given moisture content. This indicated that a portion of the moisture in the bed was trapped in a form that did not affect flowability. It was proposed that water within the bed existed in four forms: (i) in macro-agglomerates of sand particles that are easily visible, (ii) in meso-agglomerates of sand that are still visible, (iii) in micro-agglomerates that are not visible, and (iv) on the surface of individual non-porous sand particles. Any water in the macro-agglomerates was not captured in samples, as these macro-agglomerates were too large to be fluidized and, therefore, it is assumed that these agglomerates immediately descended through the bed to the grid plate. The meso-agglomerates and micro-agglomerates were small enough to remain fluidized within the bed. Samples of the bed therefore contained meso-agglomerates, micro-agglomerates and individual dry and wet sand particles.

Visual observations confirmed the presence of meso-agglomerates above 0.10 wt % (Figure 3.8). From Figure 3.7, it was concluded that moisture content is not a reliable indicator of solids flowability at high moisture levels, as water can be distributed in four forms, each of which has a different effect on solids flowability and on the overall bed fluidity.

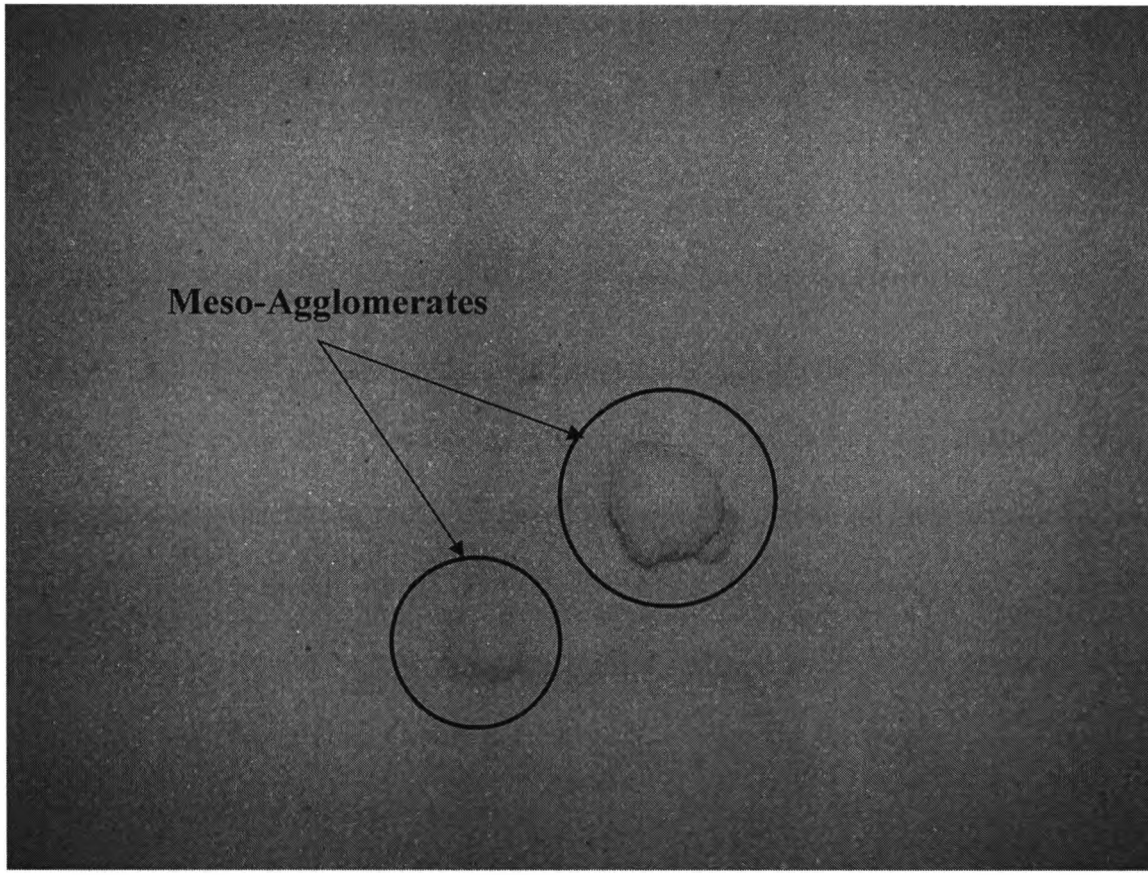

Figure 3.8 A sample containing meso-agglomerates

When the water was injected into the bed, agglomerates formed immediately at the end of the spray cavity. As agglomerates grew they incorporated dry particles onto their surface. This resulted in a relatively dry surface on the agglomerates; therefore the flowability of a given sample that contained both individual particles and agglomerates was better than expected as an agglomerate did not have a sticky or cohesive surface to negatively impact the flowability.

After drying for an initial period of time, water on the surface of the particles and within the agglomerates evaporated. In addition, some of the agglomerates attrited and

fragmented redistributing water towards more individual particles which then continued to dry.

3.6.2. Frequency analysis using fast Fourier techniques

Acoustic and vibration data were recorded throughout the drying phase. These data were analyzed offline in 60 s consecutive intervals to determine any changes in the measurements with drying time. Figure 3.9 shows the power spectral density of three recorded vibration segments of 60 seconds during drying, normalized to the power spectral density of the signal recorded from a bed at 0.025 wt % moisture. The normalized power spectral densities clearly show that the frequencies of the signals change significantly with the moisture content, and, therefore, with the fluidization quality in the bed. Similar results were obtained for both microphones on the bed wall.

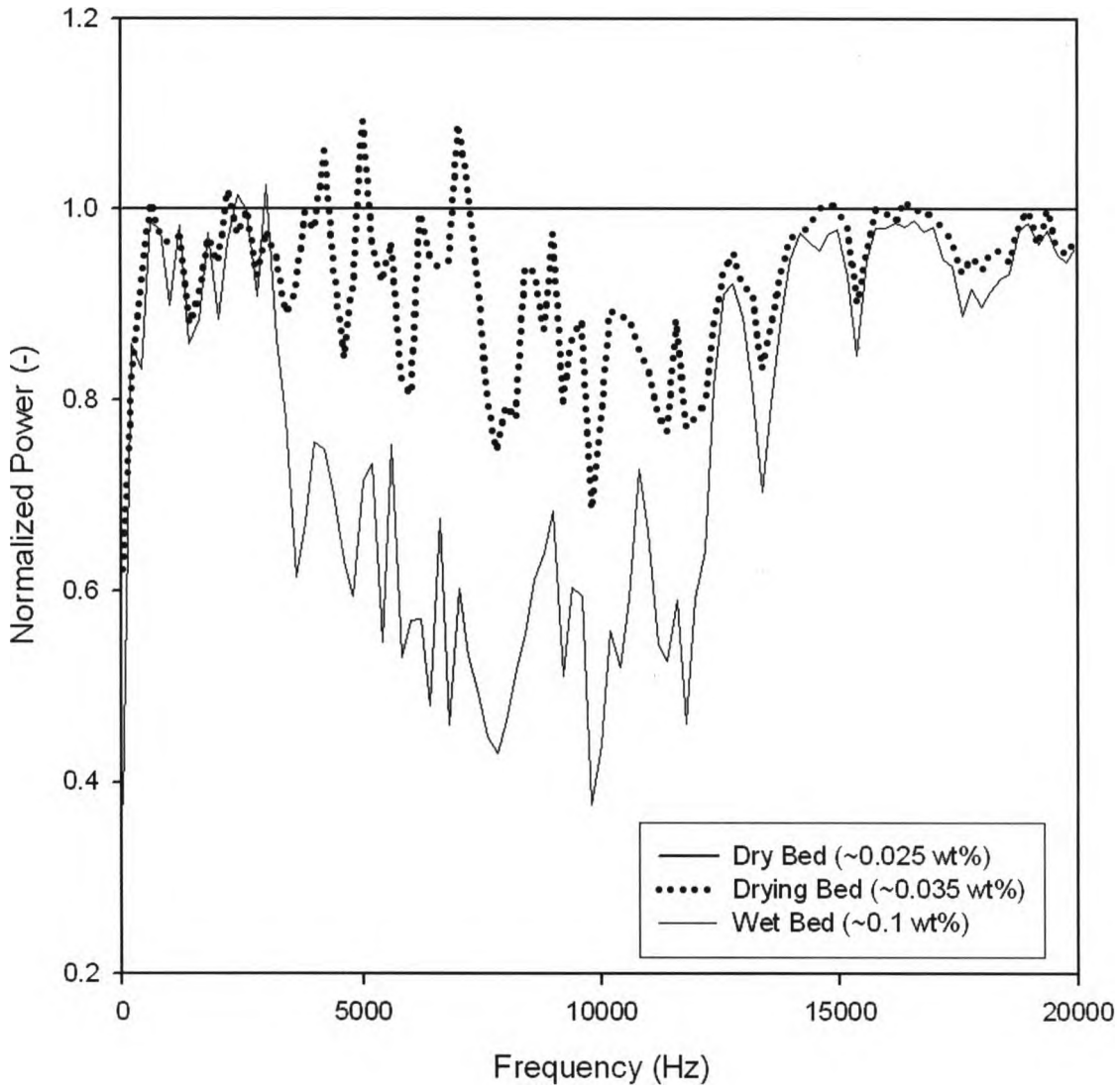

Figure 3.9 Normalized power spectral densities of vibration measurements recorded during Trial #1. from the wet bed 5 minutes after refluidization, drying bed after 45 minutes after fluidization and dry bed after 90 minutes after refluidization

3.6.3. Frequency analysis using wavelet techniques

After dividing the signal into 60 s consecutive intervals, the signals were decomposed into scales using a discrete Debauchies 4 wavelet. The wavelet standard deviation of the coefficients spectral density was normalized to the spectrum of the dry bed and plotted in

Figure 3.10. Figure 3.10 shows that the variation in the standard deviations of wavelet coefficients changed with the moisture content and fluidization quality. This indicates that as bed dries, the signal fluctuations become smaller. One possible source of this change is the large fluctuations due to sloshing from gas misdistribution being reduced. As the settled agglomerates on the gas distributor break up and fluidization quality improves, the sloshing stops and there are many smaller fluctuations from bubbles.

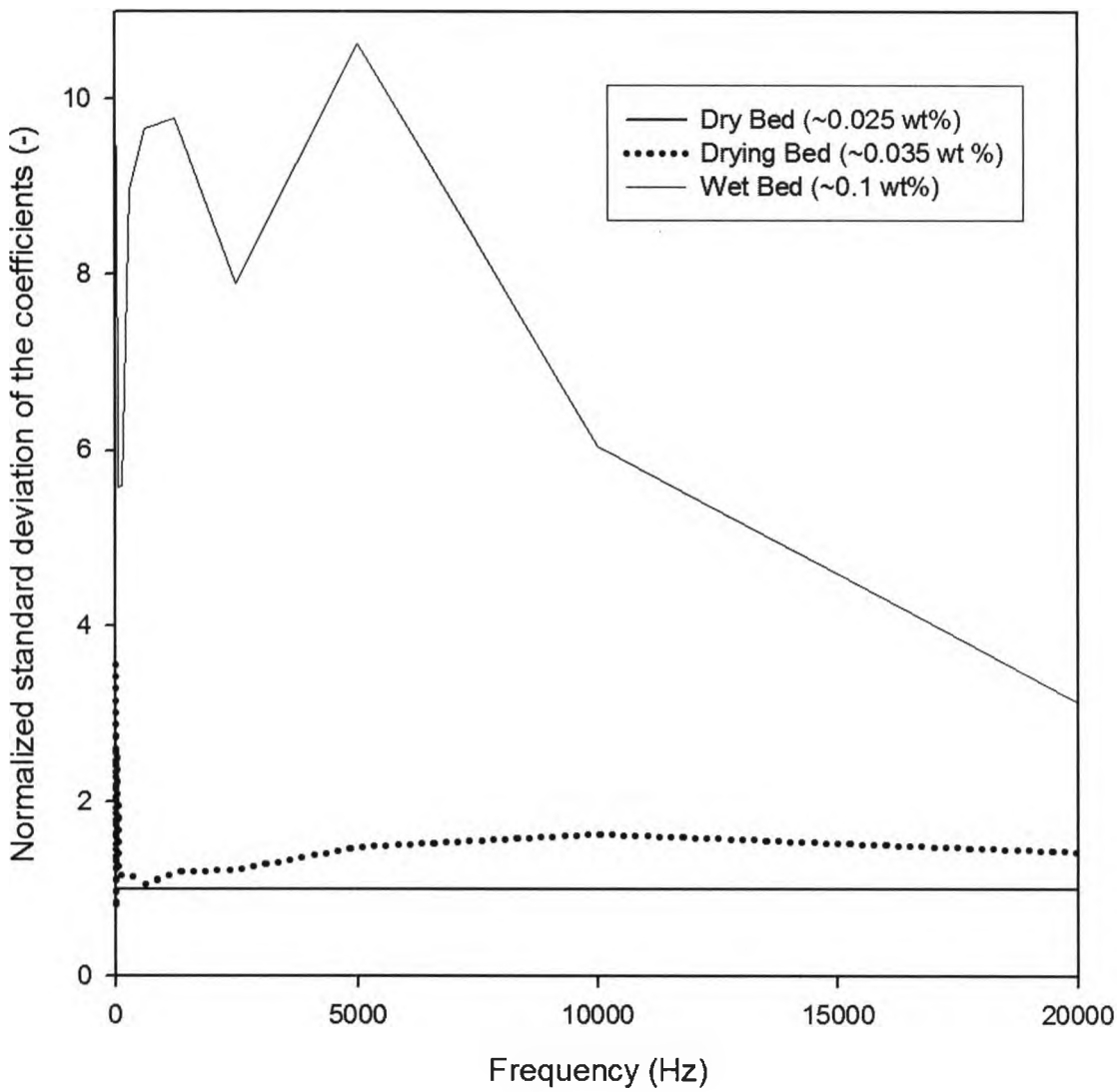

Figure 3.10 Normalized standard deviation of the coefficients of vibration measurements recorded during Trial #1 from the wet bed 5 minutes after refluidization, drying bed after 45 minutes after fluidization and dry bed after 90 minutes after refluidization

3.6.4. Multi-linear and Power law Regressions for bed fluidity detection

Throughout the study, both the power spectral density and the wavelet spectra were consistently well correlated to the fluidization quality within the bed. However, due to changes in the process over time (loss of solids and equipment modifications such as new fluidization gas lines), the base line values for a dry bed drifted. It was therefore necessary to develop a method that was resistant to process changes and would remain reliable over long periods of time. Data from the power spectral density and wavelet spectral density of the signals were therefore regressed to correlate with median avalanche times. Using regression it was possible to identify which portions of the acoustic or vibrations signals were consistently correlated to the fluidization quality within the bed.

To account for the effect on fluidization quality of the initial distribution of water, two types of regressions were performed: multi-linear regression of the sensor measurements after 10 minutes after refluidization and a power law regression of the sensor measurements for the entire 90 minutes after refluidization.

The regressions identified the important parameters for each sensor. The number and type of parameters were determined by maximizing the F-statistic. The parameters identified for each sensor are listed in Tables 3.2 and 3.3. These parameters were then

used to evaluate the fluidization quality of the bed by creating a predicted median avalanche time.

Table 3.3.2 Parameters from the power law regression of all data after refluidization

Analysis	Techniques	Sensors		
		Microphone at 2.3 m	Microphone at 2.8 m	Accelerometer
fast Fourier analysis	power at	7.5 kHz 7.9 kHz 8.5 kHz 11.5 kHz	3.3 kHz 11.1 kHz	7.3 kHz 13.5 kHz 14.1 kHz 17.3 kHz
			average frequency	average frequency
wavelet analysis	avg. of coefficients at	19th octave		
	std. dev. of coefficients at	5th octave 7th octave 10th octave	11th octave	
	normalized std. dev. of coefficients at	14th octave	4th octave	8th octave 11th octave

Table 3.3.3 Parameters from the multi-linear regression of data after the bed is well-mixed

Analysis	Techniques	Sensors		
		Microphone at 2.3 m	Microphone at 2.8 m	Accelerometer
fast Fourier analysis	power at	3.1 kHz 11.7 kHz 15.1 kHz 16.1 kHz	7.1 kHz	7.3 kHz 15.1 kHz
		noise index		
wavelet analysis	normalized std. dev. of coefficients at	5th octave	9th octave 10th octave 16th octave 18th octave 19th octave	3rd octave 9th octave 14th octave 18th octave
	intermittency index	3rd octave	13th octave	1st octave 2nd octave 6th octave
			std. dev. of octaves	

Figures 3.11-3.16 show the multi-linear and power law regressions for the vibration measurements and the acoustic emission measurements from the two microphone positions. For all sensors, the comparison between the predicted and measured median avalanche times, obtained by a power law regression of all refluidization data, was poor

at large avalanche times. These measurements were from samples taken from the bed within minutes after refluidization. The water from the injection had not yet had sufficient time to be mixed throughout the bed. Therefore, the solids, sampled locally far from the injection site, were not always representative of the solids moisture content and therefore the fluidity.

The correlation between predicted and measured median avalanche times improved when the regression was restricted to sensor measurements between 10 – 90 minutes after refluidization. This eliminated any non-representative samples from insufficient mixing of injected water into the bed.

Provided that the bed was well mixed, there was still some spread in the results. As the median avalanche time was calculated from a distribution of avalanches it was possible to have tails and outliers which could affect the results.

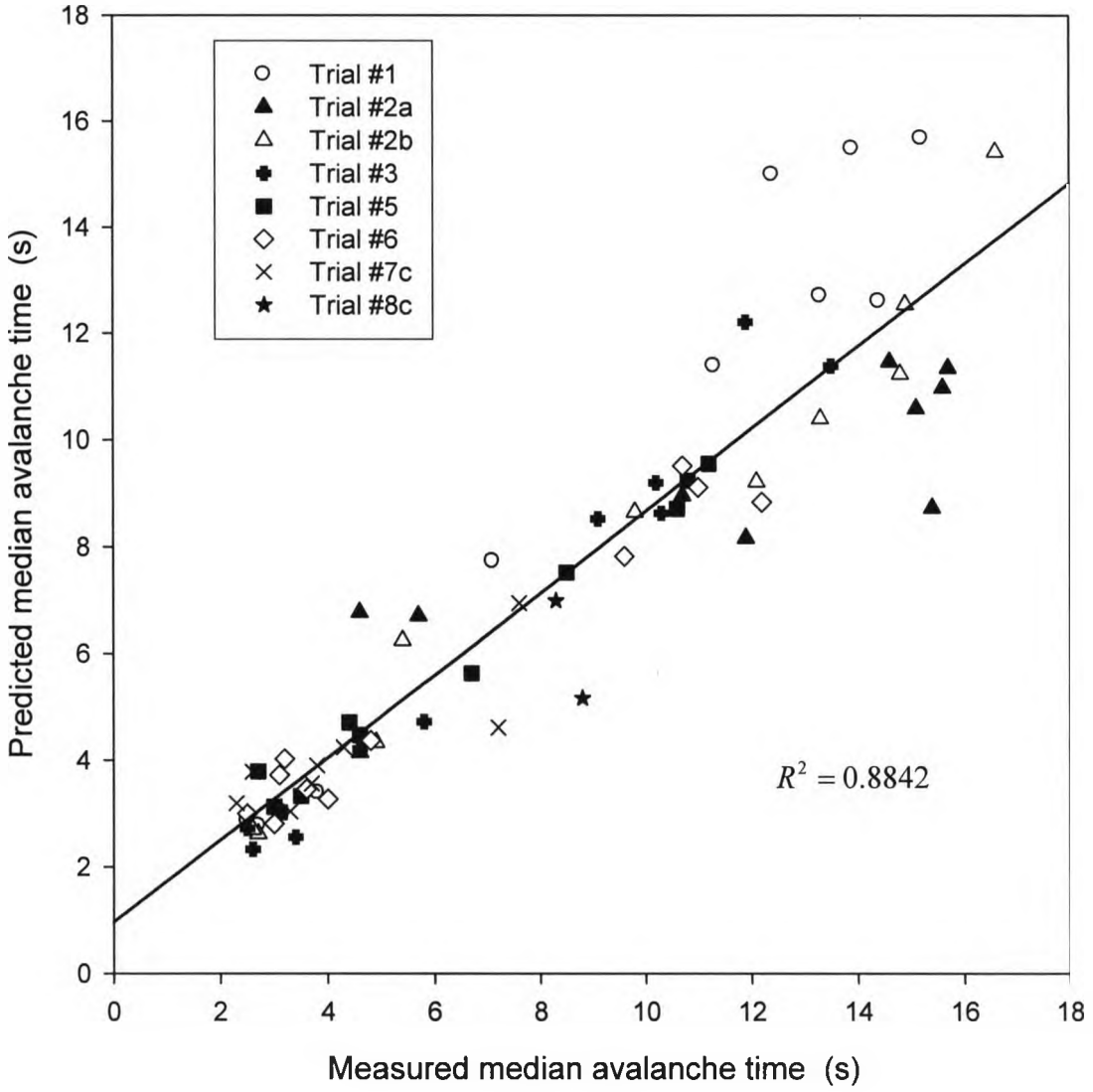

Figure 3.11 Comparison between predicted and measured median avalanche times for accelerometer measurements, fitted with a power law regression of all data immediately after refluidization

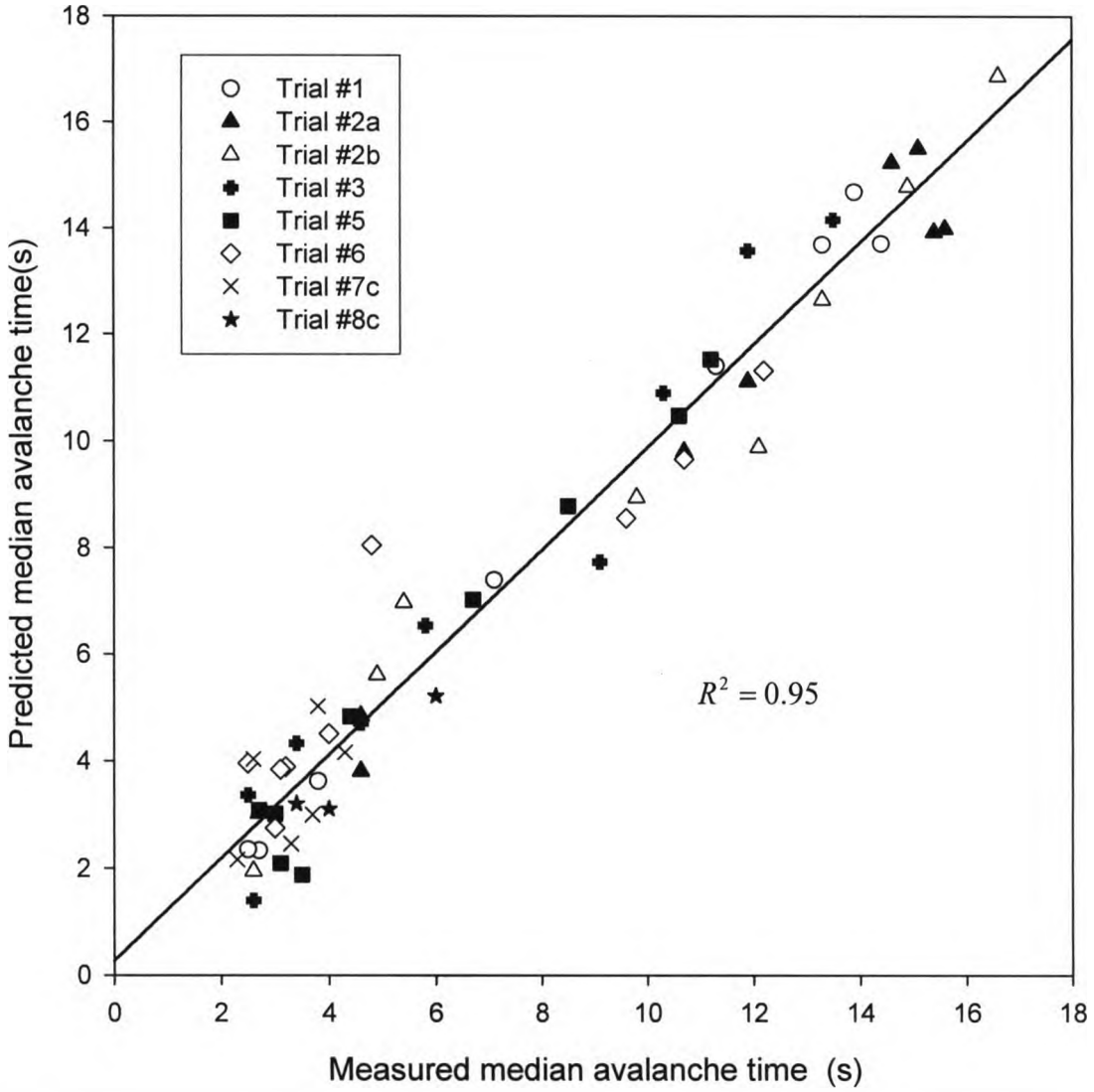

Figure 3.12 Comparison between predicted and measured median avalanche times for accelerometer measurements, fitted with a multi-linear regression of data obtained between 10 – 90 minutes

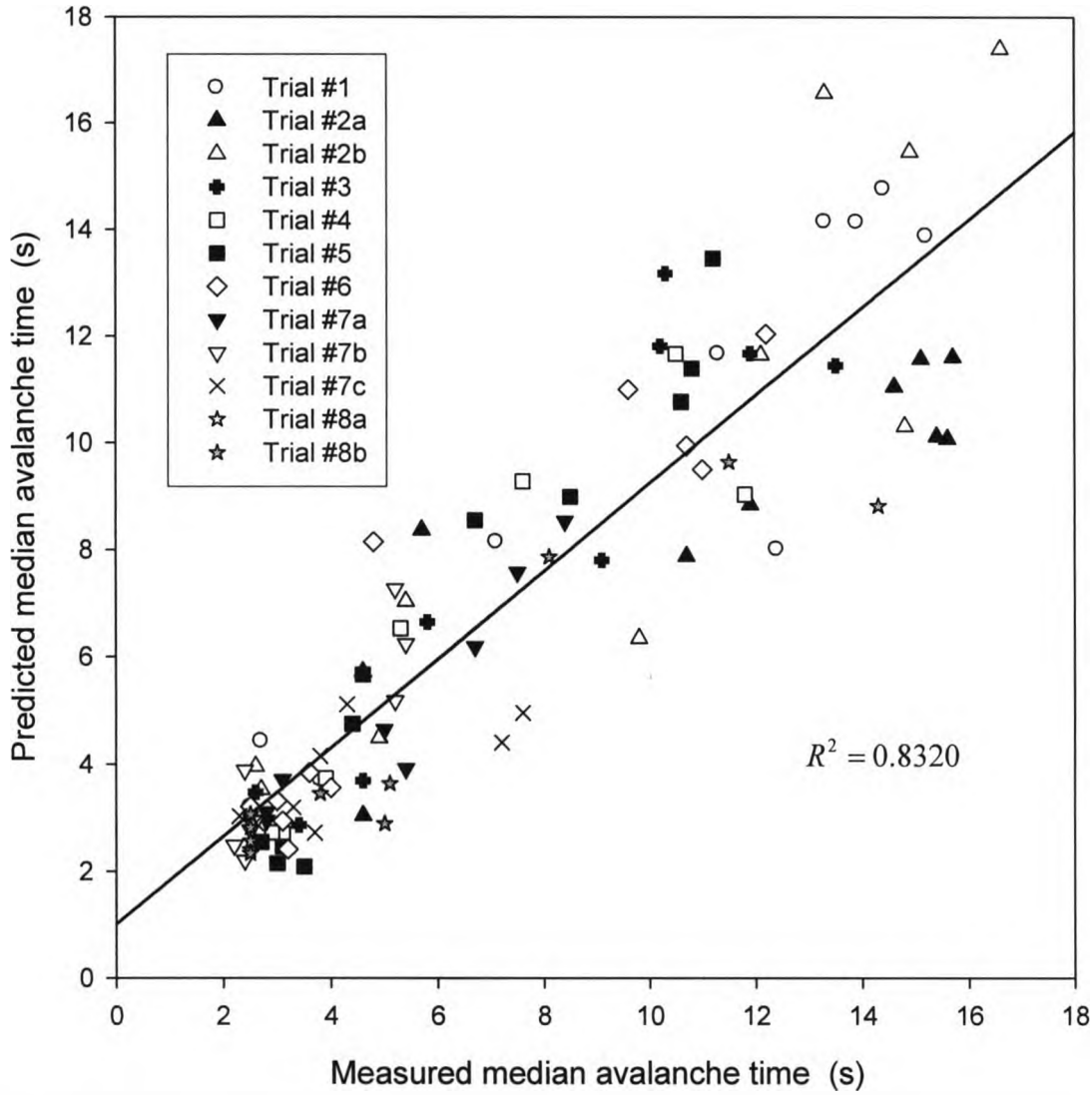

Figure 3.13 Comparison between predicted and measured median avalanche times for acoustic measurements (microphone at 2.3 m), fitted with a power law regression of all data immediately after refluidization

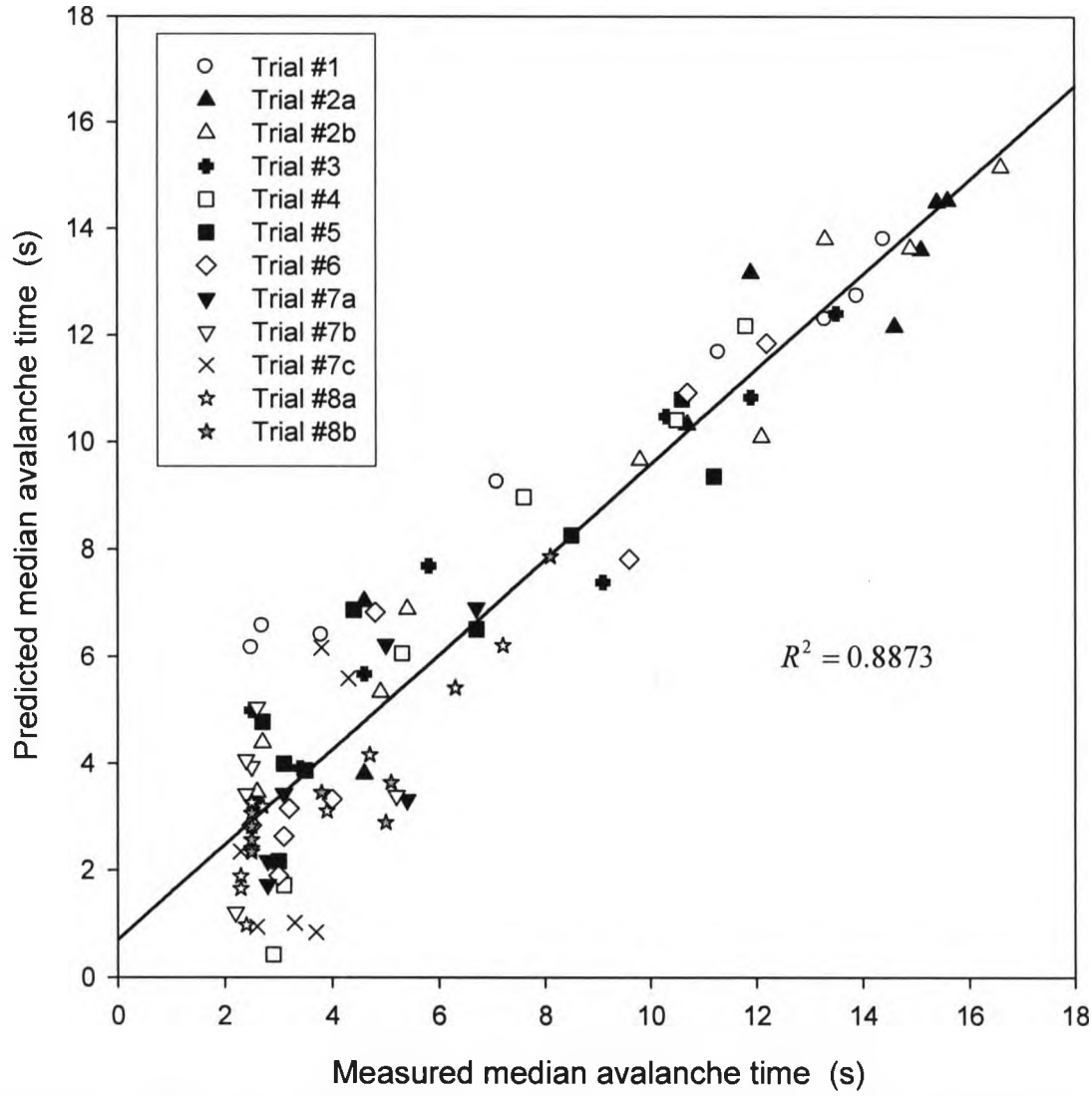

Figure 3.14 Comparison between predicted and measured median avalanche times for acoustic measurements (microphone at 2.3 m), fitted with a multi-linear regression of data obtained between 10 – 90 minutes

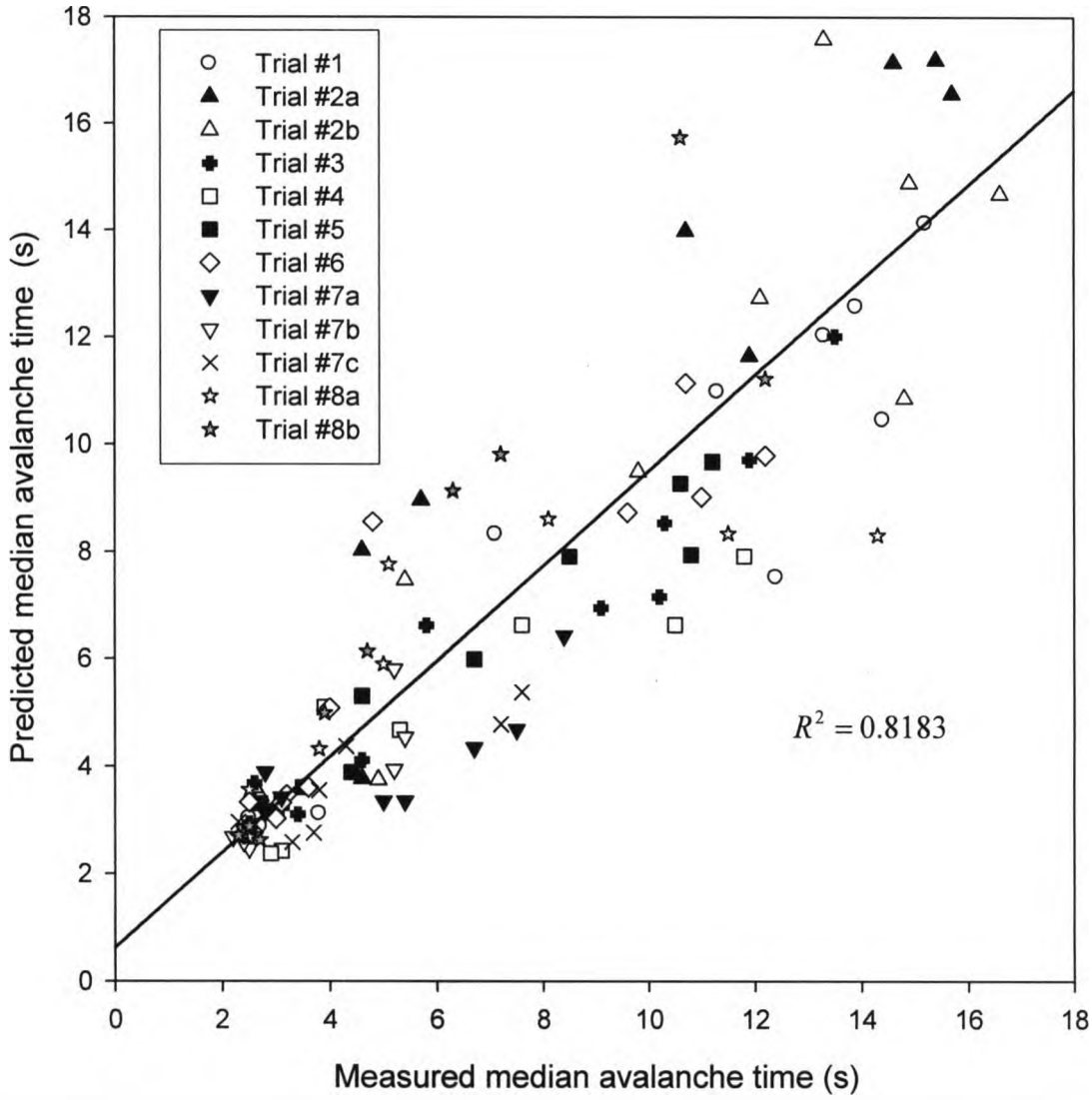

Figure 3.15 Comparison between predicted and measured median avalanche times for acoustic measurements (microphone at 2.8 m), fitted with a power law regression of all data immediately after refluidization

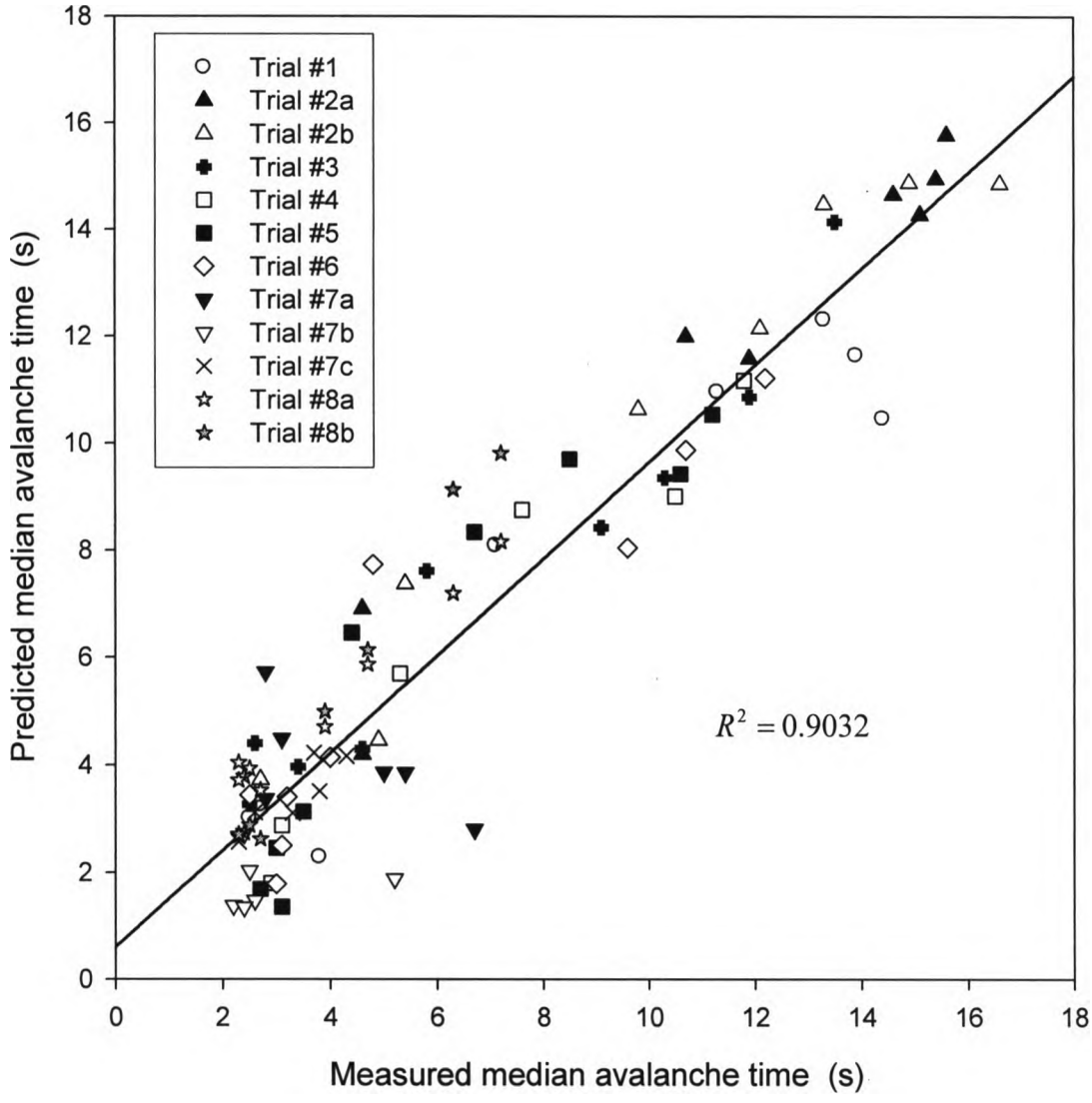

Figure 3.16 Comparison between predicted and measured median avalanche times for acoustic measurements (microphone at 2.8 m), fitted with a multi-linear regression of data obtained between 10 – 90 minutes

The moisture content of the solids within the bed affected the flowability of the solids and therefore the bed hydrodynamics and the acoustic emission and vibration measurements. Changes in the solids flowability would affect bubble distribution, velocity, shape and size. In addition, the more cohesive the wet solids would promote the formation of channels. Both bubble behaviour and channelling would then affect the

surface of the bed from enhanced sloshing to increased spouting with increased solids entrainment. Bubbles, channels and bed surface sloshing and spouting would all provide specific acoustic emissions and contribute to the vibrations within the bed. Therefore as the solids flowability and bed hydrodynamics changed during drying. The sensor measurements also changed accordingly and could be related to flowability through the sample median avalanche times.

The correlation between predicted and measured avalanche times was affected by sensor type and position. The sum of squares of the residuals for the accelerometer was nearly 50 % lower than that of both microphones demonstrating that the accelerometer was the most accurate sensor. One possible explaination of this is that the accelerometer is better for detection the low frequency sloshing when the bed is poorly fluidized.

3.6.5. Evaluation of Mixing Time

The fluidization quality of the bed was evaluated most accurately using predicted median avalanche times from the multi-linear regression of data obtained from sensor measurements between 10 – 90 minutes after refluidization. When data from the first 10 minutes after refluidization was included in the regression, the error increased substantially the bed was not yet well mixed so that, samples that were taken to measure the flowability did not represent the entire bed.

Multi-linear regressions were applied to all data after refluidization to obtain predicted median avalanche times. Sum of squares errors were then calculated for correlations with

measured median avalanche times. Figures 3.17 – 3.19 show the normalized sum of squares errors calculations with time throughout the entire phase for all the sensors.

Initially, the sum of squares errors was high and then decreased to low and approximately constant levels. The time at which the errors dropped indicated a mixing time, the time required for the injected water to become well distributed within the bed.

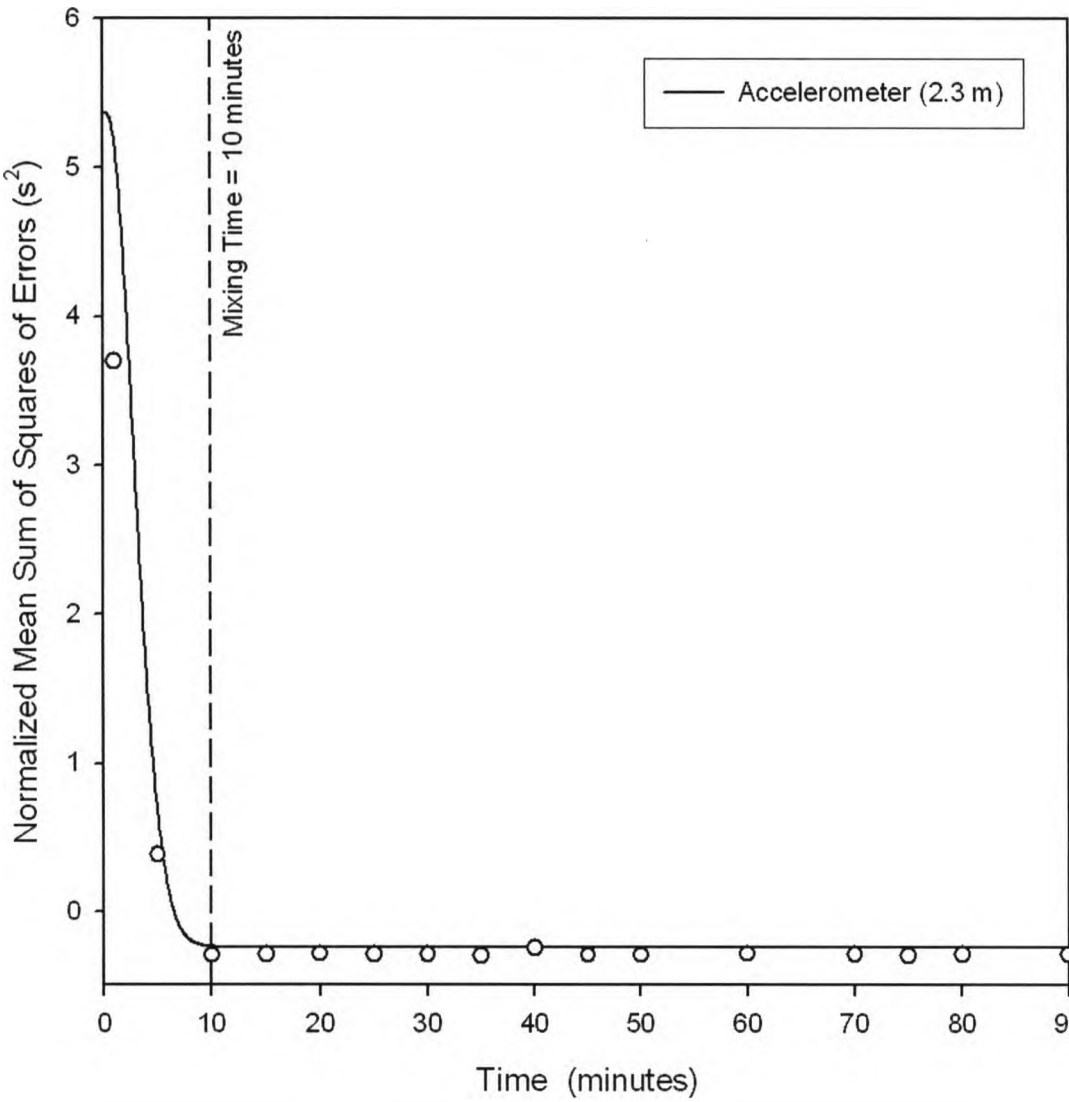

Figure 3.17 Evaluation of the time required to achieve a well-mixed bed from the Normalized SSE of vibration measurements

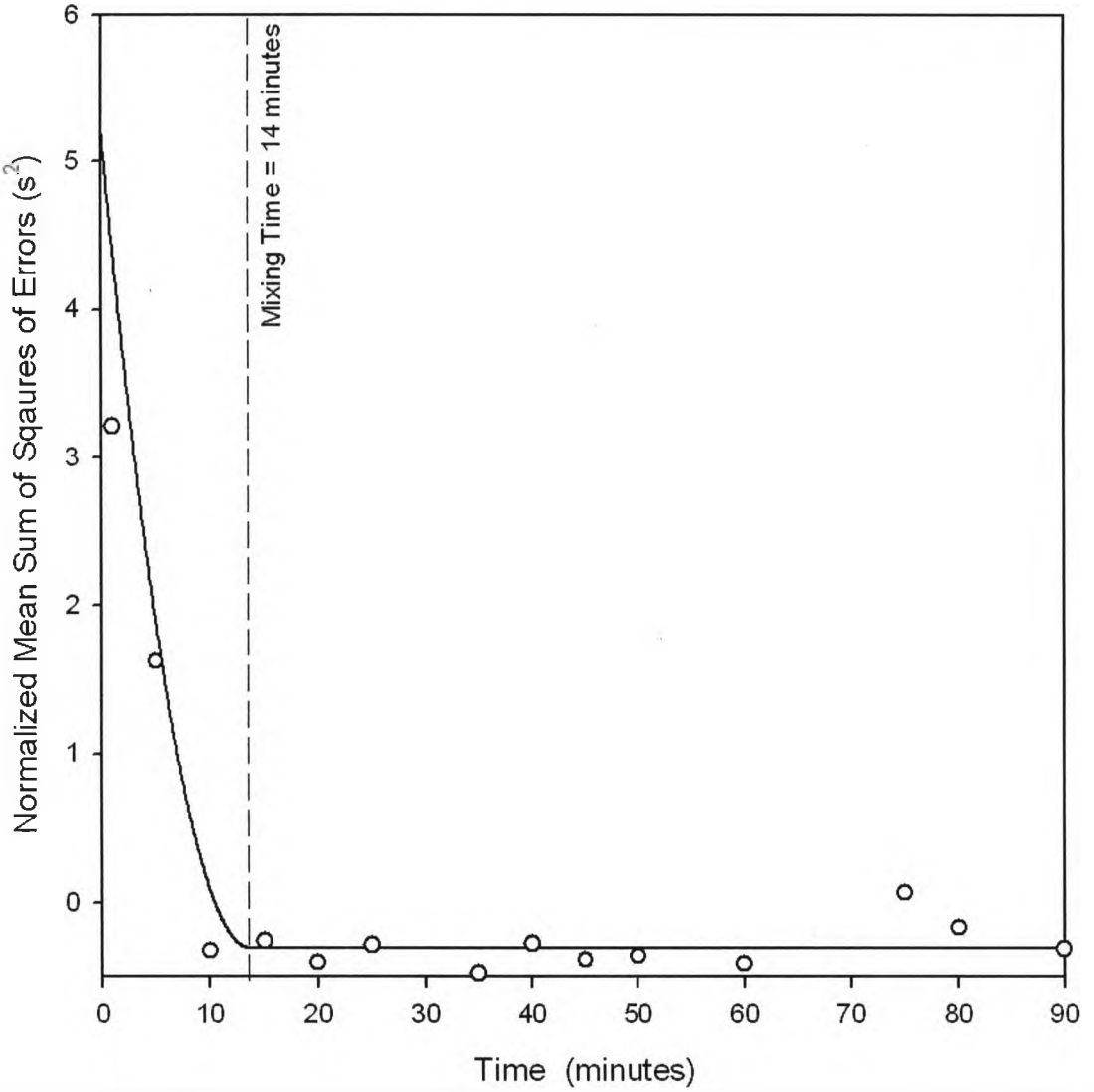

Figure 3.18 Evaluation of the time required to achieve a well-mixed bed from the Normalized SSE of acoustic measurements (microphone at 2.3 m)

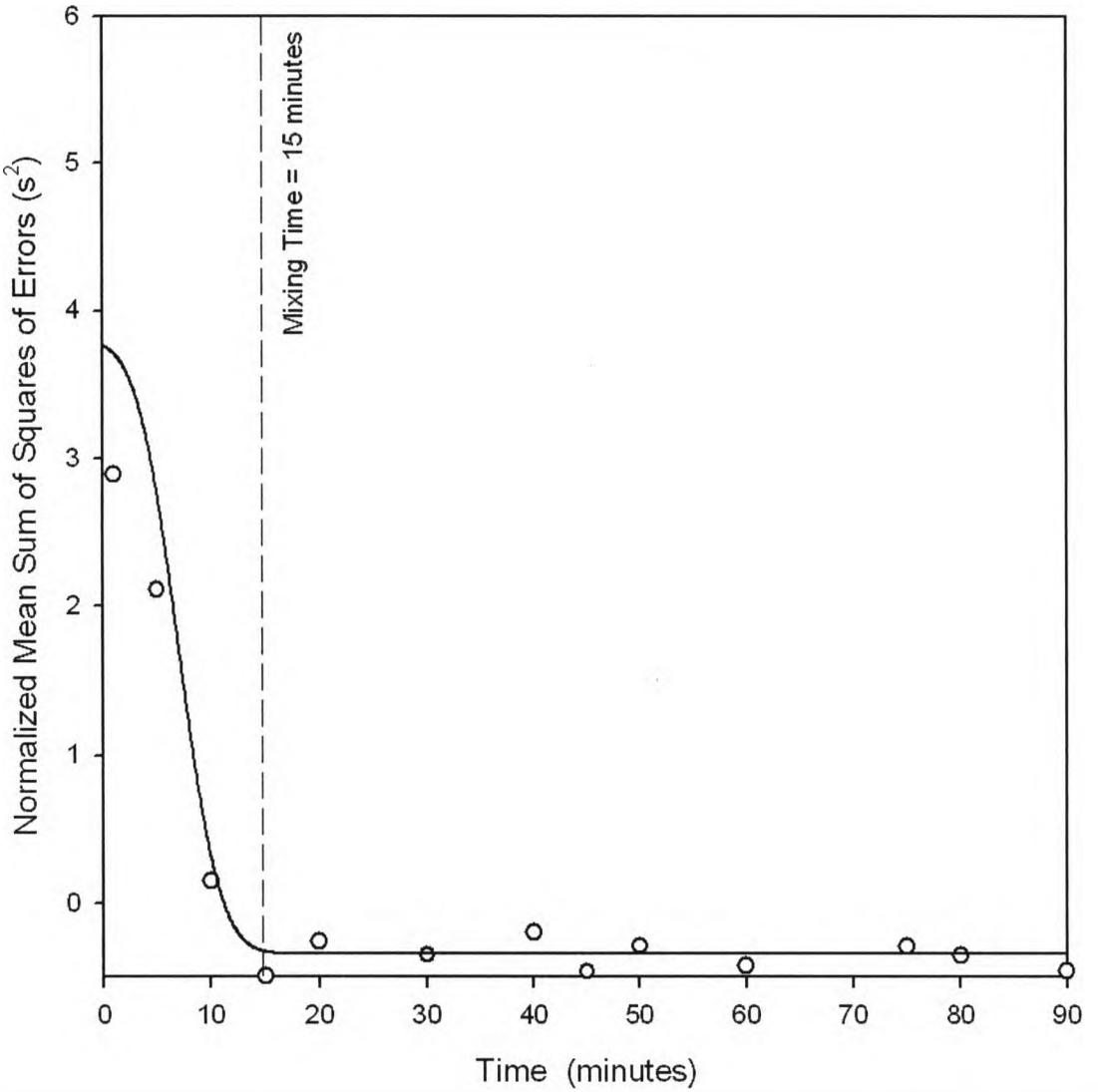

Figure 3.19 Evaluation of the time required to achieve a well-mixed bed from the Normalized SSE of acoustic measurements (microphone at 2.8 m)

A comparison of figures 3.17 – 3.19 shows that the estimated mixing times ranged from 10 minutes from vibration measurements to 14 and 15 minutes from the acoustic measurements at 2.3 and 2.8 m respectively. These results may not necessarily considered significantly different, however, the variations in these mixing times can be attributed to the different sensor measurements and locations. It was concluded that 10 – 15 minutes was required for the entire bed to completely mix.

3.7. Conclusions

- Moisture content is not an accurate way of predicting the flowability of solids after spraying of water into a fluidized bed.
- Avalanche testing is an accurate way of measuring the flowability of powders and, therefore, provides a direct measurement of the fluidization quality inside a gas-solid fluidized bed of powders.
- Two microphones and an accelerometer were used to successfully detect the fluidization quality of a large scale gas-solid fluidized bed of particles, using multi-linear and power law regressions of traditional (Fourier analysis) and advanced (wavelet decomposition) signal analysis. The measurements were well correlated to physical measurements of fluidization quality in the bed.
- Sensor location was found to have an effect on the measurements due to the asymmetrical geometry of the bed. Both non-intrusive microphones were successfully able to correlate to fluidization quality. Vibration measurements provided the most accurate predictions of fluidization quality. The vibrations were measured using an accelerometer mounted to a rod that represented a thermocouple and therefore also demonstrated that the measurements could be easily applied to commercial units.
- The time required for the bed to mix completely was evaluated by comparing the error in the SSE of the multi-linear regressions of the acoustic and vibrometric measurements.

3.8. Acknowledgments

The authors would like to acknowledge the help of Dr. Gareth Chaplin on the equipment and adapting his scheduled experiments to incorporate our needs. The authors would like to thank Syncrude Canada Ltd. for both their funding and their advice. Thanks also to NSERC, OGS and OGSST for their funding of this work.

3.9. Symbols

C Energy of the signal (units)

f Frequency, (Hz)

F Maximum frequency, (Hz)

I Local Intermittency index, (units)

j Positive integer, number of power spectral density bin, (-)

J Positive integer, number of power spectral density bins, (-)

m Positive integer, number of level in a wavelet decomposition of a signal, (-)

n Positive integer, number of points in a series or signal, (-)

p Power at a given frequency, (-)

t time, (s, min)

U_g Superficial gas velocity, (m/s)

Greek symbols

α Noise index of the signal, (units)

β Linear constant, (units)

μ Mean of a series or signal, (units)

σ Standard deviation, (units)

3.10. References

[1] McDougall, S., Saberian, M., Briens, C., Berruti, F., Chan, E., Effect of liquid properties on the agglomerating tendency of a wet gas-solid fluidized bed. *Powder Technology.* 149 (2005) 61-67

[2] McDougall, S., Saberian, M., Briens, C., Berruti, F., Chan, E., Using dynamic pressure signals to assess the effects of injected liquid on fluidized bed properties. *Chemical Engineering and Processing.* 44 (2005) 701-708

[3] Briens, C., McDougall, S., Chan, E., Online Detection of Bed Fluidity in a fluidized bed coker. *Powder Technology.* 138 (2003) 160-168

[4] Boyd, J.W.R., Varley, J., The uses of passive measurement of acoustic emissions from chemical engineering processes. *Chemical Engineering Science.* 56 (2001) 1749 - 1767.

[5] McDougall, S., Saberian, M., Briens, C., Berruti, F., Chan, E., Characterization of Fluidization Quality in Fluidized Beds of Wet Particles. *International Journal of Chemical Reactor.* 2 (2004) A26

[6] Rees, A. C., Davidson, J. F., Dennis, J. S., Hayhurst, A. N., THE APPARENT VISCOSITY OF THE PARTICULATE PHASE OF BUBBLING GAS-FLUIDIZED BEDS: A comparison of the falling or rising sphere technique with other methods. *IChemE J.* 85 (2007) A10, 1341-1347

[7] Schügerl, K., Rheological behaviour of fluidized systems. Davidson, J.F. and Harrison, D. (eds). *Fluidization,* (Academic Press, London and New York) 261-292

[8] Kai, T., Murakami, M., Yamaskai, K., Takahashi, T, RELATIONSHIP BETWEEN APPARENT BED VISCOSITY AND FLUIDIZATION QUALITY IN A FLUIDIZED BED WITH FINE PARTICLES. *Journal of Chemical Engineering of Japan.* 24 (1991) 4, 494-500

[9] Grace, J. R., The Viscosity of Fluidized Beds. *Canadian Journal of Chemical Engineering.* 48 (1970) 30-33

[10] King, D. F., Mitchell, F. R. G., Harrison, D., Dense Phase Viscosities of Fluidised Beds at Elevated Pressures. *Powder Technology.* 28 (1981) 55-58

[11] Daniels, T.C., Measurement of the Drag on Spheres Moving Through Gaseous Fluidized Beds. *Journal of Mechanical Engineering.* 4 (1962) 2, 103-110

[12] Geldart, D., Wong, A.C., FLUIDIZATION OF POWDERS SHOWING DEGREES OF COHESIVENESS—II.EXPERIMENTS ON RATES OF DE-AERATION, *Chemical Engineering Science.* 40 (1985) 4, 653-661

[13] Lorences, M. J., Patience, G.S., Diez, F.V., Coca, J., Fines effects on collapsing fluidized beds, *Powder Technology.* 131 (2003) 234-240

[14] Yutani, N., Ho, T.C., Fan, L.T., Walawender, W.P., Song, J.C., STATISTICAL STUDY OF THE GRID ZONE BEHAVIOR IN A SHALLOW GAS-SOLID FLUIDIZED BED USING A MINI-CAPACITANCE PROBE, *Chemical Engineering Science.* 38 (1983) 4, 575-582

[15] Ropchan, W.T., Heat transfer and grid jets, *PhD Thesis,* Stanford University, (1981).

[16] Karamavruç, A.I., Clark, N.N., A fractal approach for interpretation of local instantaneous temperature signals around a horizontal heat transfer tube in a bubbling fluidized bed, *Powder Technology.* 90 (1997) 235-244

[17] Moore, A.D. (Ed.), Electrostatics and its Applications, *Wiley*, USA, (1974)

[18] Briens, C. L., Briens, L. A., Barthel, E., Le Blévec, J. M., Tedoldi, A., Margaritis, A., Detection of local fluidization characteristics using the V statistic, *Powder Technology.* 102 (1999) 95-103

[19] Briens, L.A., Briens, C.L., Cycle Detection and Characterization in Chemical Engineering, *AIChE Jounal.* 48 (2002) 5, 970-980

[20] Tardos, G., Mazzone, D., Pfeffer, R., Destabilization of Fluidized Beds Due to Agglomeration – Part II: Experimental Verification, *Canadian Journal of Chemical Engineering.* 63 (1985) 384-389

[21] McLaughlin, L.J., Rhodes, M.J., Prediction of fluidized bed behaviour in the presence of liquid bridges, *Powder Technology.* 114 (2001) 213-233

[22] van Ommen, J.R., Schouten, J., Coppens, M.O., van den Bleek, C.M., Monitoring Fluidization by Dynamic Pressure Analyis, *Chemical Engineering Technology.* 22 (1999) 9, 773-775

[23] Schouten, J.C., van den Bleek, C.M., Monitoring the Quality of Fluidization Using the Short-Term Predictability of Pressure Fluctuations, *AIChE Journal.* 44 (1998) 1, 48-60

[24] van Ommen, J.R., Coppens, M.O., van den Bleek, C.M., Schouten, J.C., Early Warning of Agglomeration in Fluidized Beds by Attractor Comparison, *AIChE Journal.* 46 (2000) 11, 2183-2197

[25] Chaplin, G., Pugsley, T., Winters, C., Application of chaos analysis to pressure fluctuation data from a fluidized bed dryer containing pharmaceutical ganule, *Powder Technology.* 142 (2004) 110-120

[26] Bénoni, D., Briens, C.L., Baron, T., Duchesne, E., Knowlton, T.M., A procedure to determine particle agglomeration in a fluidized bed and its effect on entrainment, *Powder Technology.* 78 (1994) 33-42

[27] Tsjujimoto, H., Yokoyama, T., Huang, C.C., Sekiguchi, I., Monitoring particle fluidization in a fluidized bed granulator with an acoustic emission sensor, *Powder Technology.* 113 (2000) 88-96

[28] Villa Briongos, J., Aragón, J. M., Palancar, M. C., Fluidised bed dynamics diagnosis from measurements of low frequency out-bed passive acoustic emission, *Powder Technology.* 162 (2006) 145-156

Chapter 4. Evaluation of the spray stability on liquid injection in gas-solid fluidized beds by passive vibrometric methods

Garret Book, Katherine Albion, Lauren Briens, Cedric Briens, Franco Berruti

4.1. Introduction

For many gas solid fluidized bed operations, gas atomized liquid feed is injected via spray nozzles. These injections can be used to introduce feedstocks or coolants to different chemical reactors such as gas-phase polymerization reactors and fluidized catalytic cracking (FCC) units [1-6].

In 2008, the production of synthetic crude oil produced in fluid coking units by Syncrude Canada Ltd. accounted for approximately 15% of all oil production in Canada [1]. In these units, bitumen is mixed with steam in order to atomize it and disperse it throughout the bed by injection nozzles. The efficiency and rate of cracking is dependent on the liquid-solid contact within the unit which in turn is highly dependent on the effectiveness of liquid dispersion from the initial injection [3].

In almost all cases, a stable or non-pulsating spray with a controlled droplet size is considered optimal for reactor operation as this avoids large liquid-solid agglomerates which settle to the bottom of the reactor, potentially causing a catastrophic loss of fluidization or "bogging" [3,4].

The objective of the current research was to compare spray performance and stability, using a variety of sensors and advance analysis, in both open air and fluidized bed conditions.

4.2. *Literature Review*

From examination of the literature, there are two main strategies used to investigate nozzles: a direct investigation of their spray performance by measuring the contact between solids and liquids in the bed or by measuring their stability, recognizing that this is a critical factor in ensuring good liquid solid contact in the fluidized bed.

4.2.1. Spray Performance

Spray performance is generally measured in terms of droplet size distribution, liquid distribution and stability of the spray (i.e. pulsations in the flow). Spraying into open air and spraying into fluidized beds of solids are required to fully investigate spray performance. Both are required because in open air the droplet size and stability can be measured and in a fluidized bed the liquid distribution can be measured. In many studies [1, 3, 4, 6], there are a series of experiments both in open air and in the fluidized beds.

A basic way of evaluating spray performance uses high speed video or images in open air tests [3-7]. This allows for the spray expansion angle to be measured using optical algorithms [6]. While imaging techniques are relatively easy, translating the results to fluidized bed experiments can be difficult.

Ariyapadi et al. [4] used an X-ray observation technique to validate their model of the entrainment of solids in the gas-liquid jet within a fluidized bed. This observation technique visually showed the spray jet interacting with the solids in the bed in the way predicted by the model.

House et al. [5] used a tracer approach to determine the dispersion of liquid in a fluidized bed. A sugar solution in water was injected into the fluidized bed after a small injection of *n*-propanol to allow the spray to stabilize. The *n*-propanol sprayed into the bed first to allow the flow to fully develop and then evaporated quickly. The gas velocity was brought just below fluidization velocity and allowed to dry, finally the bed was emptied and the sieved. House et al [5] found that the sugar had formed bridges so the solids were trapped in granules of different sizes and by measuring the mass of sugar in these granules, it was possible to calculate the liquid to solid ratios providing a rating of the dispersion of nozzles.

Knapper et al. [8] used a more advanced technique in a fluid coking pilot plant. Copper naphthenate dissolved in bitumen was injected into the pilot scale hot coker unit. The coke particles were sampled during the injection and were analyzed offline by Inductively Coupled Plasma (ICP) to evaluate the gross concentration of copper left on the coke particles. Energy dispersive X-ray (EDX) determined the surface coating of copper on individual particles. This method was successful at differentiating between high and low performance spray nozzles. High performance spray nozzles have a stable spray with a well atomized liquid phase.

A temperature tracer technique has also been used to evaluate liquid dispersion of nozzles. In order to compare the local solid-liquid mixing of a free spraying nozzle and the same nozzle with a draft tube in a fluidized bed, McMillan et al. [9] sprayed cold ethanol into a fluidized bed and then used a series of fast response thermocouples at various lengths along the jet and radial positions from the center of the jet to measure the temperature. Theoretically if mixing was perfect the temperature should be the same all throughout the jet. However, McMillan et al. [9] found that this was not the case even though the presence of a draft tube increased the local liquid solids mixing.

Portoghese et al. [6] used multiple novel techniques to investigate the effect of varying gas to liquid ratio, liquid mass flow rate and nozzle size on the contact efficiency of the spray. In open air, a laser was passed through the gas-liquid jet onto a photocell target. The signal attenuation was defined as the difference between the value of the undisturbed signal (when there was no spray) and the average of the signal calculated over a steady state spray. Automatic computer algorithms calculated the spray expansion angle. Portoghese et al. [6] tested these same nozzles in a gas fluidized bed of silica sand. A triboelectric probe was made by inserting a steel tube into the bed opposite the nozzle and electrically isolating it from the metal walls of the bed. When particles contacted the probe, they became triboelectrically charged creating a current in the probe. This current was amplified, converted to a voltage and recorded. When wet particles contacted the probe, there was a different charging effect due to their different surface properties. The

signal was compared to a reference signal in order to develop a nozzle performance index (NPI) validated previously with temperature measurements.

To improve the technique developed by Portoghese et al. [6], Leach et al. [10] added a defluidization step after spraying which allowed for wet agglomerates to settle as well as allowing charged solids in the bed return to an charge neutral state more slowly. This provided a more distinctive signal to be analyzed. Leach et al. [1] further improved on his method by adding an active voltage to the probe rather than relying on passive tribocharging. In this way, it was possible to calculate the effective resistance and conductance of the fluidized bed. The initial distribution of the water in the bed was highly correlated with the conductance of the bed and a new nozzle performance index was calculated. Leach et al. [1] also examined nozzle performance in open air using a Malvern Mastersizer to evaluate the size distribution of the droplets; the droplet size had a strong impact on solid liquid contact when the droplet size was significantly larger than that of the solids.

Using a patented Phase Doppler Particle Analyzer (PDPA), Rahman et al. [11] fully characterized the atomization of nozzles in open air. Using Stokes, Reynolds and Weber numbers, the spray was characterized at many distances from the tip of the nozzle both axially and radially. This method is impressive in that it can define the size and velocity of droplets at many locations within the gas liquid jet.

The literature has focused on the performance of nozzles based on liquid to solid contact efficiency in fluidized beds and compared it to measurements in open air such as droplet size distribution, laser attenuation or spray dispersion angle. While this approach successfully determined nozzle performance, it cannot be applied to many industrial beds.

4.2.2. Spray Stability

Generally, stable spray is defined as a spray that is non-pulsating with a controlled droplet size [3]. Ariyapadi et al. [3] correlated spray stability coefficients calculated from a static pressure transducer upstream of the nozzle to a triboelectric probe downstream of a nozzle located inside a fluidized bed of solids. In open air tests, the stability of the nozzle spray determined with a static pressure transducer correlated with acoustic results, measured by a microphone encased in copper and placed directly in the spray. Ariyapadi et al. [3] showed that upstream measurements could be used to evaluate downstream characteristics.

A patent filed by Cody et al. [12] was on the upstream monitoring of nozzles on industrial cokers at Exxon for controlling flow rates. Accelerometers and dynamic pressure transducers were used on the feed conduits outside industrial cokers on 2 phase feed nozzles and the signals were analyzed using fast Fourier transforms. The results were compared to a reference power spectral density at a known and correct operating flowrate.

Building on the previous two studies, Maldonado et al. [7] used an advance dynamic pressure transducer at a frequency of 2 kHz in order to evaluate nozzle stability in open air. Once again the fast Fourier transform was used to analyze the pressure signal. In this case a parameter was calculated based upon the power of the frequencies from 0 to 40 Hz where the dominant frequencies were.

4.3. Experimental Equipment and Procedure

Two different experimental set ups were used: open air test facility and fluidized bed test facility. Two sets of trials were performed in the fluidized bed test facility: One set with the bed filled with solids and fully fluidized and one set with the bed empty of solids.

4.3.1. Injection System

The injection system consisted of a gas-liquid pre-mixer, a conduit and a nozzle. The conduit is required in industrial applications to account for wall thickness, insulation and any accumulation of material on the internal surfaces, thereby ensuring that the spray is always injected into a well fluidized zone. Table 4.1 summarizes the various pre-mixers and nozzles that were tested in this study.

Table 4.1 Summary of trials

Trial	Nozzle	Gas-liquid Pre-mixer	Conditions in Open Air		Conditions in Fluidized Bed		Conditions in Empty Bed	
			Mix Gas	Air	Mix Gas	Air	Mix Gas	Air
#1	Simple Constriction -1 / Shroud	Venturi-2		√				
#2	Simple Constriction -1 / Shroud	BFC-1		√				
#3	Simple Constriction -1 / Shroud	BFC-2		√				
#4	Simple Constriction -1 / Shroud	Venturi-1			√	√		
#5	Simple Constriction -1	Venturi-2		√				
#6	Simple Constriction -1	BFC-1		√				
#7	Simple Constriction -1	Venturi-1		√	√	√		
#8	Snake Head	Venturi-1		√	√	√		√
#9	Snake Head	BFC-1		√				
#10	TEB-1	Venturi-2		√		√		√
#11	TEB-1	Venturi-1		√	√	√		√
#12	TEB-1	BFC-2		√				√
#13	TEB-1	BFC-1		√	√	√		√
#14	TEB-2 / Shroud	Venturi-2				√		
#15	Simple Constriction-2	Venturi-2				√		
#16	TEB-2	Venturi-2				√		

4.3.1.1. Pre-mixers

There were two basic types of gas-liquid pre-mixers where the atomization gas was mixed the pressurized water before flowing down a conduit to the nozzle. The bilateral flow conditioner (BFC) was the simplest pre-mixer. Pipes for the atomization air and pressurized liquid entered a mixing chamber at an angle in the direction of flow. The two injection ports were located 90 ^{o} from each other along the circumference of the mixing chamber. At the end of the mixing chamber there was a contraction to reduce the diameter to the nozzle conduit diameter of 1 inch (0.0254 m). There were two sizes for each type of pre-mixer.

4.3.1.2. Nozzles

Three basic types of nozzles and one shroud design were investigated: i) Simple constriction nozzle ii) TEB nozzle iii) Snake head nozzle. The simple constriction nozzle constricted the flow of the liquid and atomization gas causing a two-phase jet to form into the open air or fluidized bed. The angles of decrease in this constriction as well as the final outlet diameter are design parameters of this nozzle. For the TEB nozzle, as the two phase flow enters the nozzle, it passes through a fast constriction followed by a slow expansion and finally through another constriction to form the two phase jet. The angles of these constrictions and expansions as well as their final diameters can be changed. For the snake head nozzle, rather than straight angles the flow was constricted with a cone with concave sides. Additionally the two phase jet of a nozzle could be changed with a special shaped shroud.

4.3.2. Open Air Nozzle Test Facility

Nozzles were tested in the open air nozzle test facility (Figure 4.1). The facility was constructed from aluminum pipe in a rectangular prism and encapsulated with transparent plastic sheeting. A liquid drain was located in the center of the facility to allow sprayed water to accumulate and empty.

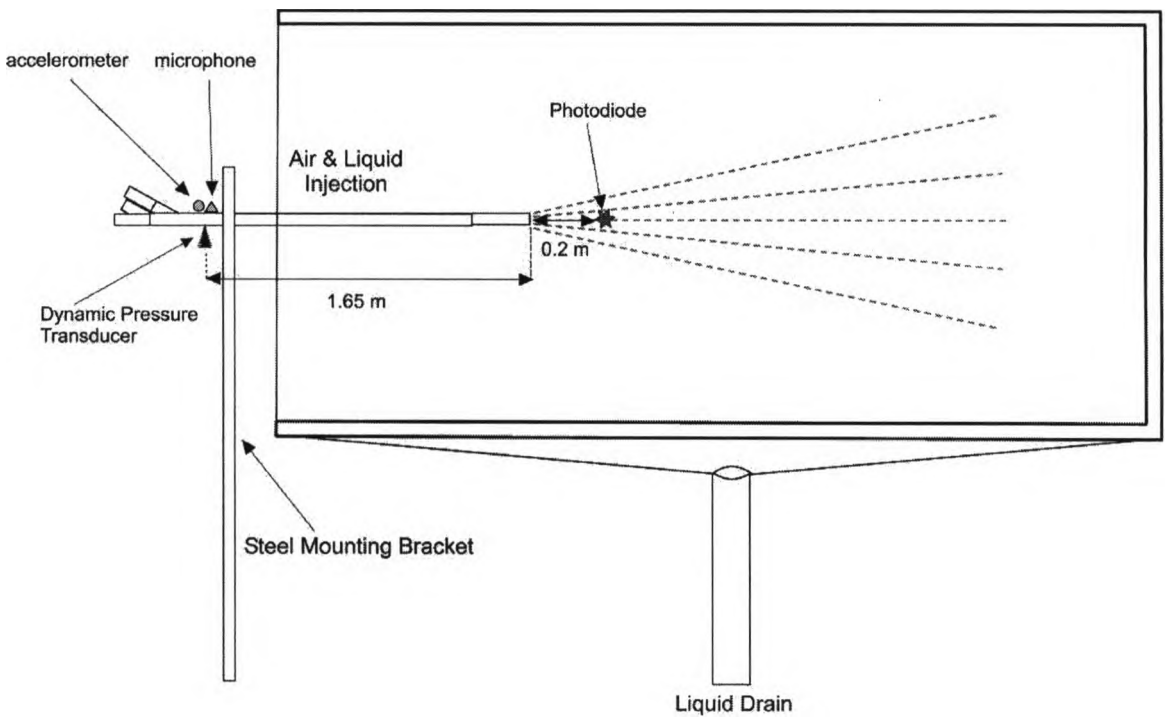

Figure 4.1 Open air nozzle test facility for nozzle stability – Side View

The nozzle and gas-liquid pre-mixer assembly were mounted such that the nozzle tip extended approximately 1 m into the facility. The nozzle injected de-ionized water from a pressurized tank. Nitrogen combined with medical air was used as the atomization gas. The steel mounting bracket (Figure 4.1) was made of the same thickness steel as the walls

of the fluidized bed. A port hole was cut into the bracket exactly as for the fluidized bed. This mounting ensured that the nozzle assemblies were secured in the same way for both the open air and the fluidized bed trials.

A prepolarized microphone was mounted 1.65 m from the tip of the nozzle facing vertically downward, flush with the conduit (Figure 4.2). A uni-directional accelerometer was mounted to the conduit in the same orientation as the microphone 2.5 cm closer to the gas-liquid pre-mixer. A high frequency dynamic pressure transducer was mounted diametrically opposite from the microphone.

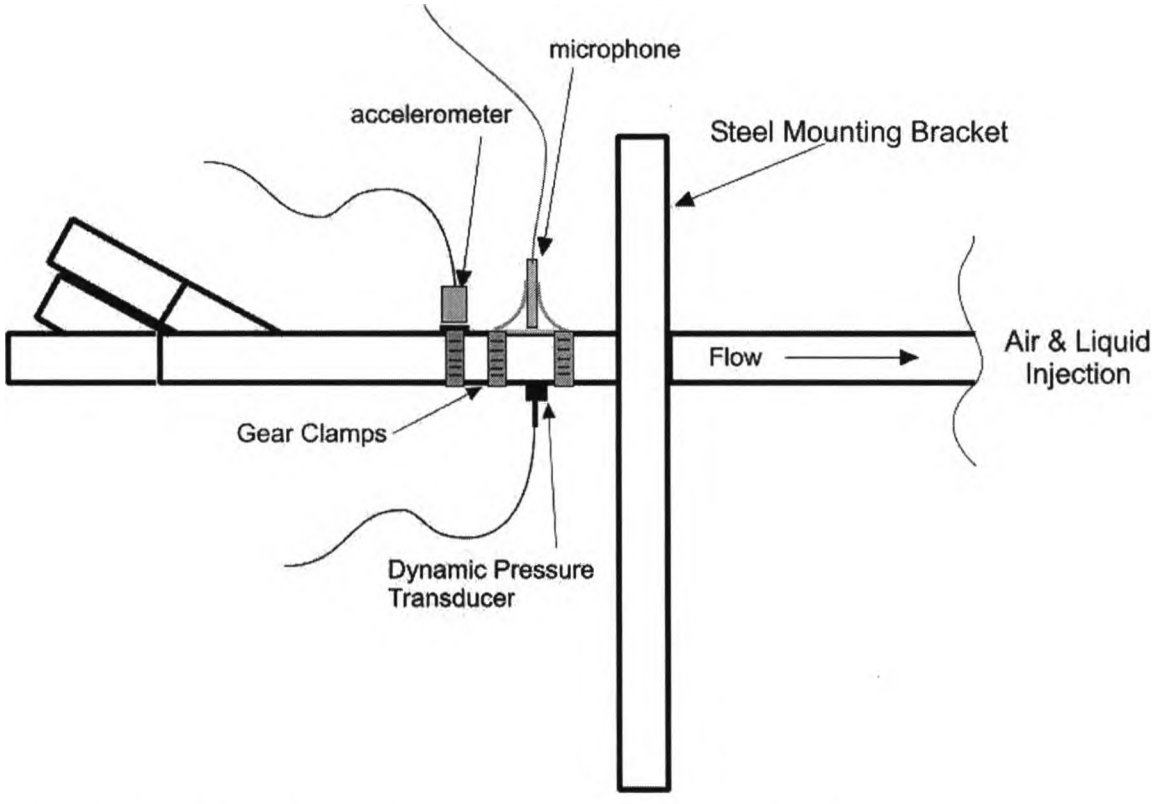

Figure 4.2 Open air test facility for nozzle stability - mounting of sensors

A laser was located 0.2 m from the tip of the nozzle in the open air facility, mounted such that the beam passed through the center of the spray and then into the photodiode target

located directly across the nozzle test facility (Figure 4.3). The photodiode produced differing voltages depending on the intensity of light transmitted through the spray.

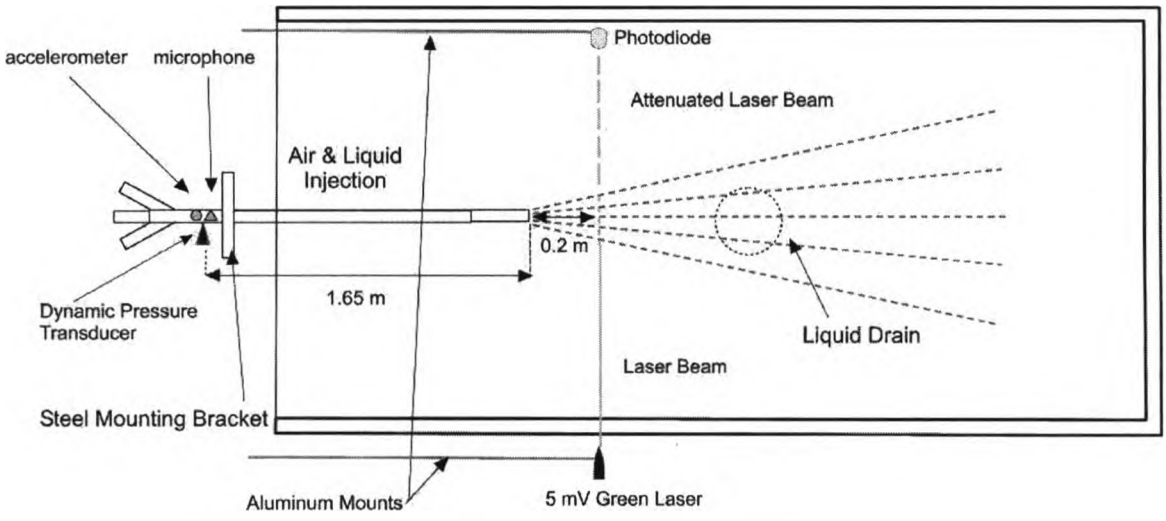

Figure 4.3 Open air nozzle test facility for nozzle stability - top view

For all trials, 21 L of water was sprayed into the facility. For the standard experiment of an air to liquid ratio by mass (ALR) of 2 %, this corresponded to a velocity of 4.5 m/s and spray time of 9.5 s. For some trial a gas mixture of 18% Helium in Nitrogen was used at a gas to liquid ratio by mass (GLR) of 0.85%. The difference in mass ratios kept the volumetric flow constant. Table 1 summarizes the nozzle configurations and settings. During each trial the microphone, accelerometer, dynamic pressure and photodiode signals were recorded at a sampling frequency of 40 000 Hz. The signals were cropped, keeping only 8 s of stable measurements, to eliminate the measurements recorded during the unstable start and finish of the spray.

4.3.3. Fluidized Bed Test Facility

The fluidized bed was 5.6 m high and trapezoidal shaped with a 0.2 m wide short end and a 1.2 m wide long end. The bed was fluidized by air, with a constant temperature of approximately 22 °C and relative humidity of 15 %. The air entered through a windbox at the bottom of the column and was distributed via a perforated plate distributor. Fines entrained in the fluidization gas were separated using a series of cyclones followed by a bag house filter. The solids in the bed were sand, Barco 71, supplied by Optma mineral. The sand had a Mohs hardness of 7, was resistant to grinding, inert and maintained its initial properties throughout the experiments. The sand had a Sauter mean diameter of 150 μm and d_{p50} of 212 μm, a specific gravity of 2650 kg/m^3 and a bulk density of 1590 kg/m^3.

The industrial nozzle and pre-mixer assembly were inserted approximately 1 m into the bed, 0.9 m above the grid plate as shown in Figure 4.4. For each trial, 21 L of water was injected into the fluidized bed or sprayed into the empty bed. For most trials, the atomization gas was a mixture of nitrogen and air. For selected trials (4, 7, 8, 11 and 13), the atomization gas was mixture of 18 % helium and 82 % nitrogen to investigate the effect of gas properties on stability and performance. This mixture was used because it was found to have similar properties to that of the steam used in fluid coking units. The mixed gas to liquid flow ratio by mass (GLR %) was 0.85 %. Due to the difference in the molecular mass in gases, this ensured that injection velocity, injection time and volumetric flow rate were maintained between air trials and mixed gas trials. Table 4.1 summarizes the trials.

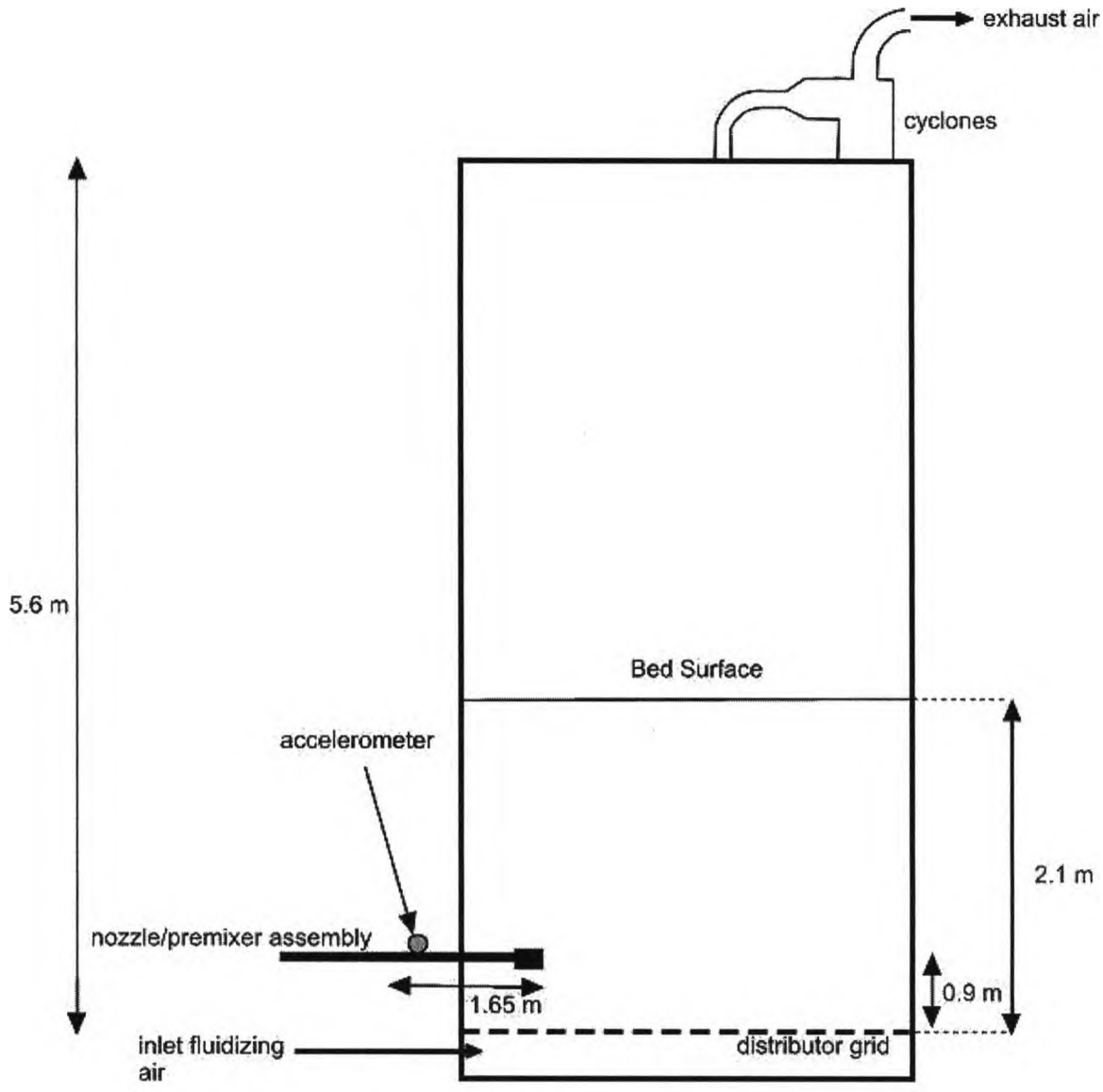

Figure 4.4 Pie shape fluidized bed apparatus for nozzle testing

Figure 4.4 shows the nozzle and premixing assembly and the location of the accelerometer. For each trial, accelerometer measurements were recorded at a sampling frequency of 40 kHz.

4.4. Results & Discussion

4.4.1. Open Air Test Facility

Measurements were made using the microphone, accelerometer, dynamic pressure transducer and photodiode. Figure 4.5 shows examples of these recordings for Trial #11. Measurements from the microphone and accelerometer were similar. Fluctuations in the pressure transducer measurement appeared to be slower and the magnitude of the photodiode measurements was very small.

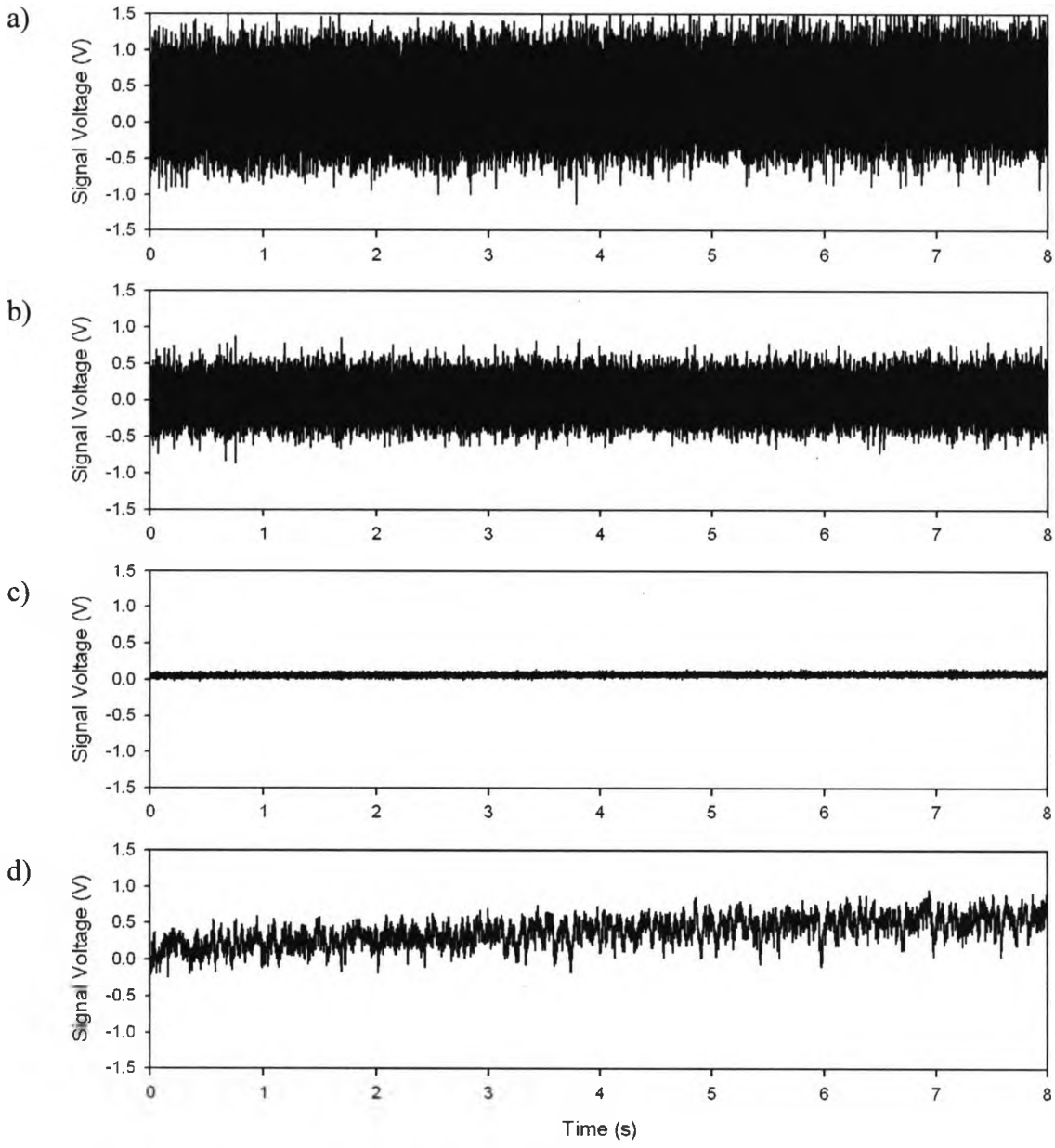

Figure 4.5 Measurements with (a) microphone (b) accelerometer (c) photodiode and (d) dynamic pressure transducer for Trial #11 in the open air facility.

Wavelet analysis divides a signal into *m* multiple levels or scales corresponding to a frequency band. Due to the halving effect of the frequency at each level the scales can further be defined as octaves. The frequency correspondingly decreases with the octaves. For each octave, using a Debauchies 4 wavelet, the signal was separated into two parts: the averages and the coefficients. The coefficients of the signal indicate the fluctuations of the signal at the specified octave. The standard deviation of these coefficients indicates the variability of the fluctuations of the signal within an octave of frequency band.

The fluctuations of the coefficients in the 17^{th} octave (10 – 20 kHz) were summarized by calculating the standard deviation of the coefficients. Figure 4.6 shows the standard deviation of the coefficients in the 17^{th} octave from photodiode measurements. The greater the size and numbers of fluctuations in the spray, there will be more and larger fluctuations in the signal. Therefore, the largers the standard deviation of the coefficients, the less stable the spray.These measurements and analysis separated the trials into three groups:

i) Trials 8 and 11 had low standard deviations that indicated a very stable spray,

ii) Trials 1,5,10 and 13 had intermediate values and intermediate spray stabilities

iii) Trials 2, 6, 9 and 12 had high standard deviations indicating low stabilities.

The trials in the open air facility used a range of nozzle and pre-mixer combinations. Photodiode measurements and analysis classified these combinations as providing high, intermediate and low stability sprays. These groups showed that, in the open air trials, the pre-mixer had a significant effect on the spray stability. A high spray stability was

obtained with a venturi-1 pre-mixer. With the exception of Trial 13, intermediate spray stabilities were obtained with a venturi-2 pre-mixer and low stabilities were obtained with BFC pre-mixers. The type of nozzle had no significant effect on the spray stability in open air trials.

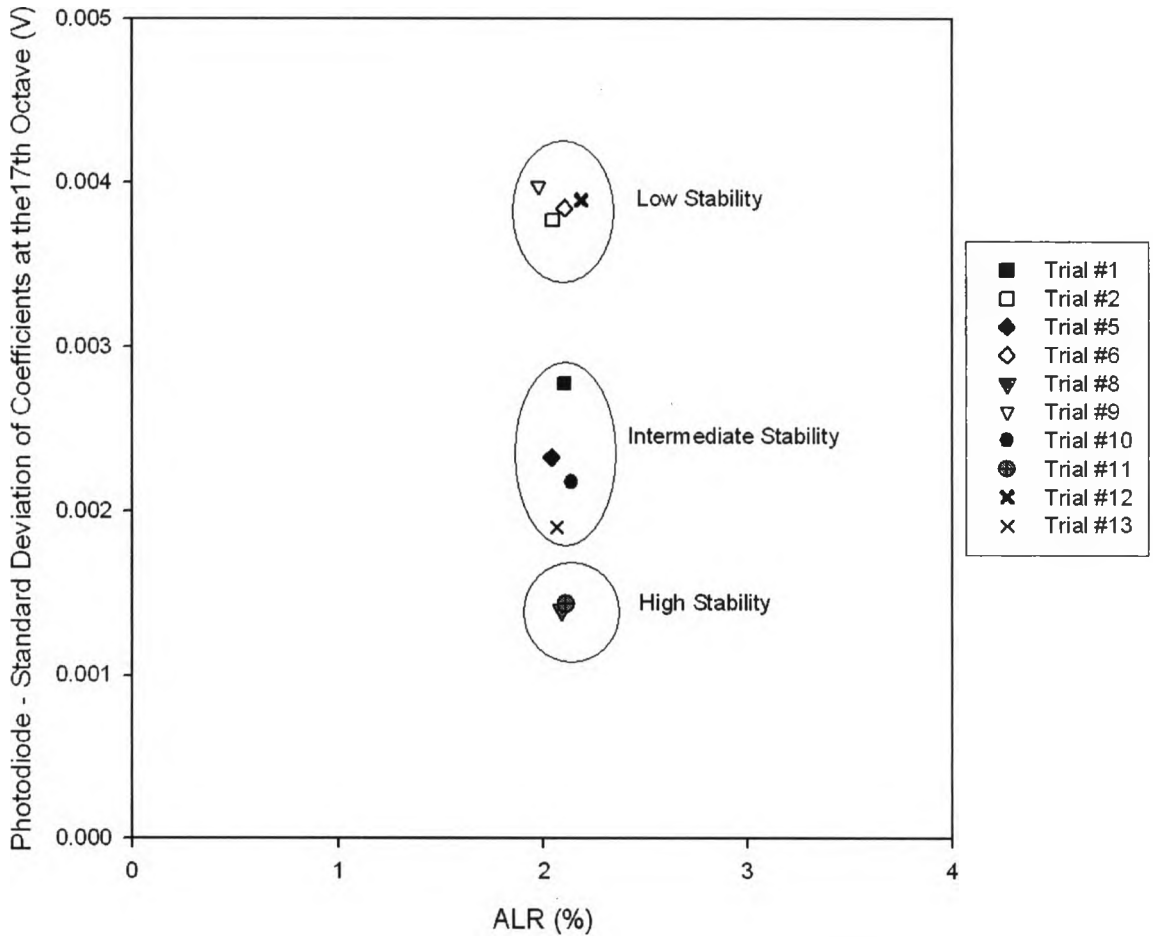

Figure 4.6 Standard deviation of coefficients within the 17th octave (10 – 20 kHz) for the photodiode in the open air test facility.

The photodiode allowed direct measurement of the spray stability. Photodiode measurements, however, cannot be made in a fluidized bed. Therefore, microphone, accelerometer and dynamic pressure transducer measurements were also made in the open air test facility to develop correlations with the photodiode measurements. Figures

4.7 – 4.9 show the correlations between the standard deviation of the wavelet coefficients in the 17^{th} octave from the photodiode measurements with the standard deviation of the wavelet coefficients in selected octaves from the dynamic pressure transducer, microphone and accelerometer measurements, respectively. Only the comparison with the accelerometer (Figure 4.9) provided a positive correlation with the photodiode measurements of spray stability. From the accelerometer measurements, a standard deviation of wavelet coefficients below 0.03 indicated highly stable sprays, between 0.03 and 0.065 indicated intermediate spray stability and above 0.065 corresponded to low spray stability.

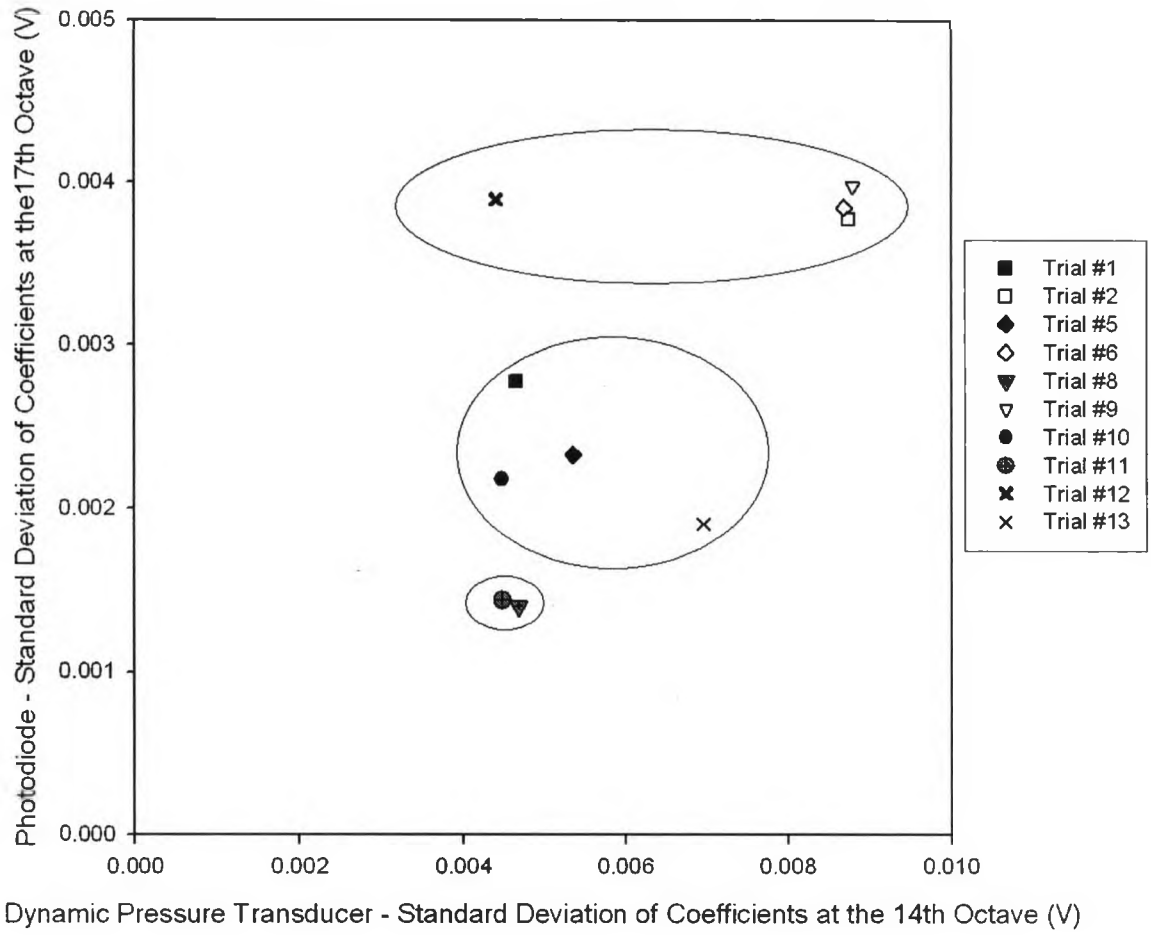

Figure 4.7 Correlation between the photodiode at the 17th octave (10 – 20 kHz) and the dynamic pressure transducer at the 14th octave (1.25 – 2.5 kHz).

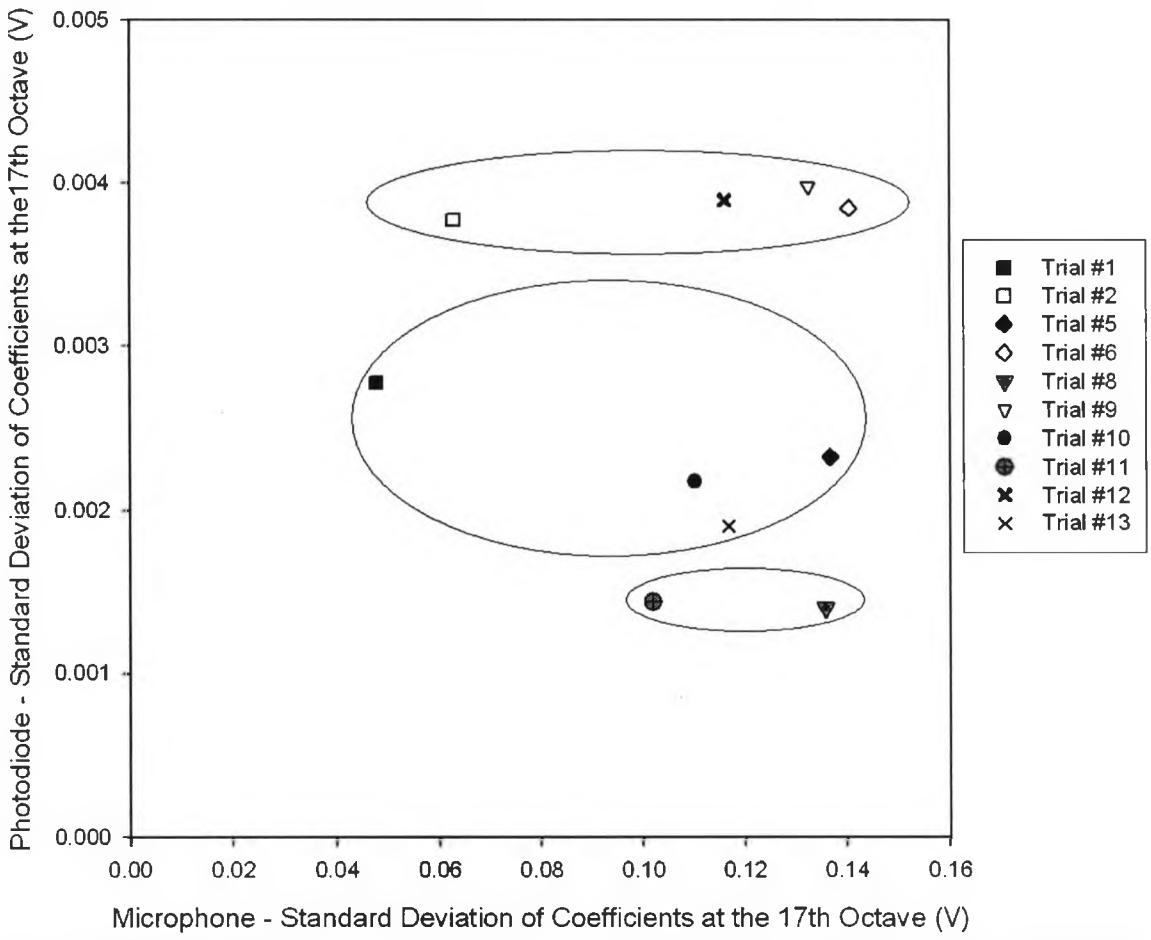

Figure 4.8 Correlation between the photodiode at the 17th octave (10 – 20 kHz) and the microphone at the 17th octave (10 – 20 kHz).

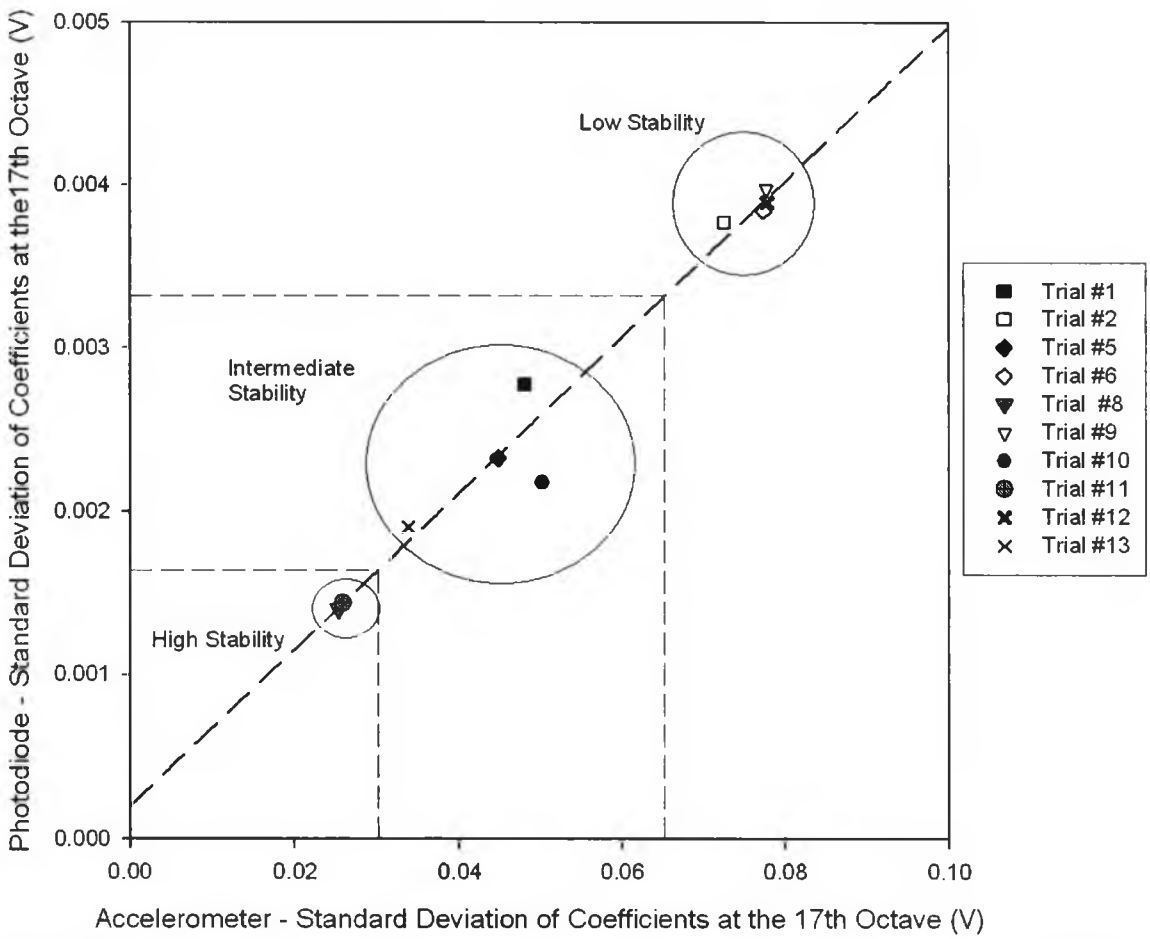

Figure 4.9 Correlation between the photodiode at the 17th octave (10 – 20 kHz) and accelerometer at the 17th octave (10 – 20 kHz).

4.4.2. Fluidized Bed

It was impractical to implement the laser-photodiode system on the fluidized bed as it was unlikely the laser could penetrate the emulsion phase of the bed. The dynamic pressure transducer did not show a good correlation to the physical measurements of the laser-photodiode in open air. Therefore, the accelerometer measurements and correlations developed in the open air test facility were applied to the fluidized bed. Figure 4.10 shows the standard deviation of wavelet coefficients at the 17th octave from the accelerometer on the nozzle conduit in the fluidized bed. Similar to the open air

results, the accelerometer provided a method to evaluate spray stability with enough resolution and sensitivity to differentiate between nozzle and pre-mixer assembly combinations. The stability ratings of the various nozzle and pre-mixer assembly combinations, however, were different from the open air ratings. For example, Trial 10 which consisted of a TEB-1 nozzle with a venturi-2 pre-mixer, was rated as highly stable in the fluidized bed but only intermediately stable in the open air. The results from the fluidized bed trials showed that the pre-mixer did not have a significant effect on the spray stability as the same pre-mixer could contribute to either a high or intermediate spray stability rating.

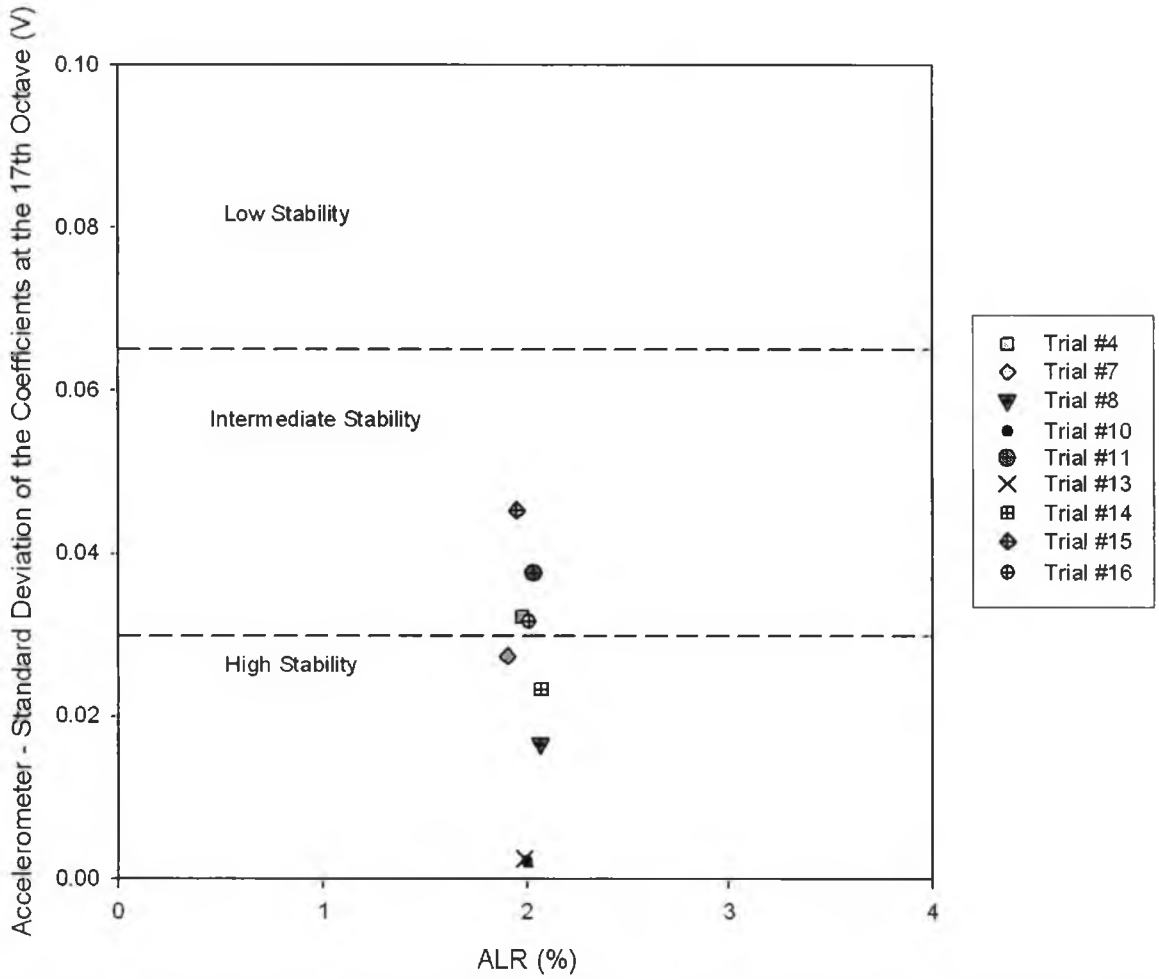

Figure 4.10 Standard deviation of coefficients at the 17th octave (20 kHz) for the accelerometer in the fluidized bed.

4.4.3. Open air stability versus Fluidized bed stability

The spray stability ratings changed from the open air test facility to the fluidized bed test facility. Since the results from the open air facility correlated well to an independent physical measurement, two possible reasons for the differences were proposed: (i) a change in measured stability as a result of additional fluctuations from the fluidization or (ii) the measurements were affected by the mounting of the nozzle/pre-mixer assembly. To determine the effect of fluidization on the spray stability, the bed was emptied of solids and trials were repeated, spraying into the empty bed rather than the fluidized bed.

Figure 4.11 shows the standard deviation of the wavelet coefficients in the 10 – 20 kHz band from the accelerometer measurements for the open air, fluidized bed and empty bed trials. In general, this standard deviation decreased from the open air to fluidized bed to the empty bed trials. Although the movement of the fluidized bed would have caused movement on the end of the inserted nozzle, the more secure mounting of the nozzle/pre-mixer assembly in general decreased the fluctuations from movement measured by the accelerometer compared to the open air trials. Removal of the fluidized solids further decreased the measured fluctuations.

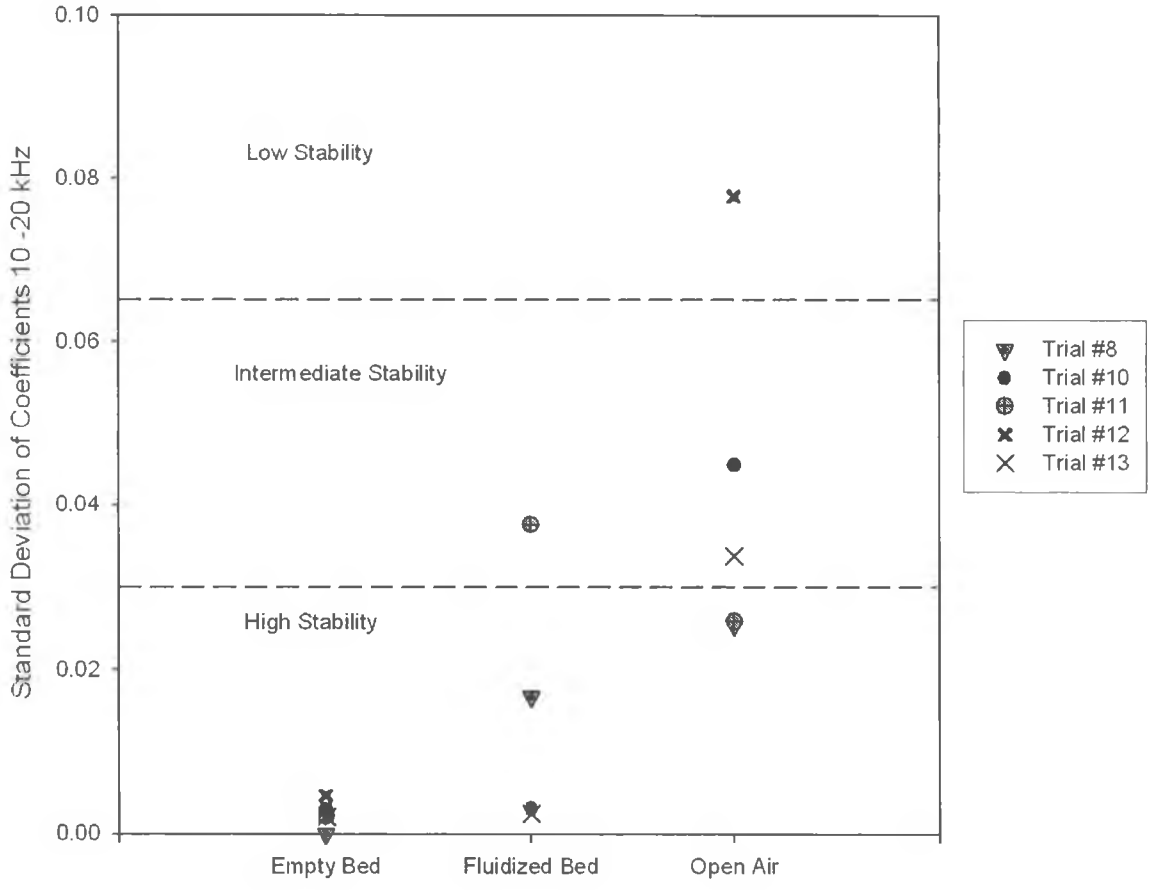

Figure 4.11 Comparison of spray stability results dependent on apparatus used in testing. Spraying into open air, fluidized bed or de-fluidized empty bed

All of the trials conducted in the empty bed indicated highly stable nozzle/pre-mixer assembly combinations. Differences in the trials could not be identified; Figures 4.12 and 4.13 further compare the results from the open air, fluidized bed and empty bed trials.

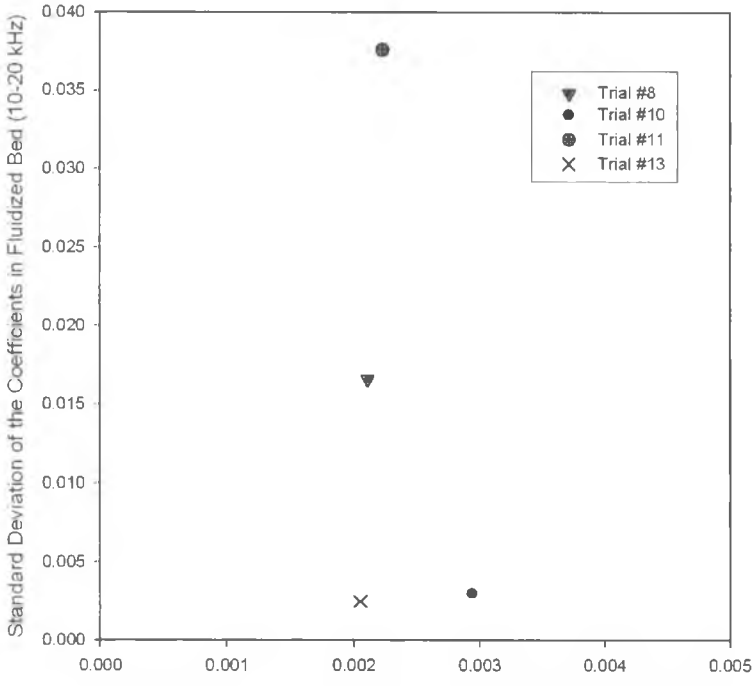

A)

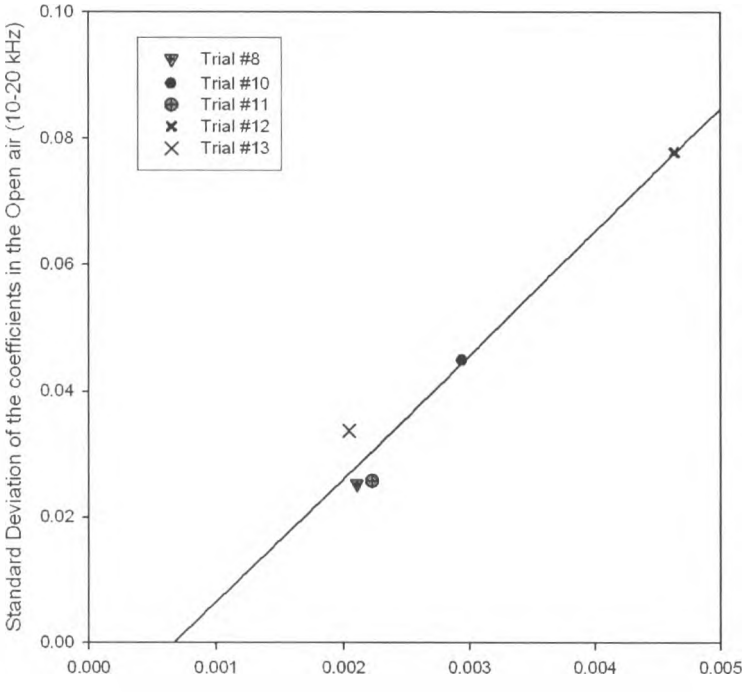

B)

Figure 4.12 Relationship between the measured spray stability in the empty bed and the a) Fluidized bed; b) Open air test facility

Figure 4.12a shows that the empty bed and the fluidized bed results are independent of each other. Figure 4.12b shows that measured stability in the open air test facility and in the empty bed are strongly correlated. This indicates that fluidization significantly affects measurements of spray stability. The vibrations of the bed created due to the fluidization are measured by the accelerometer on the conduit disrupting the accelerometers ability to evaluate stability. The accelerometer is capable of indicating spray stability in the open air, but when the nozzle and pre-mixer assembly is put directly into the fluidized bed the measurements are dominated by the vibrations due to fluidization.

All of the measurements were normalized by the average standard deviation. Figure 4.13 shows that this normalization allowed comparisons of the spray stability rankings for the open air, fluidized bed and empty bed trials. The ranking was almost identical for the open air and empty bed trials.

The boundary lines between high and intermediate stability and intermediate and low stability were also calculated based on the average standard deviation coefficients in the open air. This allowed for the spray stabilities determined in the fluidized and empty bed trials to be grouped according to their stability.

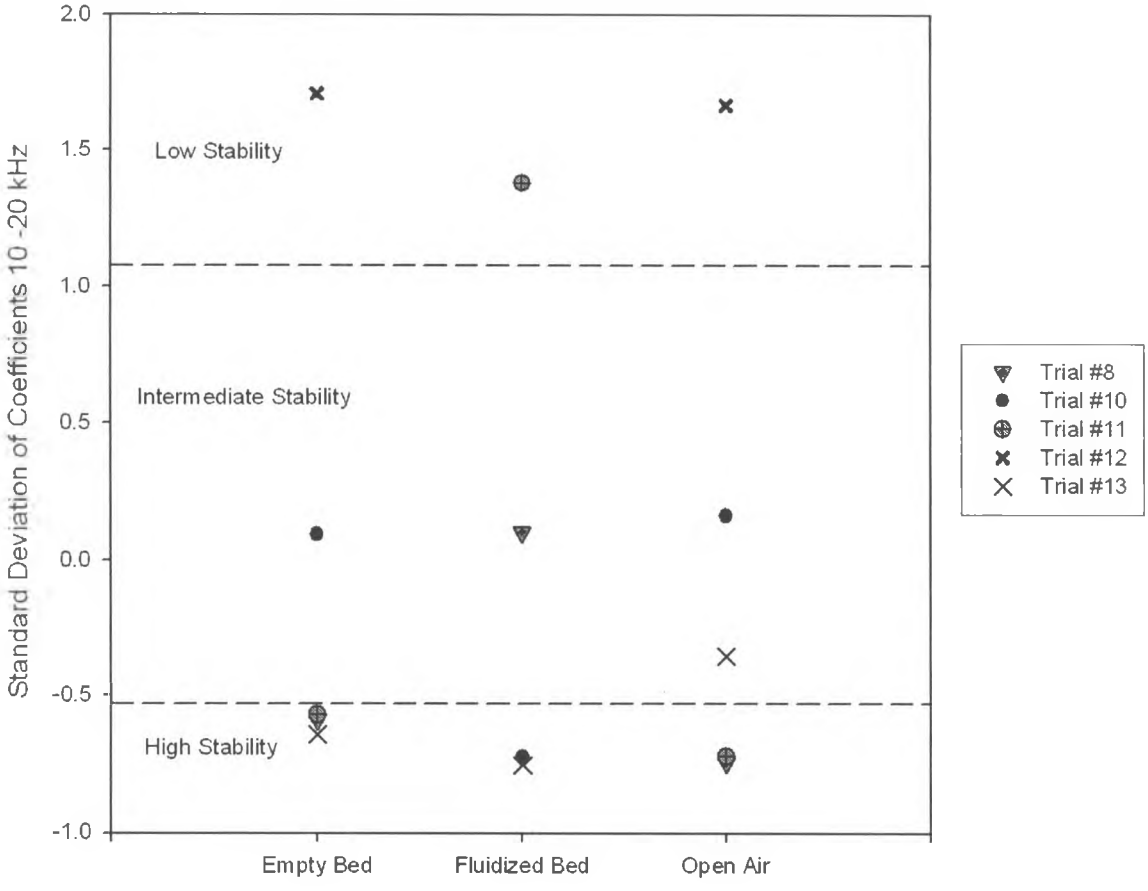

Figure 4.13 Normalized comparison of spray stability results dependent on apparatus used in testing. Spraying into open air, fluidized bed or de-fluidized empty bed

4.4.4. Applicability of the technique

Figure 4.14 shows a flow diagram of the connections between the results from the open air, fluidized bed and empty bed trials.

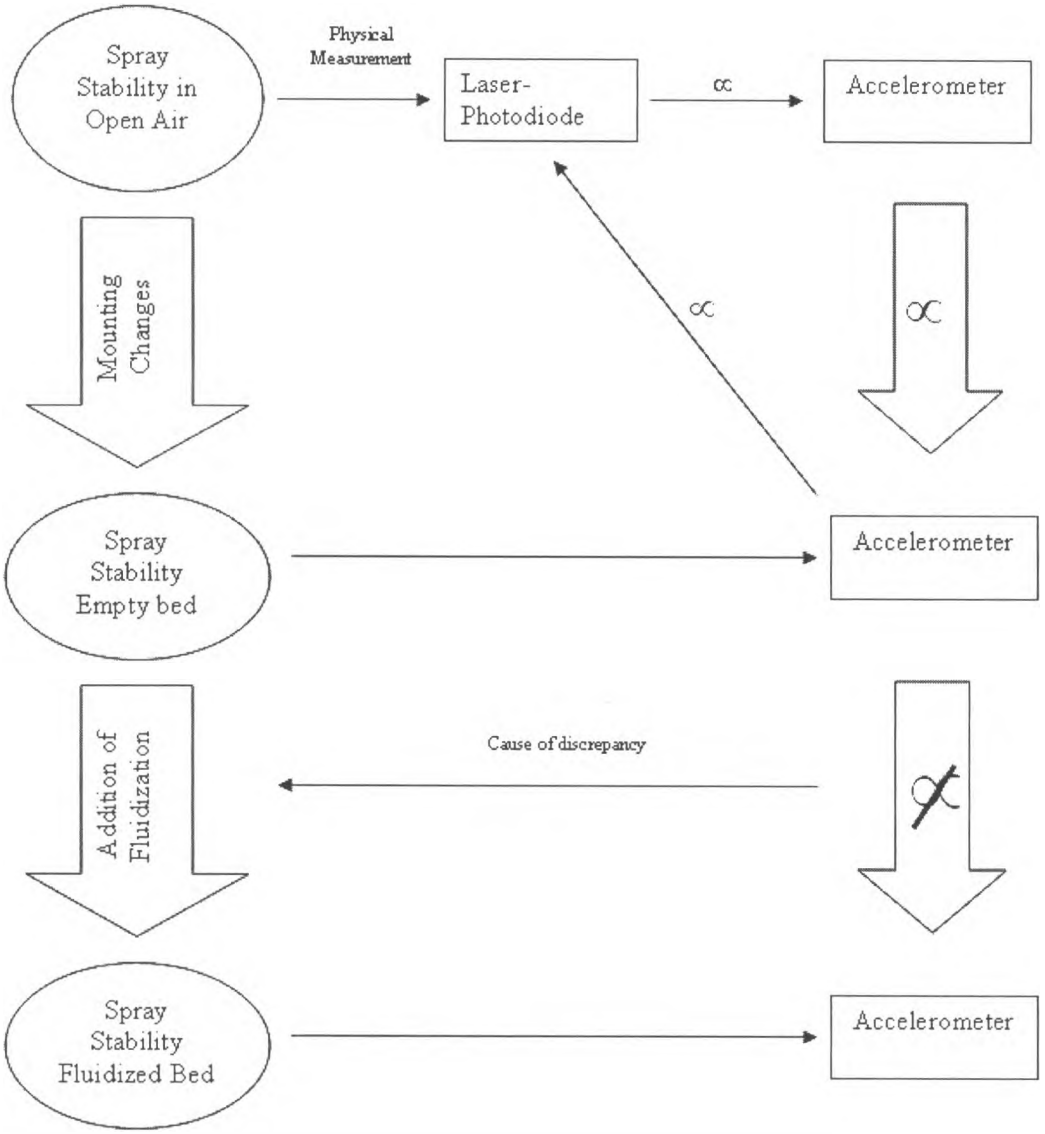

Figure 4.14 Flow diagram of relationships between results of the 3 apparatuses

The results demonstrate that the measured spray stability in the fluidized bed was not related to the measured stability from the open air or empty bed trials due to fluidization. This limits the calibration of accelerometers in open air trials for later measurement of stability in a fluidized bed. If, however, fluidization is kept relatively constant, then the accelerometer measurements could be used to evaluate relative spray stability.

4.4.5. Effect of Air to Liquid Ratio

One of the most common changes in the operation of a nozzle/pre-mixer assembly is the air to liquid ratio (ALR), whether this is due to overpressure of atomization gas or a sudden increase or decrease in liquid supply. Figure 4.15 shows the effect of ALR on spray stability in both the open air test facility and in the fluidized bed. As the ALR increased, all nozzle and pre-mixer configurations showed a decrease in stability. As the ALR increased, the velocity of flow increases and the pseudo-viscosity of the two phase flow decreased, resulting in a higher Reynolds number and more turbulent, unstable fluid flow. The relationship between ALR and stability is not constant.

Figure 4.15 shows that the relationship between the spray stability and ALR is dependent upon the nozzle/pre-mixer assembly combination. For example, Trial #10 in the open air facility, showed a linear relationship with a lower slope than the other trials. Trial #10 combined a TEB-1 nozzle with a venturi-2 pre-mixer. The venturi-2 pre-mixer had small atomization gas ports and a small diameter throat which significantly affected the pressure drop and therefore the spray stability.

A)

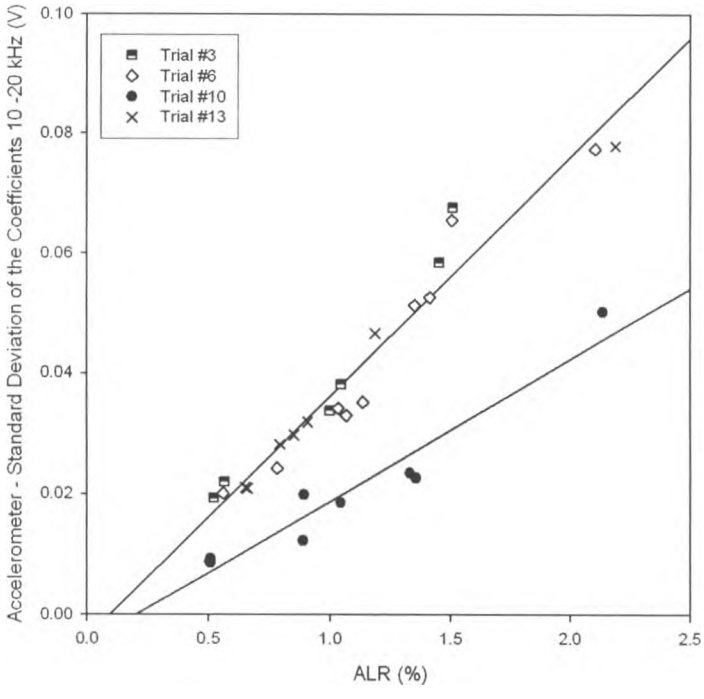

B)

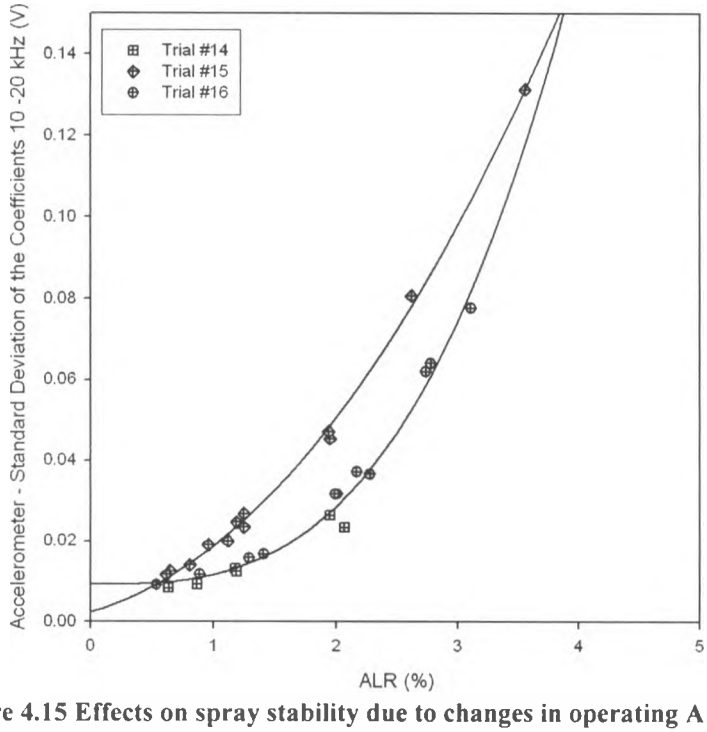

Figure 4.15 Effects on spray stability due to changes in operating ALR A) Open Air Trials B) Fluidized Bed Trials

4.4.6. Mixed gas study

Often industrial nozzles will use high temperatures or pressures with steam for atomization and heavy oil as a fluid. In these cases, the properties of air, water and pure nitrogen do not represent the operational reality of the equipment. Therefore, trials were performed with an inert helium/nitrogen gas mixture in the fluidized bed. This mixed gas was found to exhibit similar fluid properties as steam at operational temperature and pressure allowing for better estimation of spray stability in industrial applications.

In previous trials, ALR was calculated by finding the ratio mass flow rate of atomization air to mass flow rate of liquid. Since the mass of helium is much lighter than air, using the same gas to liquid mass ratios would result in different injection velocities and characteristics. Therefore, for mixed gas runs, the GLR was calculated using similar volumetric gas to liquid ratios.

Figure 4.16 shows that the trials with air, water and nitrogen underestimated the spray stability. This indicates that selection of atomization gas for testing of nozzles/pre-mixers is crucial. When a nozzle/pre-mixer combination is being tested, the ideal situation would have the tests use the same atomization gas in the tests as in the potential application. If using the same atomization gas is difficult or impossible, it is important to use a gas with similar properties. This will prevent over or under estimation of the stability of nozzle/pre-mixer combinations due to atomization gas properties.

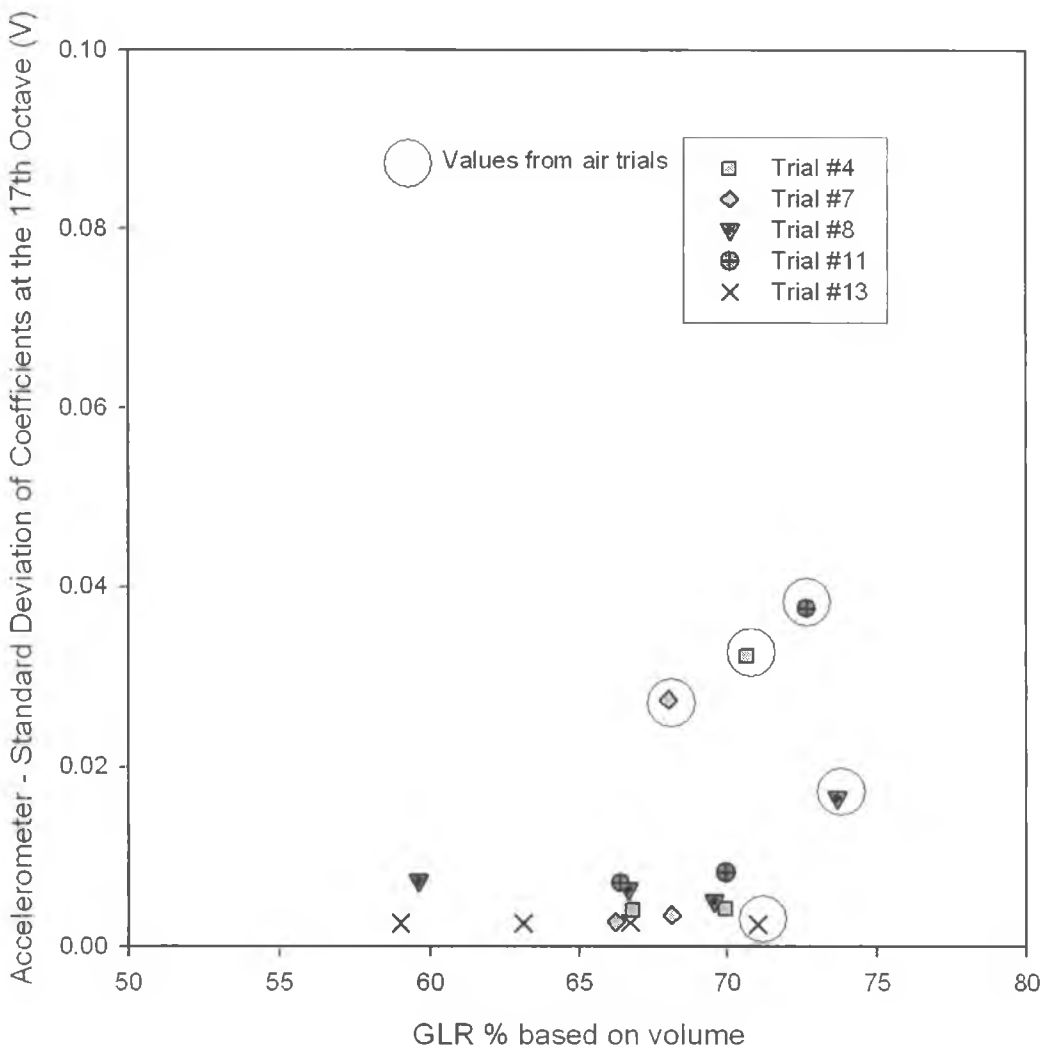

Figure 4.16 Effects of gas to liquid ratio on the spray stability in a fluidized bed

4.5. Conclusions

Novel methods of monitoring spray stability were investigated and correlated to independent methods of measuring stability. Accelerometers on the conduit after the gas-liquid pre-mixer were able to measure spray stability using advanced signal analysis techniques. A series of industrial sized nozzles and gas-liquid pre-mixers were tested in an open air test facility, a fluidized bed of solids and an empty fluidized bed. It was demonstrated that the fluidization in a reactor has strong effects on the measured spray

stability through the introduction of vibrations not related to the two phase flow in the conduit leading up to the nozzle. The effects of gas to liquid ratio and atomization gas properties were investigated and comparisons were drawn between the results in the open air test facility and fluidized bed.

4.6. Acknowledgments

The authors would like to acknowledge the help of Dr. Gareth Chaplin on the equipment and adapting his scheduled experiments to incorporate our needs. The authors would like to thank Syncrude Canada Ltd. for both their funding and their advice. Thanks to NSERC, OGS and OGSST for their funding of this work.

4.7. Symbols

C Energy of the signal (units)

f Frequency, (Hz)

F Maximum frequency, (Hz)

G_{bed} Bed conductance, (Siemens/mhos)

I current, (ampres)

L Local Intermittency index, (units)

m Positive integer, number of level in a wavelet decomposition of a signal, (-)

n Positive integer, number of points in a series or signal, (-)

p Power at a given frequency, (-)

R_1 Resistor used in the active conductivity circuit, (kΩ)

R_{bed} Bed resistance, (kΩ)

t time, (s, min)

U_g Superficial gas velocity, (m/s)

V_{app} Applied voltage, (Volts)

V_m Measured voltage, (Volts)

Greek symbols

α Noise index of the signal, (units)

β Linear constant, (units)

μ Mean of a series or signal, (units)

σ Standard deviation, (units)

4.8. References

[1] Leach, A., Chaplin, G., Briens, C., Berruti, F., Comparison of the permformance of liquid-gas injection nozzles in a gas-solid fluidized bed. *Chemical Engineering and Processing: Process Intensification.* 48 (2009) 780-788

[2] Briens, C., McDougall, S., Chan, E., Online Detection of Bed Fluidity in a fluidized bed coker. *Powder Technology.* 138 (2003) 160-168

[3] Ariyapadi, S., Berruti, F., Briens, C., Knapper, B., Skwarok, R., Chan, E., Stability of Horizontal Gas-Liquid Sprays in Open-Air and in Gas-Solid Fluidized Bed. *Powder Technology.* 155 (2005) 161-174

[4] Ariyapadi, S., Berruti, F., Briens, C., Griffith, P., Hulet, C., Modeling the Injection of Gas-Liquid Jets into Fluidized Beds of Fine Particles. *The Canadian Journal of Chemical Engineering.* 81 (2003) 891-899

[5] House, P., Briens, C., Berruti, F., Chan, E., Effect of spray nozzle design on liquid-solid contact in fluidized beds. *Powder Technology.* 186 (2008) 89-98

[6] Portoghese, F., Ferrente, L., Berruti, F., Briens, C., Chan, E., Effect of injection-nozzle operating parameters on the interaction between a gas-liquid jet and a gas-solid fluidized bed. *Powder Technology.* 184 (2008) 1-10

[7] Maldonado, S., Fleck, B., Heidrick, T., Amirfazli, A., Chan, E., Knapper, B., Development of an Experimental method to evaluate stability of gas-liquid sprays. *Atomization and Sprays.* 18 (2008) 699-722

[8] Knapper, B., Chan, E., Gray, M., Mikula, R., Meauserment of Efficiency of Distribution of Liquid Feed in a Gas-Solid Fluidized Bed Reactor. *International Journal of Chemical Reactor Engineering.* 1 (2003) A35

[9] McMillan, J., Zhou, D., Ariyapadi, S., Briens, C., Berruti, F., Characterization of the contact between Liquid Spray Droplets and Particles in a Fluidized Bed. *Industrial Chemical Engineering Res.* 44 (2005) 4931-4939

[10] Leach, A., Portoghese, F., Berruti, F., Briens, C., A new and rapid method for the evaluation of the liquid-solid contact resulting from liquid injection into a fluidized bed. *Powder Technology.* 184 (2008) 44-51

[11] Rahman, M., McMillan, J., Hiedrick, T., Fleck, B,. Charactering the Two-phase, Air/Liquid Spray Profile Using a Phase Doppler Particle Analyzer. *14th Int Symp on Applications of Laser Techniques to Fluid Mechanics*, Lisbon, Portugal, 07-10 July, 2008

[12] Baker, C., Cody, G., Joseph, C., Sela, U,. Acoustic Monitoring of Two-Phase Feed Nozzles. US Patent 5 004 152, 1991

Chapter 5. General Discussion and Conclusions

This research investigated novel sensors and advanced signal analysis techniques for monitoring fluidized beds and associated spraying processes. It was divided into three chapters: Chapters 2 focused on the use of triboelectric probes for the monitoring of fluidization and drying while investigating the effect of vibration on both. Chapter 3 focused on the use of passive sensors (accelerometers and microphones) for the monitoring of fluidization quality. Two microphones were placed on the outside wall of the fluidized bed and an accelerometer was placed on a rod simulating an industrial thermocouple to correlate sensor measurements with the measured median avalanche time from samples from the bed. Chapter 4 developed non-intrusive methods to evaluate spray stability through correlation of measurements from an accelerometer, a microphone and dynamic pressure transducer to the physical measurements of a laser-photodiode system.

5.1. Chapter 2 – Triboelectric Probes

Three triboelectric probes were installed in a small, vibrating fluidized bed of solids in order to investigate the effects of vibrations on fluidization and drying. Both pressure and bed height were recorded.

It was found that minimum bubbling velocity and minimum fluidization velocity decreased with increasing vibration. A critical vibrational amplitude was observed such that with higher amplitudes minimum fluidization velocity was not affected.

Using advanced signal analysis and multi-linear regression, a bubbling index was developed to detect bubbles using triboelectric probes. This allowed the triboelectric probes to be used to monitor the level of fluidization in the bed.

Triboelectric probes were also used to monitor drying and determine the effect of vibration on drying. Vibration greatly accelerates the drying of fine powders by breaking up wet agglomerates.

5.2. Chapter 3 - Fluidization Quality

Two microphones were installed on the wall of a large fluidized bed of silica sand and an accelerometer was attached to a rod simulating an industrial thermocouple for fluid coking. To change the fluidization quality in the bed, water was injected either through industrial sized nozzles or a small scale laboratory nozzle. The acoustic signals from both microphones and the vibrometric signal from the accelerometer were all extensively analyzed using wavelets and Fourier transforms to identify trends in the signals over time. Samples of solids from the bed were characterized for moisture content and the flowability (through avalanche properties). Using either multi-linear or power law regression, it was possible to identify the wavelet and frequency parameters in the acoustic or vibrometric signals which correlated to the flowability and therefore fluidity of the bed.

The accelerometer mounted on the rod was the most accurate sensor for predicting median avalanche time. Unlike the microphones directly on the wall, the rod was in

direct contact with the fluidized solids in the bed, directly transferring vibrations to the sensors. Thermocouples are commonly installed on industrial cokers and therefore the external attachment of an accelerometer to a thermocouple would not require any intrusive modifications to a unit.

Errors in the predicted mean avalanche time were high immediately following the injection of water into the fluidized bed. At this time, the bed solids were not fully mixed such that samples removed from the bed did not truly represent the entire bed. Eliminating sensor measurements from the first 10 minutes of fluidization the therefore reduced the prediction errors dramatically. The mixing time of the bed was calculated by determining the time at which the predicted error reduced to a low and stable level.

5.3. Chapter 4 - Spray Stability

Spray stability is a common way to rate and select nozzles for applications. The stability of industrial sized coking nozzles and gas-liquid pre-mixers were investigated both in an open air test facility and in a fluidized bed of silica sand.

Signals from an accelerometer, a microphone and a dynamic pressure transducer, all on conduits leading up to the nozzles were compared to signals from a laser-photodiode system through the spray. Using wavelet analysis it was possible to correlate the stability of the spray calculated by the laser-photodiode system to the measurements of the accelerometer upstream of the nozzle. In the open air the gas-liquid pre-mixer had a dominant effect on spray stability.

Using the method developed in the open air test facility, nozzle and pre-mixer combinations were retested in the fluidized bed. The results did not agree with those in open air. By emptying the fluidized bed and retesting, it was found that spraying into the empty bed was similar to spraying into open air; vibrations from fluidization affected the measurements in the fluidized beds.

The accelerometer could not therefore be calibrated in open air to measure the spray stability in fluidized beds. However, the accelerometer was capabable of simple detection of malfunction or sputtering of the flow.

In both open air and in fluidized bed trials it was found that, as the gas or air to liquid ratio was increased, the spray stability decreased. Additionally, it was found that the gas properties of the atomization gas affected the measured spray stability.

5.4. Overall Conclusions

The results presented in this thesis demonstrate the potential uses for triboelectric probes, passive acoustic and vibration measurements combined with advanced signal analysis as monitoring tools for industrial gas fluidized beds of solids.

The monitoring methods investigated and developed in this thesis would compliment methods used currently for the monitoring of fluidized beds and would be easily implemented and economically viable.

5.5. Acknowledgements

The authors would like to thank Syncrude Canada Ltd. for both their funding and their advice. Thanks to NSERC, OGS and OGSST for their funding of this work.

Appendix 1. Detection of drying end point in a large gas-solid fluidized bed by passive acoustic and vibration methods

Garret Book, Katherine Albion, Lauren Briens, Cedric Briens, Franco Berruti

A 1.1 Introduction

The fluidized bed is one of the most widespread technologies used in industrial drying operations. Fluidized bed dryers are prevalent in pharmaceutical, food, fertilizer and energy industries, as well as many other chemical industries where drying or wet granulation of solid materials is required [1]. They are used to dry a very diverse set of products such as coal, biosynthesis products, pharmaceutical granules and food stuffs [2].

Drying of these products is of critical importance. The under drying of foodstuffs can affect the way a product tastes, as well as the amount time it takes to spoil. Pharmaceutical granules are turned to tablets for consumption. The way pharmaceutical granules are dried affects the granule size distribution and moisture content which in turn affects crucial properties of the tablets produced (e.g. hardness, friability, disintegration time, etc) [2]. Coal particles tend to contain a considerable amount of moisture in thermal power stations and can require drying. If the coal is not dry and flowable, it can cause creates a series of major problems during transport [3].

The rapidly moving solids in a fluidized bed affords good solids mixing and creates a large surface area between the solids and drying gas for heat and mass transfer to occur.

This shortens the required time to dry the product without damaging heat sensitive materials by raising the temperature. Additionally, the fluidized solids can be moved easily in and out of the dryer via gravity and transported by pneumatic transport. The high rates of heat and mass transfer as well as high rates of solids transport to and from fluidized beds make them and important addition in industrial drying operations [2].

Despite the advantages of using fluidized beds for drying, there are several difficulties associated with fluidized bed drying. Generally, there is a requirement of both laboratory and pilot-plant trials to estimate performance of industrial units as there is a lack of reliable mathematical models for fluidized bed driers. This renders the development and scale up of fluidized bed dryers for an application more expensive. Another issue is that the fluidization quality in the beds is degraded when the particles are cohesive or difficult to fluidize. The moisture content itself tends to make the particles more cohesive [2]. Raising the fluidization gas velocity can help improve fluidization. However, higher fluidization velocities can cause several undesirable phenomena such as particle entrainment and attrition [2, 4].

Daud [2] produced a review of recent advances in fluidized bed dryer that aimed to alleviate these problems. Daud [2] reviewed two areas: 1) various mathematical models which could be applied to scale up and, 2) external means of improving fluidization via vibration, agitation, rotation and centrifugation. The mathematical models for these innovative types of fluidized beds are not well developed however both vibrated and agitated beds have been used successfully in industry [2].

Successful monitoring of fluidized bed drying is crucial. Monitoring of drying is of critical importance as under drying can cause early spoilage of product, reduce product quality and make the solids have low flowabilty making them more difficult to transfer. Over drying can result in particles which are more prone to attrition and static charging. Additionally over drying can lead to the thermal degradation of the product [1].

A monitoring system for the determination of drying end point should ideally be reliable, easy to implement, non-intrusive, low cost and applicable to a wide range of operating conditions. Passive acoustic and vibration methods have the potential to satisfy all of these requirements [5]. Additionally, preliminary studies have shown that, with advanced signal analysis, passive acoustics and vibrations can be correlated to the fluidization quality of a fluidized bed of particles [6].

In situations where bulk solids are dried specifically to improve flowability (e.g. transport of coal [7]) it desirable to determine the flowability of the solids directly as the moisture content can be misleading. This is because the relationship between moisture and flowability changes with both how much moisture is present and the method of distribution.

The objective of this study was to investigate passive acoustic and vibration methods for the reliable monitoring of drying through flowibility and detection of the drying end point in a large, industrial size fluidized bed.

A 1.2 Literature Review

Various methods to identify the drying end point have been developed. In most cases, these methods are based on the solids moisture content rather than the solids flowability.

Alden et al. [8] developed a working model for the determination of moisture content via temperature difference. They assumed that the temperature of the moist solids in the bed was equivalent to the temperature read by a wet-bulb thermometer operating in similar conditions. Measuring the instantaneous temperature difference between the temperature of the solids and the wet bulb temperature that would be measured for a saturated sample when heated by the drying air, provided the moisture content of the sample. A specific temperature difference was identified for the system by taking frequent samples and calibrating with the measured moisture content. There are two problems with this approach:

3) With wet beds, it would be impossible to achieve fluidization if moisture was uniformly distributed on the surface of the bed particles, since the particles would be too cohesive for proper fluidization. In reality, most of the moisture is trapped within agglomerates or granules whose surface is relatively dry. The surface temperature of an agglomerate is affected not only by its average moisture but also by heat and mass transfer within the agglomerate.
4) The temperature measured by a thermocouple immersed in a fluidized bed is an unknown combination of the fluidization gas temperature, the dry particles temperature and the surface temperature of the wet agglomerates.

In wet granulation a binder liquid is added to constituent powders which agglomerate to form granules. In the pharmaceutical industry these wet granules need to be dried to a specific moisture content. This is so they have appropriate properties to be turned into tablets. Therefore a great deal of research has gone into determining the drying end point of pharmaceutical granules. As some of these monitoring methods can be applied to other solids, it makes the literature extremely relevant.

Watano et al. [9] used the fact that wet granules have different infrared (IR) absorption characteristics than dry granules to develop infrared moisture sensors. These sensors were used to monitor the drying of lactose and cornstarch granules although the IR absorption characteristics were not specifically calibrated to moisture content. Other works built on these results by calibrating near IR absorbtion to the moisture content measured by Karl-Fischer titration, a volumetric titration where water is reacted with a base. The technique was capable of monitoring in real time so that process conditions could be altered to improve product characteristics and reliability [10-12].

Räsänen et al. [13] used near infrared (NIR) to study the influence of process parameters in the dehydration behaviour of two pharmaceutical solids, wet theophylline granules and disodium phosphate. It was found that three carefully selected wavelengths from NIR absorption spectra were sufficient to indicate the moisture content of the solids.

Wildfong et al. [14] and Morris et al. [15] used the NIR technique to successfully accelerate drying by appropriate monitoring and control. This was accomplished by

initially setting the inlet air temperature above the melting point of the pharmaceutical product. In the first part of drying the evaporative cooling protects the product, then, as the NIR identified a critical moisture content where evaporation can no longer cool the product sufficiently, the inlet gas temperature is reduced to a level which is unlikely to harm the product. This managed to reduce the drying time required for most pharmaceutical products tested, demonstrating the usefulness of NIR techniques.

Unfortunately, IR adsorption can give misleading results as it is a local measurement and depends on the beds fluidization to mix the particles to give average bed moisture. In the presence of large agglomerates or poor fluidization, IR adsorption can give a result which is not the real average bed moisture. Another potential problem with IR adsorption based process control is that dust will adhere to the surface of the sensors, causing changes in the IR adsorption that are unrelated to changes in bed moisture.

Inexpensive, passive triboelectric probes were successfully used to reliably measure moisture contents down to 100 ppm and detect drying end points in fluidized beds of glass beads, ceramic microspheres and silica sand [1, 16, 17]. These probes are constructed easily by inserting a metal rod into the fluidized bed. The rod is insulated from the bed wall to prevent grounding. The impact of particles on the probe causes surface or tribo charging of the solids which results in a current through the probe. The current generated is highly dependent on the surface properties of the solids which are in turn highly dependent on the moisture content of the bed.

Portoghese et al. [1, 16] correlated the W-statistic of the triboelectric signal to the moisture content of fluidized beds of glass beads and silica sand measured via Karl-Fischer titration. Triboelectric probes have also been used with cohesive powders in a vibro assited fluidized bed to determine drying end point and to detect the breakup of wet agglomerates [17]. Interestingly, Portoghese et al. [1, 16] found that, during the drying procedure, the surface moisture of the bed particles would initially increase as the breakup of wet agglomerates overwhelmed moisture removal by evaporation. Triboelectric probes are very sensitive to any change in the surface properties of the solids or the probe surfaces. Therefore any impurities in the solids or oxidation on the sensor affects the results.

Chaplin et al. [18] calibrated capacitance tomography with X-ray tomography to study the hydrodynamics of fluidized bed drying of pharmaceutical granules. They found that capacitance tomography gave similar radial profiles to X-ray tomography on a time averaged basis. As expected, the hydrodynamics of the bed changed as the product was dried. Later, Chaplin and Pugsley [19] used the S-statistic chaotic attractor comparison method on the tomographs to indicate the solid moisture content. A reference state of 9-wt% moisture was selected. The S-statistic then compared the tomographs from a drying trial to the reference state to evaluate the statistical differences. Chaplin et al. [20] later performed S-statistic analysis on dynamic pressure signals to the same effect. Unfortunately this method could only indicate if the bed was at the reference moisture content level and could not monitor the progress of drying.

Portoghese et al [21] developed a conductance method to evaluate the solid-liquid contact after spraying water into the bed. A metal electrode with an applied voltage from a signal generator was inserted into a fluidized bed and electrically isolated from the steel bed walls. By doing this it was possible for the conductance of the bed to be measured. When water was sprayed into the bed the conductance of the emulsion phase increased showing a clear correlation between the moisture content and the measured conductance. Therefore, this technique could theoretically be used to monitor drying and identify the drying endpoint. One concern is that conductance probes are very sensitive to salt impurities as these affect the conductance of the bed.

Acoustic and vibration sensors have been investigated for the monitoring fluidization quality and fluidized bed drying. Tsujimoto et al. [22] used a single high frequency (140 kHz) passive acoustic sensor on both agitated and traditional fluidized bed granulators and found that unstable fluidization due to increases in moisture content could be monitored. Bojarra and Briens [23] investigated acoustic and vibration monitoring of fluidized bed drying of pharmaceutical placebo granules. Although passive acoustic emissions could not reliably monitor the granule moisture content, vibrations of the bed could indicate the drying a specific criterion to indentify an appropriate end point. Book et al. [6] found that by placing a microphone in the bag house exhaust above a vibrated fluidized bed of cohesive particles, it was possible to monitor the drying, including the breakup of agglomerates. In this case the audible frequency range from 0.2 – 20 kHz was the focus.

Vervloet et al. [24] recorded acoustic and vibration signals at 400 Hz in order to compare analysis techniques with pressure fluctuations, also recorded at 400 Hz. Time-domain, frequency and state-space methods were used to analyze the signals. Vervloet et al. [25] found that time-domain analysis and frequency analysis of the signals were insufficient to detect gradual changes in the process. However, it was noted that the power spectral density did change between dry and wet beds for the pressure, acoustic and vibration signals. The state-space attractor comparison method successfully detected changes in the process hydrodynamics in all 3 sensor types, however, this method could only compare the signals to a reference level.

Accelerometers and microphones are non-intrusive and reliable sensors. In contrast to invasive sensors such as thermocouples and IR adsorption probes, they do not perform local measurements but detect changes in global bed properties. Additionally they can directly measure the flowability of the solids in the bed, not the moisture content, without taking samples. This would be especially useful with large industrial beds and silos where a global measurement is needed and the flowability of the solids, not the moisture content, is of primary concern.

Hann and Stražišar [7] investigated the effects of moisture content on the flowability of milled limestone. They measured two parameters as moisture content changed: 1) the rathole index, which is the outlet diameter needed to ensure a rathole failure and clean out in a funnel flow bin and, 2) the average unconfined yield strength of a column of compressed solids. The relationship between moisture content and solids flowability was

non-linear regardless of the measurement method used. Additionally, at low moisture contents the flowability is very sensitive to small changes.

Three ways to directly measure the flowability of a solids sample are the rathole index, the unconfined yield strength and through revolutions testing. The rathole index is determined by allowing samples of powder to empty from a funnel flow bin and determine the outlet diameter where a rathole failure and clean out is ensured. The uniaxial compression test finds the average unconfined yield strength of a column of compressed solids [7]. Bojarra and Briens [24] used a relatively novel method for the characterizion of solids flowability. Samples were rotated in a transparent drum and optical algorithms were used to characterize the sample surface as it rotated. The major benefit of revolution testing over the rathole index and the compression test, is that it is automated like the compression test but the powder flows as it would normally as in the rathole test.

A 1.3 Experimental Equipment

All experiments were performed using a large fluidized bed that is shown schematically in Figures A1.1 and A1.2. The bed was 5.6 m high and trapezoidal shaped with a 0.2 m wide short end and a 1.2 m wide long end. The bed was fluidized by air with a constant temperature of approximately 22 °C and 15 % relative humidity. The air entered through a windbox at the bottom of the column and then into the bed through a perforated plate distributor. Any entrained solids were returned to the bed through a system of cyclones and diplegs. Heat exchangers within the bed provided some heat to accelerate drying.

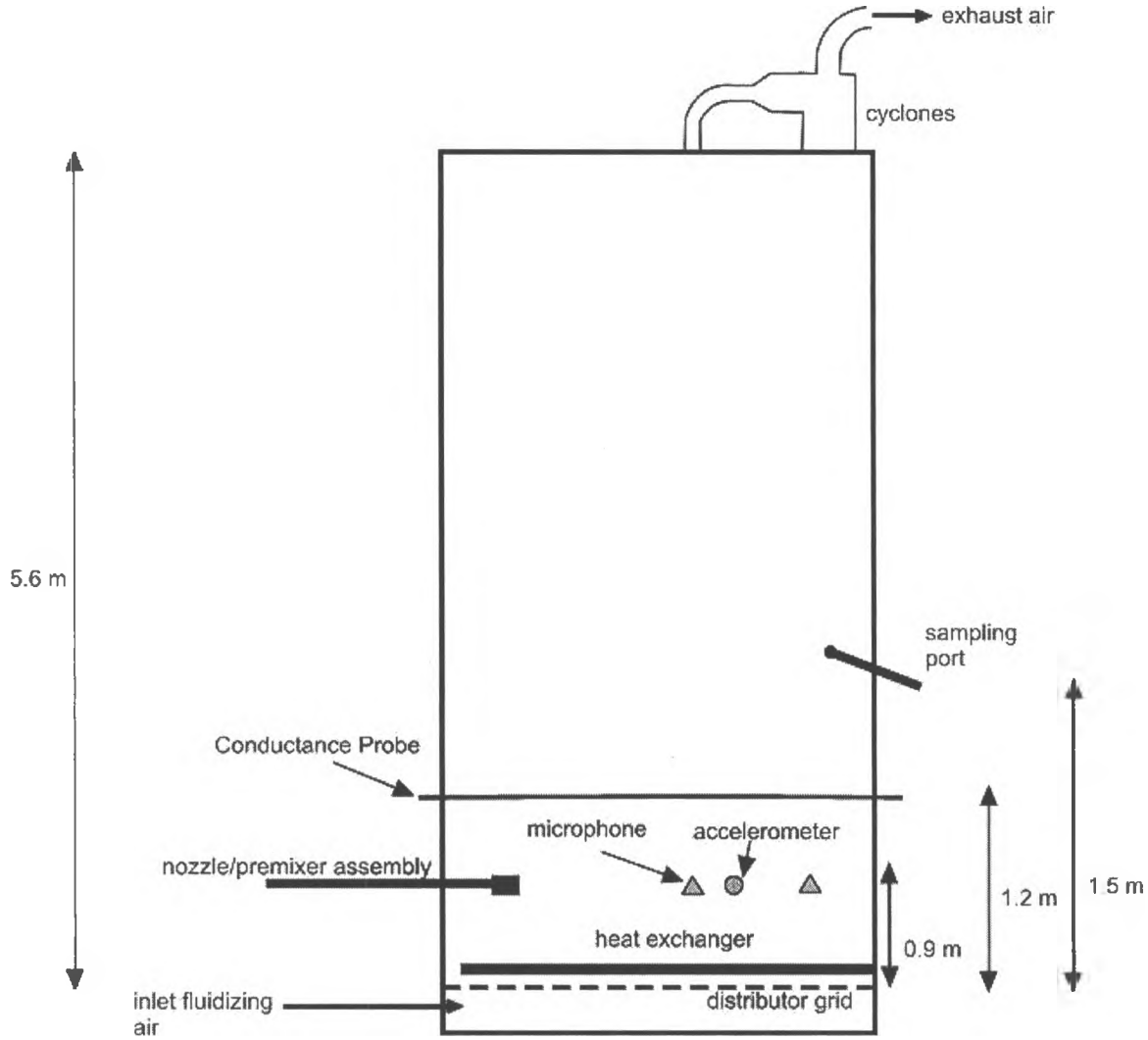

Figure A1.1 Schematic diagram of the fluidized bed, side view

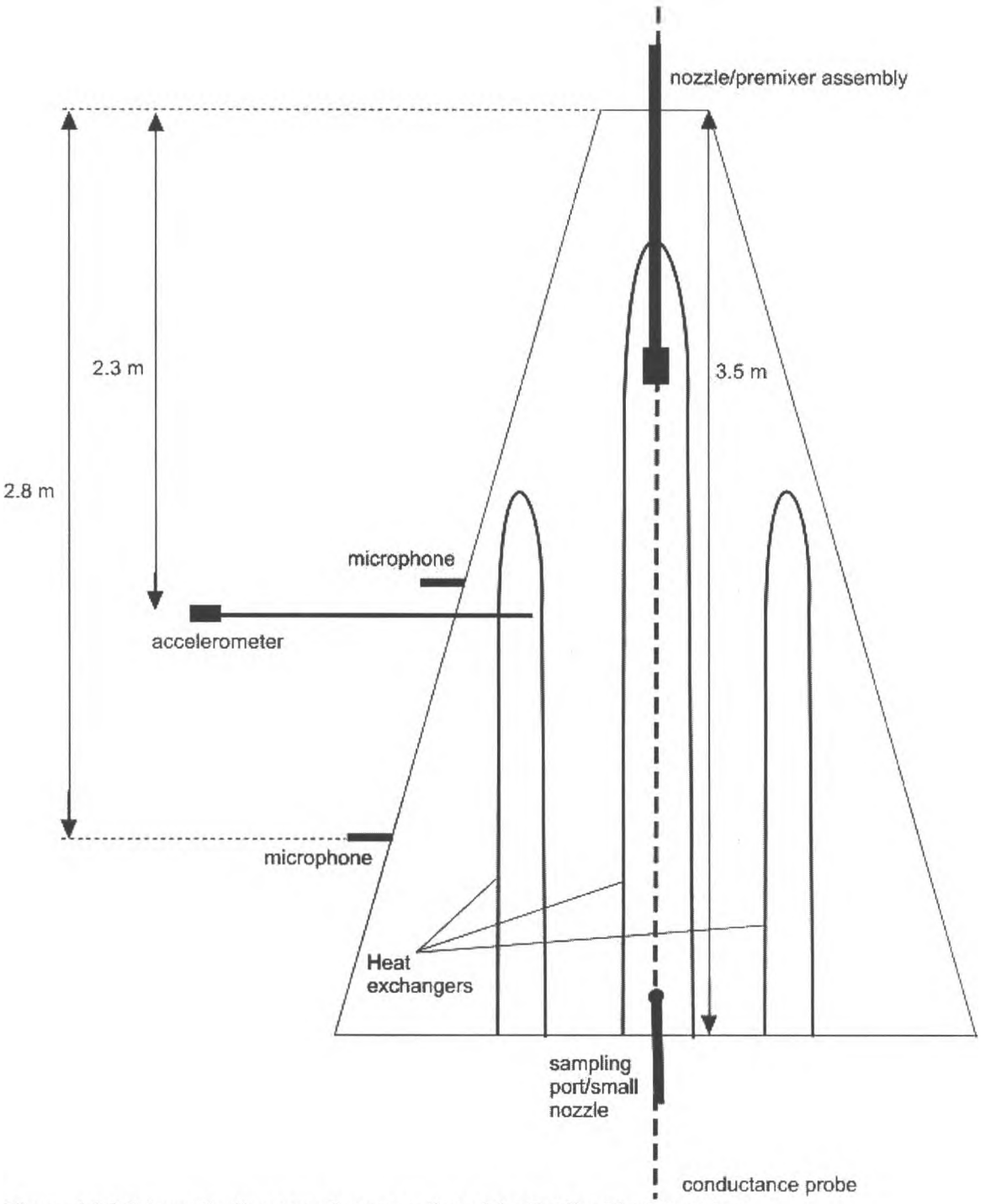

Figure A1.2 Schematic diagram of cross section of the fluidized bed, top view

About 9 tonnes of silica sand was fluidized in the bed. The sand was Barco 71 supplied by Optma mineral. The sand had a Mohs hardness of 7, was resistant to grinding, was inert and maintained its initial properties throughout the experiments. The sand had a

Sauter mean diameter of 150 μm and d_{p50} of 212 μm, a specific gravity of 2650 kg/m^3 and a bulk density of 1590 kg/m^3. The defluidized bed height was about 2 m above the distributor.

A premixer and nozzle combination were inserted 1 m into the bed and 0.9 m above the distributor grid, at the short end of the bed. The atomization gas and de-ionized water were combined in the premixer (either a venturi or bilateral flow conditioner, BFC) and then transferred through a smooth conduit before injection into the bed by the nozzle. There were two venturi pre-mixers. The venturi – 1 had a wider and longer mixing chamber as well as larger gas injection ports than the venturi – 2. The nozzles used were a TEB nozzle from Syncrude Canada Ltd, a simple constriction nozzle and a simple constrictions nozzle with a shaped shroud mounted on the nozzle tip. Table A1.1 summarizes the trials. Preliminary experiments, using samples of the bed solids, had indicated the initial injection of the liquid into the bed was completely different for each of these three sets of conditions, resulting in completely different initial distributions of the water. This ensured that the techniques developed for the drying monitoring and end point detection were independent of how the liquid was initially distributed in the bed.

Table A1.1 Summary of trials

Trial	Pre-mixer	Nozzle	Atomization gas	Water injected	Gas to liquid ratio (%)
A	BFC	TEB	Air	21 litres	1.5
B	BFC	TEB	Air	21 litres	2.8
C	Venturi - 1	TEB	Helium/Nitrogen	21 litres	0.8
D	Venturi - 2	Simple Constriction	Air	21 litres	2.8
E	Venturi - 2	Simple Constriction /Shroud	Air	21 litres	0.6

To measure the passive acoustics from the system, two prepolarized electret microphones were mounted flush onto the side of the bed, 0.9 m above the distributor grid and 2.3 and 2.8 m from the short end of the bed (Figures A1.1 and A1.2). The signals from the microphones were recorded at a frequency of 40000 Hz.

To measure the vibration of the system, a uni-directional accelerometer was mounted on the end of a 0.0064 m diameter, 0.35 m long steel rod. This rod was inserted 0.10 m into the bed at a location 0.9 m above the distributor grid and 2.3 m from the short end of the bed (Figures A1.1 and A1.2). The signal from the accelerometer was recorded at a frequency of 40 000 Hz.

To measure the conductance of the solids within the bed, a conductance probe was used (Figures A1.1 and A1.2). The probe was a 0.5 inch (0.0127 m) diameter stainless steel tube traversing the length of the bed (3.5 m). This probe was supported at both ends of the bed with nylon fittings to isolate the tube from the bed walls, which act as a ground in electrical circuit. The electrical circuitry for the conductance probe is shown in Figure A1.3. An AC Voltage (V_{app}) was applied through the use of a signal generator as a 100 Hz sine wave with a voltage of approximately 6.45 V (RMS). The voltage (V_m) was then measured across a known resistance of 49 kΩ. Both the applied voltage, V_{app}, and the measured voltage, V_m, signals were recorded at a frequency of 1 kHz.

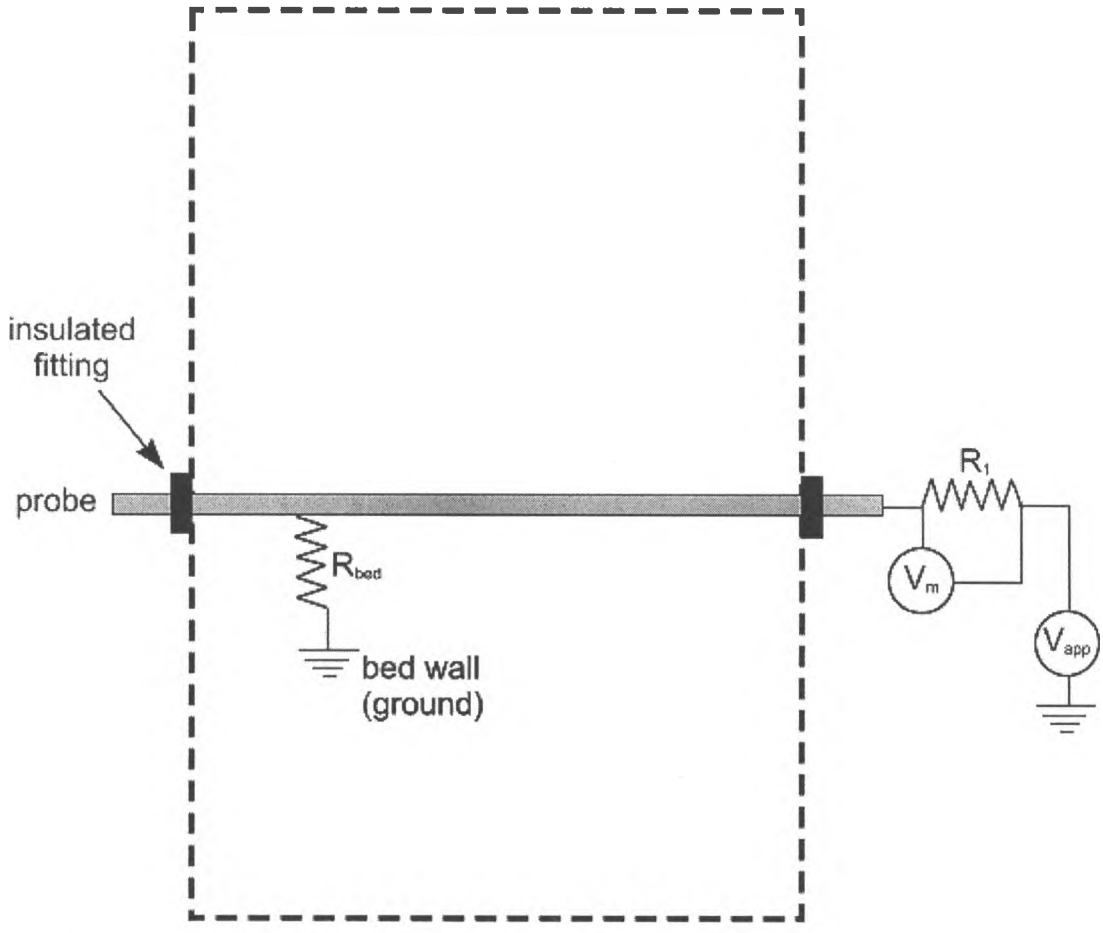

Figure A1.3 Schematic diagram of the electrical circuitry for the conductance probe

Three thermocouples were inserted 0.1 m into the column to measure the bed temperature (Figure A1.4). Thermocouple T1 was located 0.2 m above the distributor and 2.5 m from the short end, T2 was 0.75 m above the distributor and 1.9 m from the short end, T3 was 2.5 m above the distributor and located axially on the wide end of the bed. Thermocouple measurements were recorded at a frequency of 1 Hz and then downsampled to 0.1 Hz.

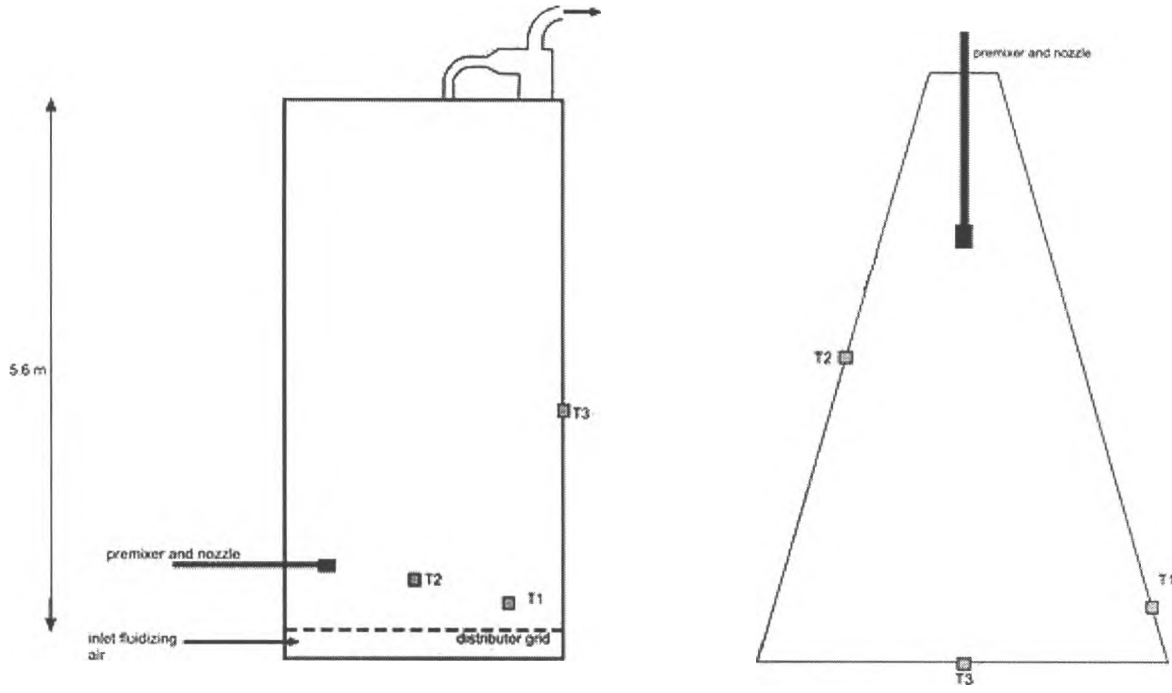

Figure A1.4 Schematic diagram of the locations of the thermocouple measurements

The flowability of samples of solids removed from the bed was measured using a Mercury Revolution Analyzer. The Revolution Analyzer rotated samples in a transparent drum at 0.3 revolutions per minute (RPM) and used optical algorithms to characterize the sample surface as it rotated. An avalanche was defined as a surface movement of 0.65% of the volume of the drum. The number, sizes and intervals between avalanches were measured as well as the angle of the sample surface relative to the horizontal. The measurements were summarized using a variety of statistics including the median avalanche time.

The moisture content of samples of solids removed from the bed was determined using a Mettler-Toledo moisture analyzer. The moisture content was determined through loss-on-drying measurements at 110 °C.

A 1.4 Experimental Procedure

The bed was initially fluidized at a superficial gas velocity of 0.15 m/s. With the large nozzle and premixer assembly, 21 litres of water were injected into the bed over 9.5 seconds. Immediately following injection, the superficial gas velocity of the fluidizing air was reduced to 0.06 m/s for 40 seconds to allow for injected water to be mixed into the bed and for large wet agglomerates to settle on the gas distributor plate. The bed was then completely defluidized and then refluidized (time t = 0 for the experimental measurements) at a superficial gas velocity of 0.12 m/s to allow the solids to dry.

During the drying phase, conductance, temperature, acoustic and vibration measurements were recorded. In addition, samples of about 5 x 10^{-4} m^3 were removed from the bed using the sampling port (Figures 3.1 and 3.2). These samples were immediately analyzed for fluidity and moisture content using the Revolution Analyzer and moisture analyzer, respectively.

A 1.5 Signal analysis methods

A 1.5.1 Acoustic and Vibration signals

The acoustic and vibration signals were analyzed offline in 60 second consecutive intervals for the frequency of fluctuations using fast Fourier and wavelet techniques. This time period was deemed to have a sufficient number of data points such that physical changes in the signal were dominant in the analysis over any random noise. A

large number of parameters were calculated and compared to the other measurements taken during drying.

A 1.5.1.1 Frequency analysis using fast Fourier techniques

The power spectral density is calculated by the product of the Fourier transform of a signal and its complex conjugate. A plot of the power spectral density versus frequency identifies dominant frequencies. Other parameters that can be examined include the average frequency and the noise index. The average frequency is calculated by:

$$\mu = \frac{\sum_{j=0}^{J-1} f(j)p(j)}{\sum_{j=0}^{J-1} p(j)} \qquad (1)$$

Where *f(j)* is the midpoint frequency of at bin '*j*' and *p(j)* is the power of the frequency at bin '*j*'

The noise index (α) of the signal is defined as the slope of line of the natural logarithm of power and frequency:

$$\ln(p) = \beta + \alpha \ln(f) \qquad (2)$$

A 1.5.1.2 Frequency analysis using wavelet techniques

For wavelet analysis of a signal, the signal is divided into *m* multiple levels or scales. Each of these levels corresponds to a frequency band, and due to the halving effect of the frequency, can further be defined as octaves. For each octave, using a Debauchies 4

wavelet, the signal was separated into two parts: the averages and the coefficients. The coefficients indicated the fluctuations in the signal at a specified scale. The coefficients can be analyzed by calculating parameters such as the average, standard deviation and intermittency. The standard deviation of the coefficients is calculated by:

$$\sigma = \sqrt{\frac{\sum_{i=1}^{n}(x_i - \mu_{coeff})^2}{n}} \qquad (3)$$

The standard deviation of coefficients can be normalized using the standard deviation of the signal. Similarly, by computing the energy of the coefficients at specified scale and dividing by the global (average) energy of the entire signal, the intermittency is determined:

$$I_{m,n} = \frac{(C_{m,n})^2}{< C^2_{m,n} >} \qquad (4)$$

Where < > indicates the mean energy of the signal and ( ) indicates the average value of the coefficients at the specific octave. The intermittency can also be calculated with respect to time at all scales, demonstrating the intermittency local to both time and scale, but this analysis was not needed in this case.

A 1.5.2 Conductance signals

Since the conductance method used AC power, root mean squared (RMS) voltages are used. The relationships used to describe bed conductivity may be written based on basic circuit analysis. Since the voltage drop across the bed resistance (R_{bed}) and R_1 must be equivalent in Figure 3.3 to the applied voltage (V_{app}) following Kirchhoff's voltage law, Kirchoff's law describes the relationship between the applied voltage and the bed resistance:

$$I = \frac{V_{app}}{R_1 + R_{bed}} \tag{5}$$

Kirchoff's law is simplified to:

$$I = \frac{V_{app}}{R_1 + R_{bed}} = \frac{V_m}{R_1} \tag{6}$$

And then rearranged:

$$R_{bed} = R_1\left[\frac{V_{app}}{V_m} - 1\right] \tag{7}$$

The bed conductance is then:

$$G_{bed} = \frac{1}{R_{bed}} \tag{8}$$

The voltage from the bed was measured at 1000 Hz and averaged over 60 s long chunks. Although this data could be presented in terms of conductance of the bed, it was found to be easier to simply work with the voltage measured.

A 1.6 Results & Discussion

When the water is injected into the fluidized bed, it wets the solids that flow within the spray zone during the injection period. With fluidization, the wet solids are dispersed and mixed throughout the bed. Some of the wet solids can form nuclei and grow into agglomerates. This tendency would be enhanced if the spray zone was small and not uniform and if the solids were not well fluidized and therefore stayed within the spray zone for an extended length of time.

Macro-agglomerates would be too large to be suspended by the fluidization gas and would therefore immediately settle onto the distributor plate. Meso-agglomerates would

be visible, but would be small enough to remain fluidized. Micro-agglomerates would be too small to be visible and would be easily fluidized. Individually wetted particles would be easily fluidized.

Drying individually wetted particles would be rapid as they are easily fluidized and exposed to excellent heat and mass transfer conditions. As agglomerates form and increase in size, drying would slow down as heat and mass transfer conditions deteriorate with external limitations from the reduction of fluidization quality resulting from agglomerates resting on the gas distributor and internal limitations within the agglomerates. In terms of solids flowability, meso and macro agglomerates generally do not affect the flow properties of the solids as they trap the moisture and have a relatively dry outer layer. However, it is still important that these agglomerates are dried fully. If they are not fully dried the agglomerates can be transferred with the rest of the solids downstream, then break up and release the trapped moisture later in the process. This release of moisture will negatively affect flowability of the bulk solids, potentially in an inopportune spot which could require a shutdown to clean out the non-flowing solids.

The methods investigated in this study can be divided into those which required sampling and those which could potentially be implemented on line.

A 1.6.1 Sampling methods

A 1.6.1.1 Effect of moisture on solids flowability

Samples were taken from the bed during the 90 minute drying time and were analyzed for flowability and moisture content using the Revolution Analyzer and the moisture balance, respectively. Additionally a number of samples were prepared offline by adding water to the silica sand and mixing the sample mechanically. Figure A1.5 shows an example of the differences in the surfaces of wet and dry samples as they are rotated in the Revolution analyzer.

a) 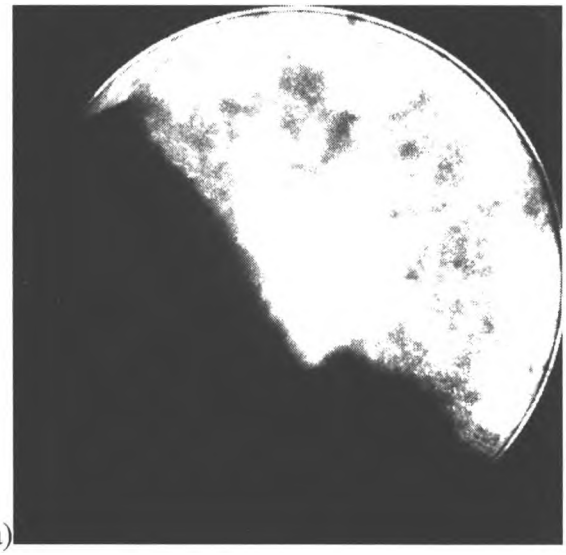

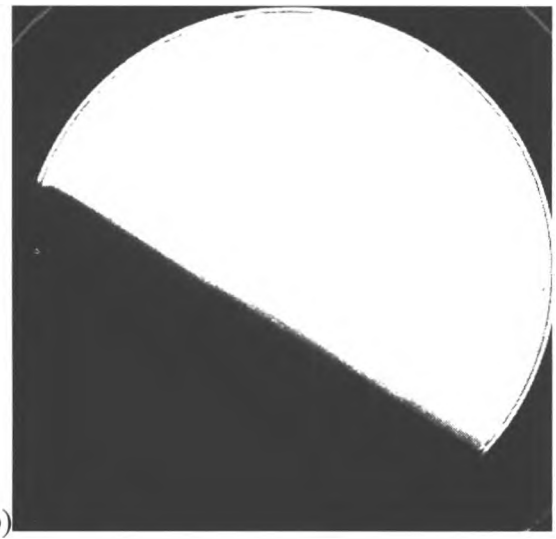

b)

Figure A1.5 Images of silica sand samples in the Revolution Analyzer when (a) the sand was cohesive and wet (0.1 wt%) and when (b) the sand was dry and free flowing

The surface of the wet sample was irregular and exhibited large avalanches at large time intervals while the surface of the dry sample only showed very small avalanches at small time intervals. As shown in Figure A1.6, there is a distribution of avalanche intervals within each sample and distinct differences between wet and dry samples. The differences between samples can be characterized by the median avalanche time. When the sample is drying the initial slope is much greater. This indicates that for dryers solids, the majority of the avalanches are faster.

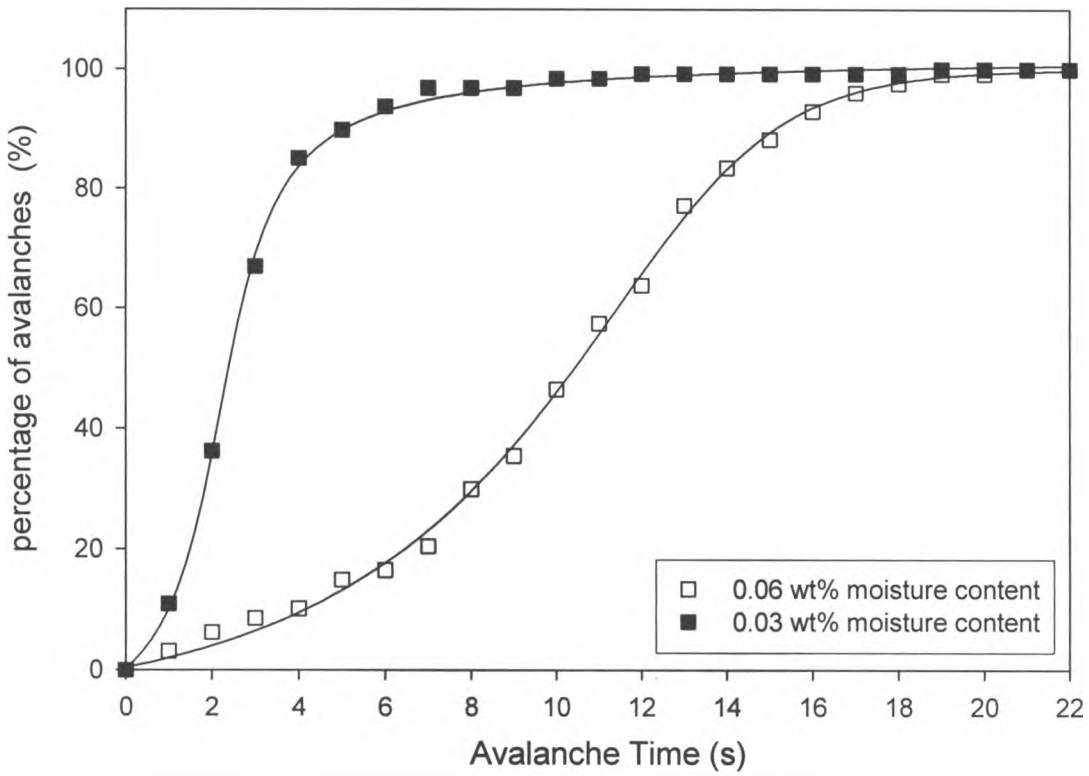

Figure A1.6 Distribution of avalanche times for two samples from Trial B

Figure A1.7 shows the relationship between the flowability of the sand, using the median avalanche time and the moisture content of the sand. It includes samples from a wide range of trials with different nozzle and pre-mixer combinations, with varying gas to liquid ratios and with the mechanically mixed samples. The mechanically mixed samples were prepared in such a way that there were no visible agglomerates.

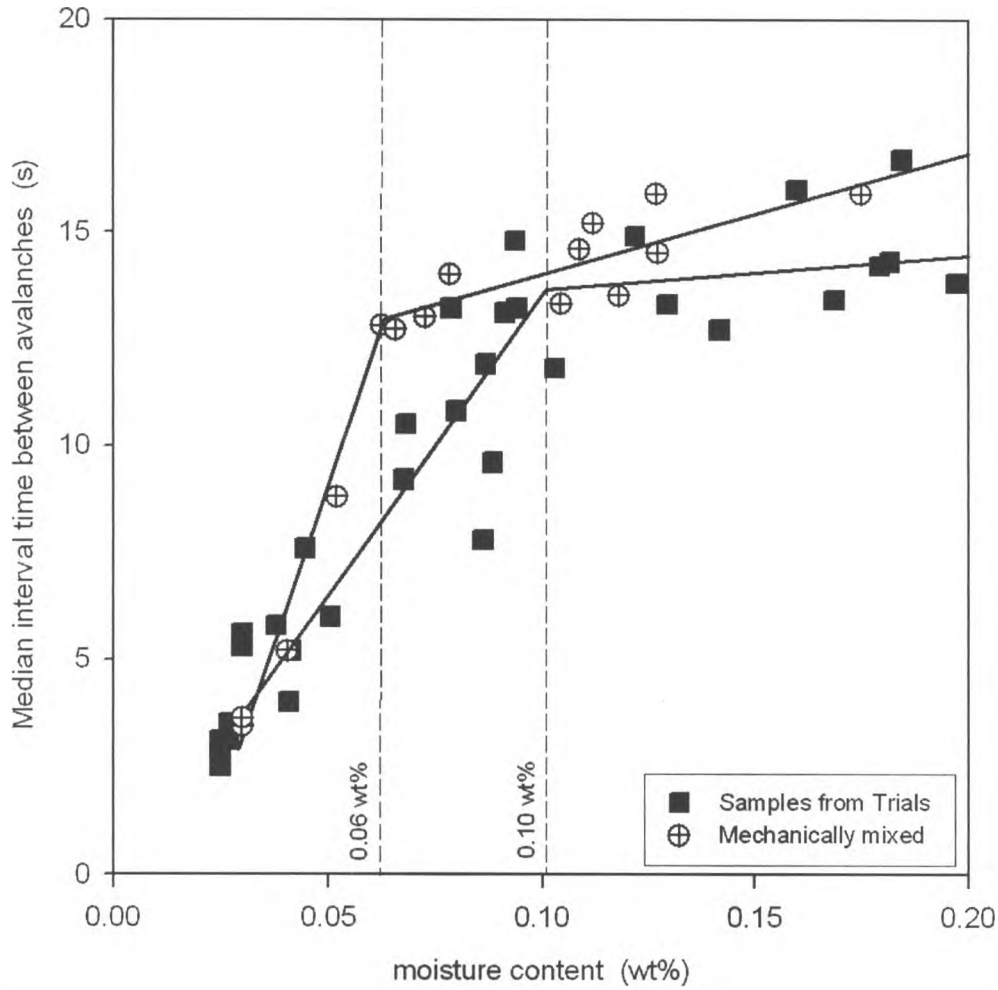

Figure A1.7 Relationship between the median avalanche time and moisture content

By fitting straight lines to the data two critical moistures could be identified. Below a moisture content of 0.06 wt %, there was a positive linear relationship between the flowability and moisture content of the sand for the mechanically mixed samples. A change in slope occurred at about 0.1 wt % for the samples withdrawn from the fluidized bed. At higher moisture content levels, there was almost no change in the median avalanche times for both mechanically mixed and fluidized bed samples.

The mechanically mixed samples had higher avalanche times than the bed samples for a given moisture content indicating that the moisture a portion of the moisture in the bed was trapped in a form that did not effect flowability. This can be explained by the fact that water within the bed existed in four forms: (i) in macro-agglomerates of sand particles that are easily visible, (ii) in meso-agglomerates of sand that are still visible but fluidizable, (iii) in micro-agglomerates that are not visible and are fluidizable, and (iv) on the surface of individual non-porous sand particles. The water in the macro-agglomerates was not captured in samples, as these macro-agglomerates were too large to be fluidized and, therefore, it is assumed that these agglomerates immediately descended through the bed to the grid plate. The meso-agglomerates and micro-agglomerates were small enough to remain fluidized within the bed. Samples of the bed therefore contained meso-agglomerates, micro-agglomerates and individual dry and wet sand particles which was confirmed through visual observations.

It was concluded that, at specific measured moisture contents, a range of solids flowabilities are possible, depending on the way the moisture is distributed. Measuring moisture content is therefore an inadequate method when attempting to achieve a specific solids flowability.

A series of tests were conducted to further compare the ability of the measured solids moisture content versus the measure avalanche behavior as methods to indicate flowability during drying.

Water was added and thoroughly mechanically mixed into a sample of sand. This wet sand sample was then divided for moisture balance and avalanche behavior testing. Several measurements were made for each test for each wet sand sample.

The coefficient of variation of the measurements of a sample was then calculated, as shown in table A 1.2.

Table A1.2 Coefficient of variation of replicate tests of moisture content and median avalanche time

Sample	Average Measured Moisture (wt %)	Coefficient of Variation – Measured Moisture	Average Median Avalanche Time	Coefficient of Variation – Median Avalanche Time
1	0.175	0.57	9.2 s	0.12
2	0.098	0.34	8.5 s	0.04
3	0.077	0.26	6.6 s	0.11
4	0.049	0.52	5.2 s	0.05
5	0.049	0.61	4.1 s	0.01
6	0.035	0.29	3.6 s	0.0161

The coefficient of variation of the moisture content measurements was larger than that for the avalanche measurements for all of the samples. This further confirms that the avalanche behavior is a better indicator of flowability than the moisture content.

A 1.6.1.2 Flowability

Figure A1.8 summarizes the median avalanche times for all five trials. The median avalanche times were initially low which reflected that the wetted solids were not yet uniformly dispersed throughout the bed. Maximum values were obtained between 10 and 20 minutes when the wetted solids and agglomerates were dispersed but had not yet dried significantly. The median avalanche times then decreased as the wetted solids dried.

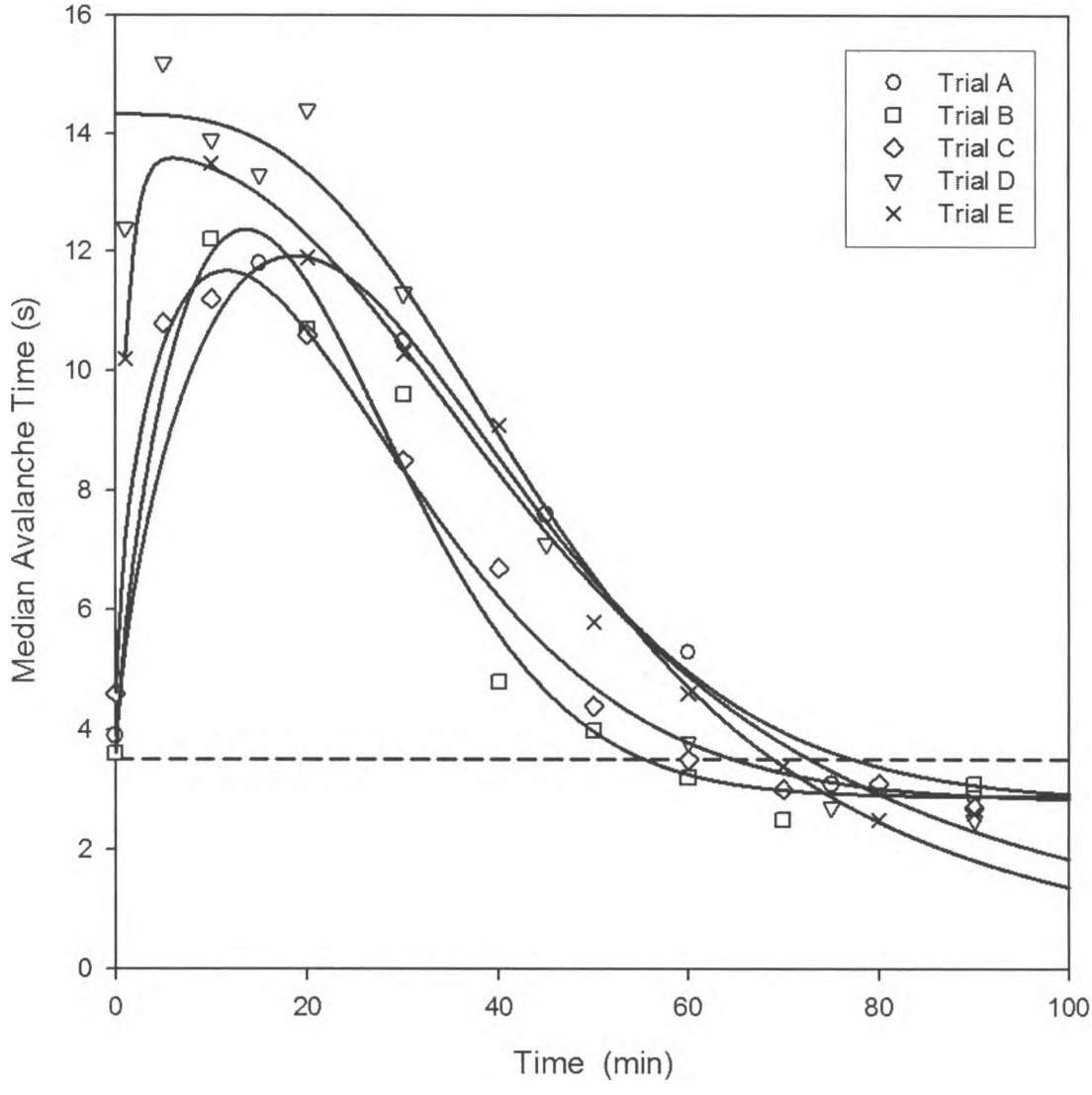

Figure A1.8 Median avalanche times during drying

Preliminary flowability experiments identified a median avalanche time of about 3.5 s for free flowing silica sand. The end-points were therefore estimated to be about 75 minutes, 55 minutes, 65 minutes, 65 minutes and 70 minutes for Trials A, B, C, D and E respectively.

There was some scatter in the measured median avalanche times for a given trial. A s the measurements were made using samples from the bed, the measured flowability was a local measurement.

Unfortunately, avalanche testing is not always be practical as it is time consuming, cannot be done online and is a local, intrusive measurement.

A 1.6.2 Potential On-line Methods

A 1.6.2.1 Conductance

Figure A1.9 shows the conductance measurements for Trials B, D and E. The measurements did not reach a maximum until about 10 minutes into the trials, again indicating that the wetted solids were not initially well distributed throughout the bed. The conductance levels remained high and then decreased quickly to a low and constant value as the bed became dry. This rapid change of slope occurred at about 65 minutes for Trial B, 60 minutes for Trials D and Trial E.

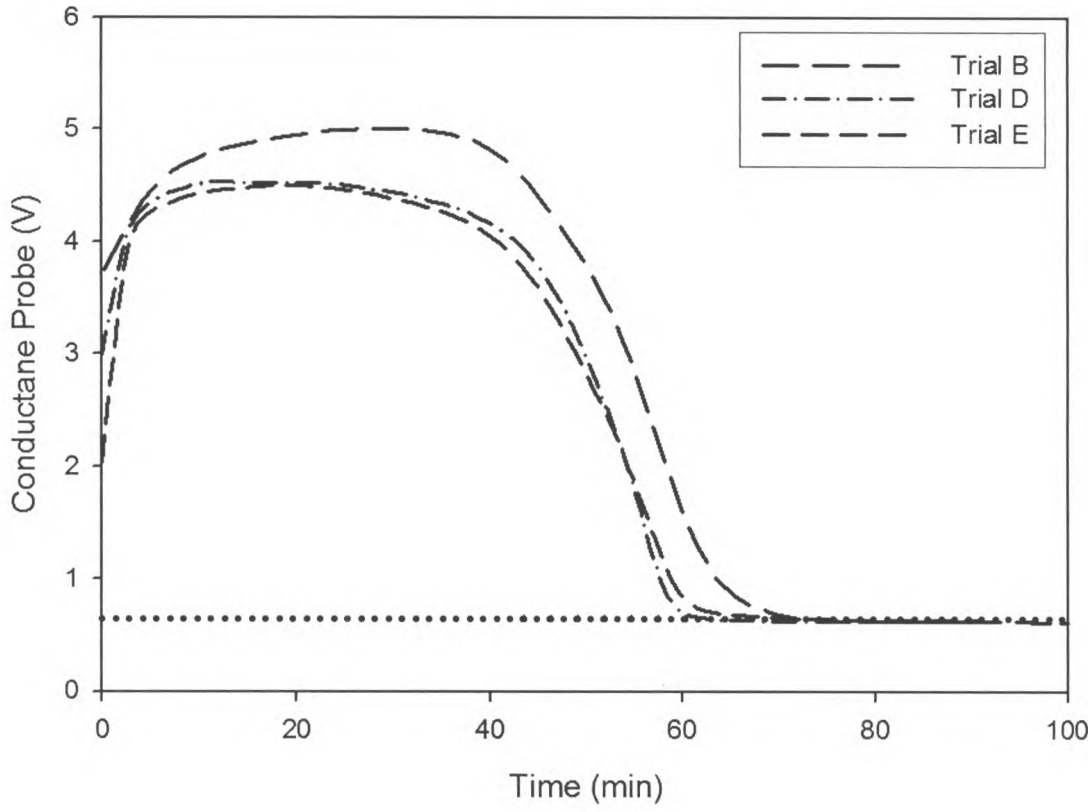

FigureA 1.9 Conductance measurements for Trial B

The conductance probe transversed the length of the bed and used the bed walls as the measurement ground. The measurements were therefore not local which was reflected in the high conductance measurements until the bed was almost completely dry and that allowed the drying end-point to be clearly identified. There were, however, many disadvantages to the conductance measurements: the probe was intrusive and therefore the measurements may not be appropriate for many applications, the measurements can reach a maximum quickly with solids above a critical moisture content, and the probe measurements must be calibrated to account for drift due to erosion or other changes of the probe surface. Finally, the conductance probe is incapable of inferring anything

regarding the flowability of the solids. All these reasons make conductance measurements useful for the laboratory but impractical in industry.

A 1.6.2.2 Temperature

Thermocouples provided three temperature measurements at various locations within the bed. Figure A1.10 shows the temperature measurements within the bed for Trial B, D and E. The temperature measurements for Trial B decreased until about 60 minutes and 57 and 56 minutes for Trials D and E respectively. During this time, the wet solids were being dispersed through the bed, but also started to dry. The temperature started to increase when the individual wetted particles and the surface of agglomerates were dry. The temperature then continued to increase as the interior of agglomerates became dry and/or weak agglomerates were broken and further dried. The minimum temperature measurements corresponded fairly well to the drying end-point times obtained from the sampled avalanche profiles and conductance measurements.

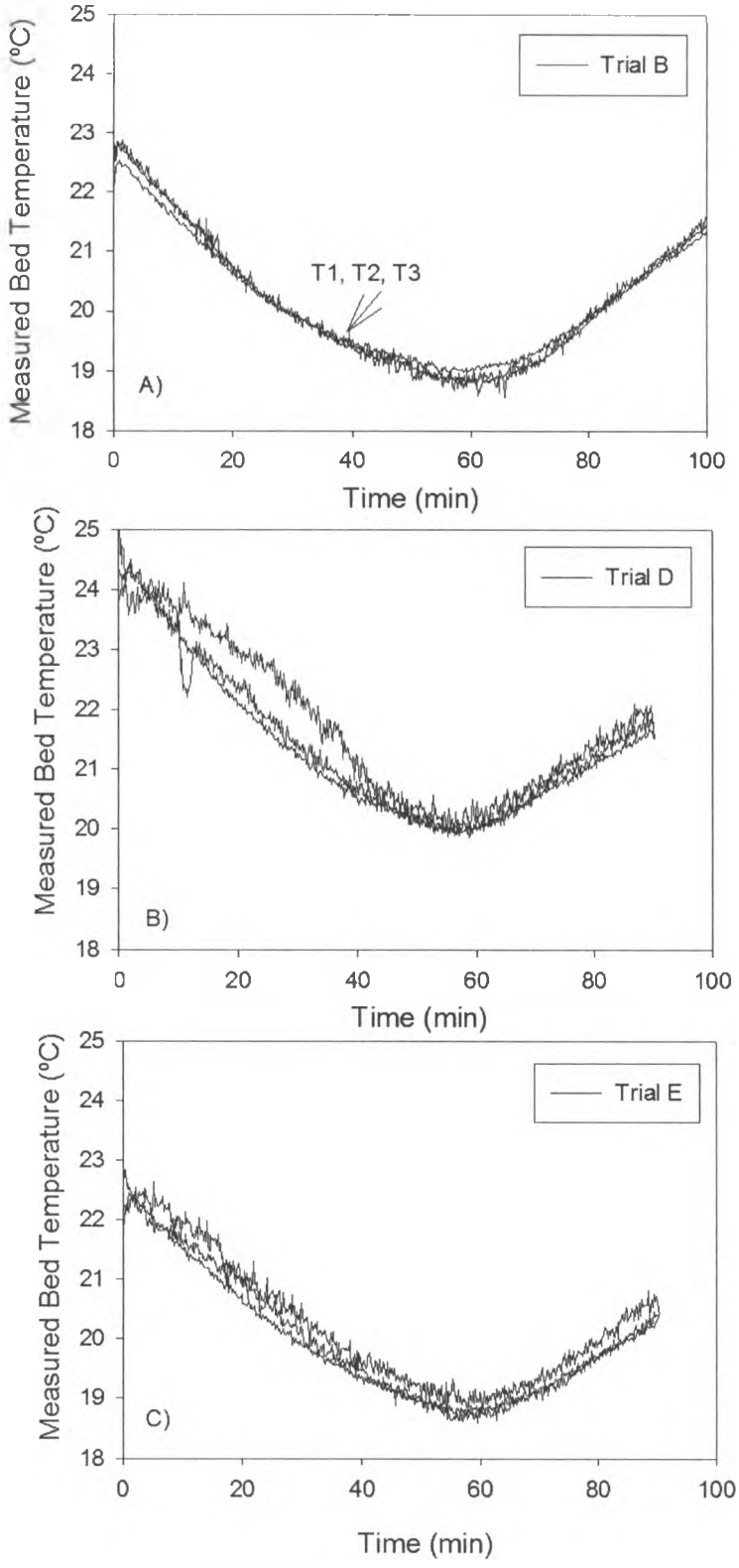

Figure A1.10 Measured bed temperatures for
A) Trial B
B) Trial D
C) Trial E

Although temperature measurements are easy to make, there are several disadvantages to using these measurements for monitoring drying: 1) the measurements are intrusive 2) the measurements are local and therefore many measurements are required to indicate the overall bed conditions 3) the measurements would be affected by local hydrodynamics 4) the measurements do not directly indicate flowabiliy.

A 1.6.2.3 Acoustic measurements

Acoustic measurements were taken using two microphones located 0.9 m above the distributor and 2.3 and 2.8 m from the short end of the bed. The measurements were divided into 60 s consecutive segments and extensively analyzed. These segments were then smoothed to form continuous drying curves. Figure A1.11 shows 1 second of a typical raw acoustic signal from Trial A at 15 minutes from the microphone at 2.3 m.

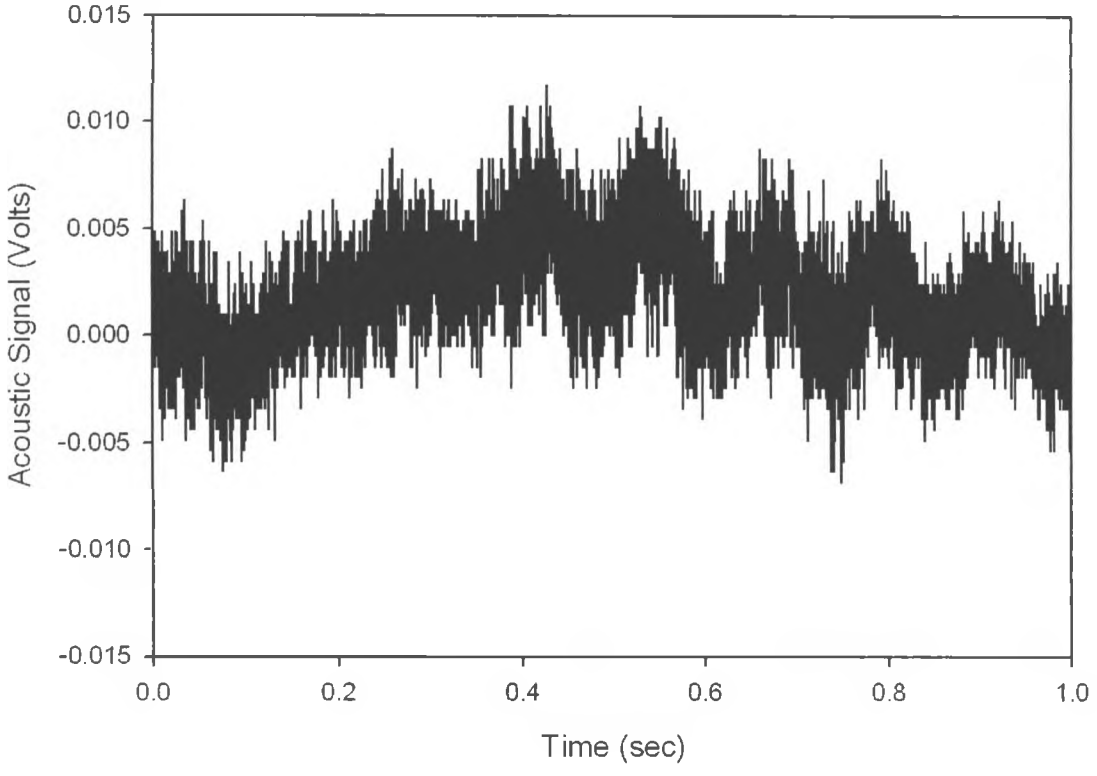

Figure A1.11 Raw acoustic signal from the microphone at 2.3 m in Trial A at 15 minutes

Although some analysis techniques clearly indicated the progression of drying, individual techniques were affected by parameters such as power supply and mounting of the microphone to the bed.

The power spectra of the 60 s long segements were calculated using the Fourier transform and parameters such as signal power, average frequency and noise index were produced. The chunks of signal were also decomposed using the Debauchies 4 wavelet transform. Using a least squares method all of the values calculated from the wavelet and Fourier analysis were regressed to identify important parameters and correlate the signals to the measured avalanche time from samples. A combination of several analysis techniques with regression against median avalanche times provided a method for the non-invasive

acoustic measurements to consistently and reliably identify the drying end-point. Figures A1.12 and A1.13 show the median avalanche times predicted from these regressions versus the measured median avalanche times.

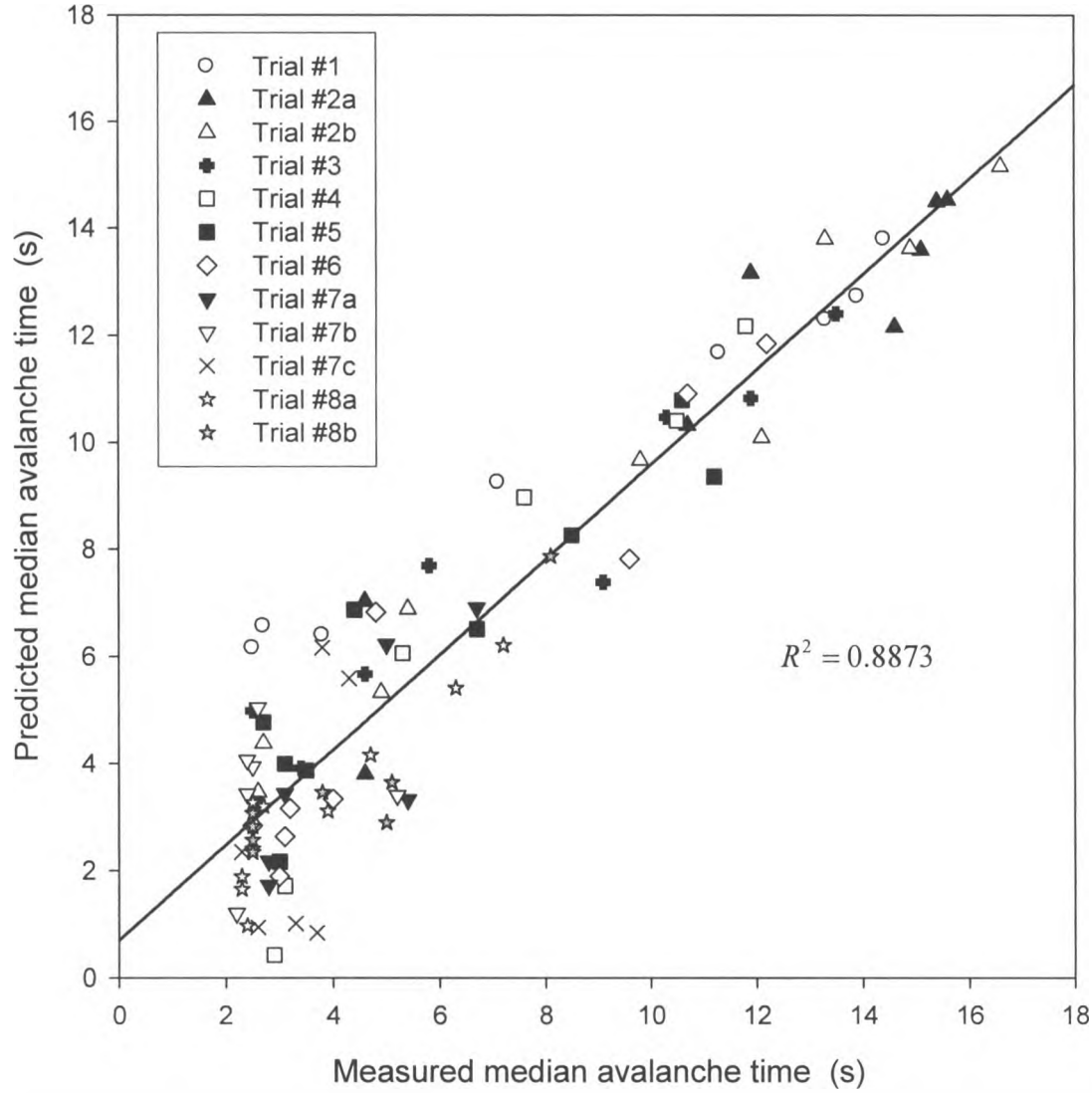

Figure A1.12 Comparison between predicted and measured median avalanche times for acoustic measurements (microphone at 2.3 m), fitted with a multi-linear regression

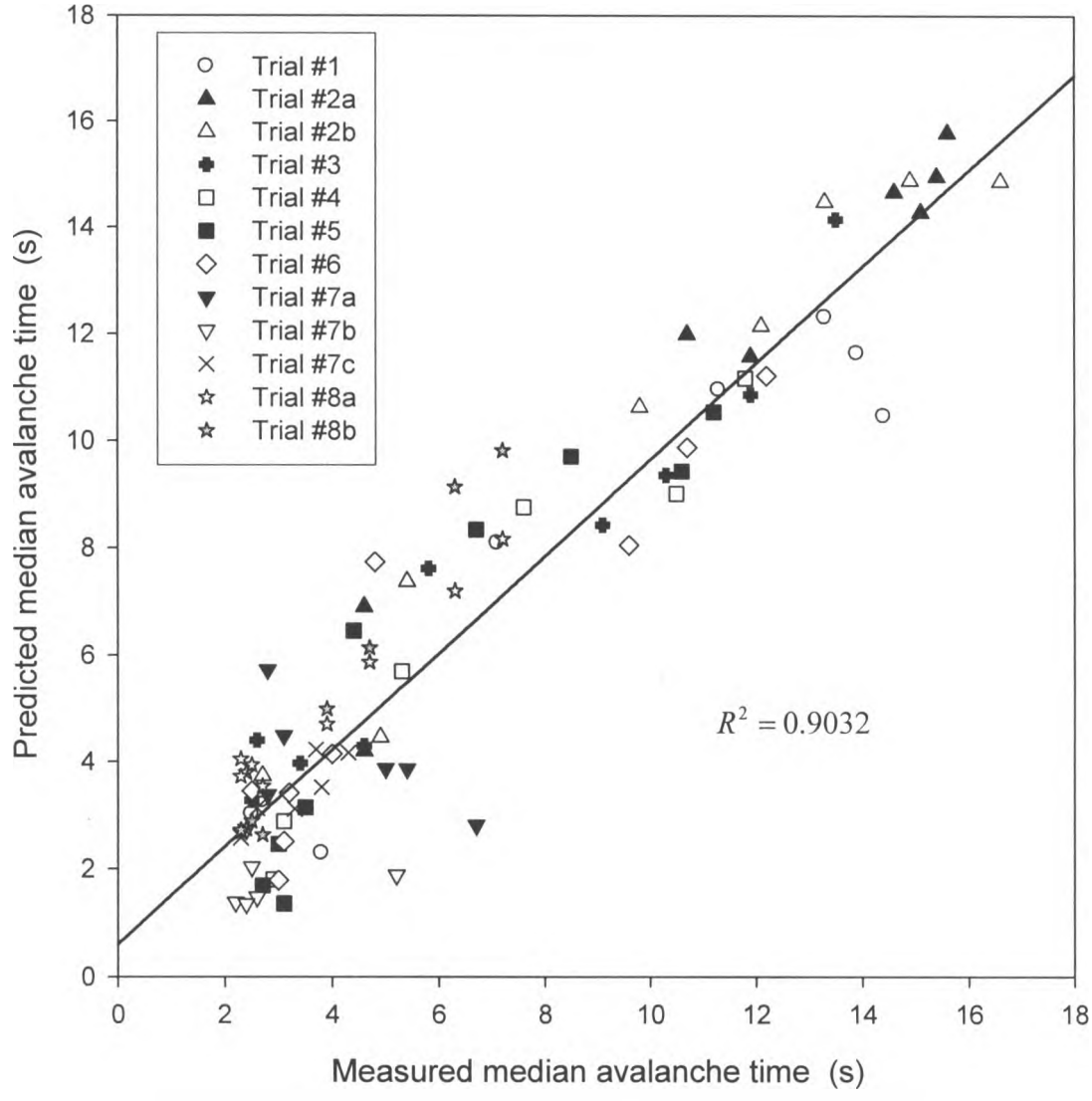

Figure A1.13 Comparison between predicted and measured median avalanche times for acoustic measurements (microphone at 2.8 m), fitted with a multi-linear regression

Once the regressions were determined, a predicted avalanche time was calculated for every minute of the drying run from the acoustic signal. The regressions had different associated errors when determining a dry bed. This meant that there was some scatter in predicted median avalanche time even when the bed was dry. The experimentally

determined median avalanche time of dry silica sand was 3.5 seconds, however, due to this error each microphone had a specific median avalanche time, below which the bed was considered dry. The microphone located 2.8 m from the short end of the bed had relatively little scatter so this value was a median avalanche time of 4 seconds. The microphone located at 2.3 m had more scatter and the median avalanche time for a dry bed was 6 seconds.

Figures A1.14 and A1.15 shows the predicted avalanche time drying curves smoothed to be continuous. For both microphones, the drying endpoint can be clearly identified where the predicted median avalanche time curves, calculated from the acoustic signal, approach and cross a value of 4 s for the microphone at 2.8 m and 6 s for the microphone at 2.3 m. The microphone located at 2.3 m was less accurate, as seen in figures A1.12, showing that sensor location is an important consideration.

The major advantages of acoustic analysis for monitoring included: (i) measurements are non-invasive and can be implemented easily (ii) measurements indicate overall bed conditions, and, (iii) the measurements indicate the flowability of the solids.

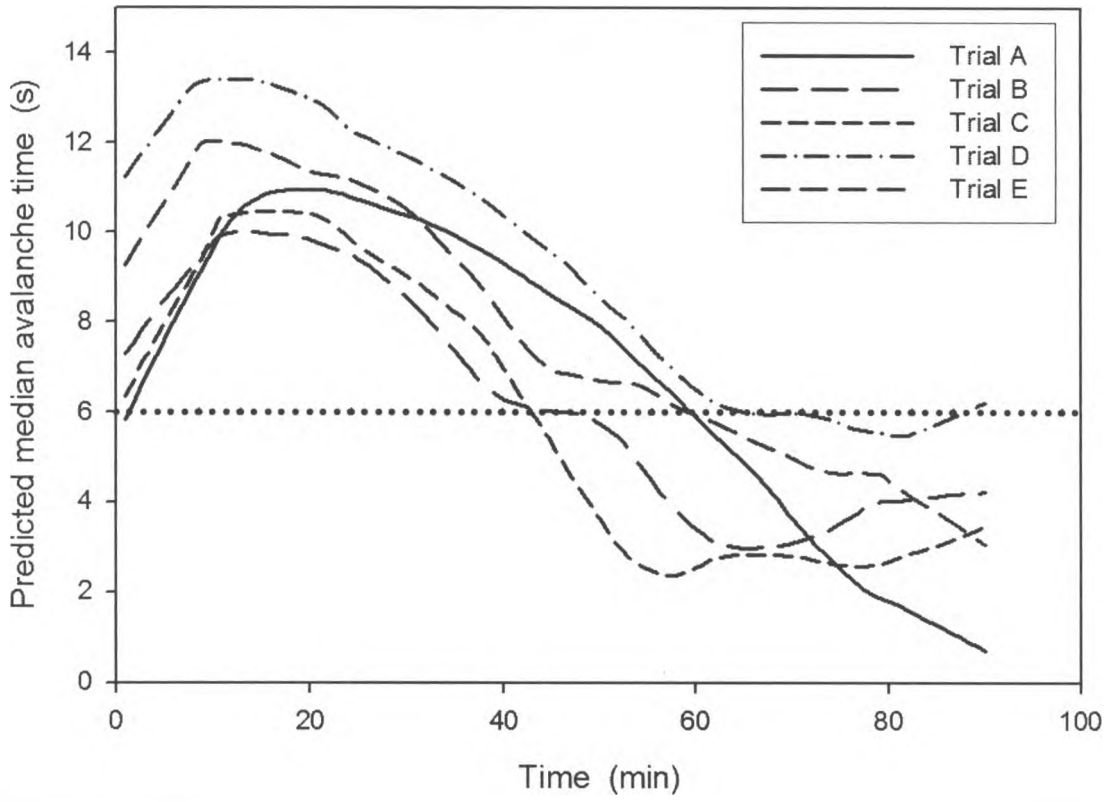

Figure A1.14 Predicted median avalanche times from acoustic measurements at 2.3 m from short end of the bed

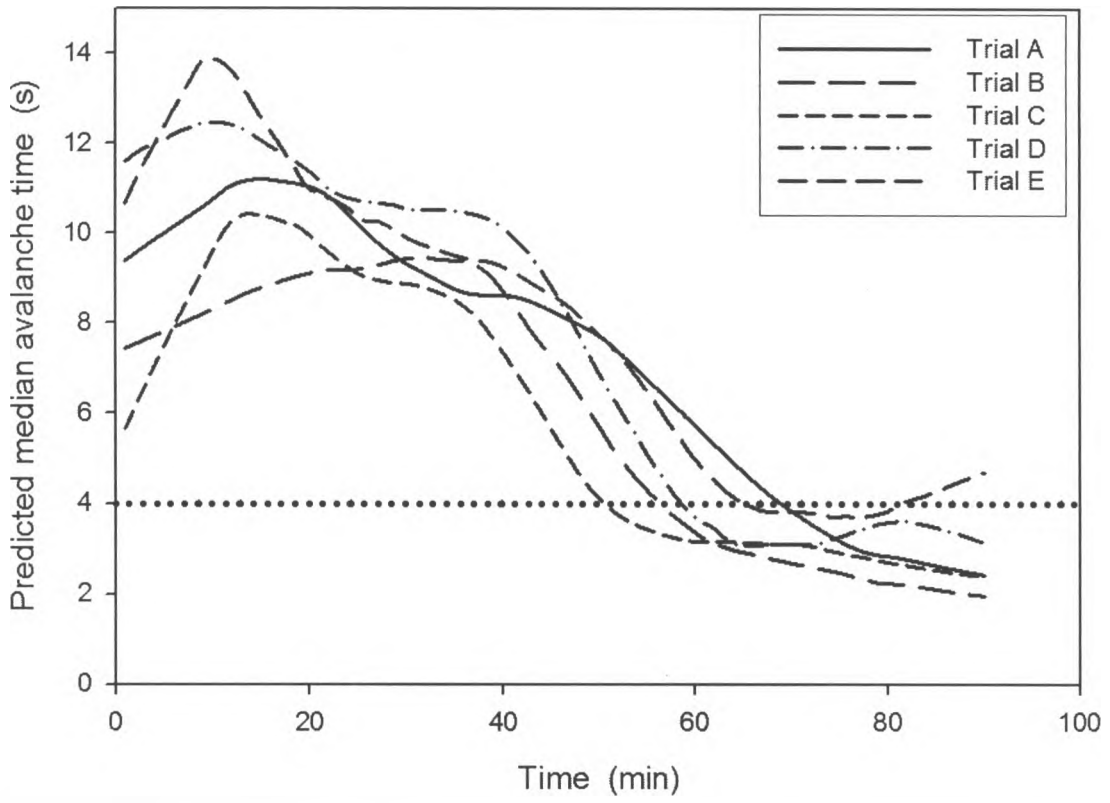

Figure A1.15 Predicted median avalanche times from acoustic measurements at 2.8 m from short end of the bed

A 1.6.2.4 Vibration measurements

The accelerometer mounted on the rod was located 0.9 m above the gas distributor and was 2.3 m from the short end of the fluidized bed. The vibration measurement were divided into 60 second consecutive chunks and analyzed in a way similar to the microphones. Much like the microphones the accelerometer had an error associated with measuring the dry bed. Figure A1.16 shows the median avalanche times predicted from the linear regression.

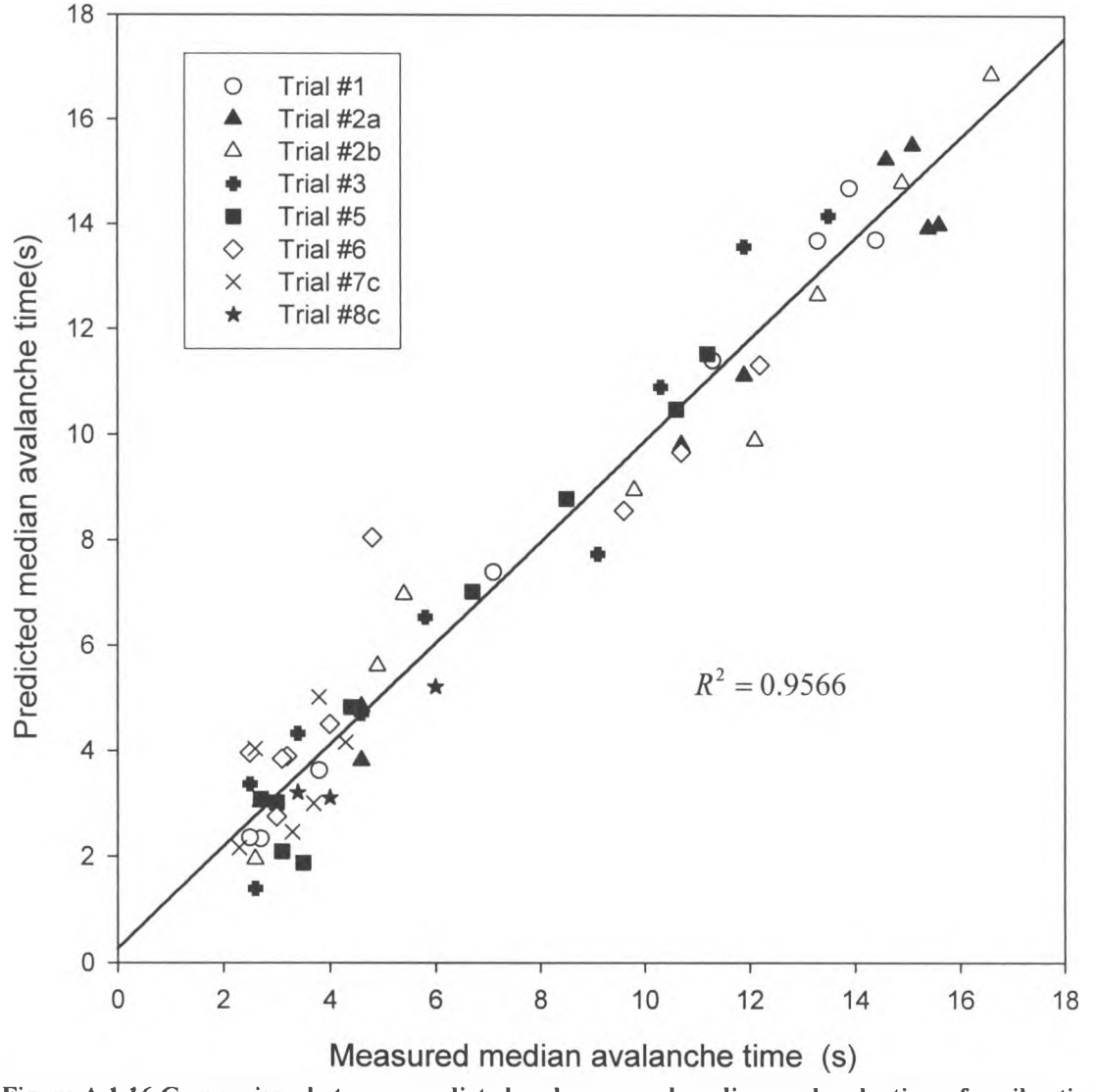

Figure A 1.16 Comparison between predicted and measured median avalanche times for vibration measurements, fitted with a multi-linear regression

It was determined that the accelerometer regression had the least scatter and below a predicted median avalanche time of 3.75 s the bed was considered dry.

Figure A1.17 shows the drying curves from the accelerometer regression. The accelerometer was able to determine the drying endpoint by predicting the median time avalanche time.

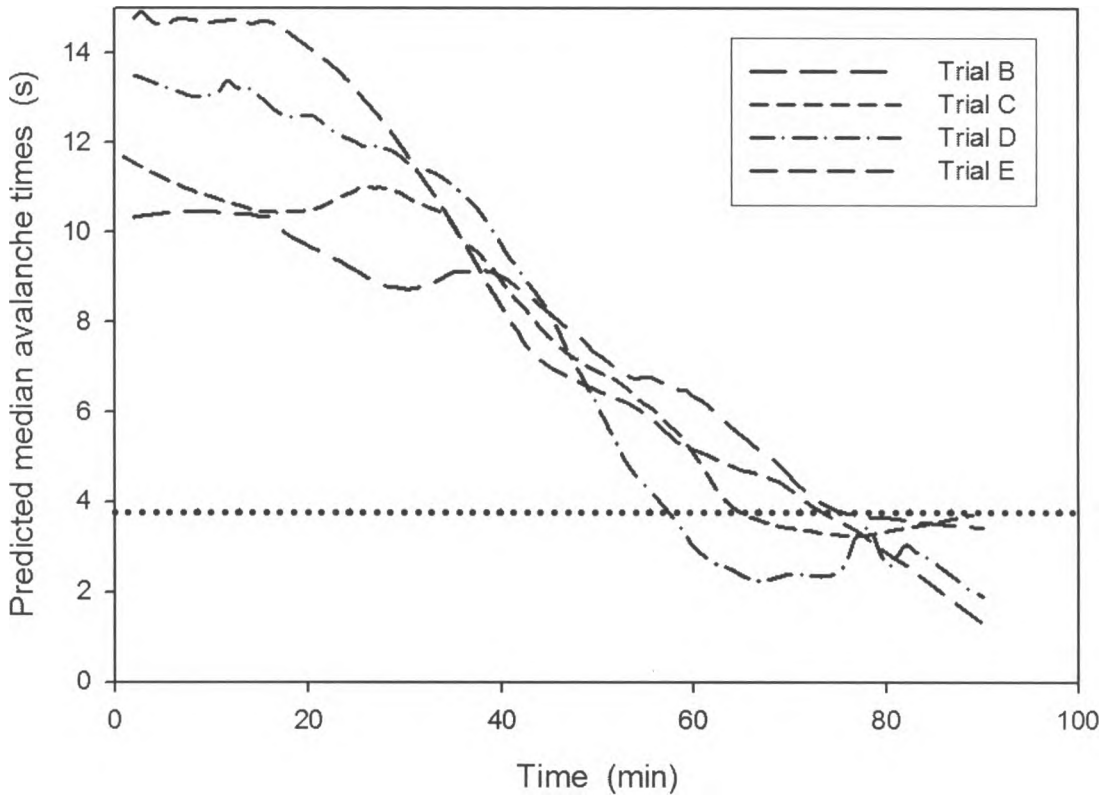

Figure 1.17 Predicted median avalanche times from vibration measurements

The accelerometer shows slightly different drying profiles than the microphones and was the predicted the bed was dry closest to the experimentally determined dry median avalanche time. This demonstrated that both sensor type and location are important parameters.

A 1.6.3 Comparison of Methods

Each method investigated in this study was capable of monitoring the drying of the solids and to determine an end point.

There is no distinct pattern of early/late detection of drying end points. However, when the goal of drying solids is to ensure flowability, there are clear advantages to using acoustic and vibration methods.

For small laboratory scale beds, sampling is an accurate way of determining moisture content in fluidized beds. Although at low moisture concentrations, loss-on-drying measurements have limited accuracy, Karl-Fischer titrations may be used. One major weakness of sampling in larger sized industrial beds is that the samples are seldom representative of the global solids moisture content. The other major weakness is that moisture contents are not indicative of the solids flowability. Depending on how the solids were initially wetted, the flowability can be different at specific moisture content.

Conductance probes are highly intrusive to the process and the measurements can become saturated. Although this method is more global than any sampling method, it can be negatively impacted by poor mixing: the conductance measured will always be that of the wettest solids in the bed due to the nature of electricity always going through the path of least resistance. Additionally, conductance is related to the moisture content of the solids and not their flowability.

In an ideal fluidized bed, with excellent mass and heat transfer, temperature would be a global measurement. In this case, temperature is local and the drying end point can be difficult to determine. Thermocouples would not be suitable for large bulk solids

applications. Similar to all of the above methods, no information about the flowability of the solids can be determined.

Flowability measurements are more accurate at low moistures than moisture content but require sampling and take a long time. Microphones and accelerometers can be mounted easily onto existing equipment and eliminate the need for sampling. They provide a more global measurement that is easy to interpret and does not saturate as for conductance probes. In addition, acoustic and vibration measurements directly indicate flowability of the solids via predicted median avalanche time. This makes them the ideal sensing method for when free flowing solids are the goal of drying.

A 1.7 Conclusions

Microphones and accelerometers showed promise for monitoring drying and determining a end point in an industrially sized fluidized bed of sand. This was accomplished by regressing the signals in order to predict the flow properties of the solids within the fluidized bed. Further trials and more work are needed..

A 1.8 Acknowledgments

The authors would like to acknowledge the help of Dr. Gareth Chaplin on the equipment and adapting his scheduled experiments to incorporate our needs. The authors would like to thank Syncrude Canada Ltd. for both their funding and their advice. Thanks to NSERC, OGS and OGSST for their funding of this work.

A 1.9 Symbols

C Energy of the signal (units)

d_{p50} median particle size (μm)

f Frequency, (Hz)

F Maximum frequency, (Hz)

G_{bed} Bed conductance, (Siemens/mhos)

i Numerical index in a series (-)

I Current, (ampres)

j Positive integer, number of power spectral density bin, (-)

J Positive integer, number of power spectral density bins, (-)

L Local Intermittency index, (units)

m Positive integer, number of level in a wavelet decomposition of a signal, (-)

n Positive integer, number of points in a series or signal, (-)

p Power at a given frequency, (-)

R_I Resistor used in the active conductivity circuit, (kΩ)

R_{bed} Bed resistance, (kΩ)

t time, (s, min)

U_g Superficial gas velocity, (m/s)

V_{app} Applied voltage, (Volts)

V_m Measured voltage, (Volts)

Greek symbols

α Noise index of the signal, (units)

β Linear constant, (units)

μ Mean of a series or signal, (units)

σ Standard deviation, (units)

A 1.10 References

[1] Portoghese, F., Berruti, F., Briens, C., Continuous on-line measurement of solid moisture content during fludized bed drying using triboelectric probes. *Powder Technology.* 181 (2008) 169 – 177.

[2] Daud, W. R. W., Fluidized Bed Dryers - Recent Advances. *Advanced Powder Technology.* 19 (2008) 403 - 418.

[3] Medhe, M., Pitchumani, B., Effect of moisture induced capilliary forces on coal flow properties. *AIChE Annual Meeting, Conference Proceedings 2006.* (2006)

[4] Wormsbecker, M., Pugsley, T., The influence of moisture on the fluidization behaviour of porous pharmaceutical granule. *Chemical Engineering Science.* 63 (2008) 4063 – 4069.

[5] Boyd, J. W. R., Varley, J., The uses of passive measurement of acoustic emissions from chemical engineering processes. *Chemical Engineering Science.* 56 (2001) 1749-1767.

[6] Book. G., Briens, L., Briens, C., Development of an acoustic method for the measurement of mixing and drying in a vibrated fluidized bed. *Canadian Acoustics - Acoustique Canadienne.* 33 (2005) 20-21

[7] Hann, D., Stražišar, J., Influence of Particle Size Distribution, Moisture Content, and Particle Shape on the Flow Properties of Bulk Solids. *Instrumentation Science and Technology.* 35 (2007) 571 – 584

[8] Alden. M., Torkington, P., Strutt, A. C. R., Control and Instrumentation of a Fluidized-Bed Drier Using the Temperature Difference technique I. Development of a Working Model. *Powder Technology.* 54(1988) 15-25.

[9] Watano, S., Takashima, H., Sato, Y., Miyanami, K., Yasutomo, T., IR Absorbstion characteristics of an IR moisture sensor and mechanism of water transfer in a fluidized bed granulation. *Advanced Powder Technology.* 7 (1996) 279-289.

[10] Rantanen, J., Lehtola, S., Rämet, P., Mannermaa, J-K., Yliruusi, J., On-line monitoring of moisture content in an instrumented fluidized bed granulator with a multi-channel NIR moisture Sensor. *Powder Technology.* 99 (1998) 163-170.

[11] Frake, P., Greenhalgh, D., Grierson, S. M., Hempenstall, J. M., Rudd, D. R., Process control and end-point determination of a fluid bed granulation by application of near infra-red spectroscopy. *Internation Journal of Pharmaceutics.* 151 (1991) 75-80.

[12] Green, R. L., Thurau, G., Pixley, N. C., Mateos, A., Reed, R. A., Higgins, J. P., In-Line Monitoring of Moisture Content in Fluid Bed Dryers Using Near-IR Spectroscopy with Consideration of Sampling Effects on Method Accuracy. *Analytical Chemistry.* 77 (2005) 4515-4522.

[13] Räsänen, E., Rantanen, J., Mannermaa, J-K., Yliruusi, J., Vuorela, H., Dehydration Studies Using a Novel Multichamber Microscale Fluid Bed Dryer with In-Line Near-Infrared Measurement. *Journal of Pharmaceutical Sciences.* 92 (2003) 2074-2081.

[14] Wildfong, P. L. D., Samy, A-S., Corfa, J., Peck, G. E., Morris, K. R., Accelerated Fluid Bed Drying Using NIR Monitoring and Phenomenological Modeling: Method Assessment and Formulation Suitability. *Journal of Pharmaceutical Sciences.* 91 (2002) 631-639.

[15] Morris, K. R., Stowell, J. G., Byrn, S. R., Placette, A. W., Davis, T. D., Peck, G. E., Accelerated Fluid Bed Drying Using NIR Monitoring and Phenomenological Modeling. *Drug Development and Industrial Pharmacy.* 26 (2000) 985-988.

[16] Portoghese, F., Berruti, F., Briens, C., Continuous on-line measurement of solid moisture content during fluidized bed drying using triboelectric probes. *Powder Technology.* 181 (2008)169-177.

[17] Brennan, W., Jacobson, M., Book, G., Briens, C., Briens, L., Development of a triboelectric procedure for the measurement of mixing and drying in a vibrated fluidized bed. *Powder Technology.* 181 (2008) 178-185.

[18] Chaplin, G., Pugsley, T., van der Lee, L., Kantzas, A., Winters, C., The dynamic calibration of an electrical capacitance tomography sensor applied to the fluidized bed drying of pharmaceutical granule. *Measurement Science and Technology.* 16 (2005) 1281-1290.

[19] Chaplin, G., Pugsley, T., Application of electrical capacitance tomography to the fluidized bed drying of pharmaceutical granule. *Chemical Engineering Science.* 60 (2005) 7022-7033.

[20] Chaplin, G., Pugsley, T., Winters, C., Application of chaos analysis to pressure fluctuation data from a fluidized bed dryer containing pharmaceutical granule. *Powder Technology.* 142 (2004) 110-120.

[21] Portoghese, F., House, P., Berruti, F., Briens, C., Adamiak, K., Chan, E., Electric Conductance Method to Study the Contact of Injected Liquid with Fluidized Particles. *American Institute of Chemical Engineering Journal.* 54 (2008) 7.

[22] Tsjujimoto, H., Yokoyama, T., Huang, C.C., Sekiguchi, I., Monitoring particle fluidization in a fluidized bed granulator with an acoustic emission sensor, *Powder Technology.* 113 (2000) 88-96.

[23] Bojarra, M., MONITORING FLUIDIZED BED DRYING OF PHARMACEUTICAL GRANULES. MESc Thesis, The University of Western Ontario, 2008.

[24] Vervloet, D., Nijenhuis, J., van Ommen, J.R., Monitoring a lab-scale fludized bed dryer: A comparison between pressure transducers, passive acoustic emissions and vibration measurements. *Powder Technology.* 197 (2010) 36 - 48.

Appendix 2. DEVELOPMENT OF AN ACOUSTIC METHOD FOR THE MEASUREMENT OF MIXING AND DRYING IN A VIBRATED FLUIDIZED BED

Garret Book, Lauren Briens, Cedric Briens
Western Fluidization Group, Faculty of Engineering
The University of Western Ontario, London, Ontario, Canada, N6A 5B9

Note: This appendix was published in the non-refereed conference proceeding at Acoustics Week in Canada 2005 October 11-14, 2005, London, Ontario, Canada

A 2.1 INTRODUCTION

Gas-solid fluidized beds can be used for physical processes such as mixing, drying and granulation. Fine powders, however, are difficult to fluidize well with gas flow. Vibration can be used to improve the fluidization.

The objective of this research was to develop a non-invasive acoustic method to detect fluidization regimes and measure mixing and drying in a vibrated fluidized bed.

A 2.1.1 Fluidization

At low gas velocities, the bed of powder is fixed. As the gas velocity is increased above the minimum fluidization velocity (Umf), the bed becomes fluidized. Increasing the gas velocity further, past the minimum bubbling velocity (Umb) the bed becomes well mixed due to the action of the bubbles. Applied vibration reduces the required gas velocity for

fluidization and bubbling. Pressure profiles and bed height methods for determining Umf and Umb are not practical for industrial applications.

The fluidizing gas dries the wet particles as it flows through the bed. For drying, the bed must be operated above Umb to provide the agitation, mixing and good heat transfer required for effective drying. Monitoring is required to ensure that the solids reach the appropriate moisture.

A 2.1.2 Acoustics

Acoustic sensors are inexpensive, can withstand a wide range of process conditions, and can provide reliable, fast, on-line and non-intrusive monitoring. Passive acoustics detect the sound generated by the process itself. In vibrated fluidized beds, acoustic emissions are caused by particles colliding with each other, the bed walls, the motion and eruption of bubbles and the vibration source [1].

A 2.1.3 Signal Analysis

The standard deviation measures the dispersion of the values within a given signal. The information entropy of a signal is a measure of the randomness. The power spectrum decomposes a signal into frequency bands that allow dominant frequencies to be identified.

A 2.2 METHOD

A Plexiglas fluidized bed (I.D. of 0.113 m and height of 0.274 m) was mounted on a vibration source and vibrated at 60 Hz with variable amplitudes. The powder was ceramic microspheres of 33 μm. This powder was non-porous and analogous to glass beads. A

microphone was attached in the baghouse at the top of the column directed down towards the bed. Each acoustic measurement was recorded at a frequency of 40000 Hz.

To determine the minimum bubbling velocity and the minimum fluidization velocity, the bed was initially very well fluidized. Acoustic emissions were recorded, the gas velocity was incrementally lowered, the bed was allowed to reach steady state, and measurements repeated. Measurements were recorded at vibration amplitudes of 0, 0.01, 0.026 and 0.05 mm.

To evaluate drying, solids were removed from the bed, water was mixed in with the solids and then the particles were replaced and the bed was re-fluidized. Measurements were recorded at gas velocities of 0.008 and 0.010 m/s and vibration amplitudes of 0 and 0.05 mm.

A 2.3 RESULTS & DISCUSSION

As shown in Figure A1.1, the standard deviation of the acoustic emissions for the vibrated bed identified both the minimum fluidization and the minimum bubbling velocities. The standard deviation indicates the amplitude of the acoustic emissions. Below Umf, the bed was fixed: the acoustic emissions were low as there was no particle movement and the bed did not easily transmit emissions from the vibration source. The standard deviation of the acoustic emissions increased significantly above Umf due to particle movement and the fluid properties of the bed allowing better transmission of emissions from the vibration source. Above Umb, the standard deviation again increased due to the emissions from bubble motion and eruption at the bed surface and the

decreased bed density for emission transmission. The power at the 60 Hz frequency of the vibration source showed similar profiles and the standard deviation was much lower in the non-vibrated bed indicating that observed variations in acoustic emissions are primarily due to the changes in transmission properties of the bed as it changes fluidization regime.

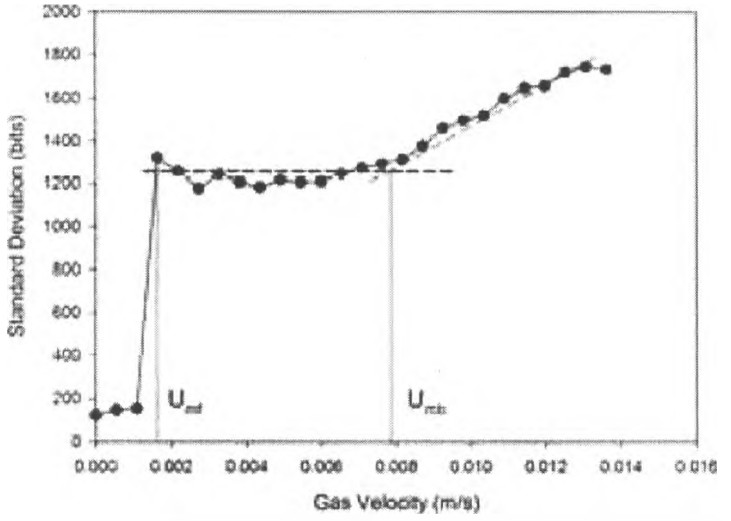

Figure A2.1Standard deviation of acoustic emissions at a vibration amplitude of 0.026 mm.

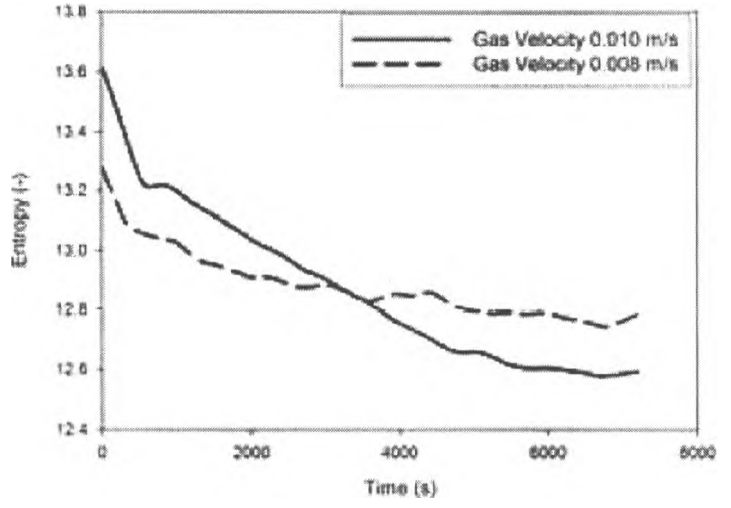

Figure A2.2 Evolution of the information entropy of the acoustic emissions as the bed dries.

Figure A1.2 shows that the drying process can be monitored with the acoustic signals. It shows how the information entropy of the microphone signal decreased gradually as drying progressed. At a superficial gas velocity of 0.010 m/s, the information entropy reached an asymptotic value at a time of about 6000 s (100 minutes). Drying at a superficial gas velocity of 0.08 m/s was not as effective, since the information entropy had not yet reached its asymptotic value after 7000 s of drying.

Figure A1.3 shows that similar results can be obtained from the standard deviation of the acoustic signals. The information entropy, however, seems more sensitive to low moistures.

Since the initial moisture was 100 ppm, the non-invasive acoustic signals therefore allow for the detection of moistures of a few tens of ppms. Very few on-line methods can achieve such sensitivity.

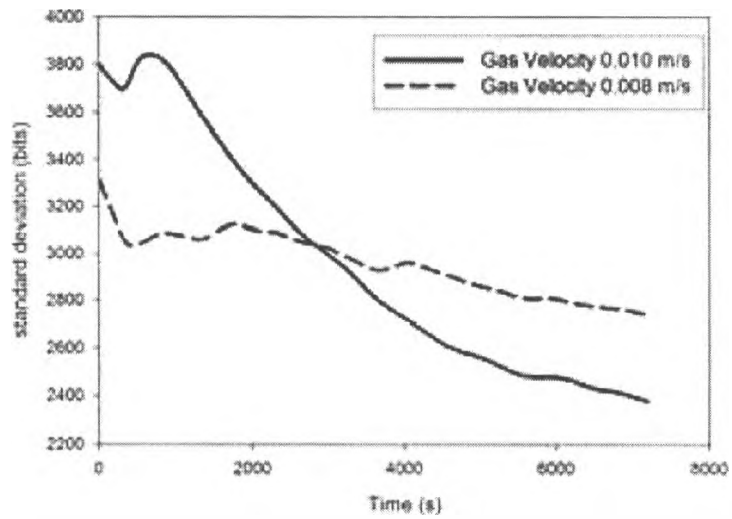

Figure A2.3 Evolution of the standard deviation of the acoustic emissions as the bed dries.

A 2.4 CONCLUSIONS

A non-invasive acoustic method was developed to identify fluidization regimes and to monitor drying within a vibrated fluidized bed.

The minimum fluidization and bubbling velocities can be reliably determined from the standard deviation of a microphone signal.

The drying of fluidized solids can be monitored by using either the information entropy or the standard deviation of a microphone signal. This acoustic method can detect moistures of a few tens of ppms.

A 2.5 ACKNOWLEDGEMENTS

The authors would like to thank the National Sciences and Research Council of Canada for their financial support of this research.

A 2.6 REFERENCES

[1] Belchamber, R. Acoustic Emission Monitoring – A New Tool for Particle Technology. *Pharmaceutical Technology Europe,* 12 (2000) 26-29.

Appendix 3. Flow Regime Detection in Pneumatic Transport of Particulates Using Non-Intrusive Acoustic Probes

K. Albion, C. Briens, L. Briens, F. Berruti, G. Book
Western Fluidization Group, Faculty of Engineering
The University of Western Ontario, London, Ontario, Canada, N6A 5B9

Note: This appendix was published in the non-refereed conference proceeding at Acoustics Week in Canada 2005 October 11-14, 2005, London, Ontario, Canada

A 3.1 Introduction

Pneumatic transport is used to convey solids in many industrial plants. Changes in particle properties or operating conditions may cause particles to settle out and deposit on the bottom of horizontal sections of the transport line. Such deposits result in unsteady solids flow, pressure surges and eventually, blockage of the line. Early detection of deposits would allow for quick corrective action.

The objective of this paper is to present an early detection method for solids deposits at the bottom of the transport line using only non-invasive sensors. External microphones were selected as non-invasive sensors and their signals were processed with advanced filters and signal analysis methods.

A 3.1.1 Pneumatic Transport and Flow Regimes

In dilute phase horizontal pneumatic transport, particles do not move forward in a straight line, parallel with the pipe wall. Gravity pulls the particles toward the bottom of the pipe, but are ideally kept in suspension by turbulent gas eddies. As the gas flowrate is reduced or the solids flowrate increased, particles eventually deposit on the bottom of the pipe [1].

Flow patterns in horizontal transport vary depending on the solids concentration and superficial gas velocity. Different flow regimes occur at different transport conditions. At high superficial gas velocities and low solids fluxes, there is fully suspended dilute phase flow; increasing the solids flux or decreasing the superficial gas velocity results in dilute phase flow with a higher concentration of solids transported along the bottom of the pipe, and later as solids deposits as dunes or a stationary bed [2].

Flow patterns in an inclined line are similar. At high gas velocities and low solids fluxes, there is dilute phase flow. Increasing the solids flux or decreasing the superficial gas velocity eventually results in solids deposition on the bottom of the pipe [3].

A 3.1.2 Acoustics

Acoustic sensors are inexpensive and can withstand a wide range of process conditions. They can provide reliable, on-line and non-intrusive monitoring. Passive acoustics detect the acoustic emissions generated by the process. In processes involving the movement of solid particles, acoustic emissions are caused by particles colliding with each other, vessel walls or other objects [4].

A 3.1.3 Signal Analysis – Wavelet Residual and V Statistic

The wavelet residual is a method used for detecting outliers in the signal [5]. Wavelets can be used to denoise signals while preserving sharp, rapid variations in the signal. However, in the present work the rejected "noise" actually contains valuable information about the process. The V Statistic is used to detect cyclic, non-periodic behaviour.

A 3.2 Method

The pneumatic transport loop consisted of a 0.1 m inside diameter, stainless steel pipe. The gas-solids mixture flows through a 5.3 m vertical transport line, a 5.5 m horizontal pipeline or 5 m inclined pipeline, with a return line into a cyclone. Each acoustic measurement was recorded at a frequency of 40 000 Hz. Acoustic sensors were located on the bottom or side of the pipe, at measurement locations of 0.05, 0.20, 0.35, 0.90, 1.05, 1.20, 1.35, 1.50, and 1.65 m from the elbow in the horizontal line for glass beads or PVC powder, or at 0.50, 1.05. 2.50 and 3.3 m from the elbow in the inclined line for polyethylene pellets. An acrylic section of pipe in each section allowed for visual observations of the flow regimes. The flow regimes could easily be determined from high speed video files.

A 3.3 Results and Discussion

The V Statistic at 0.000425 s was calculated from the wavelet residual signal. At this subperiod length, there was a significant difference in the V Statistic which allowed for regime identification. Three flow regimes were identified: conveying over settled solids,

dilute phase conveying and a transition region between the phases. Figure A3.1 shows that the narrow transition region could be detected from acoustic signals. This transition region occurred at $164 \pm 4\ s^{-0.5}$.

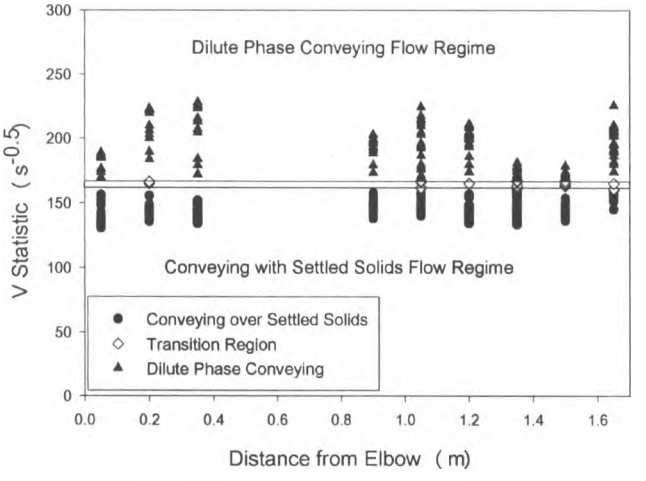

Figure A3.1 V Statistic values for glass beads using wavelet residual of acoustic signals for all distances from the elbow, identifying two main flow regimes and narrow transition region.

This method was applied to PVC powder in the same system, and resulted in a similar transition region of $169.5 \pm 5.5\ s^{-0.5}$.

Figure A3.2 is a flow regime map that was developed from the acoustic signals using the criteria shown in Figure 1. Each curve on the map represents the average value of the transition region, as it occurs relative to all solids fluxes and superficial gas velocities, and corresponds to a given distance from the elbow. The area located above each line represents the conveying with settled solids flow regime, whereas the area located below each curve represents dilute phase conveying. At 0.05 m from the elbow, the settled solids regime predominated. At distances further from the elbow, 0.35 m and 0.90 m, the position of the line changed, and there were more conditions where dilute phase flow occurred. The majority of dilute phase flow occurred at 0.90 m and 1.20 m, where the

shapes of the curves were nearly identical. Further from the elbow, at 1.50 m, there was less dilute phase flow, and the shape of the curve was similar to the curves closer to the elbow. This variation in the flows indicated where dunes existed rather than locations of a stationary bed. At 0.90 m and 1.20 m, there were breaks in the stationary bed, forming distinct dunes, existing at these locations and conditions, whereas at locations further from the elbow, a settled bed was detected.

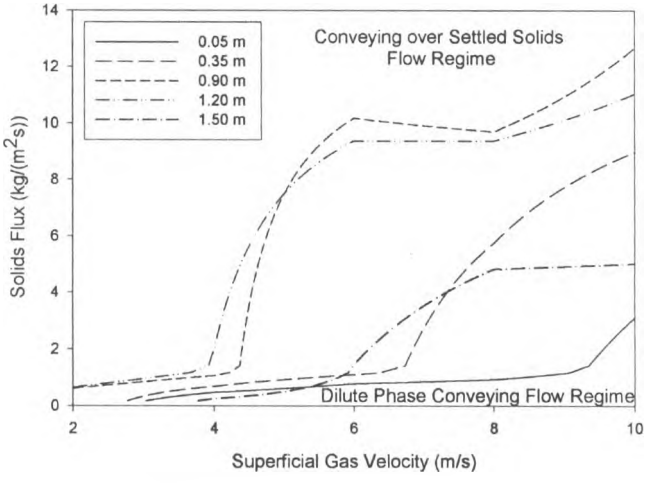

Figure A3.2 Flow regime map for glass beads at various distances from the elbow.

This flow regime method was applied to an inclined line transporting polyethylene pellets. Figure A3.3 shows the V Statistic values for the wavelet residual acoustic signal at 0.000425 s. Two regimes were identified, conveying over settled solids and dilute phase flow. There was no detectable transition region: minute changes in either gas velocity or solids flowrate were sufficient to switch from one regime to another. The boundary between the two regimes occurred at 73.0 $s^{-0.5}$.

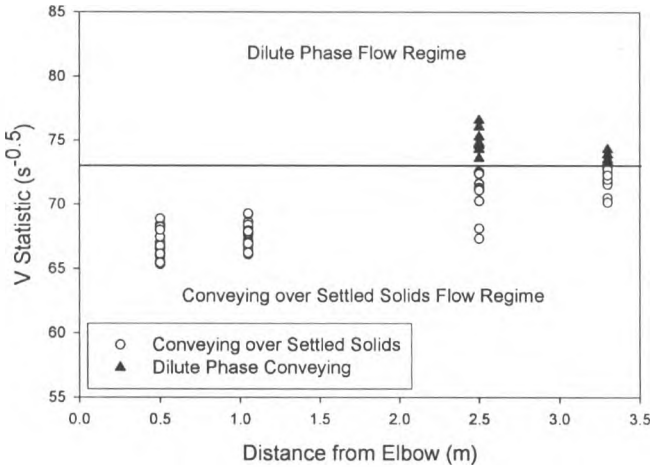

Figure A3.3 V Statistic values for polyethylene pellets from the wavelet residual acoustic signal for all distances from the elbow, identifying the two flow regimes.

A 3.4 Conclusions

Flow regimes in pneumatic transport can be detected by applying a wavelet filter to the raw acoustic signal and calculating the V Statistic at 0.000425 s on the residual signal.

There was a narrow transition region between the dilute phase regime and conveying with settled solids regime for horizontal transport of glass beads and PVC powders. There was a sharp boundary between the two flow regimes for inclined transport of polyethylene pellets.

This acoustic monitoring method is useful for process control. It allows for easy, rapid and non-intrusive on-line monitoring of flow regimes in pneumatic transport lines. It can help maintain the pneumatic transport line at conditions that maximize product quality and system efficiency.

A 3.5 Acknowledgements

The authors would like to thank the Natural Sciences and Engineering Research Council of Canada for their financial support of this research.

A 3.6 References

[1] Fan, L.S., Zhu, C. Principles of Gas-Solids Flows. United Kingdom: Cambridge University Press. (1998).

[2] Klinzing, G.E., Marcus, R., Rizk, R., Leung, L.SPneumatic Conveying of Solids, 2nd Edition. Great Britain: Chapman & Hall. (1997).

[3] Klinzing, G.E., Rohatgi, N.D., Myler, C.A., Dhodapkar, S., Zaltash, A., Mathur, M.P. Pneumatic transport of solids in an inclined geometry. *Canadian Journal of Chemical Engineering*, 67(1989), 237 - 244.

[4] Boyd, J.W.R., Varley, J. The uses of passive measurement of acoustic emissions from chemical engineering processes. *Chemical Engineering Science*, 56(2001) 1749 - 1767.

[5] Trygg, J., Kettaneh-Wold, N., Wallbacks, L. 2D wavelet analysis and compression of on-line industrial process data. *Journal of Chemometrics*, 15 (2001). 299 - 319.

Appendix 4. Flow Regime Determination in Upward Inclined Pneumatic Transport of Particulates Using Non-Intrusive Acoustic Probes

K. Albion, C. Briens, L. Briens, F. Berruti, G. Book
Western Fluidization Group, Faculty of Engineering
The University of Western Ontario, London, Ontario, Canada, N6A 5B9

NOTE: Published in Chemical Engineering and Processing, 46(6), 520-531, 2007.

A 4.1 Introduction

Pneumatic transport is used to convey solids in many industrial plants. Changes in particle properties or operating conditions, such as solid or gas flowrates, may cause particles to settle out and deposit on the bottom of the pipe diameter in the transport line. Such deposits result in unsteady solids flow, pressure surges and, eventually, blockage of the line. Early detection of deposits would allow for quick corrective action, which could take the form of an increase in gas flowrate or a momentary reduction in solids flowrate.

The objective of this paper is to develop a non-invasive method, which is independent of the pipe angle, for the early detection of solids deposits within an inclined transport line. External microphones were selected as non-invasive sensors and their signals were processed with advanced filters and signal analysis methods.

Non-invasive microphones allow for measurements without disrupting the flow within the pipe for an accurate measurement of flow conditions. This technology is easy to

implement: microphones attach to the external surface of the pipe wall and can be easily relocated, whereas conventional pressure measurements require pressure taps in fixed locations, and can interfere with the flow.

A 4.2 Background Information

This section provides background information on inclined pneumatic transport, the use of pressure drop measurements to determine flow characteristics, acoustic emissions and their detection, and on the signal analysis methods used in the present study: cycle and wavelet analyses.

A 4.2.1 Inclined Pneumatic Transport

There are two types of pneumatic transport systems: dilute phase transport, where particles occupy less than 5% of the line volume, and dense phase transport, where particles may occupy up to 50% of the line volume. The present study focuses on dilute phase transport.

In dilute phase horizontal pneumatic transport, particles do not move forward in a straight line, parallel with the pipe wall. Although gravity pulls the particles toward the bottom of the pipe, they are ideally kept in suspension due to turbulent gas eddies. However, as the gas flowrate is reduced or the solids flowrate is increased, particles eventually deposit on the bottom of the pipe [1]. Inclined pneumatic transport has potential benefits over horizontal and vertical pipelines including a shorter pipe and a smaller number of pipe elbows, resulting in less wear and a lower pressure drop [2]. Disadvantages of inclined

pneumatic transport include high energy losses, large fluctuations of gas and solids flowrates and pipeline blockage [3]. However, pneumatic transport systems with inclined lines are common in industry [4]. Since inclined pipelines experience flow instabilities, it is important to have an accurate monitoring method.

Flow patterns in pneumatic transport vary depending on the solids concentration and superficial gas velocity. Figure A4.1 describes the different flow regimes in pneumatic transport encountered in this study, as the gas flowrate is decreased or the solids flowrate increased. Figures A4.1a and A4.1b show fully suspended dilute phase flow, Figures A4.1c and A4.1d illustrate dilute phase flow with a higher concentration of solids transported along the bottom of the pipe, and Figures A4.1e and A4.1f show solids deposits as dunes or a stationary bed [5-8].

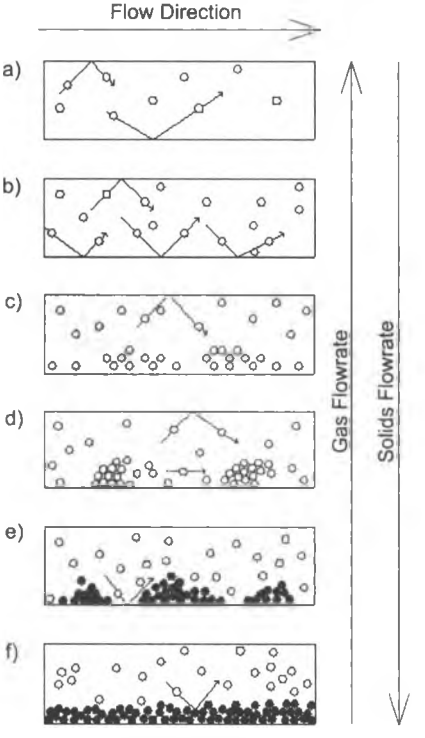

Figure A4.1. Flow regimes encountered in pneumatic transport (Adapted from [1]).

The state diagram allows for identification of the flow regimes discussed above, based on the pressure drop per unit length of pipe as a function of the gas velocity. Traditionally, the pressure minimum curves on the state diagram have been used to distinguish between dilute and the dense phase flow regimes [5].

A 4.2.2 Acoustics

Acoustic sensors are inexpensive and can withstand a wide range of process conditions. They can provide reliable, on-line and non-intrusive monitoring. There are two acoustic monitoring methods:

- active acoustics detect the effect of the process on a transmitted acoustic wave; and
- passive acoustics detect the acoustic emissions generated by the process.

Generally, passive acoustic methods are much easier to implement and are preferred when the process acoustic emissions are strong, which is the case with pneumatic transport.

Acoustics is defined as the study of sound. Sound results from pressure vibrations that can be detected by the human ear or microphones. The vibrations are caused by rapid, linear motion of a particle or elastic solids about an equilibrium position [9].

In processes involving the movement of solid particles, acoustic emissions are caused by particles colliding with each other, vessel walls or other objects. When rigid particles

impinge upon each other, the result is acoustic emissions in either sonic [10] or ultrasonic ranges depending on the particle size, shape and acoustic properties [11].

The microphones used in this study were prepolarized electret condenser microphones, which transform sound pressure fluctuations into capacitance variations, which are further converted into an electrical voltage signal. They produce an oscillating voltage proportional to the original pressure oscillations [9].

A 4.2.3 Signal Analysis – The V Statistic for the Detection and Characterization of Non-Periodic Cycles

Hurst [12] developed the rescaled range technique for the analysis of time series. The time series is divided into time intervals of length τ. The data is rescaled to have a mean of 0, and a standard deviation of 1. The rescaled range is calculated for each time interval, with the average of the rescaled ranges, $(R/S)_\tau$, calculated for all intervals of length τ. By changing the length of τ and plotting $\ln(R/S)_\tau$ against $\ln(\tau)$, a curve is produced from which Hurst was able to detect and characterize non-periodic cycles such as the floods of the Nile River [12]. The $\ln(R/S)_\tau$ against $\ln(\tau)$ curve can have two linear regions. The region between the linear segments corresponds to the cycle time of the measured signal. This cycle time, however, can be difficult to determine if the change is gradual [13].

Peters [14] extended Hurst's analysis with the V Statistic to facilitate the detection of cyclic, non-periodic behaviour in the stock market. The V Statistic is calculated through:

$$V_\tau = \frac{(R/S)_\tau}{\tau^{0.5}}. \qquad (1)$$

The V Statistic is plotted against ln(τ); the maximum V Statistic occurs at the cycle time determined by the intersection of the linear Hurst curve regions. The V Statistic provides an accurate measure of the cycle length [13].

A 4.2.4 Signal Analysis – Wavelets

Wavelet transforms are applied to complex signals for de-noising, data compression and feature extraction. Wavelet transforms decompose the original signal into scaled and shifted versions of the original wavelet, resulting in a signal with multiple scales. When low-frequency components of a spectrum are preferred, a stretched version of the wavelet function is used, whereas the opposite is true for higher frequency components [15].

Very rapid signal analysis can be achieved with the discrete wavelet transform. For a signal of length 2^j, filtering is performed j times, resulting in j levels of different scales, each separated by a factor of 2. The wavelet filter produces wavelet coefficients, whereas the scaling filter describes the signal, whose coefficients represent the signal in the next scale. This allows for exact reconstruction of the original signal through the use of the average value and wavelet coefficients. The size of the transformed signal is the same as the original signal if the average value is used. The wavelet residual is a method used for detecting outliers in the signal [15].

Wavelets can be used to denoise signals. An advantage of wavelet filters is that sharp, rapid variations in the signal are preserved. Sometimes, as in the present work, the rejected "noise" actually contains valuable information about the process.

A 4.2.5 Signal Analysis Methods to Determine Flow Regimes

Briens et al. [13, 16] developed a variety of methods based on the V Statistic and applied them to the detection of flow regime transitions in different multiphase systems. Albion et al. [17] developed a method to determine the flow regime in horizontal pneumatic conveying based on the value of the V Statistic at a certain subperiod length. These methods are easy to implement, rapid and tolerate signal contamination by electrical noise. They are ideally suited to the monitoring of industrial processes. Dhodapkar and Klinzing [18] detected flow patterns in a horizontal pneumatic transport system by applying the power spectra to the recorded pressure fluctuations, at low frequencies. Luewisuthichat et al. [19] and Kikuchi et al. [20] also studied three-phase systems and used the correlation dimension to detect the transition between flow regimes. Srivastava et al. [21] studied circulating fluidized beds using electrical capacitance tomography and determined that ECT could successfully image flow patterns in gas-solids flows.

A 4.3 Equipment and Experimental Methods

A 4.3.1 Pneumatic Transport System

The pneumatic transport loop consisted of a 0.1 m inside diameter, stainless steel pipe, shown in Figure A4.2. Air was supplied from a compressor, controlled using a regulator and set and monitored using a valve, calibrated pitot tube, pressure transducer and

voltmeter. Air flows through a horizontal pipeline located underneath the storage silo from which powder is fed into the line with a vibrating feeder. Figure A4.2a shows a 5.0 m vertical transport line and a 5.5 m horizontal line, whereas in Figure A4.2b, the gas-powder mixture flows upwards through a 4.0 m vertical transport line, a 4.0 m inclined line, and a return horizontal line into a cyclone where solids are separated from the gas stream. The inclined line was at inclinations of 15^{o} and 25^{o} from the horizontal. The gas and small entrained particles enter a baghouse filter for further separation, whereas the solids return to a solids hopper. A diverter valve located in the cyclone dipleg allows for the measurement of the solids mass flowrate.

A 4.3.2 Powder Characteristics

Three different solids, polyethylene pellets, glass beads and polyvinylchloride (PVC) powder, were used to test the detection method over a wide range of particle sizes and densities. The apparent particle density, equivalent particle diameter and terminal velocity for each solid is shown in Table A4.1.

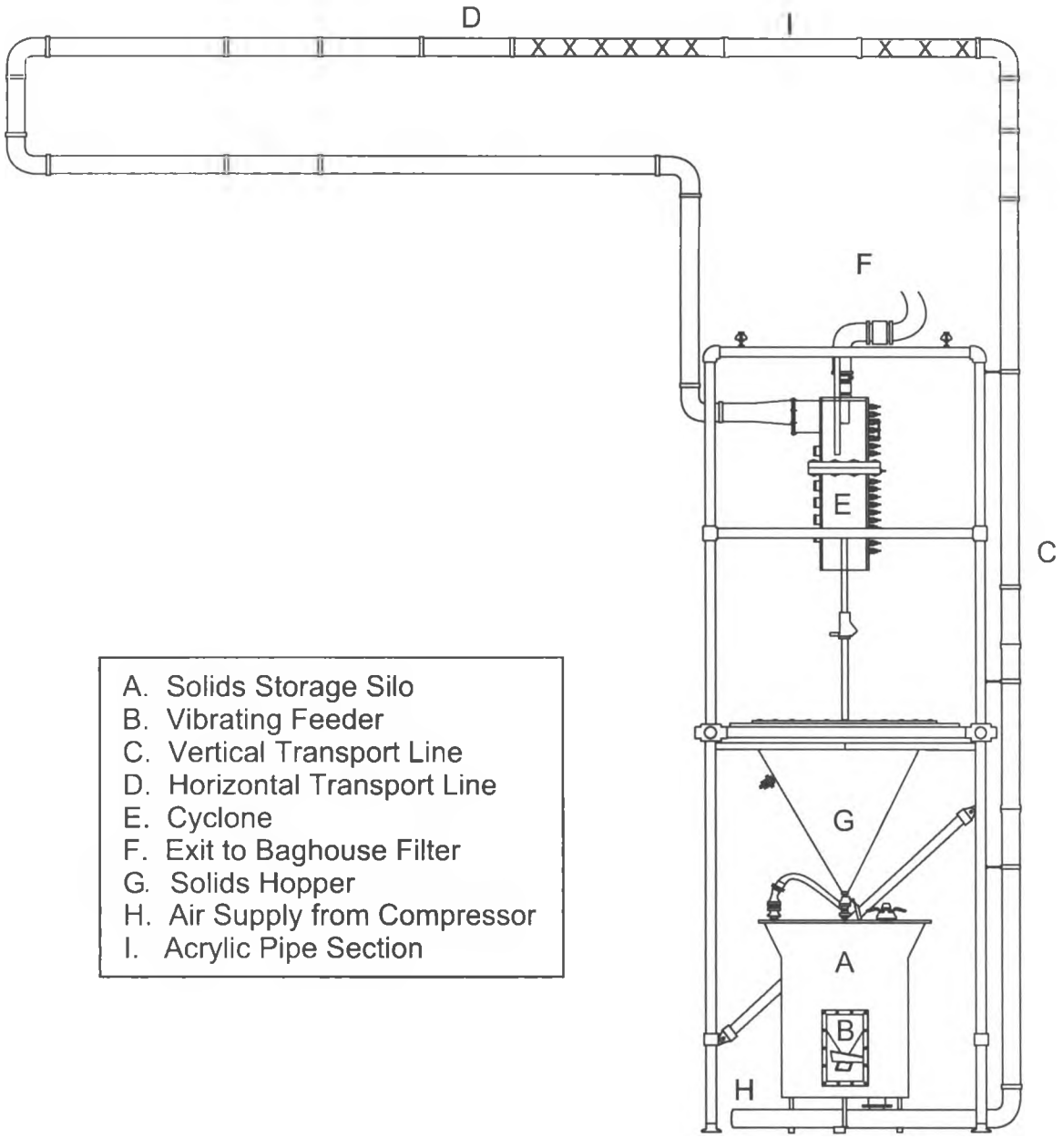

Figure A4.2a. Schematic diagram of the pneumatic transport system containing the horizontal line. X indicates location of acoustic probe measurements.

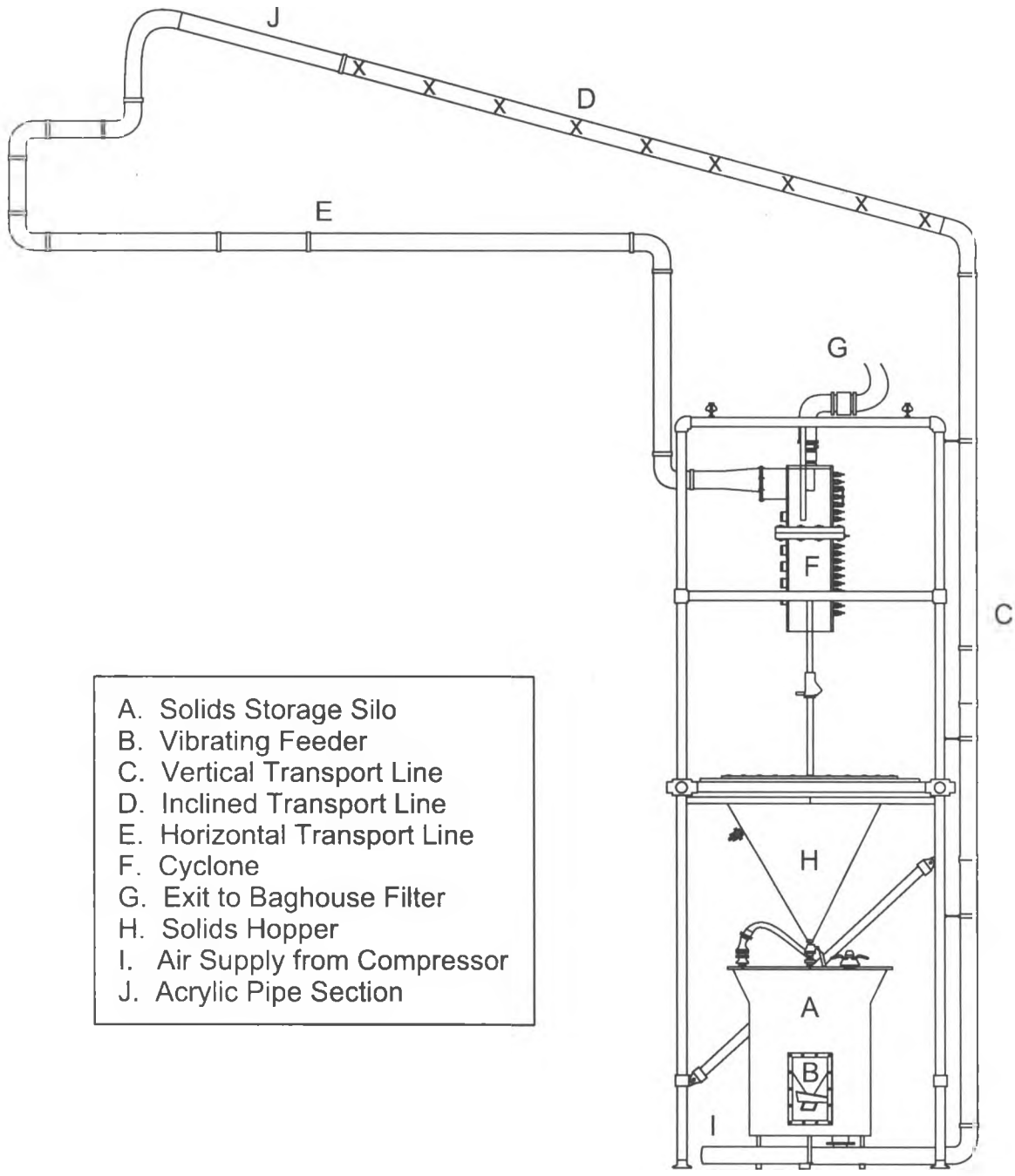

Figure A4.3b. Schematic diagram of the pneumatic transport system containing the inclined line. X indicates location of acoustic probe measurements.

A 4.3.3 Powder Flow Properties

Flow regimes in the pipeline are controlled through the variation of the solids flux and superficial gas velocities. The solids fluxes and superficial gas velocities studied for each solid are shown in Table A4.1.

Table A4.4.1. Physical properties of powders studied and operating conditions

	Glass Beads	PVC	Polyethylene Pellets
Apparent particle density (kg/m^3)	2 600	1 380	950
Equivalent particle diameter (μm)	171	154	2 800
Terminal velocity (m/s)	1.2	0.63	5.5
Solids Fluxes ($kg/(m^2s)$)	1.24, 5.97, 13.5, 28.3	0.234, 4.29, 15.8, 23.5	0.0485, 0.823, 6.89, 13.5
Superficial Gas Velocities (m/s)	2, 4, 6, 8, 10	2, 4, 6, 8, 10	7, 9, 11, 13, 15

A 4.3.4 Acoustic and Pressure Sensors

Six prepolarized electret microphones manufactured by PCB were used to simultaneously record acoustic signals at different locations along the inclined pipeline. Data was acquired using a National Instruments card and board. Each measurement was recorded at a frequency of 40 000 Hz. Acoustic sensors were located on the side of the pipe, at each measurement location on the 15° and 25° inclined pipe sections, and on the top of the pipe for measurements on the horizontal line. No significant differences were found between measurements on the top and on the side of the pipe. This allowed

measurements to be easily made for all configurations and for comparison of the results. Measurement locations of 0.05, 0.20, 0.35, 0.90, 1.05, 1.20, 1.35, 1.50, 1.65 m from the elbow in the horizontal line are shown in Figure 4.2a, whereas measurement locations of 0.20, 0.30, 0.50, 1.05, 1.50, 1.75, 2.00, 2.50, 3.30 and 3.95 m from the inclined elbow are indicated in Figure 4.2b. Acoustic sensors were secured to the pipeline using a strip of shim shaped to the form of the sensor, and attached to a thin foam base. This base was held to the pipe with Velcro wrapped around the pipe circumference.

Four differential pressure transducers produced by Omega were used to record pressure signals simultaneously with the acoustic sensors at different locations along the inclined line. Pressure taps were located on the top of the pipe at measurement locations of 0.15, 0.40, 0.65, 0.90, 1.15, 1.40, 1.65, 2.40, 2.90, 3.40 and 3.90 m from the inclined elbow.

A 4.3.5 Visual Observations

An acrylic section of pipe in the inclined and horizontal pipelines allowed for visual observations of the flow regimes. The flow regimes could, thus, easily be determined.

A 4.3.6 Experimental Method

For each measurement, the superficial gas velocity was set at the desired flow rate before solids were added to the transport line. Once the flow stabilized, acoustic and pressure measurements were recorded. After each measurement, the solids feeder was stopped and the gas flow maintained until the pipeline was completely cleared of solids.

A 4.3.7 Signal Analysis Methods

Raw signals were recorded by LabVIEW in a binary format. From these raw signals, a notch filter was used to filter out 60 Hz electrical noise. The V Statistic was calculated using a smallest number of divisions of 10 and a minimum subperiod length of 10, which provided 10 000 R/S values. The V Statistic used in further analysis occurred at a 0.000425 s subperiod length. For further refinement, a wavelet filter was used at 95% compression, and the wavelet residual was calculated. A 95% compression means that 95% of the wavelet coefficients, the smaller ones, are set to zero. The wavelet residual was also analysed using the V Statistic.

A 4.4 Experimental Results and Discussion

A 4.4.1 Raw Acoustic Signals

Figures A4.3a and A4.3b show that the presence of solids deposits cannot be detected from the raw signals. These figures show the acoustic raw signal of glass beads, filtered to eliminate the 60 Hz electrical noise, recorded under ideal dilute phase conveying and conveying over settled solids conditions. These signals were all recorded at the 25^{o} angle from the horizontal at 1.05 m from the elbow, and show 1 s of data. Each signal is centred around 0 V and has the same standard deviation. The flow regime cannot be

determined from a visual observation of the raw acoustic signals. This trend continues for the other solids, angles and locations examined.

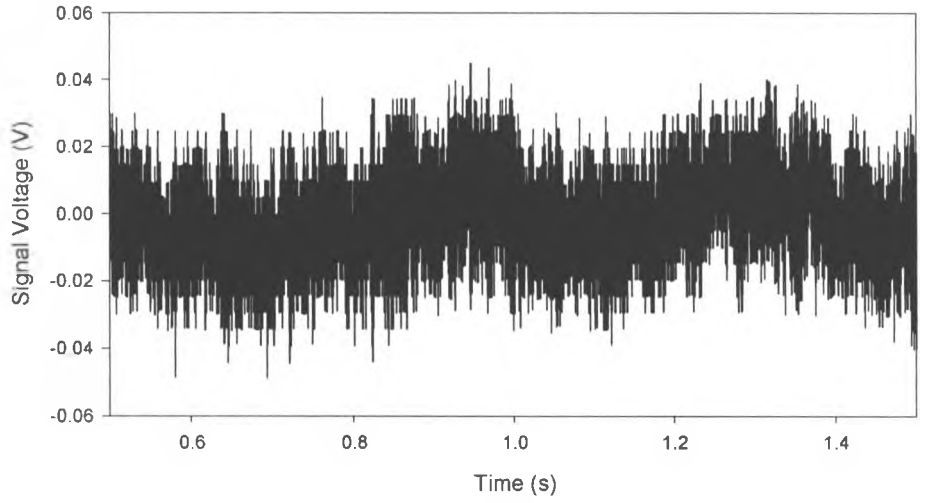

Figure A4.4a. Acoustic raw signal for dilute phase conveying of glass beads at x = 1.05 m from the elbow at an angle of 25°, U_g = 4 m/s and F_s = 1.24 kg/(m^2s).

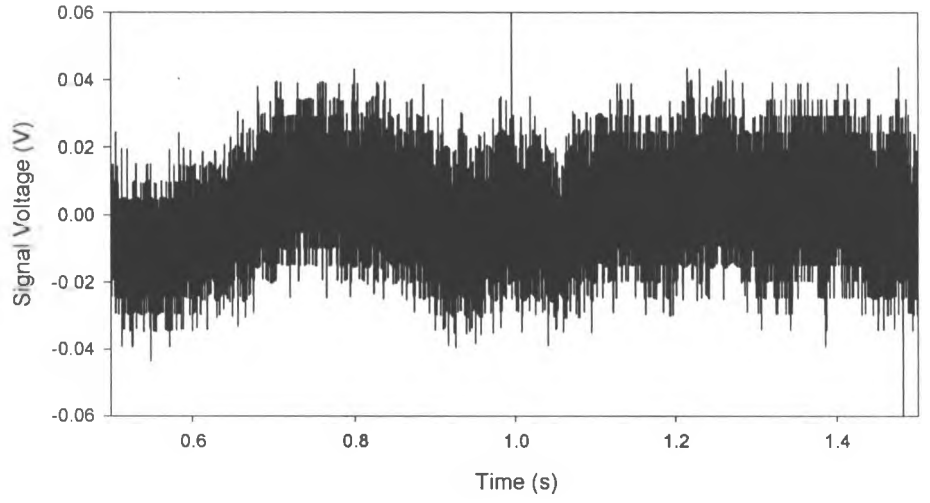

Figure A4.5b. Acoustic raw signal for conveying over settled solids of glass beads at x = 1.05 m from the elbow at an angle of 25°, U_g = 10 m/s and F_s = 28.3 kg/(m^2s).

A 4.4.2 Raw Pressure Signals

The sampling frequency of the differential pressure transducers was 40 000 Hz; this was reduced to 1 000 Hz for analysis. Figure 4.4a is the raw pressure signal for glass beads under dilute phase conveying, whereas Figure 4.4b is the pressure signal under conveying of settled solids. These signals were recorded at 0.40 m from the elbow on the 25° inclined line. The signals had nearly the same mean (7.36 V vs. 7.38 V) and the standard deviations were the same. These figures correspond to the same flow conditions as presented in the previous acoustic signals and were recorded at the same time. The flow regime cannot be determined from the pressure signals.

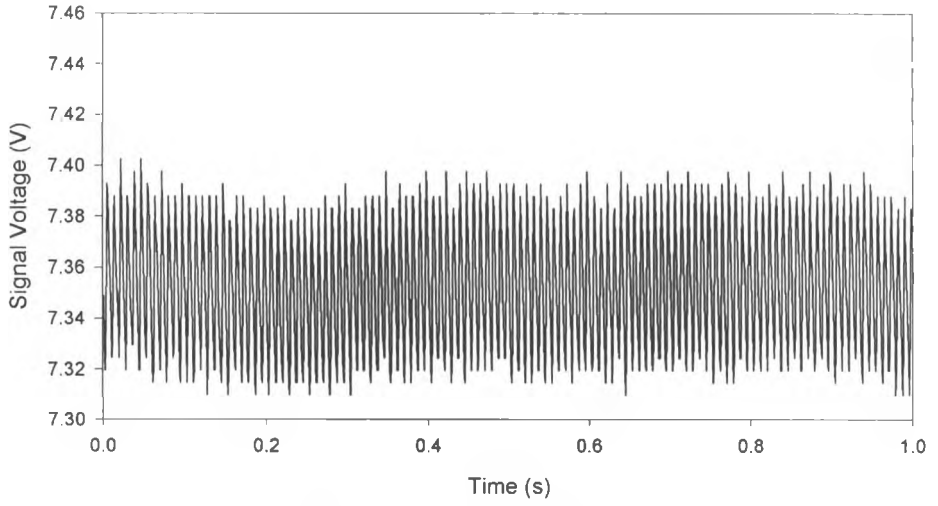

Figure A4.6a. Pressure signal for dilute phase conveying of glass beads at x = 0.40 m from the elbow, at an angle of 25°, U_g = 4 m/s and F_s = 1.24 kg/(m^{2}s).

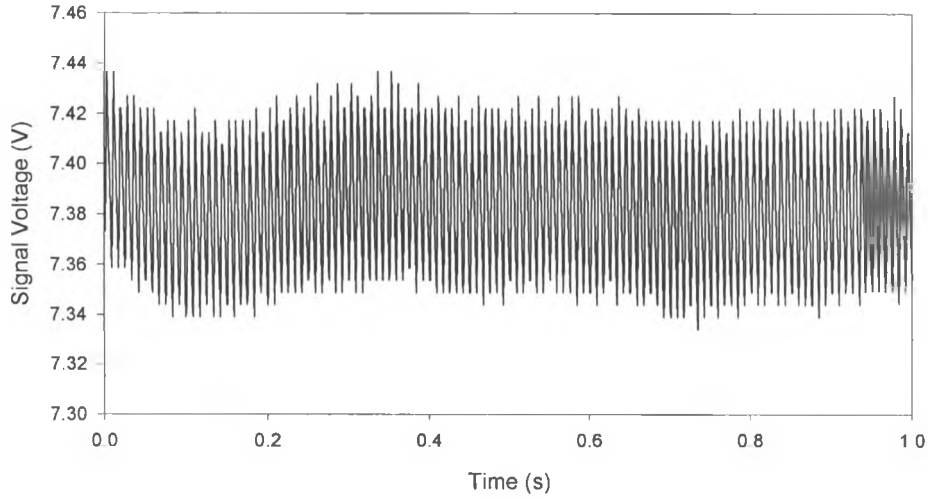

Figure A4.7b. Pressure signal for conveying over settled solids of glass beads at x = 0.40 m from the elbow, at an angle of 25°, U_g = 10 m/s and F_s = 28.3 kg/(m^2s).

A 4.4.3 Wavelet Residual Acoustic Signals

Figures 4.5a and 4.5b were obtained from the data presented in Figures A4.3a and A4.3b for dilute phase conveying and conveying over settled solids flows, after the application of a wavelet filter. These figures show the residual signal of a 95% compression Daubechies 4 wavelet filter. The signals for each flow regime have similar means and standard deviations. In these signals there are no periodic components to the signals; the mean is always at 0 V. As well there are few spikes or irregularities in the signal. The flow regime cannot be determined from a visual observation of the wavelet residual acoustic signals. These results are the same for the other solids, angles and locations examined.

A 4.4.4 V Statistic

The V statistic of the acoustic signals clearly discriminates between the flow regimes. Figure 4.6a represents the V Statistic curves from the signals shown in Figures A4.3a and

A4.3b. The V Statistic curves for dilute phase conveying and conveying over settled solids flow regimes show weak cyclic components, and increase regularly. The curves are clearly distinct, especially at small subperiod lengths. Similar results were obtained with the PVC and polyethylene pellets.

Figure A4.6b shows the V Statistic curves of the wavelet residual signals corresponding to Figures A4.5a and A4.5b. The cyclic behaviour in the raw signal V Statistic curve has been reduced through the use of the filter. These curves do not reach a maximum V Statistic peak. However, they both increase regularly. The difference in the V Statistic is especially marked at small subperiod lengths between flow regimes. This trend continues for the PVC and polyethylene pellets.

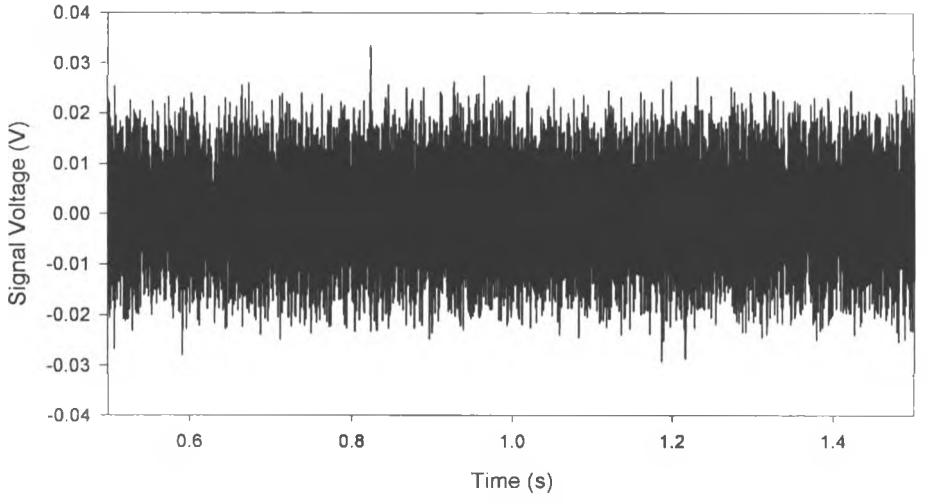

Figure A4.8a. Wavelet residual signal for dilute phase conveying of glass beads at x = 1.05 m from the elbow, at an angle of 25°, U_g = 4 m/s and F_s = 1.24 kg/(m^2s).

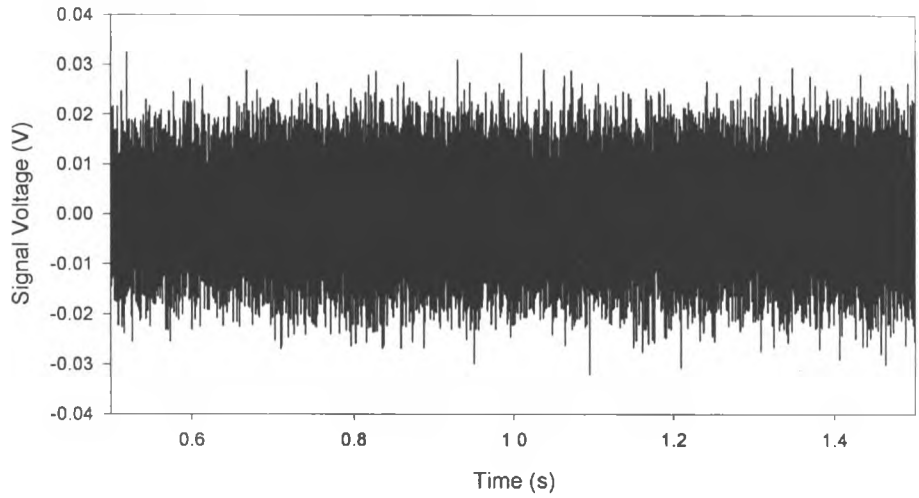

Figure A4.9b. Wavelet residual signal for conveying over settled solids of glass beads at x = 1.05 m from the elbow at an angle of 25°, U_g = 10 m/s and F_s = 28.3 kg/(m^{2}s).

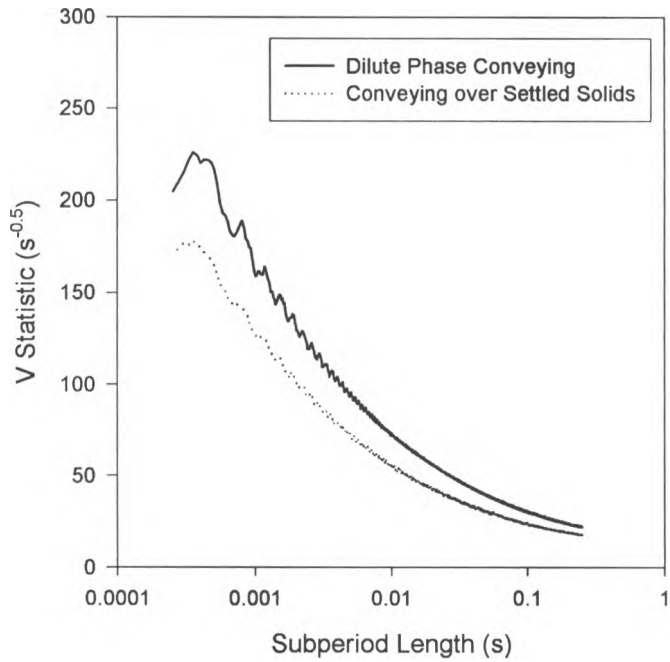

Figure A4.10a. V Statistic curves of raw signals for dilute phase conveying (U_g = 4 m/s, F_s = 1.24 kg/(m^{2}s)), and conveying over settled solids (U_g = 10 m/s, F_s = 28.3 kg/(m^{2}s)) for glass beads at x = 1.05 m from the elbow at an angle of 25°.

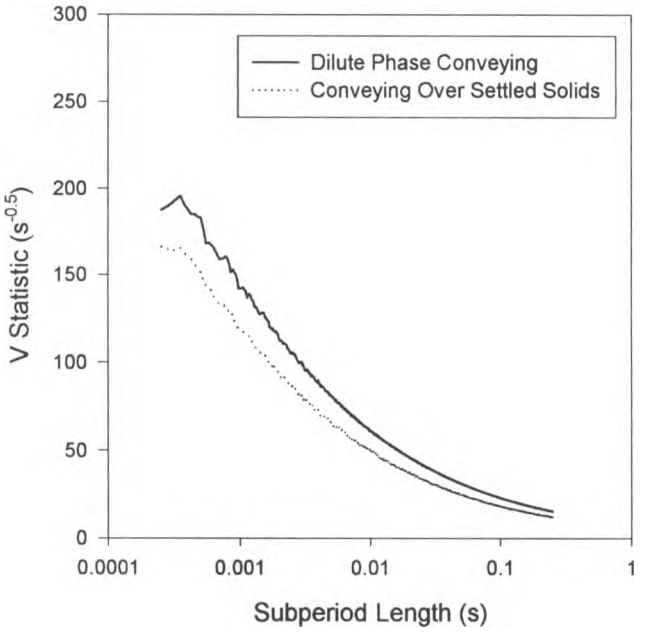

Figure A4.11b. V Statistic curves of wavelet residual signals for dilute phase conveying (U_g = 4 m/s, F_s = 1.24 kg/(m^{2}s)), and conveying over settled solids (U_g = 10 m/s, F_s = 28.3 kg/(m^{2}s)) for glass beads at x = 1.05 m from the elbow at an angle of 25°.

Figure A4.7 shows the resulting V Statistic curves of the wavelet residual signals corresponding to dilute phase flow and conveying over settled solids, as well as from the vibrating feeder and the flow of gas without solids in the system. Similar trends were obtained with power spectra. The V Statistic curve from the feeder has a different shape compared to the curves for gas and solids flow: this curve reaches a maximum V Statistic peak with a cycle time of approximately 0.001 s. Results from this study can therefore be generalized to lines equipped with different feeders.

Figure A4.7 also shows that the V Statistic curve corresponding to gas flow reaches a peak with a cycle time at approximately 0.0005 s. This cyclic behaviour was damped with the addition of solids in the system with greater damping occurring at higher solids

fluxes. The cycle at 0.0005 s observed with pure gas practically disappeared in the settled solids regime.

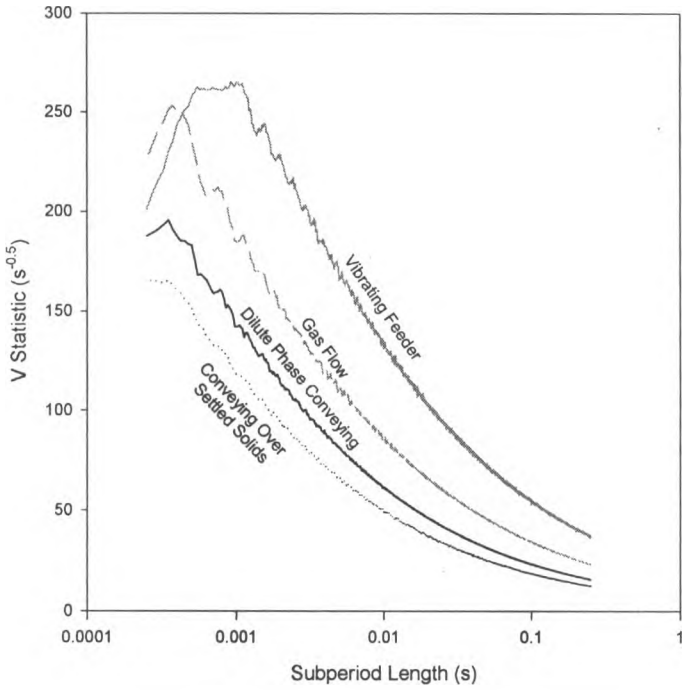

Figure A4.12. V Statistic curves of wavelet residual signals for dilute phase conveying (U_g = 4 m/s, F_s = 1.24 kg/(m^2s)) and conveying over settled solids U_g = 10 m/s, F_s = 28.3 kg/(m^2s)) for glass beads, vibrating feeder (corresponding to F_s = 1.24 kg/(m^2s)) and gas flow (U_g = 10 m/s) at x = 1.05 m from the elbow at an angle of 25°.

A 4.4.5 V Statistic and Distance

The V Statistic was calculated for measurements recorded at all distances from the elbow, angles, solids fluxes and gas velocities. As shown in Figure A4.6b, since a maximum V Statistic is not always present, the V Statistic at 0.000425 s was used for the analysis of flow regime transitions. At this subperiod length, Figures A4.6a and A4.6b show that there is a significant difference between the V Statistic curves corresponding to the different flow regimes.

Figures A4.8a, A4.8b, and A4.8c demonstrate that the V statistic of the acoustic signals can reliably distinguish between the flow regimes. They show all the V Statistic values at various distances from the elbow and the different angles, for the glass beads. Three flow regimes are identified in the chart: conveying over settled solids, dilute phase conveying and a transition region between the two flow regimes.

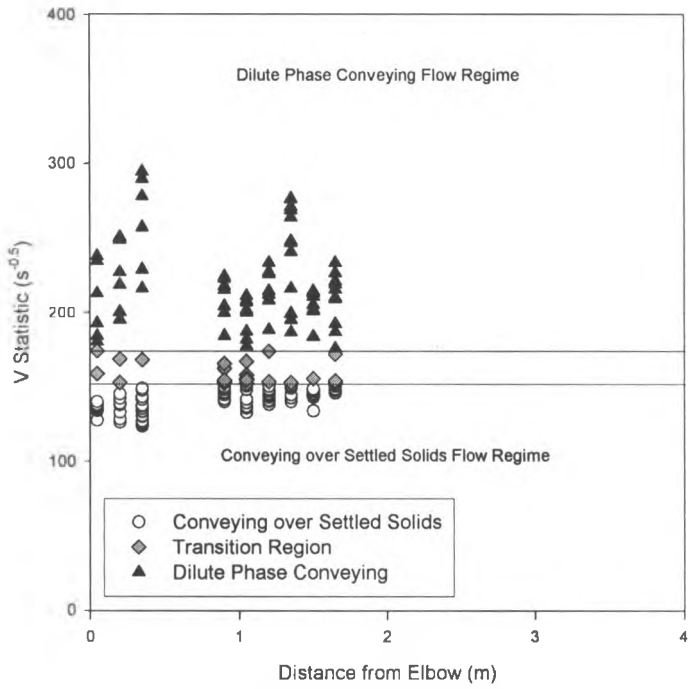

Figure A4.13a. V Statistic values for glass beads from the raw signal at 0.000425 s at an angle of 0° and all distances from the elbow.

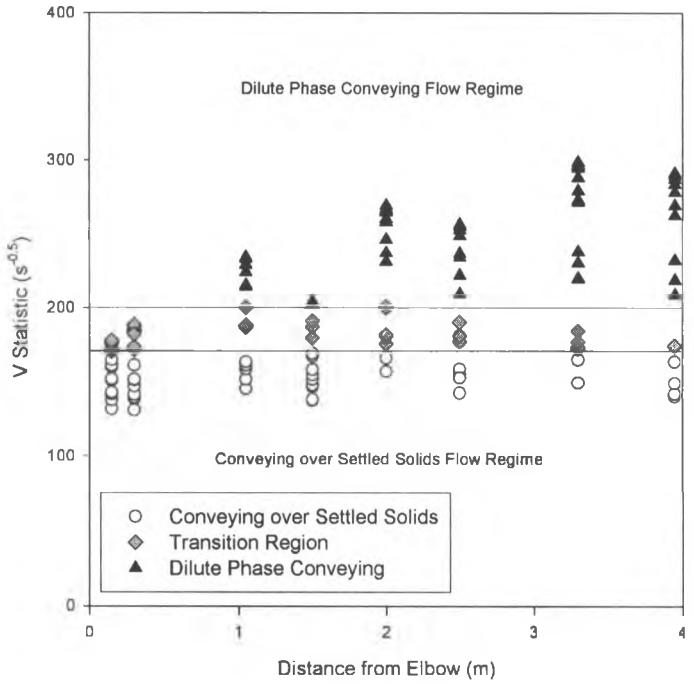

Figure A4.14b. V Statistic values for glass beads from the raw signal at 0.000425 s for an angle of 15° and all distances from the elbow.

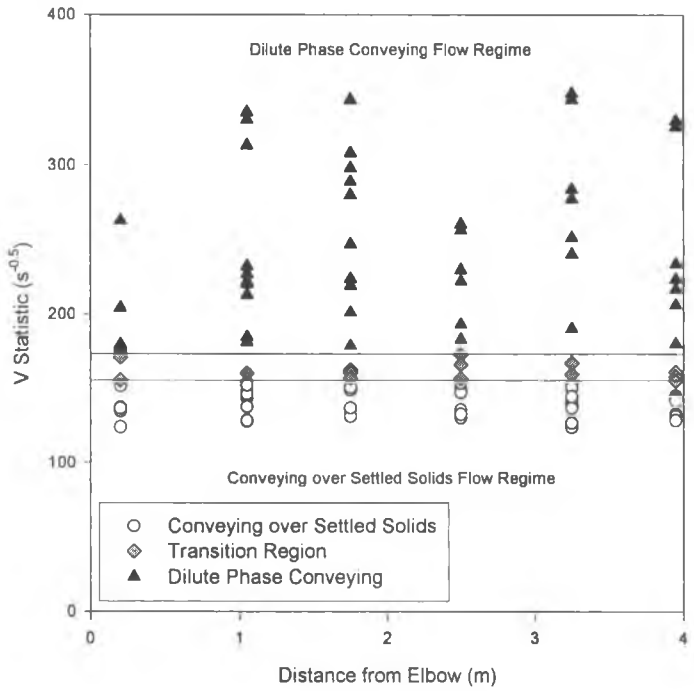

Figure A4.15c. V Statistic values for glass beads from the raw signal at 0.000425 s for an angle of 25° and all distances from the elbow.

For each solid and angle a different transition region exists, as shown in Figure A4.9. Above this transition region is dilute phase conveying V Statistic values, whereas below the transition region is conveying over settled solids V Statistic values. The critical V Statistic value is lower for the polyethylene pellets compared to the V Statistic values for the PVC and glass beads. Although this method is very reliable, the critical V Statistic value varies greatly with solid type and line inclination.

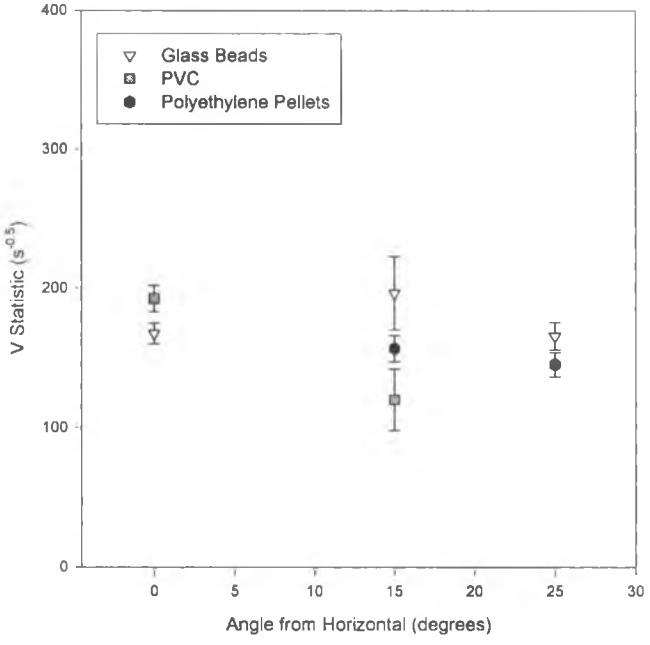

Figure A4.16. Raw signal V Statistic transition regions for each solid and angle from the horizontal.

To improve this method, the V Statistic at 0.000425 s was calculated from the wavelet residual signal. Figures A4.10a through A4.10g show that the range of V Statistic values has been condensed with less variation in each regime. Figures A4.10a, A4.10b and A4.10c show the narrower transition region for glass beads at 0^{o}, 15^{o} and 25^{o}. Figures A4.10d and A4.10e show the narrow transition region for PVC at 0^{o} and 15^{o}, whereas Figures A4.10f and A4.10g show the narrow transition region for polyethylene pellets at

15° and 25°. Figure A4.11 shows the new transition region values for each solid and angle: the critical V Statistic value varies much less with solid type and line inclination than when the raw acoustic signals were used (Figure A4.9). As shown by Figure A4.11, when the wavelet residuals are used, the transition region is narrower and is the same for the PVC and glass beads at each angle studied. However, the transition region is different for the polyethylene pellets compared to the powders, although the values for the pellets at the 15° and 25° angles are the same.

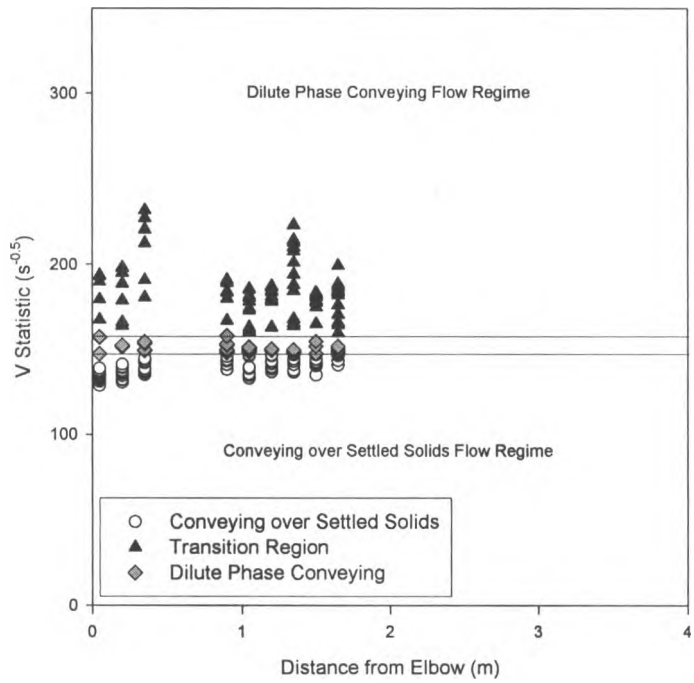

Figure A4.17a. V Statistic values for glass beads from the wavelet residual signal at 0.000425 s for all distances from the elbow at an angle of 0°.

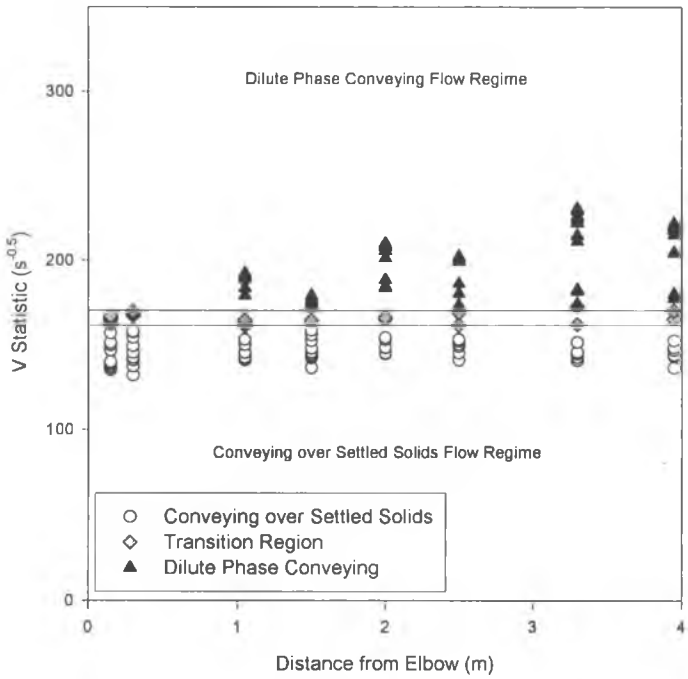

Figure A4.18b. V Statistic values for glass beads from the wavelet residual signal at 0.000425 s for all distances from the elbow at an angle of 15°.

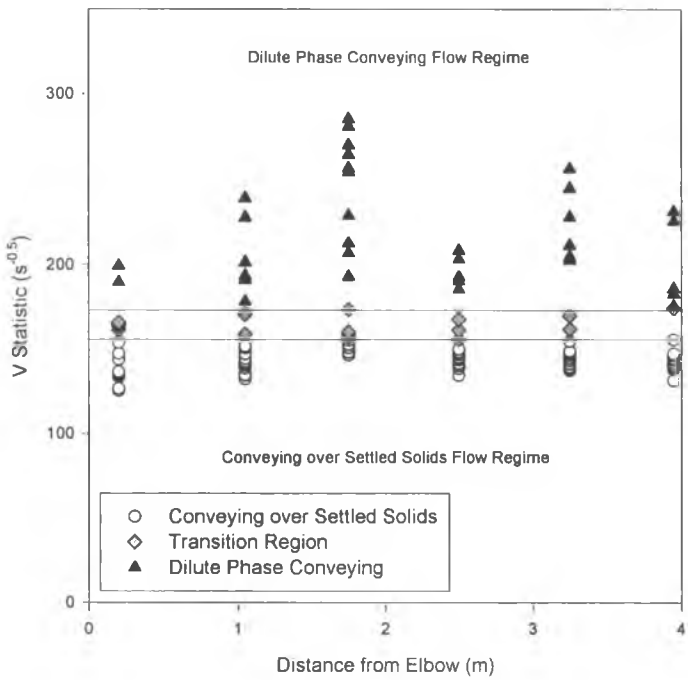

Figure A4.19c. V Statistic values for glass beads from the wavelet residual signal at 0.000425 s for all distances from the elbow at an angle of 25°.

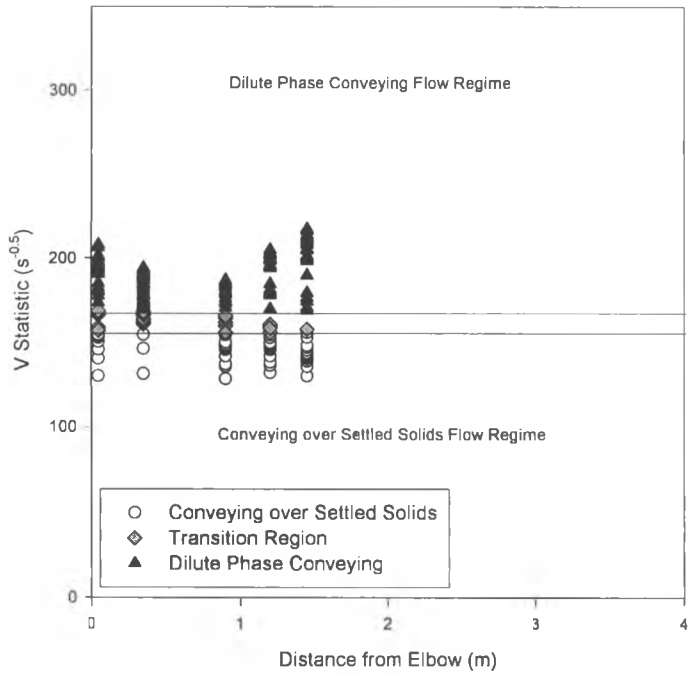

Figure A4.20d. V Statistic values for PVC from the wavelet residual signal at 0.000425 s for all distances from the elbow at an angle of 0°.

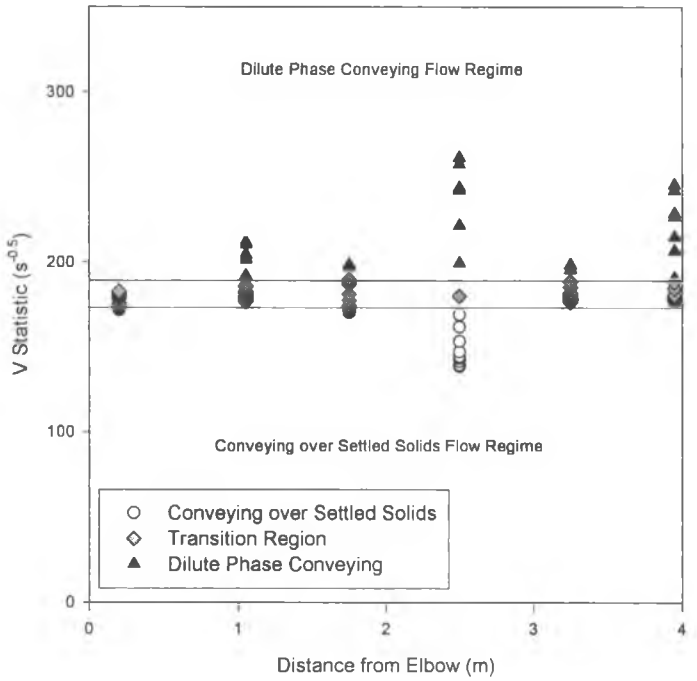

Figure 4.4.21e. V Statistic values for PVC from the wavelet residual signal at 0.000425 s for all distances from the elbow at an angle of 15°.

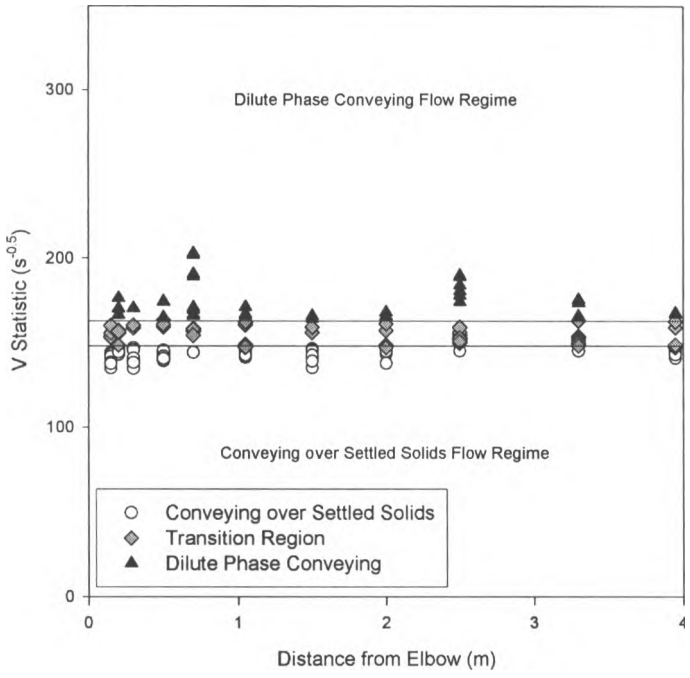

Figure 4.4.22f. V Statistic values for polyethylene pellets from the wavelet residual signal at 0.000425 s for all distances from the elbow at an angle of 15°.

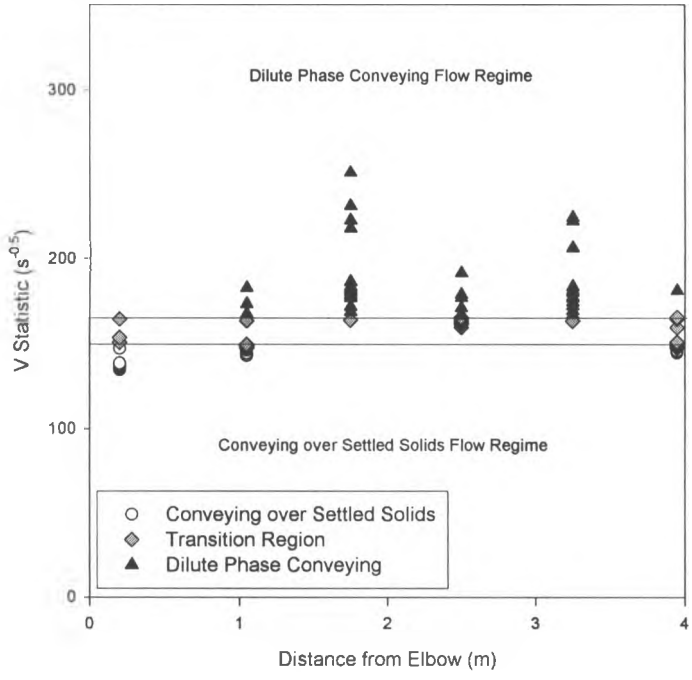

Figure 4.4.23g. V Statistic values for polyethylene pellets from the wavelet residual signal at 0.000425 s for all distances from the elbow at an angle of 25°.

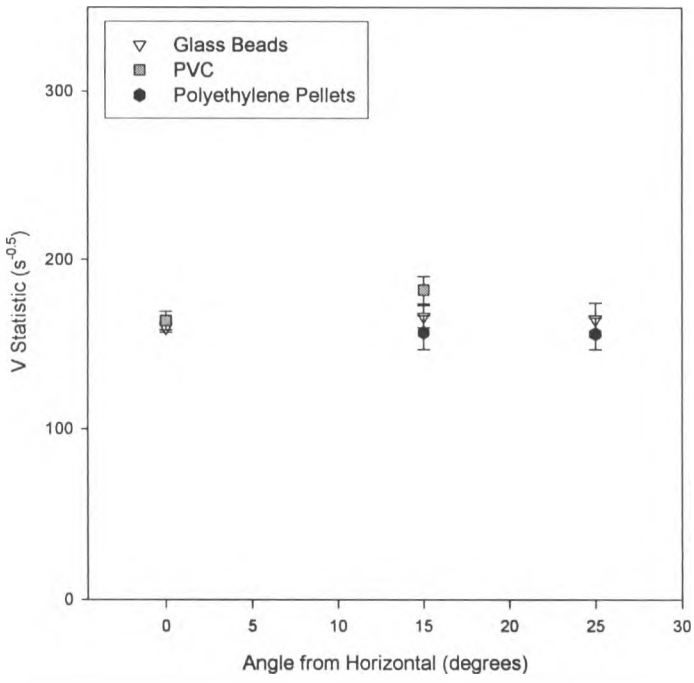

Figure 4.4.24. Wavelet residual V Statistic transition regions for each solid and angle from the horizontal.

The choice of the V Statistic at 0.000425 s allows for easy determination of the flow regime based on the value of the V Statistic relative to the transition value. The advantage of a transition region is the accurate classification of each flow regime, with few flow conditions that fall within the transition region. The dilute phase conveying regime corresponds to Figures 4.1a and 4.1b. The conveying over settled solids is represented in Figures 4.1e and 4.1f, while the transition region is shown in Figures 4.1c and 4.1d.

Pressure signals cannot be used to reliably detect the flow regimes. Figure 4.12 represents the wavelet residual of the pressure signals at 0.000425 s for glass beads at an angle of 15°. It is evident that the V Statistic values of the pressure signals cannot be used to determine the flow regime. The flow regimes that were determined from visual

observations and confirmed with the acoustic signals could not be detected from pressure signals. The V Statistic values which correspond to a specific flow regime are scattered and a transition region does not exist. Pressure signals from polyethylene pellets and PVC show the same behaviour. Other methods that were used to examine the pressure signals included the V Statistic of the raw signal, Hurst's Rescaled Range analysis, power spectra, signal mean, standard deviation and coefficient of variation, with similar poor results. Also, the correlation dimension used by Luewisuthichat et al. [19] and Kikuchi et al. [20], and the power spectra used by Dhodapkar and Klinzing [18] did not detect flow regimes using the acoustic signals.

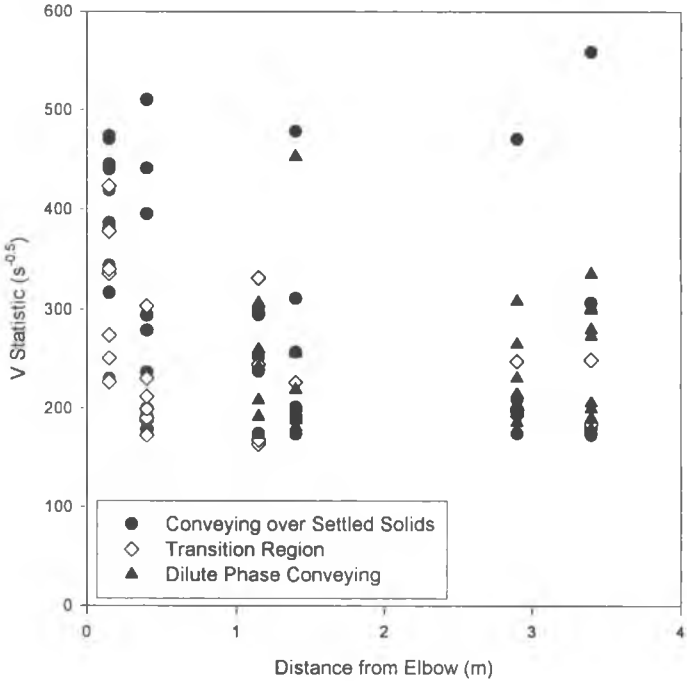

Figure 4.4.25. V Statistic values from the wavelet residual pressure signal for glass beads at 0.000425 s for various distances from the elbow at an angle of 15°.

A 4.4.6 Flow Regime Maps

Figure A 4.13 is the flow regime map for glass beads at 1.05 m from the elbow at 0°, 15° and 25° angles. Each curve on the map represents the average value of the transition region for a given distance from the elbow and angle from the horizontal. The map was developed using acoustic measurements and verified with visual observations. Conditions located above each line are associated with the conveying over settled solids flow regime, whereas conditions located below each curve are associated with dilute phase conveying. Figure 4.13 shows that the angle of the pipe has a strong and complex effect on the flow regime boundary. For a given gas velocity, deposits occur in inclined lines at a much lower solids flux than in a horizontal line of the same diameter due to particle-wall interactions causing particles to decelerate.

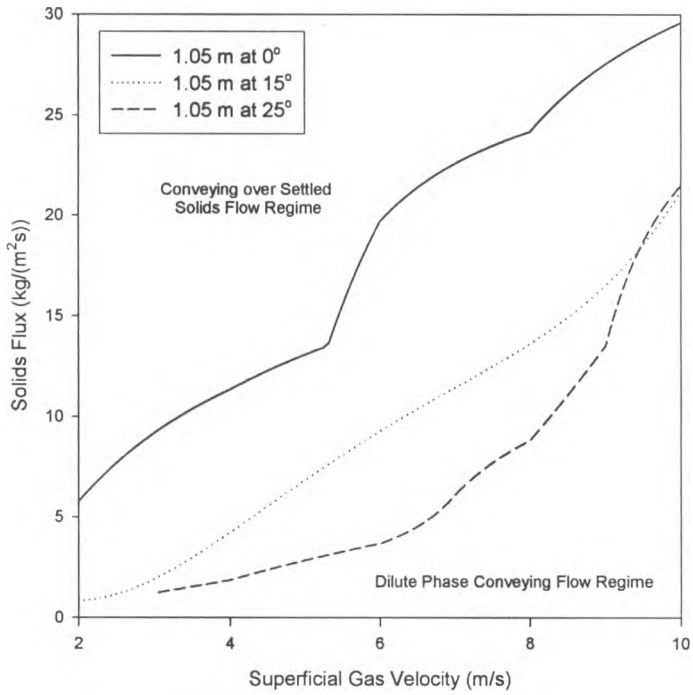

Figure 4.4.26. Flow regime map for glass beads at 1.05 m from the elbow for each angle.

Figures 4.14a, 4.14b and 4.14c are flow regimes maps for glass beads, PVC and polyethylene pellets at an angle of 15^{o} and different locations along the pipe. Close to the elbow, the settled solids regime predominates. At distances further from the elbow there are more conditions where dilute phase flow occurs. The increase in settled solids at the elbow can be attributed to the acceleration region, where particles fall out of suspension after the elbow. The majority of dilute phase flow occurs away from the elbow where the curves are nearly identical for glass beads and PVC. The variation in the location of the transition region along the pipe shows that there is an effect of location on the flow regime. Figures 4.14a, 4.14b and 4.14c also show that the particle size has an effect on the flow regime; deposits are more likely with the polyethylene pellets than with the glass beads and PVC powder. This suggests that the lower transition region for the polyethylene pellets was due to the larger particle size, since the pellet diameter was about 20 times larger than the PVC and glass beads diameters.

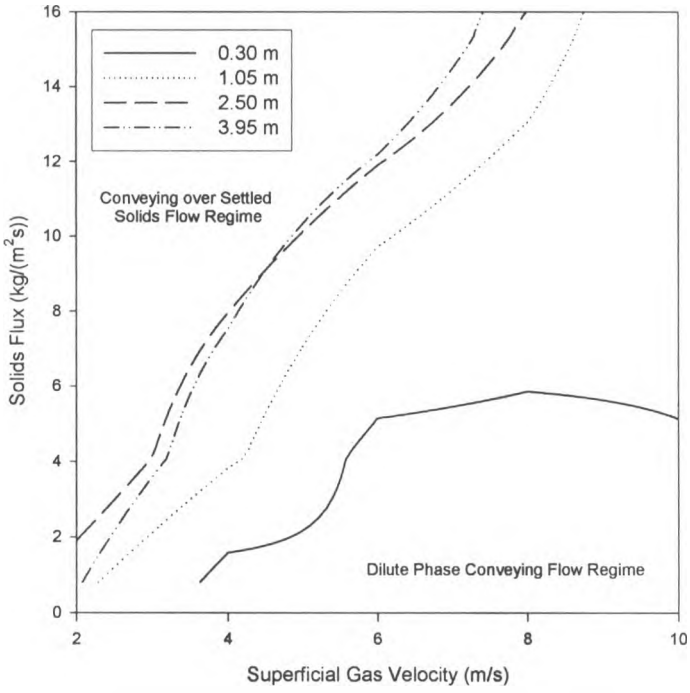

Figure A 4.4.27. Flow regime map for glass beads at various distances from the elbow at an angle of 15°.

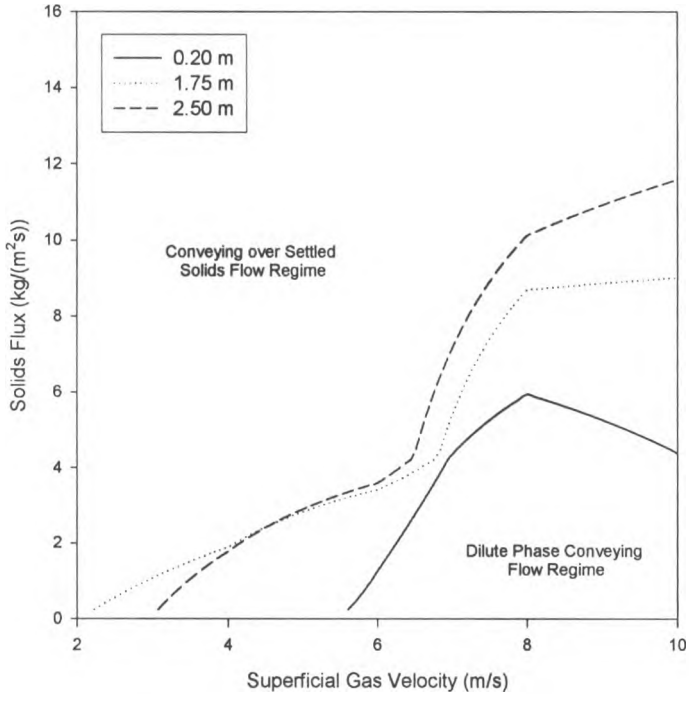

Figure A 4.4.28. Flow regime map for PVC at various distances and angles from the elbow at an angle of 15°.

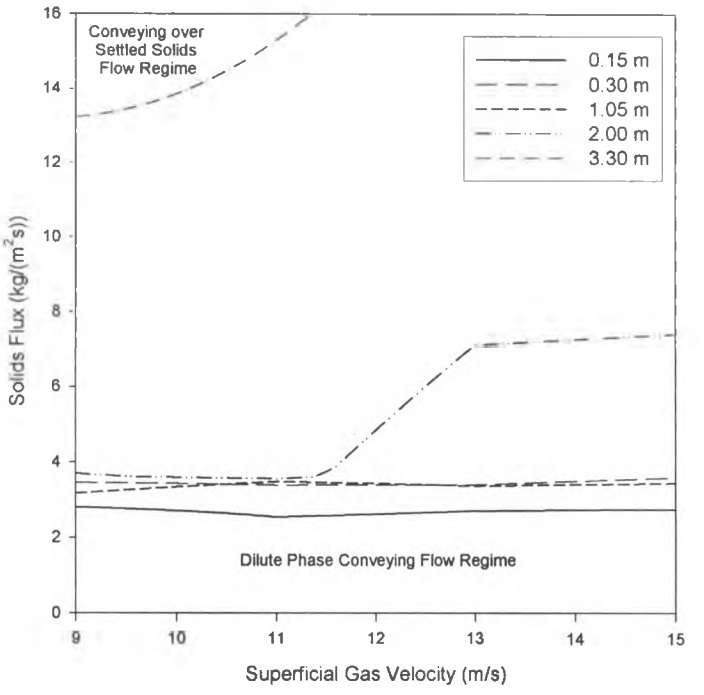

Figure A 4.4.29. Flow regime map for polyethylene pellets at various distances from the elbow at an angle of 15°.

A 4.5 Conclusions

Flow regimes in inclined pneumatic transport can be detected from acoustic probe measurements by using the V Statistic analysis. This detection method is applicable to all the distances, angles and solids studied in the inclined line.

Although the V Statistic of the raw signal can discriminate between dilute phase and settled solids flow regimes, the method can be improved through wavelet filtering. A wavelet filter was applied to the raw signal, and the V Statistic was calculated from the residual signal. This resulted in better discrimination between the dilute phase and settled solids regimes.

After applying the wavelet residual filter, the transition region for each solid and pipeline angle can be characterized by a similar V Statistic, with the exception of the polyethylene pellets. These results suggest that the critical value of the V Statistic may be independent of particle shape and density but dependent on the particle diameter since the polyethylene pellets size was about 20 times larger than the PVC and glass beads sizes.

This monitoring method is useful for process control. It allows for easy, non-intrusive, on-line monitoring of flow regimes. Through monitoring, detection of a V Statistic value above the critical transition value indicates pneumatic conveying in dilute phase, whereas a V Statistic below the critical transition value represents pneumatic conveying with settled solids. Use of this method for early detection of deposited solids can allow for quick corrective action to ensure overall product quality and system efficiency.

A 4.6 Acknowledgements

The authors would like to thank the Natural Sciences and Engineering Research Council of Canada and Syncrude Canada Ltd. for their financial support of this research.

A 4.7 References

[1] Fan, L.S., Zhu, C. Principles of Gas-Solids Flows. United Kingdom: Cambridge University Press. (1998).

[2] Ginestet, A., Guigon, P., Large, J.F., Sen Gupta, S., Beeckmans, J.M. Hydrodynamics in a flowing gas-solids suspension in a tube at high angles of inclinations. *The Canadian Journal of Chemical Engineering, 71* (1993) 177 - 182.

[3] Levy, A., Mooney, T., Marjanovic, P., Mason, D.J. A comparison of analytical and numerical models with experimental data for gas-solid flow through a straight pipe at different inclinations. *Powder Technology, 93* (1997) 253-260.

[4] Zhu, K., Wong, C.K., Rao, S.M., Wang, C.H. Pneumatic conveying of granular solids in horizontal and inclined pipes. *AIChE Journal, 50* (2004) 1729-1745.

[5] Klinzing, G.E., Marcus, R., Rizk, F., Leung, L.S. Pneumatic Conveying of Solids, 2nd Edition. New York: Chapman and Hall. (1997).

[6] Wirth, K.E., Molerus, O. The influence of pipe geometry on the critical velocity of horizontal pneumatic conveying of coarse particles. *Powder Technology, 42* (1985) 27-34.

[7] Wirth, K.E. Critical velocity of solids transport through horizontal circular pipelines. *German Chemical Engineering, 6* (1983) 45-52.

[8] Wirth, K.E., Molerus, O. Prediction of pressure drop in horizontal segregated pneumatic conveying with particle strands sliding along bottom of the pipe. *German Chemical Engineering, 4* (1981) 278-284.

[9] Valentino, M. Microphone Handbook. *PCB Piezotronics Vibration Division,* http://www.pcb.com/Linked_Documents/Vibration/Microphone_Handbook.pdf. (2005).

[10] Albion, K., Briens, L., Briens, C., Berruti, F. Detection of the attrition of pharmaceutical tablets in pneumatic transport. *International Journal of Pharmaceutics, 322* (2006) 119 - 129.

[11] Boyd, J.W.R., Varley, J. The uses of passive measurement of acoustic emissions from chemical engineering processes. *Chemical Engineering Science, 56* (2001) 1749 - 1767.

[12] Hurst, H.E. Long-term storage capacity of reservoirs. *Transactions of the American Society of Civil Engineers, 116* (1951) 770 - 808.

[13] Briens, L.A., Briens, C.L. Cycle detection and characterization in chemical engineering. *AIChE Journal, 48* (2002) *(5),* 970 - 980.

[14] Peters, E.E. Fractal Market Analysis: Applying Chaos Theory to Investment and Economics. Toronto: John Wiley & Sons, Inc. (1994).

[15] Trygg, J., Kettaneh-Wold, N., Wallbacks, L. 2D wavelet analysis and compression of on-line industrial process data. *Journal of Chemometrics, 15* (2001) 299 - 319.

[16] Briens, C.L., Briens, L.A., Barthel, E., LeBlevec, J.M., Tedoldi, A., Margaritis, A. Detection of local fluidization characteristics using the V Statistic. *Powder Technology, 102* (1999) 95 - 103.

[17] K. Albion, L. Briens, C. Briens, F. Berruti. Flow regime detection in horizontal pneumatic transport of fine powders using non-intrusive acoustic probes. *Powder Technology, 172* (2007) 157 - 166.

[18] Dhodapkar, S.V., Klinzing, G.E. Pressure fluctuations in pneumatic conveying systems. *Powder Technology, 74* (1993) 179 - 195.

[19] Luewisuthichat, W., Tsutsumi, A., Yoshida, K. Deterministic chaos analysis of particle dynamics in three-phase systems. *Journal of Chemical Engineering of Japan, 29* (1996) *(4),* 675-682.

[20] Kikuchi, R., Tsutsumi, A., Yoshida, K. (1996). Fractal aspect of hydrodynamics in a three-phase fluidized bed. *Chemical Engineering Science, 51(11),* 2865-2870.

[21] Srivastava, A., Agrawal, K., Sundaresan, S., Reddy Karri, S.B., Knowlton, T.M. Dynamics of gas-particle flow in circulating fluidized beds. *Powder Technology, 10* (1998) 173-182.

Appendix 5. Signal Analysis

Briens [1] performed extensive work on time series analysis of signals for the identification of flow regime changes in multiphase reactors. This was the main source of the methods to calculate the statistics used in this thesis.

Below are brief descriptions of the various statistical methods cited in this work. Details on the methods and their validations are provided in Briens [1].

Power Spectral Density - The power spectral density is calculated by the product of the Fourier transform of a signal and its complex conjugate. If x(t) is a function, its Fourier transform is:

$$x(\omega) = \frac{1}{2\pi}\int_{-\infty}^{\infty} x(t)e^{-i\omega t}\,dt \qquad \textbf{(A5.1)}$$

and its spectral density at the angular frequency ω is:

$$s(\omega) = x(\omega) \bullet x^{*}(\omega) \qquad \textbf{(A5.2)}$$

where $\omega=2\pi f$ and $x^{*}(\omega)$ is the complex conjugate of $x(\omega)$. The power spectral density is a plot of $s(2\pi f)$ versus the frequency f.

The Fourier Transforms were calculated using Haar windows.

Wavelet analysis - During wavelet analysis of a signal, the signal is divided into *m* multiple levels or scales. This is accomplished by performing a transform on the data which retains all the information while reducing the length. Each of these levels corresponds to a frequency band, and due to the halving effect of the frequency, can further be defined as octaves. At each octave, using a Debauchies 4 wavelet, the signal was separated into two parts: the averages and the coefficients. The coefficients indicated the fluctuations in the signal at a specified scale.

Walker [2] provides an overview of the theory and methodology of wavelets as well as their scientific applications.

W-statistic – The W-statistic is the ratio of the average amplitude of the small fluctuations of a time series to the average amplitude of all of the fluctuations in the raw time series. The small fluctuations are extracted by using wavelet analysis to decompose the time series into averages and coefficients. The coefficients are the small fluctuations of the time series. By selecting a compression ratio, a threshold is selected, below which fluctuations are considered small. Once the small fluctuations have been identified the W-statistic is calculated for a signal $y(t)$ with the small fluctuations $y_s(t)$ by:

$$\text{W-Statistic} = \sqrt{\frac{\int_0^T (y_s(t) - \bar{y}_s)^2 \, dt}{\int_0^T (y(t) - \bar{y})^2 \, dt}} \qquad \textbf{(A5.3)}$$

where $\bar{y}_s$ and $\bar{y}$ are the average values of the small signal component and the raw signal respectively and T is the sampling time [3].

Hurst exponent – The Hurst exponent is a measure of the persistence of a signal and is calculated from the rescaled range analysis. Details on the calculations are provided in Briens et al [4].

V-statistic – The V-statistic was initially developed to predict cycles in the stock market. It is also using the rescaled range analysis and is a measure of the strength of the cyclic non periodic behaviour of a time series. Details on the calculations are provided in Briens et al [4].

F-Statistic – the F-statistic provides a measure of how well a model fits a set of experimental or observed data. Pope et al [5] provides a discussion on methodology and uses of the F-statistic.

Hölder exponent - For stochastic processes or functions X(t), the local regularity of sample paths is usually measured in terms of the Hölder exponent. This is performed by a comparison of X(t) at time t to a power law. A process X is said to have Hölder regularity $h \geq 0$ at time t if there exists a local polynomial P(s) of degree n = h and a constant C, as shown in Equation A5.4.

$$\left|X(t+s)-P(s)\right| \leq C\left|s\right|^{h} \qquad \textbf{(A5.4)}$$

Where 's' is an independent variable of the poloynomial 'P'. The Hölder exponent [h] quantifies the roughness of X [2, 3]. If h is close to 0 then the signal is considered to be rough and variable whereas an "h" close to 1 indicates a smooth and regular signal. For the derivative of the function, the Hölder exponent is in the range 1<h<2; where an "h" closer to 1, the rougher the signal. The Hölder exponent therefore is a measure of signal singularity.

The Hölder exponent is estimated by calculating a parameter based on the wavelet coefficients of all scales of the decomposition. This parameter is the average of the absolute values of the coefficients to the positive integer exponent 'n'. The results are plotted on the log scale and the Hölder exponent is measured as the slope. The present study used a Hölder exponent estimated by using an 'n' of 3. Therefore, the exponent calculated is referred to as the Hölder exponent of the 3rd order [6, 7].

Multi-variable regression – Using the least of squares curve fitting method it is possible to regress many parameters to fit experimental data. After a certain number of parameters, increasing number of coefficients becomes statistically insignificant and the best model is found. The number and type of parameters are determined by maximizing the F-statistic. This results in a model of the form:

$$y = C_1 x_1 + C_2 x_2 ... C_n x_n + K \qquad \textbf{(A5.5)}$$

Where 'n' is the number of independent parameters 'x' in the model, 'C' are the corresponding coefficients and 'K' is a constant.

By taking the log of the data before performing the least squares curve fitting it is possible to make a power law model of the form:

$$y = Kx_1^{C_1} x_2^{C_2} \ldots x_n^{C_n} \qquad \textbf{(A5.6)}$$

Where 'n' is the number of independent parameters 'x' in the model, 'C' are the corresponding coefficients and 'K' is a constant.

A 5.1 References

[1] Briens, L., Identification of flow regimes in multiphase reactors by time series analysis. Ph.D Thesis., *The University of Western Ontario (Canada)*, 2000

[2] Walker, J.S., A Primer on Wavelets and Their Scientific Applications, 2nd ED. *Boca Raton, Chapman & Hall.* (2008)

[3] Portoghese, F., Berruti, F., Briens, C., Continuous on-line measurement of solid moisture content during fluidized bed drying using triboelectric probes. *Powder Technology.* 181 (2008)169-177.

[4] Briens, C.L., Briens, L.A, Hay, J., Hudson, C. and Margaritis, A., Hurst's Analysis to Detect Minimum Fluidization and Gas Maldistribution in Fluidized Beds. *AICHe J.* 43 (7) (1997) 1904 – 1908

[5] Pope, P.T., Webster, J.T., The Use of an F-Statistic in Stepwise Regression Procedures. *Technometrics*. 14 (2) (1972) 327-340

[6] Park, K., Willinger, W. [Ed] Self-Similar Network Traffic and Performance Evaluation. *New York. Wiley-Interscience*. (2000)

[7] Riedi, R. Multifractal processes. In: Doukhan P, Oppenheim G, and Taqqu M [Ed.] *Theory and Applications of long range dependence*. Springer, (2003) 625-716.